Discrete Element Modelling of the Sizing of Particles in Zero Gravity

Daniel Truter

A research report submitted to the Faculty of Engineering and the Built Environment, University of the Witwatersrand, Johannesburg, in partial fulfilment of the requirements for the degree of Masters of Science in Engineering.

Johannesburg 2020

Declaration

I declare that this project report is my own, unaided work, except where otherwise acknowledged. It is being submitted for the degree of Master of Science in Engineering in the University of the Witwatersrand, Johannesburg. It has not been submitted before for any degree or examination at any other university.

....

Signed on the ....11th.... day of ....August 2020........

Daniel Truter

Abstract

This report focuses on the discrete element method and experimentation of sizing of particles in zero gravity conditions, with the objective of understanding the difficulties which may arise when attempting to predict the behaviour of particles under these conditions. This research will be beneficial in future asteroid mining operations.

This report first demonstrates how spherical particles behave in a zero gravity environment and how efficiently different types of sieve geometries and configurations perform. Plastic and steel pellets as well as iron ore particles were used as the screening material. The extruded sieve concept produced favourable results, with particles approaching at 60° to 90° to the sieving plane reaching efficiencies of 90%.

Probabilities were calculated for the various sieves, with the following results: rectangular (28.6%), oval (22.4%), square (14.1%) and circular (11.1%). A physical experiment was then performed for the purposes of having a comparative practical screening technique. The results of the physical experiment demonstrated similar efficiencies. In order to calibrate and validate the DEM simulation parameters for the various particles, a simulation of the physical experiment was then performed.

Screening in a zero gravity environment was then simulated. The space case sieve results were compared to the theoretical passing probability of particles, demonstrating similar efficiencies for the plastic and steel pellets. The iron ore particles reached efficiencies which were 1.5 times higher than the theoretical results; however, they were still within the range of probabilities for multibody particles.

The report shows that the main characteristics which govern the behaviour of particles during the screening process in a zero gravity environment are the coefficient of restitution, coefficient of static friction and the shape of the particle.

The overall conclusion of this report is that it is possible to predict the behaviour of material in a zero gravity environment with the use of practical experiments, careful parameter calibration and validation, and LIGGGHTS DEM simulations.

This work is dedicated to my parents, Regina, Anton and Theona Truter, and to my partner, Roxanne, who have continually supported and encouraged me, and who taught me that there are no shortcuts to any place worth going.

Acknowledgements

I would like to acknowledge and thank Mr Terrance Frangakis for his continual support, advice and guidance.

Contents

List of Figures

List of Tables

Nomenclature

Symbol	Description	Units
p	probability	-
L_A	Length of square aperture	m
d_p	Particle diameter / Particle size of which 50% of particles passed through the sieve	m
d_w	Wire diameter of wire in wire mesh screen media	m
ε	Coefficient of restitution	-
h_{final}	Final height	m
$h_{initial}$	Initial height	m
μ_s	Static friction coefficient	-
θ	Angle of inclined plane	°
F	Force	N
m	Mass	kg
a	Acceleration	m/s^2
g	Gravitational acceleration	m/s^2
T_R	Critical Raleigh time step	s
ρ_p	Particle density	kg/m^3
G_p	Particle shear modulus	Pa
γ_p	Particle Poisson's ratio	-
ø	Diameter	m
E	Young's modulus	Pa
υ	Poisson's ratio	-

Abbreviations/ Technical words	Description
NEA	Near Earth Asteroid
GEO	Geostationary Earth Orbit
DEM	Discrete Element Method
LIGGGHTS	LAMMPS Improved for General Granular and Granular Heat Transfer Simulations
LAMMPS	Large-scale Atomic/Molecular Massively Parallel Simulator
HSI crusher	Horizontal Shaft Impact (crusher)
VSI crusher	Vertical Shaft Impact (crusher)
VSMA	Vibrating Screen Manufacturers Association
Screen	Mechanical vibrating screen
Sieve	Screen media of screen which is typically constructed from woven wire
Stroke angle	Angle (measured from the horizontal) at which a screen would move
Stroke Amplitude	Distance of the stroke in the direction of stroke angle
PSD	Particle size distribution
CAD	Computer-aided design
CG	Centre of Gravity
Foreshortening	The perceived area of a sieve aperture from where a particle is approaching at an angle which is not perpendicular to the sieve.

Chapter 1 Introduction and Literature Review

1.1 Summary of Chapter 1

Chapter 1 consists of the background, problem statement, research questions, objectives and the literature review.

1.2 Research Background

There has been extensive research in the field of space mining as to whether mining in space is realistic and feasible. The main considerations in those studies however, were the economic feasibility thereof. In recent years there have been major developments in reducing the costs for transporting objects, including machines, into space. One entrepreneur in particular, Elon Musk, has been a leader in this field, and has continuing aspirations to make space travel more affordable than where it currently stood, at $17000 per kg in 2014 (Gump, 2014). This means that the possibility of mining asteroids is not as implausible as it seemed ten years ago. Some experts expect space mining to become a reality within the next ten years (Goswami, 2018). Scientists have studied asteroids and the general environment of space, and engineers have already proven that it is feasible to design and manufacture machines which can operate in space and the environment it offers (Musk, 2017).

Asteroids are classified into different types. Amongst the three most common types are carbonaceous, silicate and metallic type asteroids (Ross, 2001). The minerals within these asteroids are valuable and the asteroids can also contain water in the form of ice. Some of the minerals (eg. nickel and iron) are not particularly desirable because of their abundance on earth, but could be used in space for future structural developments (Arthur, 2016).

On Earth, mining techniques are generally limited to three methods, namely surface mining, underground extraction and in-situ extraction (Sonter, 1996). The fundamentals of these techniques are similar in the way that material is broken down and processed in smaller portions. By contrast, mining asteroids in space will involve attaching a type of space vehicle to the asteroid. It would break down the asteroid into smaller, manageable pieces, sort the pieces of asteroid using a method of screening, packaging the final product and transporting it to a space station or back to Earth. The focus of this report is the screening process of the particles recovered from breaking down of the asteroid, to assess whether the principles that govern particle sizing on Earth may be applied in zero gravity conditions, and whether there are adaptations to other mining processes that may be required.

1.3 Problem Statement

Space mining is a relatively new but fast-growing field of interest as companies around the world such as SpaceX, Planetary Resources and Deep Space Industries (DSI) are racing to be the first to achieve a viable form of mining asteroids in space (Space.com, 2018). These companies are developing concepts for salvaging asteroids and returning them to Earth for material processing. Asteroids exist in different shapes and sizes ranging from a few metres to a few hundred metres in diameter, which would be dangerous to bring through the Earth's atmosphere therefore braking methods such as propulsive braking or aerobraking would need to be investigated (Ross, 2001). This poses the question; would it not be more sensible to process the material in space and transport back only that which is desired in more manageable sizes? The idea behind this is that it will be more efficient to mine in outer space in this manner. Of course this would require the asteroid to be broken up, a feat which would need to be done without the use of explosives in order to prevent any flying, and potentially damaging debris.

On Earth there are various machines used to crush large rocks. These include jaw crushers, cone crushers, gyrasphere crushers, horizontal shaft impact (HSI) crushers and vertical shaft impact (VSI) crushers. The first three machines rely on gravity to ensure feed to the crushing chamber is maintained, and would not be viable solutions to mine in space. The HSI and VSI crusher would however, be able to operate solely with an initial push of the material into the crushing chamber. These two crushers produce cubic shaped particles (Metso, 2018) and the size of the particles varies depending on the close side setting and the speed at which the rotor rotates (between 800 – 2700 rpm) (Trio® Vertical Shaft Impact Crushers, 2016). These machines typically recirculate the material which has been crushed to ensure that the final product has reached the desired close side setting size. It is thus feasible that, with some adaptation, crushing may be possible in zero gravity.

After crushing, the loose particles would need to be contained and conveyed to a screening chamber. On Earth, screens vibrate the particles on the screen media or mesh using gravity as the force to ensure that the particles remain in contact with the screen media. The agitation mechanism allows the particles to rotate randomly into the correct orientation, which allows the particles to pass through the screen media apertures. In space, this would not be possible as the effect of vibration on the particles would be different, as the particles could have higher kinetic energy and would not remain in contact with the sieve. There are several facets which need to be explored in order to understand the behaviour of particles on screen media, including the orientation of particles relative to the screen media apertures, kinetic energy, driving force or energy required to allow a particle to successfully pass through an aperture in the screen media, method to ensure that a sized particle does not pass through the aperture in reverse, impacts of particles in a low energy dissipation environment, and the method of cleaning the screen media that has become blinded (ie. where particles become stuck in the apertures).

This report aims to investigate the principles which affect the screening of particles, in order to better understand the zero gravity application and to predict such application by means of DEM (Discrete Element Method) simulations, calibrated using a simple experimental approach.

1.4 Literature Review

1.4.1 Introduction

Sonter (1996) stated that space mining processes will naturally differ with respect to the desired product type. If a metal was desired and it was presented as macroscopic lumps in a silicate matrix, a process of crushing and thereafter sieving would need to take place. This generic mining separation method separates the larger particles from the smaller particles through screening. The larger particles are conveyed to a secondary crusher for further down-sizing, while the screened particles are conveyed to an area where they will be further refined, in order to obtain the metal in its purest form. This screening process forms the basis of this research.

This section will discuss the different factors which need to be considered before space mining may commence.

1.4.2 Asteroids

Near Earth Asteroids (NEA) have been grouped into several categories according to their compositions. It has been found that the most common types of asteroids are of the carbonaceous type (C-type). This classification means that they are made up of water and other elements necessary for life (Sonter, 1996). The second most common type of asteroid is classified as a silicate type (S-type), which, although stony, is mineral-rich (Arthur, 2016). These contain fragments of Magnesium silicates, and small quantities of nickel, iron and platinum (Arthur, 2016). The third type of asteroid composition which is of interest is the metallic type (M-type). These consist of large quantities of nickel and iron, although it has been found that large asteroids cannot consist of pure metal as photometric and polarimetric studies suggest that they consist of silicate-component-like stony-iron (Lupishko and Belskaya, 1988). These studies suggest that no form of water exist in this type of asteroid. This report has, therefore, excluded water from the analysis. Nickel (Ni) and Iron (Fe) are of minimal interest for return to earth but could prove to be extremely useful for construction of colonies and vehicles in space (FW:Thinking, 2013), where they could be melted down, extruded into a filament and used for 3D printing parts in space. If this process is successful, it will be possible to print steel structures at a substantially reduced cost.

Two organizations have set their targets on space exploration, namely Planetary Resources and Deep Space Industries (DSI) (Space.com, 2018)). Planetary Resources has already deployed Arkyd – a machine which was built and sent into space purely to identify whether asteroids contain precious minerals (FW:Thinking, 2013). DSI, on the other hand, has produced the first ever 3D print from an asteroid material on earth. The asteroid was crushed, powdered and processed and then used in a 3D printer (Science Plus, 2016). The printed part consisted of iron, nickel and cobalt and was produced to prove that asteroids could be used for future steel construction in space. The composition of this part was comparable to a refinery grade steel (Science Plus, 2016).

1.4.3 Transfer of mass

According to a study performed by Ross (2001), the difficulty in transferring a mass from one orbit to another is due to the change of velocity required. These changes of velocity can range between 1 km/s – 11.8 km/s, the former being the change of velocity of a NEA to Earth's orbit, and the latter being from Earth's surface to Geostationary Earth Orbit (GEO) (Lewis, 1991, cited in Ross, 2001). Findings on how to nudge NEAs into Earth's orbit temporarily have been published by Tsighua University in Beijing (Baoyin et al., 2011, cited in Goswami, 2018). This will allow space miners on Earth the opportunity to access the asteroid for mineral extraction before nudging the asteroid back out of Earth's orbit. The asteroid's trajectory would need to be determined carefully in order to carry out this dangerous task, as any mistake could result in the asteroid entering the earth's atmosphere, which could be catastrophic.

1.4.4 Spacecraft

There is an emphasized drive to reduce the costs of sending objects into space. Currently, Elon Musk is one of the leading entrepreneurs in this field as his company, SpaceX, has made immense progress in optimizing the concept of reusing the spacecraft after it lands safely on Earth. This was done in order to reduce the costs per launch for the space tourism concept. Currently, Elon Musk's largest spacecraft to date is the Falcon Heavy which can transport 30 tonnes of payload per trip (Musk, 2017). Approximately 70% of the spacecraft is reusable. The design of the previous space rocket, the BFR, consisted of a fully-reusable spacecraft which can transport a payload of 150 tonnes (Musk, 2017). The latest SpaceX launch vehicle, the Starship prototype called the Mk1, has been designed and will be the first full-sized test vehicle that is planned to take flight in 2020 (Wall, 2019). It will fly to an altitude of approximately 20 km. Soon thereafter it is predicted that the Mk4 or Mk5 of Starship will transport paying customers into space as early as 2023 (Wall, 2019). One major challenge of space travel is the transportation of the fuel the spacecraft requires as this forms the largest portion of mass and thus accumulates the most cost when sending the spacecraft into orbit. Liu Ruopeng, founder of Kuang-Chi Science Ltd., intends to compete with Elon Musk by entering the race for space tourism (Goswami, 2018). The competition will not only reduce the time to the first space tour, but will ensure that companies consider every possible way to reduce the cost per ticket for the consumer. The reduction in cost of space launches will mean that space travel could become another mode of common transport. This would also allow the transportation of space mining machines and robots into orbit that could carry out the task of space mining, which would make space mining potentially feasible in future.

1.4.5 Financial aspects

A study performed by Sonter analysed the technical and economic feasibility of mining NEAs and concluded that it is technically feasible, and that the product returned to earth could be traded for an impressive profit (Sonter, 1996). This study took into consideration the potential drop in the mineral market due to large quantities of specific minerals being sourced from space which would decrease the rarity of the mineral here on Earth.

NASA budgets $19.9 billion annually for their space programmes (NASA, 2020). China has recently increased the contribution to their space program from $695 million in 2015 to $6 billion in 2016 (Goswami, 2018). This shows an increased interest in space exploration. The justification given for the increased annual financial investment is led by China’s ambitions to investigate spaced-based solar power, lunar and asteroid mining, space settlement, and planetary defence (Goswami, 2018). The China National Space Administration (CNSA) is focused on performing feasibility studies for extracting minerals from asteroids between 2017 and 2022. One asteroid, in particular, 1996 FG3, is one NEA which is near enough to be processed for research and the collection of titanium and platinum mineral samples (Goswami, 2018). These budgets may seem low as studies performed in 1996 suggested that an initial capital of $100 billion would be required in order to start space mining (Kargel, 1996, cited in Ross, 2001). In today’s value it is converted to $164 billion – an amount far greater than the amounts budgeted for by NASA and CNSA combined.

1.4.6 Material processing on Earth

1.4.6.1 Separation techniques

There are many different types of separation techniques which are used in industry today. Amongst the most common are magnetic separation, eddy current separation and different types of mechanical screening. Other interesting separation techniques exist such as the X-ray fluorescence separator which is used in the final recovery process in diamond mines. This process utilizes two physical properties of diamonds; they are hydrophobic in nature and that they fluoresce when they are exposed to x-rays (Diamcormining.com, 2018).

Material separation occurs during recycling of automobiles through the use of manual and mechanical techniques. Due to the relatively low cost of mechanical separation techniques it has become the preferred process of material separation. Automobiles are shredded into thousands of pieces and are then sorted into ferrous and non-ferrous metals. Ferrous metals are separated from other materials through a magnetic process. Non-ferrous metals are separated with an eddy current separator (Coulter et al., 1998). For separating polymers of different densities a fluid is used. The material with the greater density sinks while other polymers float (Coulter et al., 1998).

Screens are the most common type of machine used in the mining industry for separating large particles from smaller particles.

1.4.6.2 Types of screens

Rotary screens are used in industry to separate solids from liquids (Defender Rotary Screens, 2016). This is done by feeding the solid-liquid mixture onto a rotating drum which has openings to allow liquid to pass through while transporting the solids over the drum to a discharge chute.

Vibrating screens have a bed with apertures which vibrate to allow motion of particles across the bed, with smaller particles passing through the apertures. All screens attempt to achieve complete stratification through the method of exciting material at an acceleration of more than 3 times the acceleration due to gravity. Screens operate with different motions and each motion has its own advantages for specific applications. Each screen is designed for a specific application and can very rarely be modified to suit another application. Circulatory motion screens are usually inclined at 20° and can process tonnages of up to 1700 tonnes per hour in some applications (Xinhai, 2018).

Vibrating screens are designed for the type of screen media which they will be fitted with and these may also vary according to the application. The type of screen media chosen is based on the desired percentage open area of the screen, the wear resistance of the media as well as the maintainability of the screen media when it is worn. The types of screen media are (Screen Media, 2013):

- perforated plates – steel plates with apertures profiled through the thickness of the plate,
- woven wire mesh – wires layered horizontally and vertically to form sieve apertures,
- polyurethane and rubber panels – moulded panels with apertures moulded into the material,
- wedge wire panels – wires moulded into polyurethane or rubber panels to form apertures.

1.4.6.3 Screening parameters

Studies have been performed on vibrating screens to determine the efficiencies which could be attained by changing the physical and operational parameters. Screen manufacturers use different programs to size screens correctly according to the defined requirements but most of these software programs are based on a modified formula that was initially generated by the Vibrating Screen Manufacturers Association (VSMA) (Olsen and Carnes, 2001). This formula considers 12 factors which have been tested over years of research.

Olsen and Carnes (2001) argued that the original formula considered 12 factors to reduce the manual calculation time, but with today's computer power they urge screen engineers to include 6 additional subtle factors which they felt are necessary to increase the accuracy of the solutions. Table 1 lists the 12 originally generated factors as well as the 6 additional factors which are suggested above. Their relevance to the zero gravity application are also assessed.

Table 1: Parameters which determine the screening efficiency of vibrating screens.

Parameters	**Description**	**Relevance to Zero gravity Application**
Basic Factors		
Basic capacity per square foot	Capacity in tonnes per hour	Relevant
Inclination angle	Screen angle determines the effective screen opening area (foreshortening) – See Figure 1.	Not relevant
Deck factor	Not the whole length of the lower decks are being used – See Figure 2	Not relevant
Oversize factor	Percentage of input particles which are larger than the screen openings.	Relevant
Half size factor	Percentage of input particles which are less than half the size of the screen openings.	Relevant
Slot factor	Determined by the shape of the screen openings.	To be investigated
Spray factor	Effect of a water spray system on a screen.	Not relevant
Material condition	Dictated by the effect of moisture content on the feed material.	Not relevant
Particle Shape	Dictated by the shape of the particle ie. Cubic or elongated.	Relevant
Open area factor	The available open area of the screen media.	To be investigated
Weight factor	Determined by the density of the feed material.	Not relevant
Efficiency factor	The ratio between the amounts of particles which should theoretically pass through versus the amount of particles which actually pass through.	Relevant
Additional Factors		
Type of stroke factor	Determined by the type of stroke of the screen – See Figure 3.	Not relevant
Stroke length factor	Dictated by the stroke length of the screen.	Not relevant
Timing angle factor	Considers larger particles in large screen openings requiring a greater vertical lift to clear the material from the opening.	Not relevant
Frequency or the revolutions per minute (RPM) factor	Determined by the frequency of vibration and the particle size.	To be investigated
Near size factor	The amount of particles which are close to the screen media opening size (within approximately 25%).	Relevant
Bed depth factor	Based on the bed depth size compared to the size of the screen openings – See Figure 4.	Relevant

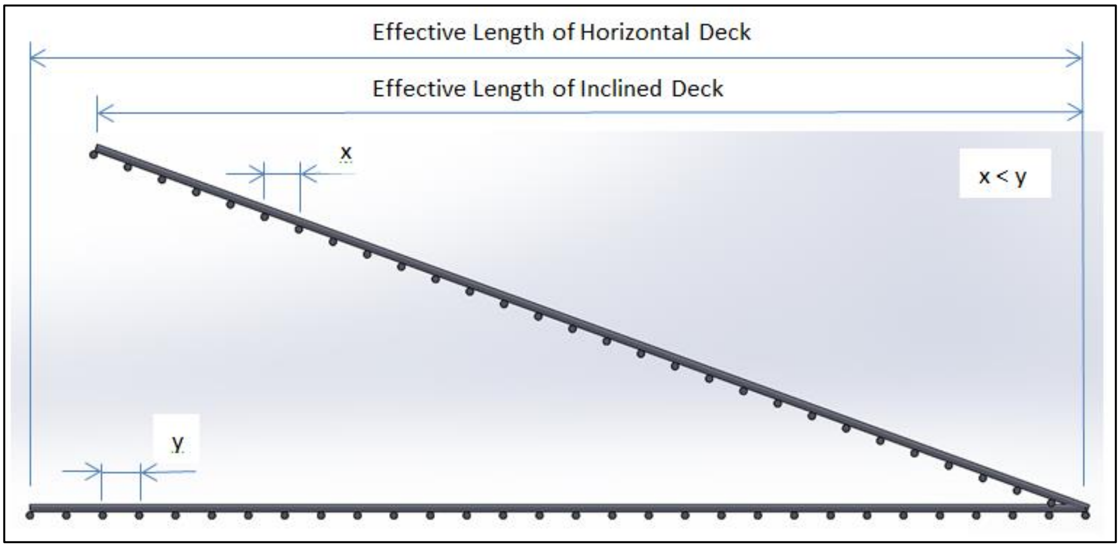

Figure 1: Foreshortening - effective open area of horizontal deck vs effective area of 20° inclined deck.

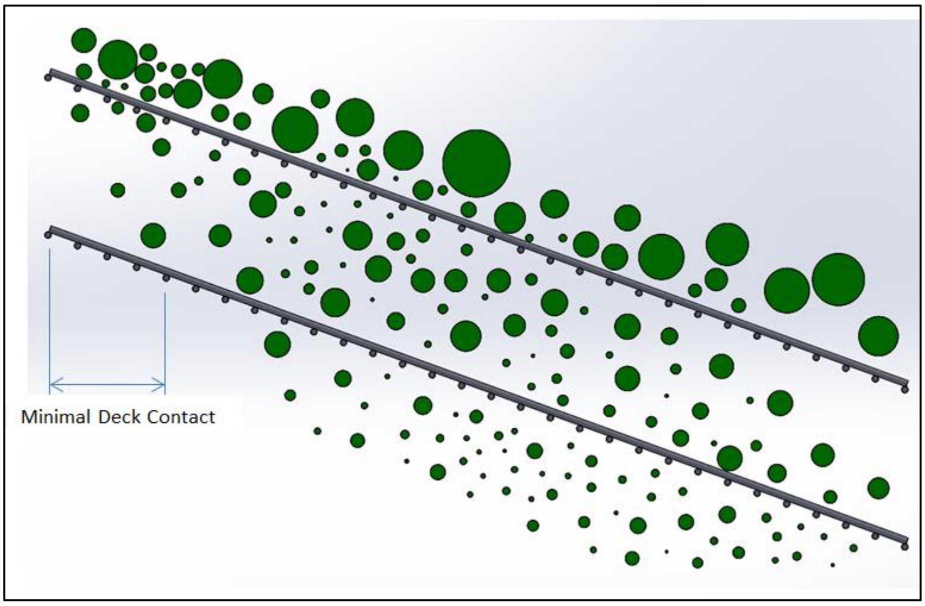

Figure 2: Deck factor illustration

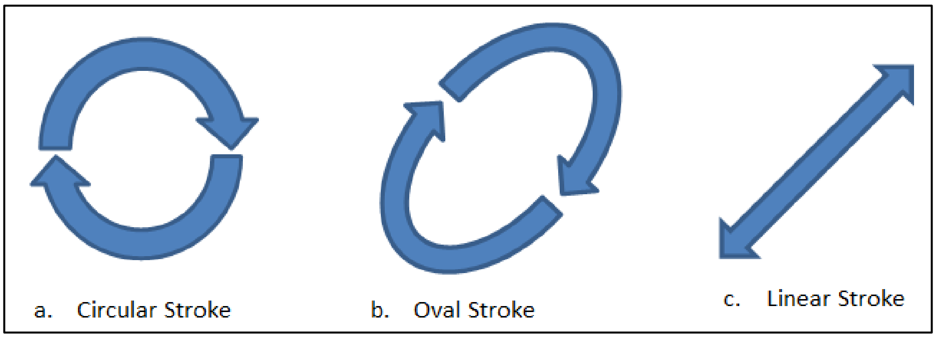

Figure 3: Illustration of a circular, oval and linear stroke

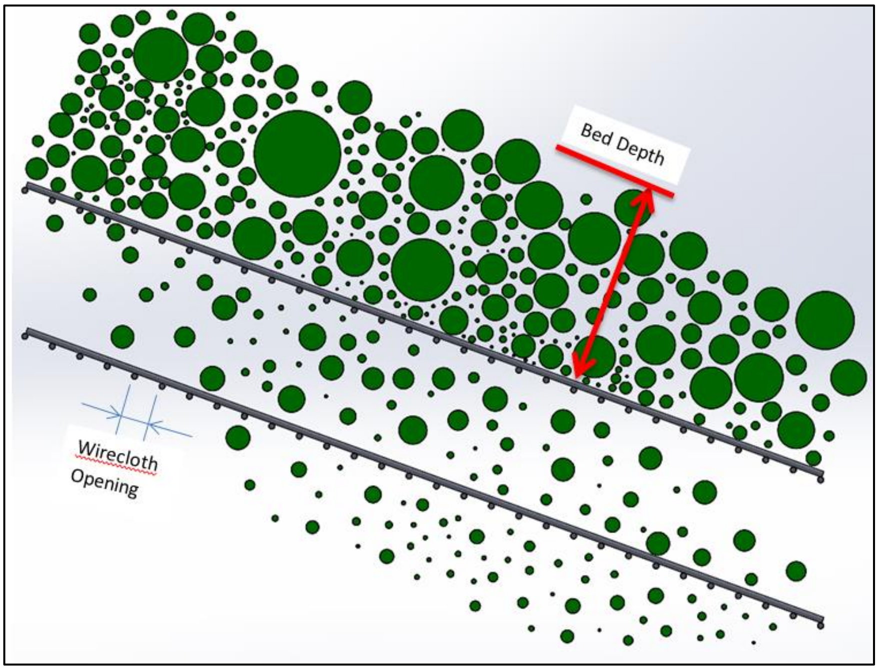

Figure 4: Large bed depth compared to small screen media opening.

Table 1 lists all the factors which influence the efficiency of screening and whether or not they will be relevant in determining the efficiency of screening in space. Three factors, in particular, need to be investigated further to understand whether they will affect screening efficiency in space or not. These factors are namely: slot factor, open area factor and the frequency or RPM factor. It is thought that the latter factor will not directly affect the efficiency but investigation of inducing a vibration at a frequency may provide useful insights.

It is common knowledge in the screen design and engineering community that vibrating screens perform optimally when they are actuated at an acceleration of 3–5 times the acceleration due to gravity, or g. According to Newton's second law of motion, to achieve this, a screen with a mass of 4000 kg would require an actuating force in excess of 200 kN (when also considering the mass of the material on the bed). This force is easily generated through the use of electric motors which are designed to induce vibrations to a screen at various frequencies. These motors use counterweights which are designed to cause an imbalance which result in the vibrating motion.

The work done by Olsen and Carnes (2001) on the RPM factor explains why, in industry, screens operate with a stroke (or a throw) of between 8–10 mm for particles larger than 10 mm, a stroke between 4-6 mm for particles smaller than 10 mm and a stroke of 1-2 mm for particles smaller than 3 mm. The stroke is dependent on the frequency at which the vibrating motors operate. To achieve a stroke of 4-6 mm a 4-pole motor (1470 RPM) operating at a frequency of 24.5 Hz is used and to achieve a stroke between 8-10 mm a 6-pole motor (960 RPM) operating at a frequency of 16 Hz is used. For the purposes of this research report it is anticipated that a larger stroke would be desirable, therefore the frequency of vibration of 16 Hz will be used.

The particles flowing over the vibrating screen are in contact with the screen for a minimal amount of time so that the particle is understood to be "hopping" on the screen media. Screens operating with large bed depths have ranges of different sized particles and the main phenomenon which plays an important role in the efficiency of the screen in this case is stratification. This is a process whereby the smaller particles are excited through vibrations and manage to find their way through the spaces between the larger particles to the top of the screen media (as seen in Figure 5). This means that the smaller particles are positioned at the bottom of bed depth and have a greater probability of falling through the screen media due to their contact time being increased.

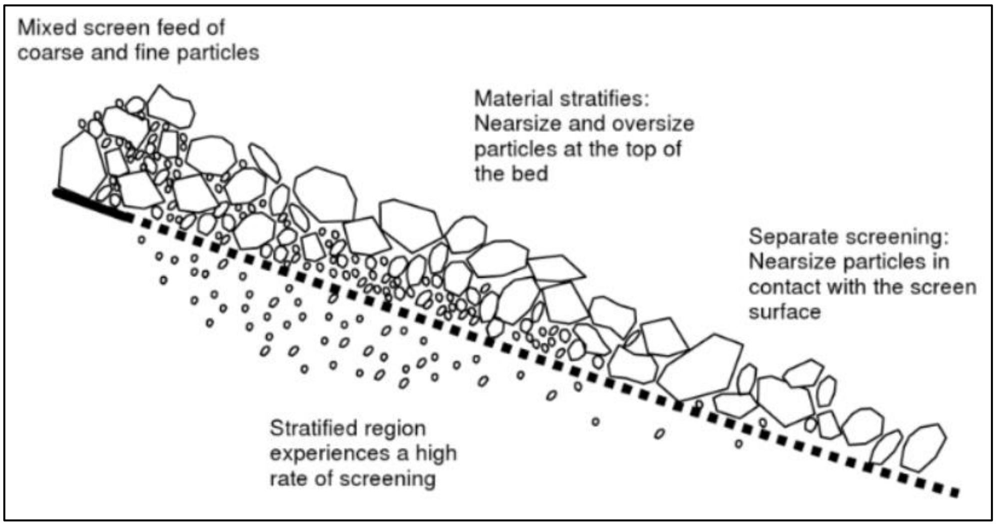

Figure 5: Stratification of material due to a vibrating screen deck (Courtesy JKMRC and JKTech Pty Ltd, as cited in Mineral Processing & Metallurgy, 2018).

1.4.7 Screening in zero gravity vs screening on Earth

The difference between screening in zero gravity versus screening on Earth is the fact that space does not consist of an atmosphere and a gravitational field. The zero gravity environment is the main concern as it heavily restricts the principles of screening to be applied to screens in space. On Earth, gravity is the external force which ensures that particles vibrating on a screen surface return to the screen surface after being accelerated upwards at 3-5 g. In space this force will not be applied and alternative parameters of screening will play a predominant role for the efficiency of screening. One advantage which the zero gravity environment has is the fact that the sieve will not have to be underneath the material being screened, it could be positioned around all sides of the material. Imagine a cube with one side being the inlet for material to enter and the opposite side being the exit for the oversize material. The remaining 4 sides could consist of a screen media which would mean 4 sides will be screening versus the single side screening on Earth.

1.4.8 Probability of particles passing through sieves

Probability plays an important role in the screening process as particles experience opportunities where they may pass through the sieve apertures. Screen designs on Earth rely heavily on ensuring particles have the most particle-on-sieve encounters (Retsch.com, 2019) to increase the chances to pass through the apertures. Therefore the probability of a single particle passing through a sieve aperture in one interaction is usually never considered. This research report, however, will consider the probability of a single particle passing through a single sieve aperture and will be compared to the results obtained in the DEM simulations and the physical experiments.

Gupta and Yan (2006) found that Gaudin developed a formula which governs the probability of a single particle passing through a square aperture. The formula is based on the assumption that the particle does not touch any sides of the aperture while approaching at 90° to the plane of the opening. The formula is given by:

$$\boldsymbol{p} = \left[\frac{(\boldsymbol{L_A} - \boldsymbol{d_p})}{(\boldsymbol{L_A} + \boldsymbol{d_w})}\right]^{\boldsymbol{2}} \tag{1}$$

where

L_A - is the length of the square aperture

d_p - the particle size of which 50% passed through the screen (Gupta and Yan, 2006). This could be found in the particle size distribution (PSD) data, from the d_{50} measurement

d_w - is the wire diameter of the wire in wire mesh screen media

The equation was further derived to include the additional probability of the particles colliding with the wire diameters and deflecting through the aperture openings. Theoretically this can be calculated with the use of a spherical particle and the angle at which the particle contacts the edge of an aperture (θ). Figure 6 below illustrates trajectory of the spherical particle after it collides with the wire diameter due to the overlap.

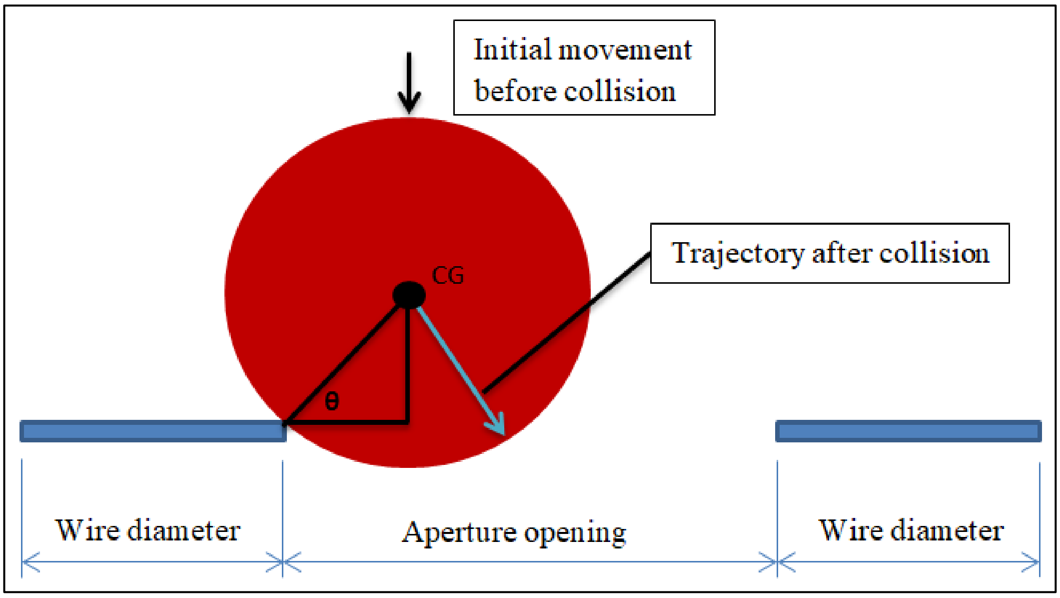

Figure 6: Particle colliding with wire diameter and deflecting through the aperture.

Using the above figure the following probability equations for the square, rectangular, circular and oval apertures can be derived (T Frangakis 2020, personal communication, 14 February):

Square:

$$p_{square} = \left[\frac{(L_A - d_p \cos\theta)}{(L_A + d_w)}\right]^2 \tag{2}$$

Rectangle:

$$p_{rectangle} = \frac{(L_A - d_p \cos\theta)(3L_A - d_p \cos\theta)}{(L_A + d_w)(3L_A + d_w)} \tag{3}$$

assuming the longest side of the rectangle is 3 times that of the shortest side.

Circle:

$$p_{circle} = \frac{\pi}{4}\left[\frac{(L_A - d_p \cos\theta)}{(L_A + d_w)}\right]^2 \tag{4}$$

Oval:

$$p_{oval} = \frac{\pi}{4}\left[\frac{(L_A - d_p \cos\theta)(3L_A - d_p \cos\theta)}{(L_A + d_w)(3L_A + d_w)}\right] \tag{5}$$

assuming the major axis of the oval is 3 times that of the minor axis.

1.4.9 Efficiency of screening and error percentage

Similar to how the probability equation quantifies the theoretical probability of particles passing through sieves, the screen efficiency quantifies the collective percentage of all the particles which physically pass through the sieve. The screening efficiency is calculated using the following formula provided by the VSMA handbook (Vibrating Screens, 1968):

$$Efficiency = \frac{\%\ of\ undersize\ in\ feed\ which\ actually\ passes}{\%\ of\ undersize\ in\ feed\ which\ should\ pass} \tag{6}$$

Predictions of results are not always entirely accurate therefore a deviation percentage is used to calculate the difference between the experimental value and the simulated value as a percentage. For this calculation the following formula is used:

$$\text{Deviation }\% = \frac{|\text{experiment value} - \text{simulation value}|}{\text{experiment value}} \times 100 \tag{7}$$

1.4.10 3D printing

3D printing is rapidly growing in the commercial industry. Steel printers, such as the one which DSI used to 3D print a part using material from a M-type asteroid, are common machines in the market (Cherdo, 2019). These devices use different techniques for 3D printing one of which is the process of extruding a filament (a material which could be melted down and formed), of the operator’s choice, to produce parts which have been designed on a computer aided design (CAD) program. The process starts with inserting cylindrical resin pellets (for polymer 3D printing) of approximately ø2 mm x 2 mm long of the desired material into the hopper which is then moved to the heating element and forced through the extrusion nozzle to form the filament which is used by the 3D printer. The 3D printer then melts down the filament and places layers of material to form a part which is a precise replica of the CAD model. The process to make steel filament is the same except it starts with melting down a powder instead of pellets (Cherdo, 2019).

This research report will focus on the sizing of particles to obtain small particles so that in the space application these small particles could be used to make filament for the purpose of steel 3D printing.

1.4.11 Discrete Element Method (DEM)

Discrete Element Method (DEM) is a numerical technique used to simulate the flow of granular material. It considers interactions between particles and particles as well as between particles and wall surfaces. Weak forces between particles may also be defined to simulate a material with a certain moisture content (Coetzee, 2017). During the movement of granular materials, particles may break into smaller particle sizes but this is sometimes not considered in order to simplify the simulation. Results produced by DEM software include the position and velocity of particles, as well as the magnitude and orientation of contact forces which may be experienced by particles as would occur in reality (Cavarretta et al., 2012). This method of analysis, although well established, often lacks in-depth experimenting for the validation of the results it produces (Grima and Wypych, 2011).

LIGGGHTS (LAMMPS Improved for General Granular and Granular Heat Transfer Simulations) is an open source DEM software program which is used to perform simulations of bulk material flow (Kloss et al., 2012). Accurate DEM simulations make use of suitable contact models in conjunction with Newton's second law of motion to determine the resulting forces acting on discrete particles within a stipulated system (Horn, 2012). In order for the software to determine the movement of particles it calculates the velocities, accelerations and the positions of the particles as well as the effects of the collisions with other particles and system geometry. The DEM model is first set up with parameters which have been calibrated with the material which is to be simulated. Thereafter the model is validated through the use of an experiment (Cheung and O'Sullivan, 2008). Once the above two steps have been carried out correctly it is possible to use those parameters to predict how similar particles will behave in other environments. It is therefore necessary to investigate the different input parameters which will have the most influence on the accuracy of the results in zero gravity application. Stated below are the input parameters of LIGGGHTS:

1. Coefficient of restitution (COR) is a measure of the amount of useful kinetic energy which is lost due to a collision between any two bodies (Ranjan, 2017). This input parameter is dependent on the velocity before and after the impact of the particle. The coefficient of restitution is often determined by a simple rebound test governed by the following equation (Bennett and Meepagala, 2005):

$$\varepsilon = \left|\frac{v_{final}}{v_{initial}}\right| = \sqrt{\frac{h_{final}}{h_{initial}}} \tag{8}$$

where v_{final} is the relative velocity after impact, $v_{initial}$ is the relative velocity before impact, $h_{initial}$ is the initial height from which the particle has been dropped and h_{final} is the height to which the particle has rebounded.

It is important to note that this equation may only apply on Earth where the kinetic energy can be transformed into other forms of energy such as sound and heat. Where the effects of energy conversions are different, as in space where sound may not exist, a different value of coefficient of restitution may occur.

A global parameter for the coefficient of restitution is initially used due to the quantity of collisions between the respective particles being fewer than the collisions between the particles and the wall geometry. Therefore the coefficient of restitution value is initially given that of the particle to wall until the parameter is calibrated in Section 2.4.1.6.

2. Particle shape plays an important role in DEM simulation (Combarros et al., 2014) as it determines whether the particles are more susceptible to a rolling or bouncing motion during a collision. For the purposes of screening it determines whether a particle may orientate itself in a position which will allow it to pass through the screen media apertures. Two methods are commonly used for particles in DEM simulations:
    i. Spherical particles with modified DEM input parameters to provide results which accurately simulate the desired bulk material or;
    ii. Multibodies which consist of many spheres which are clumped together to replicate the actual particle shape.

Cavarreta et al. (2012) stated that O'Sullivan and Cui (2009) obtained results which accurately compared to their experimental results when using DEM particles which were closely spherical while in their physical experiment they used precision steel balls, whereas Barreto (2009) did not achieve accurate results probably because he used particles which were not completely spherical which significantly influenced the behaviour of the bulk material. The results of these papers proved that DEM is heavily dependent on the particle geometry being used. Many types of equipment use the QicPic system (Cavarretta et al., 2012) to analyse the particle's size and shape by dynamically measuring the particles and by producing three results, namely the aspect ratio, sphericity and convexity (Sympatec, 2018). This enables particle shape to be accurately represented in DEM.

3. Particle density is calculated by dividing the particle's mass by its volume (Flint et al., 2002).

4. Young's modulus (E) is a measure of the stiffness of a material (Budynas, Nisbett and Shigley, 2011). It is common practice in DEM simulation to assume a value of $5x10^6$ for Young's Modulus because any value higher than this results in a dramatic increase in simulation time, while values of this order do not significantly affect simulation results (Yan et al., 2015).

5. Cohesion energy density quantifies the amount of energy required to break the cohesive bond between particles. This will not be explored in this research.

6. Coefficient of static friction is the amount of resistance a particle experiences before a force starts moving the particle in the direction of the applied force, when the particle is in contact with a surface. One method that may be used to test for the coefficient of static friction is through the use of an inclined plane test. This test inclines a plane on which a particle is placed until sliding occurs. Once the particle begins to move the angle at which the plane is set (θ_s) is recorded and used in the following equation for determining the coefficient of static friction (μ_s) (Pstcc.edu, 2019):

$$\mu_s = \tan\theta_s \tag{9}$$

   The coefficient of kinetic or sliding friction is used to determine the resistance force experienced by an object while it slides at a constant velocity. The coefficient depends on the nature of the two surfaces in contact and their respective surface roughness's.

   For the purposes of this research report the coefficient of static friction will be experimentally determined and will initially be used. This value acts as a global friction coefficient and is used in the case of kinetic friction as well (gran model hertz model — LIGGGHTS v3.X documentation, 2016). Similar to the coefficient of restitution, after the use of the initial value, the coefficient of static friction is calibrated in Section 2.4.1.6.

7. Poisson's ratio is a material property defined for a body as the ratio between the transverse strain and the longitudinal strain when the body undergoes stress due to a

load being applied to it (Silver.neep.wisc.edu, 2018; Engineeringtoolbox.com, 2018). This value was shown to have an insignificant effect on the results of the bulk material flow behaviour (Horn, cited in Guya 2018). In DEM, the Poisson's ratio (υ) can be used to define the Shear modulus (G) and the Young's modulus (E) of a substance using; $G = \frac{E}{2(1+\upsilon)}$. Therefore using a small value for Young's modulus in the simulation results in the shear modulus/ Poisson's ratio obtaining a small value.

8. Particle size is the physical size of the particle being simulated. Often spheres are clumped together to form more complex geometries to accurately represent actual sizes of granular materials (Coetzee, 2017).

9. Time step is a DEM simulation parameter which defines the time interval between iteration of particles' position, velocity and acceleration as they interact with one another and wall surfaces. This parameter is directly related to the simulation time and is dependent on the particle size. The larger the particle size the larger the time step required which results in a shorter simulation time (Grima and Wypych, 2011). The time step is required to be less than the critical Rayleigh time step. This is calculated using:

$$\boldsymbol{T_R = \frac{1}{2}\pi d_p \left(\frac{\rho_p}{G_p}\right)^{1/2} \left(0.1631\gamma_p + 0.8766\right)^{-1}} \tag{10}$$

where T_R is the critical time step, d_p is the particle diameter, ρ_p is particle density, G_p is the particle shear modulus and γ_p is the particle Poisson's ratio (Ren et al., 2012). A study performed showed that the particle shear modulus has a small impact on the results of the DEM simulation as long as a value of 1 MPa or greater was selected (Cole, 2020). A value higher than this increases the simulation time exponentially and is not necessary for the accuracy of the results.

The critical time step defines the point where the simulation would be numerically unstable (O'Sullivan and Bray, 2004). One instance in particular which shows this, is the requirement for having a small enough time step to produce results where particle interaction may be detected, as illustrated in Figure 7 below. Two particles travelling toward each other need to have a time step such that their collision is detected, as in the case of the two particles on the right of Figure 7 (Guya, 2018). If the time step is too large a collision may not be detected, and particles may pass through one another. This is not possible in reality.

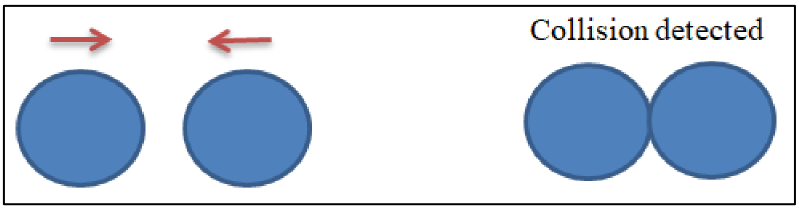

Figure 7: Timestep illustration

Out of the 10 input parameters mentioned above only the parameters relevant to segregation of cohesionless granular materials will be focused on. The parameters which are to be investigated and calculated are the coefficient of restitution, particle shape, particle density, coefficient of static friction, particle size and the critical time step.

The LIGGGHTS script also makes use of the Hertzian granular contact model which considers the contact between any two curved bodies of different radii to either be a point or a line as shown in Figure 8 (Williams and Dwyer-Joyce, 2001). Once a force is applied between these two bodies the contact area enlarges due to elastic deformation and the loads experienced by the bodies are distributed as pressures.

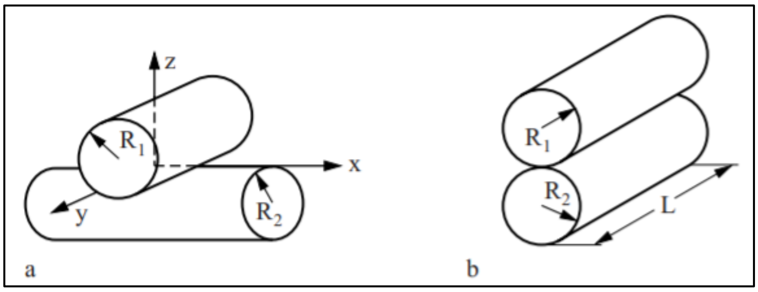

Figure 8: (a) Two crossed cylinders in contact; (b) Two cylinders in contact with parallel axes (Popov, 2010)

The granular contact model makes use of the following equation in order to calculate the force between two particles:

$$F = \underbrace{(k_n \underbrace{\delta n_{ij}}_{\substack{normal\\overlap}} - \gamma_n \underbrace{v n_{ij}}_{\substack{normal\\relative\ vel.}})}_{normal\ force} + \underbrace{(k_t \underbrace{\delta t_{ij}}_{\substack{tangential\\overlap}} - \gamma_t \underbrace{v t_{ij}}_{\substack{tangential\\relative\ vel.}})}_{tangential\ force} \quad (11)$$

The DEM simulation parameters require calibration and validation by means of physical experiments. Therefore the DEM and experiment processes are represented in Figure 9 and Figure 10 below. These illustrate the steps in order to successfully compare the results obtained in the DEM simulations and the physical experiments.

DEM process:

Figure 9: DEM process

For this research project laboratory experiments will be conducted to determine particle characteristics including coefficients of friction and restitution and sieving experiments, before the final simulation of the application is conducted.

Experiment process:

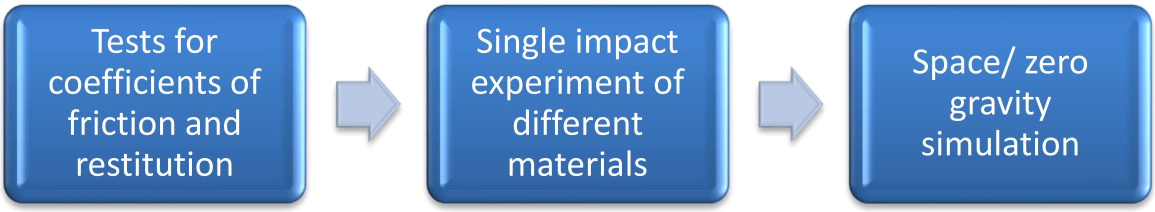

Figure 10: Experiment and simulation processes

1.4.12 DEM simulations of screening

Various studies have been conducted to analyse screen performance using different DEM software, including LIGGGHTS. These include studies by Sawant, Mohan and Sawant (2016) who investigated the effects of vibration frequency as well as vibration amplitudes on the performance of screening. Their findings were that vibration frequencies between 20 Hz to 30 Hz, and larger vibration amplitudes of between 5 - 7 mm, increased the screening efficiency. Barrios et al. (2013) investigated the behavioural difference between an experiment with iron ore particles and the DEM simulations of overlapping sphere multibodies and single spheres. Their findings were that overlapping spheres could achieve results within 6% of the experimental results while the single sphere results differed by more than 30%. It was said that it was possible to improve the result of the single sphere simulation by changing the static friction coefficient so much that much of the physical meaning of the parameter was lost. This, along with the use of multibodies, will form the approach for the research conducted in this report.

Delaney et al. (2012) conducted a study investigating the validity of approximating realistic granular flow with spherical particles. The study concluded that this approximation proved to be inadequate and that experiments and DEM simulations of non-spherical particles should be conducted. This illustrated that one of the most important parameters for running accurate DEM simulations is to ensure the best particle shapes, which closely represents the material being investigated, is used. According to research performed by Barrios et al. (2013) the sphericity and aspect ratio calculated for the tetrahedral-shaped overlapping spheres (see Figure 11) almost matched the physical measurements taken from a sample of iron ore pellets.

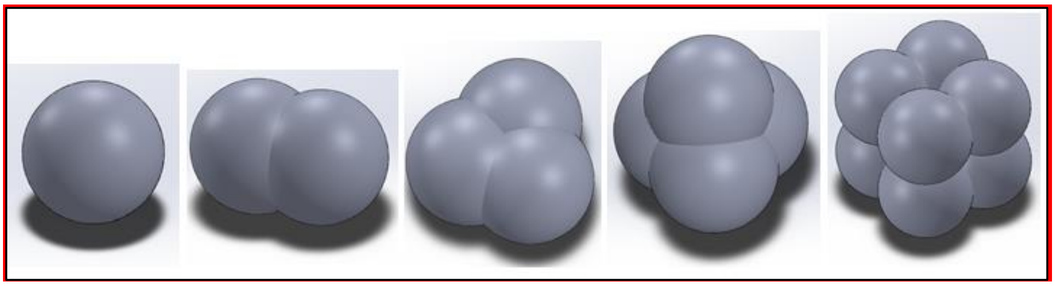

Figure 11: Illustration of shapes made from spheres which are to be used in DEM simulations (Coetzee, 2017)

In order to satisfy the required parameters for the simulations certain approximations will be made. These include approximations for Young's Modulus as well as the particle shape used in the simulations. The former is approximated much smaller than the actual value, as the DEM time step is inversely proportional to the shear modulus, which depends on the Young's Modulus. This results in a reduction of simulation time while not affecting the accuracy of the results. (Jahani et al., 2016).

1.4.13 Gap in the research

This literature review consisted of studies where the feasibility of space mining was investigated but lacked investigations of how the practicality of space mining would be carried out. A 3D printed steel part has been made from an asteroid material and thus it is desired that an asteroid of iron, nickel and cobalt be crushed down and screened to achieve a final product of powder. Similar to mines on earth the space mining process will require multiple crushing and screening stations to acquire the desired powdered product. Initially the particles would need to be crushed to particles smaller than 2 mm x 2 mm x 2 mm cubes. Realistically screens would be positioned in series so that there would be multiple stages of screens allowing the particles to be sized progressively until the final product is reached. The cubic pellets will then be transported to other crushing or grinding stations to be ground down to a powder and then melted down and extruded into a filament and used in a 3D printer to produce steel parts in space.

In order to design machines for the space mining industry, designers and engineers first need to understand the dynamics of particles in a zero gravity environment and the potential problems which may be presented. This research will investigate the physics of screening in a zero gravity environment. In order to do so the mechanics of screening in a gravitational field will be reviewed experimentally before exploring how these principles may be extended for use in a zero gravity environment.

1.5 Research Questions

The main questions set out in this research are:

A. Which system and particle characteristics govern the behaviour of particles during screening within a gravitational field, and in zero gravity?
B. How may the behaviour of particles in a zero gravity screening application be suitably simulated?

1.6 Research Objectives

The research objectives are as follows:

1) Conduct a physical experiment with different sieve geometries using spherical plastic and steel pellets, as well as iron ore particles, to assess screening efficacy in a high kinetic energy environment.
2) Calibrate and validate DEM models for spherical plastic and steel pellets, and iron ore particles, based on the physical experiment
3) Assess the effect of sieve geometry and efficacy in screening particles in a zero gravity environment by means of DEM simulation.

1.7 Research Methods

1.7.1 Research design

The theory on which this research is based will be tested and analysed through experimentation and simulation. The theory and formulas presented by VSMA over the last few decades have proven that highly vibrated particles are screened more efficiently than particles which are not excited at all. Due to this reason it makes sense to think that particles in space would act in the same way as they do on Earth if the same vibratory environment could be created for it. Therefore the desire to simulate a situation where particles will be highly vibrated in zero gravity exists but where the vibration is likely due to particle and surface interactions, in addition to the vibration of the screen. These simulation parameters will be validated using a laboratory experiment. Mentioned below is the breakdown of the simulations and experiments which are to be conducted and the reasons why each step is necessary to determine the efficacy of screening in space.

Preliminary simulation:

- Assess sieve geometry and efficacy in a high kinetic energy environment. This would be done using DEM simulations, and would explore different sieve and aperture geometries. The stroking frequency of the sieve geometry would be 16 Hz so as to remove this parameter from the comparison between screens operating on Earth versus screens operating in zero gravity.

Physical experiment:

- Construct and test a small laboratory experiment with the sieve geometry now set from the first simulation. The materials to be tested will be plastic pellets, steel pellets and iron ore particles. This test would explore only a single impact scenario to assess the probability that a particle could pass through a sieve aperture. The behaviour of spherical vs non-spherical particles will also be assessed in relation to the probability of the particle passing through the aperture.

Final simulation:

- Carry out DEM calibration of the plastic pellets, steel pellets and iron ore particles and simulate the laboratory experiment to validate the DEM model.
- Assume a space application geometry and carry out DEM simulations of the single impact test to test efficacy and practicality of sieving in space.

Note that the intention is not to determine an optimal geometry for sieving in zero gravity but rather to explore the potential thereof.

1.7.2 Material to be analysed

Three different spherical pellets (white, yellow and steel) will be tested to provide a benchmark to which the iron ore particles can be compared. These spherical pellets are all 6 mm in diameter and consist of different densities.

Material of all types, shapes and sizes exist in space in the form of asteroids. Asteroid mining which this research will investigate is extracting minerals from the M-type asteroid to be used for steel 3D printers. The types of minerals in M-type asteroids are iron, nickel and cobalt therefore for the purposes of this research iron-ore will be investigated as the equivalent space material. Materials which are available to be used for testing include iron-ore in the size range of 2 – 16 mm. Only undersize iron-ore particles, -6 mm, will be used in the experiments to ensure each particle has an opportunity to pass through an 8 mm aperture.

The desired particle shape to be used in the experiments is of a cubical nature as this is the shape which is most likely to be produced by VSI's and HSI's – the type of crusher most likely to succeed in a zero-gravitational environment. The different samples of iron ore material will be screened to sort the sizes of the test sample. The shape which will be used in the simulation will be determined in the preliminary simulation. The types of shapes to be tested will consist of spheres in different forms; the single sphere and four spheres forming a tetrahedral shape (see Figure 11).

1.7.3 Experimental equipment

The simulations conducted in LIGGGHTS will require inputs for the parameters. The following list illustrates which parameters will be tested and which will be obtained from literature.

1. Coefficient of restitution – conduct an experiment to identify the coefficient of restitution between the material and the object or surface it will be interacting with. To do this, particles of a spherical shape will be used in a rebound test where the initial and final heights are measured.
2. Particle shape – modelled after visually inspecting the particles.
3. Particle density – acquired from literature.
4. Young's Modulus (E) – acquired from literature.
5. Cohesion energy density – literature suggests that it is not necessary to include this parameter for dry materials.
6. Coefficient of static friction – initially acquired from literature but to be tested later to determine the effects on the overall behaviour.
7. Poisson's ratio – acquired from literature.
8. Particle size – measured from the particles which are to be used in the experiment.
9. Time step – calculated using the critical Rayleigh time step equation.

A personal computer with Bash on Ubuntu 14.04 will run a simulation using LIGGGHTS 3.8.0 which will produce results in the form of code. LIGGGHTS will require two types of inputs; parameter inputs as well as geometric inputs. The geometric inputs will be designed in the NX computer aided design environment. Once the results are obtained by LIGGGHTS and converted into the VTK format (an action included in the LIGGGHTS execution code) it will be run in Paraview to visually display the results to the viewer. This will easily present whether or not the design is sufficient for the purposes of this investigation.

1.7.4 Data collection and analysis procedures

The preliminary simulation will be performed to determine which sieve configuration will be used including the type of screen media openings best assists screening efficacy. The shape to be simulated plays an important role in the DEM simulation therefore intensive investigation in this area will be required. The DEM simulation of the single impact experiment under Earth conditions must be carried out. Once this is completed the physical single impact experiment performed will validate the DEM simulation parameters. Once the experiment has validated the DEM model, the simulation of the zero gravity condition may be performed and will represent how particles can be expected to react in space. The results obtained from these simulations and experiments will be the first step to determining whether it is feasible to use screening as a form of sizing particles in space. Favourable results, such as efficiencies which are comparable to those which could be expected on Earth, means that this research will be able to be used as the basis for a space screen design.

Chapter 2 Experimental Methods and LIGGGHTS Calibration

2.1 Summary of Chapter 2

This chapter will address the experimental setup of the preliminary, physical and final experiments and simulations to achieve the objectives set out in Chapter 1. The calibration of the LIGGGHTS variables required in order to run an accurate simulation will also be discussed.

2.2 Preliminary LIGGGHTS simulation

To generate a design for particle sizing for the space application it is important to first understand how particles behave in a high kinetic energy environment. The objective of the preliminary simulation is to assess the effects of the following on the screening ability:

- Number of particles (200, 600 and 1800);
- Stroke angle (the direction in which the sieve should stroke as seen in Figure 12);
- Shapes of the sieve apertures (square, rectangular, circular and oval); and
- Sieve configurations (flat and extruded)

In order to test for this a preliminary LIGGGHTS simulation will be set up using generic default parameters. This includes values such as 0.5 for the coefficient of friction, 0.3 for the coefficient of restitution, a Poisson's ratio of 0.45 and a Young's Modulus of $5x10^6$ GPa.

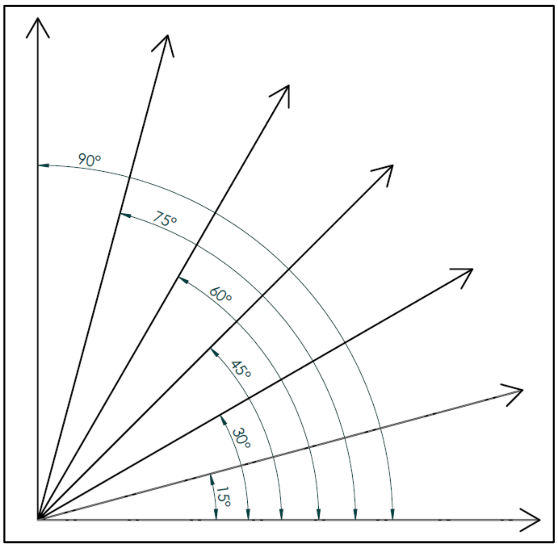

Figure 12: Stroke Angles in Increments of 15°

2.2.1 LIGGGHTS simulation setup

A box will be modeled with a sieve with shaped apertures (square, rectangular, circular or oval apertures) dividing the box in half (see Figure 13 and Figure 14). All the particles will be randomly inserted in the top half of the box (via the insertion plane which uses a defined input velocity) while the entire box, including the sieve divider, stroked (moved back and forth in the direction of the stroke angle). This will allow particles to pass through the mesh and oftentimes pass back through the mesh. A surface (later referred to as the counting plane) positioned on the other side of the mesh will count the number of particles which pass through the mesh (from the top half to the bottom half). The counting plane will only count particles which pass through the plane from above and only count each particle once in the entire simulation. In order not to count the particles which pass back through the sieve a manual count will be done once the simulation has ended. The reason the particles remain in the simulation and are not removed once screened is to test the ability of each sieve configuration to retain the screened particles in the bottom chamber.

The specific details of the simulation and the results thereof will now be presented as useful insights were gained that were relevant to the subsequent direction that the research took.

The sieve box consisted of the following dimensions: length = 200 mm, width = 100 mm and height = 200 mm. The sieve was positioned midway between the top and the bottom surfaces of the box.

The CAD models used were purely 2D walls and sieve surfaces as this reduced mesh size and thus reduced simulation run time. The one problem which this brought with it was that the Raleigh time step needed to be carefully calculated in order to ensure that particles' interaction with walls and sieves were detected correctly.

The method of trial-and-error was used to determine the best amplitude of the sieve-box to ensure that enough kinetic energy was transferred to the particles. Therefore the amplitude of the stroke was tested to be 28.3 mm (20 mm in the x- and y-directions). This provided a realistic stroke should linear vibration be used in the zero gravity (space) application. This approximation was based on the performance of the particles in the trial-and-error box-sieve configuration simulation. With a smaller stroke the particles reached a point where they would float in the one chamber and not enough particle-to-particle and particle-to-wall collisions were experienced, therefore the particles stagnated in empty space.

The total simulation time for each run was 0.5 seconds – 8 strokes in each simulation which equated to an operating frequency of 16 Hz and was comparable to the frequencies of screens operating on Earth. Gravity was not considered in this simulation therefore it was set to zero. The particle shapes which were used were spherical particles with diameters of 2, 3, 5 & 6 mm. The sieve aperture size used was 4 mm therefore the 3 and 5 mm diameter particles represented the near-size undersized and oversized particles respectively. The 2 and 6 mm diameter particles represented the undersize and oversize particles respectively. Each of the four particle sizes comprised of 25% of the particles in the simulations.

The angle of stroke of the sieve box was varied between 0° and 90° in intervals of 15° to find the most acceptable stroke to optimize throughput results in a zero gravity environment. This is illustrated in Figure 12. This was necessary because the first handful of set ups of the DEM simulation showed that a large stroke was preferred over small vibrations as in the latter case particles became "lost" in empty space in the box after making contact with the sieve and other particles, and then not interacting with the sieve again.

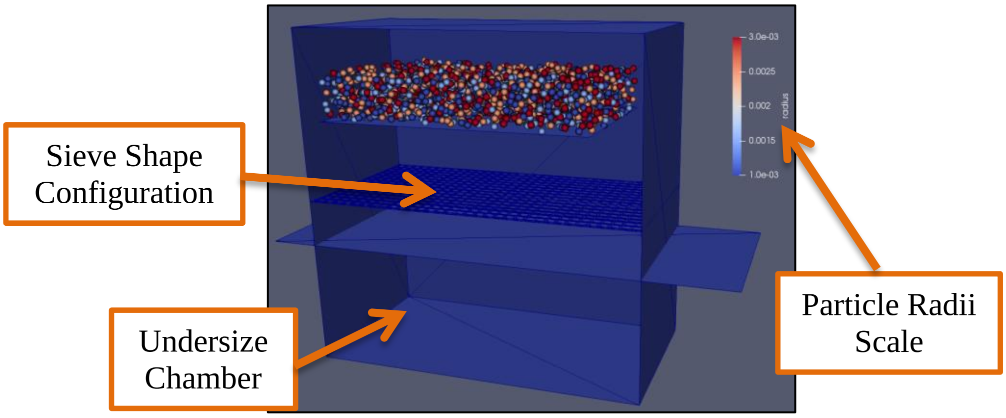

Figure 13: Top isometric view of the sieve box with particles positioned in the top chamber.

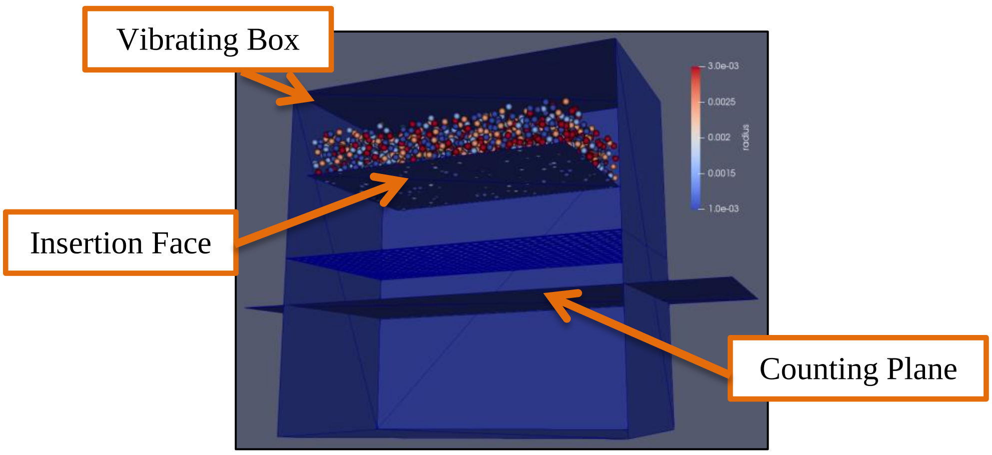

Figure 14: Bottom isometric view of the sieve box with particles positioned in the top chamber.

2.2.2 Sieve geometry

Four different aperture geometries – square, rectangular, circular and oval – were used in the simulation. These types of sieve geometry were tested with 2 different configurations; flat and extruded sieve apertures to further identify the best sieve type and configuration for a zero gravity application. These are explained in more detail in the following sub-section.

2.2.2.1 Sieve configurations

Flat configuration: Simulated with a flat piece of steel with punched out shapes.

Extruded configuration: Simulated with angled extruded apertures as per Figure 15. It was decided that this would assist in guiding the particles through the mesh shapes. The purpose of the optimised sieve configuration is to maximise the total top surface area used in the extruded configuration by increasing the number of apertures in the sieve surface. The first advantage which the extruded sieve is expected to have is that it would retain more particles in the bottom chamber once the particles have been screened. The second advantage is that should this configuration be selected for the space application the structural integrity of this design would be better. This sieve configuration may be directly compared to the flat sieve configuration as the same overall sieve area is used.

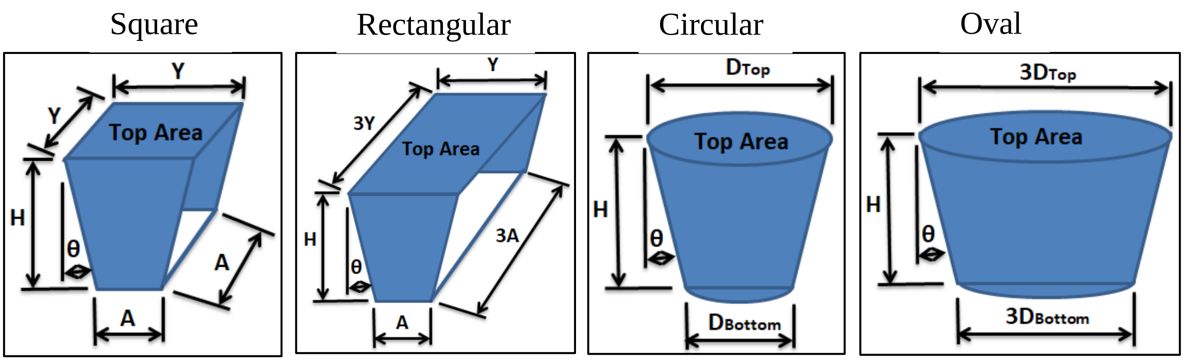

Figure 15: Extruded sieve configurations.

2.2.2.2 Sieve Shapes

Both of the above configurations were applied to each of the shapes below (shown in Figure 16). These shapes, through means of CAD software, were modeled and patterned multiple times to form part of a complete sieve. This CAD model was then saved as a stereolithography (.STL) file to be used in the LIGGGHTS code.

Dimension A would be the cut size of the sieve and was given a value of 4 mm. The cut size defines the size of particles which would be able to pass through the sieve. For the extruded sieve configurations the cut size dimension is given to the bottom area of the extruded shapes as this dimension determines the particle size which is allowed to pass through the sieve apertures. The longest dimension of the rectangular and oval aperture was selected to be 3A to ensure the results obtained are distinguishable from the square and circular aperture.

The following values were assigned to the dimensions in Figure 15:

$A = D_{Bottom} = 4$ mm

$H = 4$ mm

$\theta = 10°$

Therefore using Pythagoras Y and D_{Top} could be calculated:

$Y = D_{Top} = 5.411$ mm

Square	**Circular**
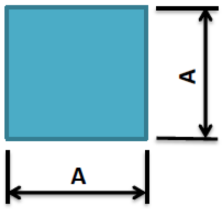 Open Area = A x A = 0.004 x 0.004 = 1.6 x10^{-5} m²	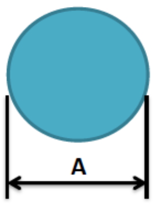 Open Area = π x (A/2)² = π x (0.004/2)² = 1.256 x10^{-5} m²
Rectangular	**Oval**
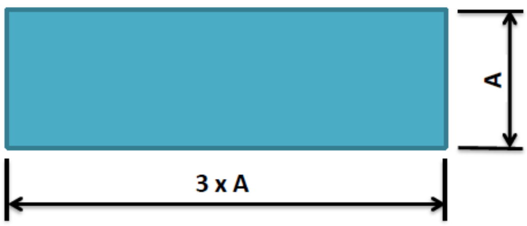 Open Area = A x (3 x A) = 0.004 x (3 x 0.004) = 4.8 x10^{-5} m²	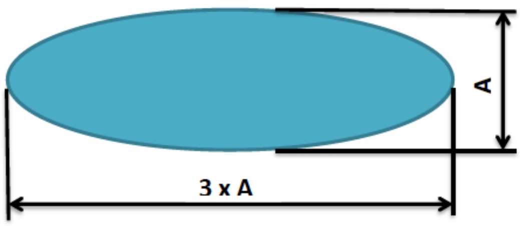 Open Area = π/4 x A x (3 x A) = π/4 x 0.004 x (3 x 0.004) = 3.77 x10^{-5} m²

Figure 16: Sieve shape open areas used in preliminary simulations

2.2.2.3 Simulation Sieve Configurations and Shapes

The following sets of figures (Figure 17 through to Figure 20) illustrate all the sieve shapes and configurations used in the process of the preliminary simulations.

- **Square Sieve:**

Flat Configuration	Extruded Configuration
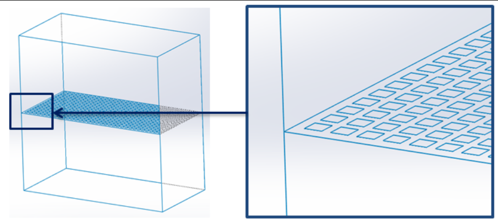	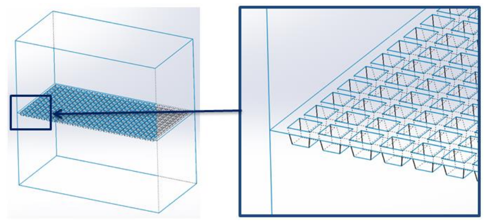

Figure 17: Preliminary simulation model of flat and extruded square sieves

- **Rectangular Sieve:**

Flat Configuration	Extruded Configuration
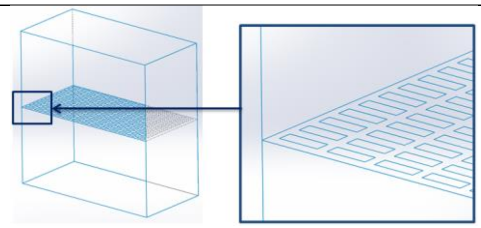	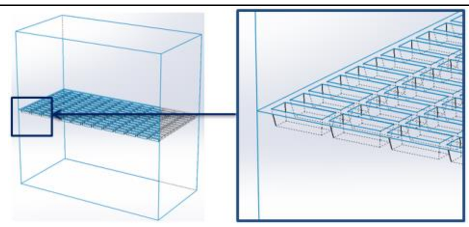

Figure 18: Preliminary simulation model of flat and extruded rectangular sieves

- **Circular Sieve:**

Flat Configuration	Extruded Configuration
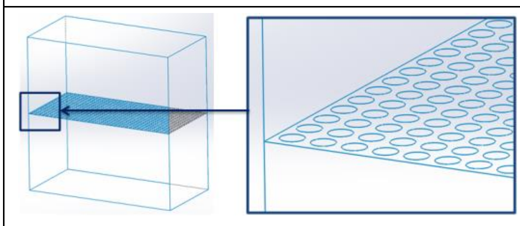	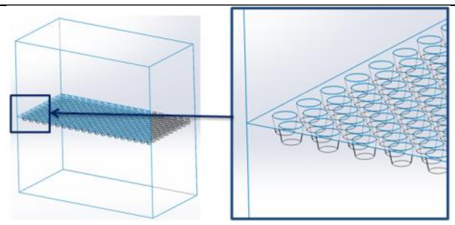

Figure 19: Preliminary simulation model of flat and extruded circular sieves

- **Oval Sieve:**

Flat Configuration	Extruded Configuration
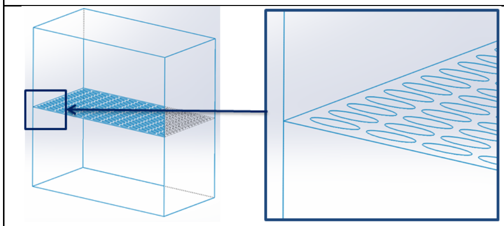	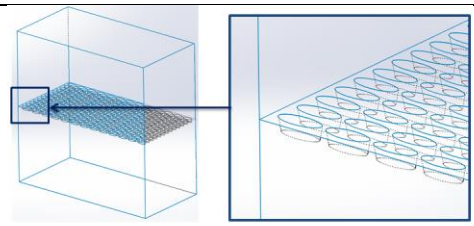

Figure 20: Preliminary simulation model of flat and extruded oval sieves

Table 2 below shows the open areas for all the sieves in square metres (m^2) and as a percentage (%) and it gives the top open area of the extrusions. It is important to note this because if the particles enter this open area nominally perpendicularly they are guided by the extruded sieve walls towards the opening (bottom) of the extrusion which increases the probability. In another case a particle approaching the aperture at an angle may not result in the particle passing through as it may deflect off the angled walls and deflect out the extruded aperture.

Due to the different sieving shapes used in the preliminary simulations it was not possible to produce screening sieves with the exact same open areas. The remainder of the apertures could not be used because a portion of an aperture would be ineffective for the application of screening. There is no point in using a half a hole (2 mm) because no simulated particle would fit through it. Therefore the open areas in square metres (m^2) and the open area percentage (%) would not be exactly the same but was within 4%, except for the extruded configuration which would optimally utilize the entire sieve area with as many sieve apertures as possible.

Table 2: Sieve open areas for top of extrusions

	Flat Sieve	**Extruded Sieve (Top)**
Square (Area m²) (Area %)	0.0084 (42.2%)	0.0099 (49.5%)
Rectangular (Area m²) (Area %)	0.0081 (40.6%)	0.0123 (61.3%)
Circular (Area m²) (Area %)	0.0084 (41.8%)	0.0092 (46.0%)
Oval (Area m²) (Area %)	0.0084 (42.2%)	0.0123 (61.3%)

Table 3 below shows the open area in square metres (m^2) and as a percentage (%) for all the sieves but gives the bottom open area of the extruded configurations. This is the area which dictates the size of particles passing through the aperture.

Table 3: Sieve open areas for bottom of extrusions

	Flat Sieve	**Extruded Sieve (Bottom)**
Square (Area m²) (Area %)	0.0084 (42.2%)	0.0054 (27.0%)
Rectangular (Area m²) (Area %)	0.0081 (40.6%)	0.0081 (40.6%)
Circular (Area m²) (Area %)	0.0084 (41.8%)	0.0050 (25.1%)
Oval (Area m²) (Area %)	0.0084 (42.2%)	0.0081 (40.6%)

2.2.3 Particles used in the simulation

The preliminary simulation was run using only spherical particles. The particle sizes to be used were undersize (2 mm), near-size undersize (3 mm), near-size oversize (5 mm) and oversize (6 mm) particles. 25% of each of the above particle sizes was inserted into the simulation. It was thought that simulating 25% of each particle size would also show which particle size is screened the most as well as which particle sizes are retained by the extruded configurations the most.

The sieve cut-size (aperture size) was selected to be 4 mm in apertures (A = 4 mm). Therefore the maximum amount of particles which could pass through the sieve is 50% of the particles (only the 2 mm and 3 mm particles). It should be noted that the efficiencies for the simulations were calculated by excluding all the oversize particles as these could not possibly pass through the sieves. Three Simulations were run for each shape type and configuration. Each run time the number of inserted particles changed between 200, 600 and 1800 particles. This was done to observe the performance of each sieve type during a small load, fairly loaded and an overloaded scenario.

2.2.4 LIGGGHTS parameters

To perform the preliminary simulation it was decided that the LIGGGHTS parameters were to be set up using the generically provided default parameters. The values of these parameters, as long as they remained consistent throughout all the preliminary simulations, would not have an impact on the objective of the preliminary simulation. These default LIGGGHTS parameters consisted of the following:

Table 4: LIGGGHTS parameters used in the preliminary simulations

LIGGGHTS Parameter	**Value (Units of measurement)**
1. Coefficient of restitution	0.3
2. Particle shape	Spherical
3. Particle density (ρ)	2500 (kg/m³)
4. Young's modulus (E)	$5x10^6$ (Pa)
5. Cohesion energy density	No cohesion
6. Coefficient of static friction	0.5
7. Poisson's ratio (υ)	0.45
8. Particle size	Diameters 2, 3, 5 & 6 (mm)
9. Time step (calculated below)	$5x10^{-6}$ (s)
10. Gravity	0 (m/s²)

The timestep was calculated based on 20% of the Raleigh time step but due to the high frequency and stroke of the sieve box towards the particles it was necessary to reduce it further. The Raleigh time step applies to wall boundaries which remain stationary but because in this case the wall boundary would be moving, the time step was calculated using equation 10 using the following values:

d_P (Smallest particle diameter) = 0.002 m

ρ_P (Particle Density) = 2500 kg/m³

G_P (Particle Shear Modulus) = 2 MPa (as mentioned in Section 1.4.11 any value above 1 MPa is acceptable)

γ_P (Particle Poisson's Ratio) = 0.25

Equation 10 then yields:

$$T_R = \frac{\pi\ (0.002)\sqrt{\frac{2500}{2\times10^6}}}{2\ (0{,}1631\ x\ 0.25 + 0{,}8766)}$$

$$T_R = 0.0001211\ s$$

$$20\%\ T_R = 2.42\ \times 10^{-5}\ s$$

The simulation initially provided results with oversize particles in the undersize chamber which is not physically possible therefore the simulation was re-run with a much smaller time step. The simulation result was then carefully inspected to ensure that no oversize particles passed through the sieve. After this trial-and-error approach it was found that a timestep of $5x10^{-6}$ seconds produced acceptable results while still maintaining a reasonable simulation time. This means that in order to account for the fast moving boundary wall the Raleigh time step had to be scaled by a further 20%. Therefore the value of the Raleigh time step which was used in the preliminary simulation was:

$$\textbf{20\% of 20\% } \mathbf{T_R} = \underline{\mathbf{5 \times 10^{-6}\ s}}$$

2.2.5 Simulation observations

It was observed in all the extruded sieve geometries that the oversize particles would trap themselves in apertures resulting in a reduction of the open area available for undersize particles to pass through. Figure 27 below indicates where the oversize particles (ø5 mm) had lodged themselves in the extruded apertures in the first row of the sieve geometry. 14 of the 20 apertures in the first row had been blocked. This dramatically reduces the open area and thus affects the overall efficiency of the sieve box. The flat sieve configuration did not have these issues and thus the open area at the start of the simulation was equal to the open area at the end of the simulation. One possible cause for this could be due to the input code of LIGGGHTS where the Young's modulus of the particles are given a value which resembles the stiffness of rubber (in order to allow the simulations to run faster) – due to this reason they would be more prone to get wedged in the apertures during the simulations.

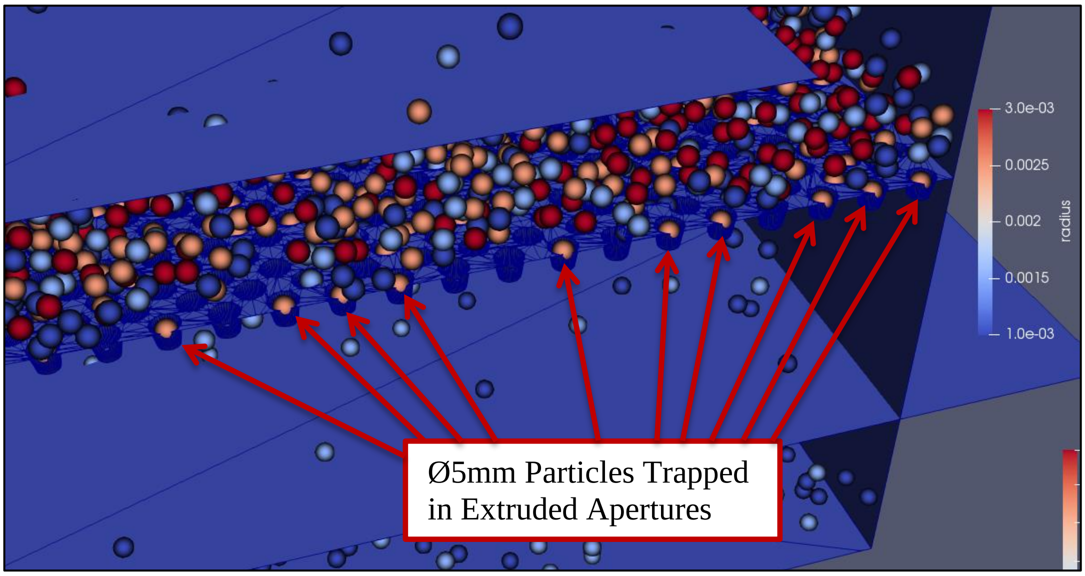

Figure 21: Sliced section of the circular extruded sieve box showing trapped ø5mm spheres.

It is important to note that upon visual inspection of the simulations that 20 - 30% of the particles which were screened were screened during the first interaction with the sieve. This observation inspired the one-time sieving technique for use in the zero gravity space case.

The simulations with 600 and 1800 particles showed that the sieve box was so full that the particles formed a bed that was 3 -5 particles high which only allowed the bottom layer of particles to have an opportunity to be screened.

One aspect which was observed during the preliminary simulation with no gravitational acceleration was that no stratification took place. A frame-by-frame visual inspection of the simulation showed that the particles would interact with the sieve and the particles which did not pass through the sieve would be pushed in the exact direction of the vibrating stroke (upwards). The particles would meet the top of the sieve box moving in the opposite direction (downwards) to impact the particles to transfer kinetic energy into the particles. The particle's velocities increased with this transfer of energy but were soon slowed down once the particles collided with other particles which reduced the particle kinetic energy again.

The energy transferred to a particle during a collision dissipates energy at the factor of the coefficient of restitution. Therefore the energy in the entire system is not ever-increasing as the sieve box moves through its strokes. In reality, some energy will cause particle chipping or fracture, or would also be dissipated in impacts with the walls or sieves.

2.2.6 Preliminary LIGGGHTS simulation results

Figure 22 shows the result of one of the preliminary simulations run with 1800 spherical particles of which 25% were 2 mm diameter, 25% were 3 mm diameter, 25% were 5 mm diameter and 25% were 6 mm diameter (as can be seen on the scale on the right of Figure 22). The screen box used in this particular simulation was a flat square aperture sieve and was stroking at 45° (vibrating linearly in this direction) and screening at a cut-size of 4 mm (aperture's smallest size).

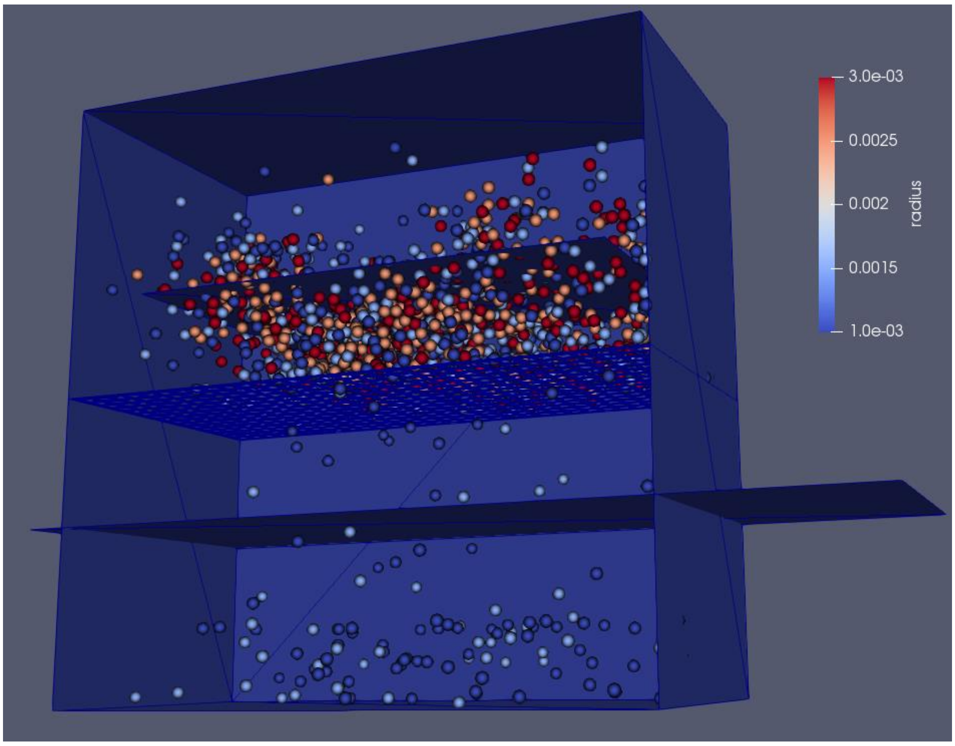

Figure 22: Results of Flat Mesh vibrating at 45° Stroke with 1800 Particles

The following figures (Figure 23 to Figure 26) show the efficiency results obtained, after eight complete strokes of the sieve box, during the preliminary simulations. They show the percentage of particles which passed through the counting plane after passing through the sieve. The counting plane only counted each particle once as they passed through the top of the counting plane. It should be noted that during this simulation particles were allowed to pass back through the sieve but these particles were still counted as a “passed particle”. Each of the sieve configurations (flat and extruded) and each of the aperture shapes (square, rectangular, circular and oval) were simulated with 200, 600 and 1800 particles and were vibrated at the different angles of stroke as previously mentioned. The points plotted in the figures are summarized in table form in Appendix E. The results of the best and the worst performing stroking angles for each sieve type and for the different number of inserted particles can be seen in Appendix F.

The blue line on the graph indicates the flat sieve configurations while the green line indicates the extruded sieve configurations. It is evident from the various graphs that the blue line generally illustrates a greater efficiency in the smaller stroking angles, between 0° and 45°, and that the green line, in some instances, illustrates greater efficiencies in the higher stroking angles, between 45° and 90°.

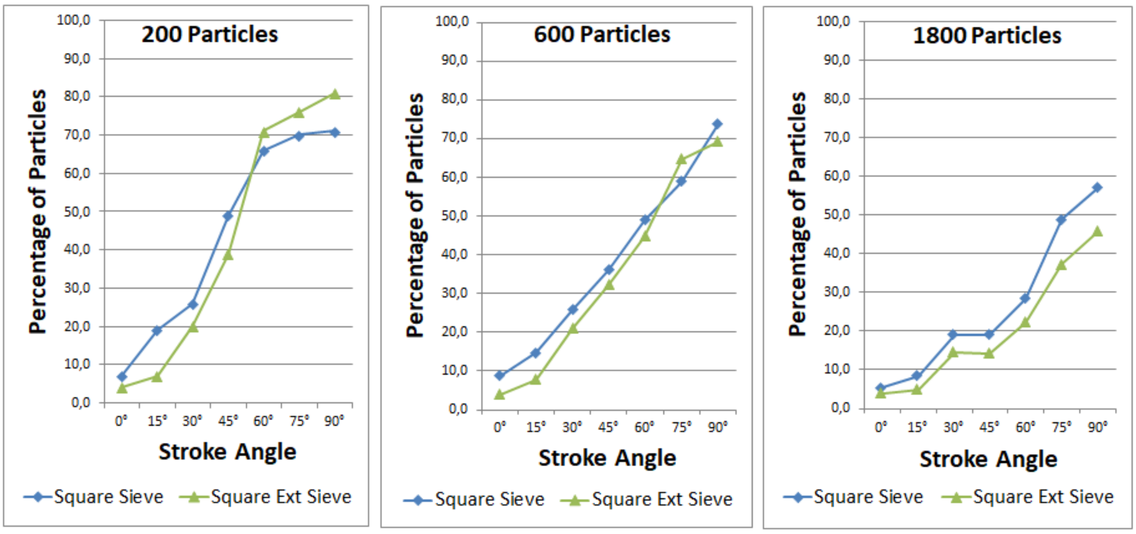

Figure 23: Efficiency results for square sieve configurations, for different number of particles

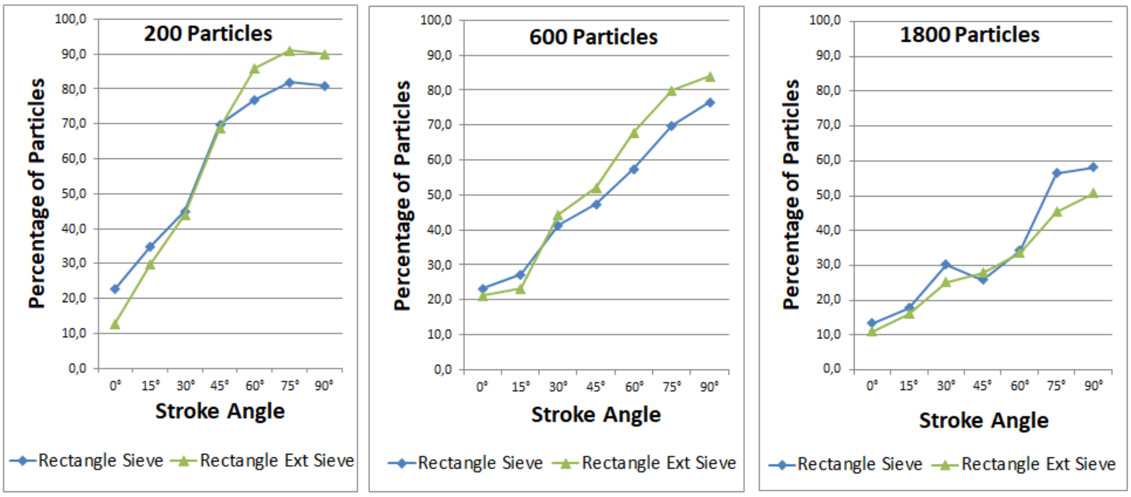

Figure 24: Efficiency results for rectangular sieve configurations, for different number of particles

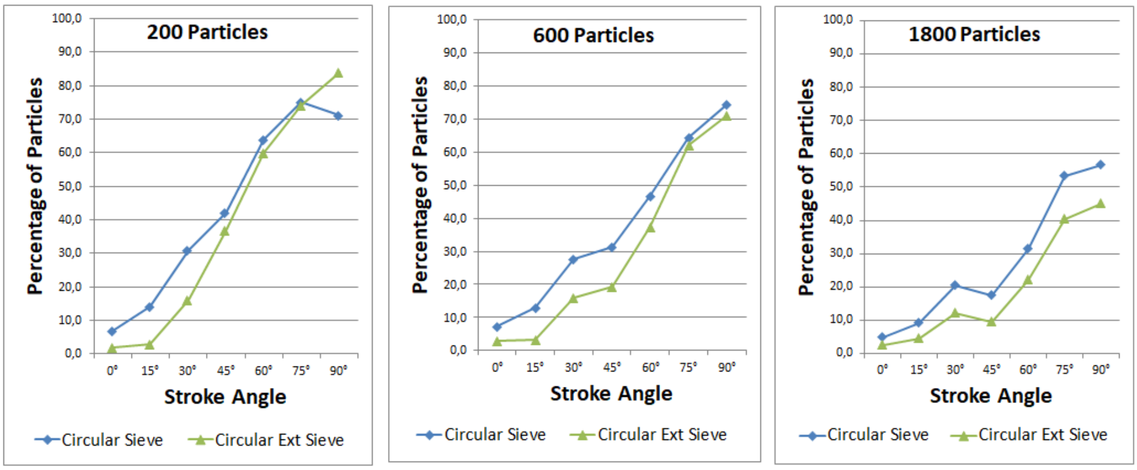

Figure 25: Efficiency results for circular sieve configurations, for different number of particles

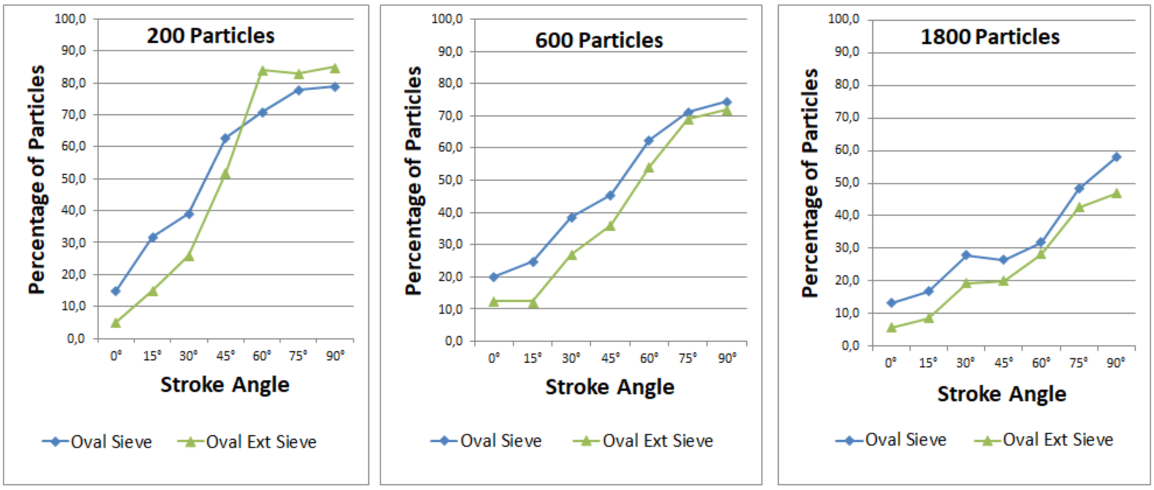

Figure 26: Efficiency results for oval sieve configurations, for different number of particles

2.3 *Physical Experiment*

2.3.1 Vertical tube experiment

The concept behind the experimental programme was to study the interaction between particles and sieves with different shaped apertures, without the effects of gravity. This should imitate a single impact scenario which allows the particles one opportunity to pass through the sieve. This is one concept which could be used in a zero gravity environment as it was observed in the preliminary simulation that the first stroke of the sieve box separated more particles than any of the other strokes. The concept was to drop particles down a long vertical tube (into a box), allow the particle to bounce off a 45° deflector plate and move horizontally towards a sieve plate mounted vertically (see Figure 27 for concept illustration as well as dimensions of the physical experimental setup).

One of three scenarios would play out when the particles interacted with the sieve plates:

1. The particle would pass through the shaped apertures (the probability for this scenario can be quantified (see Section 2.3.5)).
2. The particles would deflect off the side of a shaped aperture and pass through.
3. The particles would collide with a portion of steel between two open aperture shapes and not pass through the sieve.

The particles which managed to pass through the shaped apertures would be collected and counted and would be considered the successful particles, and would provide a percentage of success rates for each drop of particles.

To determine the length of the tube, an initial simulation was performed with the default LIGGGHTS parameters (used in the preliminary simulation) to view the smallest height at which particles could be dropped to bounce off a deflector plate and allow the particles to continue on the same path with minimal influence of gravity on the particle trajectories.. The resulting drop height was approximately 2.2 m with a 45° angled deflector plate. The design drawing of the deflector plate box can be found in Appendix A

Figure 28 shows the apparatus of physical experiment while Figure 29 shows a close-up of the physical experiment with the vertical pipe in the testing position. The vertical tube is positioned closer to the sieve plate (130 mm from the centre of the tube) in the latter figure to ensure the particles would deflect towards the sieve plate from point-blank range.
The following procedure will be used for the vertical tube test:

1. The deflector plate is positioned inside the wooden box in line with the vertical tube
2. A single sieving plate (square aperture sieving plate) is installed on the open face of the wooden box
3. The particle type (e.g. yellow pellets) is dropped from the top of the vertical tube with no initial velocity and in quick succession. Each pellet type is dropped in quantities of 50 particles while the quantity of iron ore particles will be increased to 200 (to increase the accuracy of these results)
4. The particles which pass through the sieve will then be counted and the total amount of particles left in the box will be counted to ensure no particles have been lost during the process
5. Steps 1 – 4 are then repeated for the all four particle types and for all four sieve types.

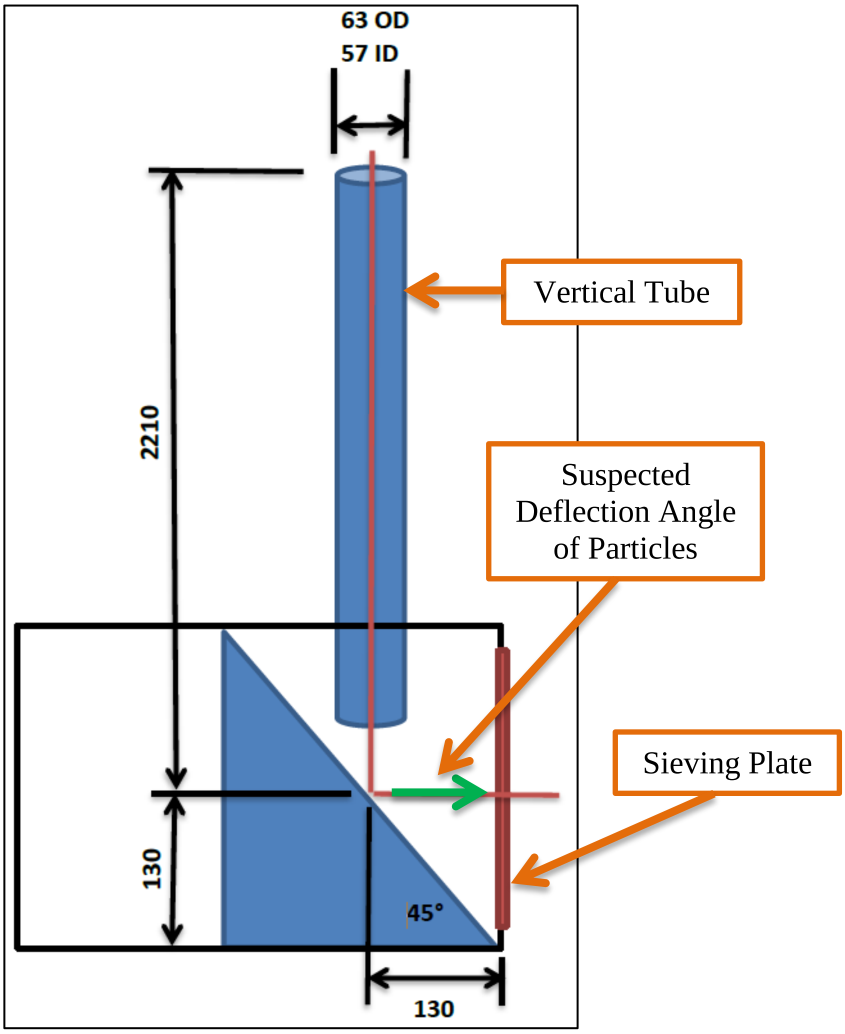

Figure 27: Concept of physical experimental setup.

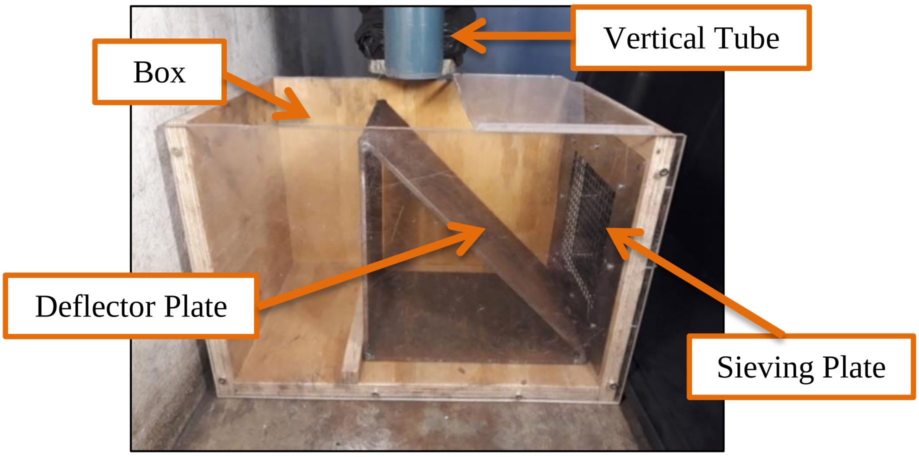

Figure 28: Physical experimental setup with mild steel deflector plate.

Figure 29: Close-up of physical experimental setup with mild steel deflector plate.

2.3.2 Sieves used in the experiment

The flat sieve geometries performed the best overall in the preliminary simulations therefore it was decided that all the aperture shapes of the flat sieves would be tested in the experimental stage. This would allow a complete comparison to be done between the physical experiment and the experimental LIGGGHTS simulation. Due to the complexity of the manufacturing process of the extruded sieves these were not manufactured and were only assessed in the simulation phase. Detailed drawings of the flat sieves with their respective sieve aperture shapes may be seen in Appendix B.

Table 5 below shows the open area (in square metres and as a percentage) of the various sieve shapes. The different aperture areas were not likely to significantly affect the probabilities of particles passing through in a single impact, so the measured results would be retained without any weighting.

Table 5: Open area of various shaped sieves used in the experiment.

	Open Area (m^2)	**Open Area (%)**
Square	0.01440	50.00
Rectangular	0.01498	52.00
Circular	0.01453	50.44
Oval	0.01478	51.31

2.3.3 Stacking densities of the sieves

The square and the rectangular sieves may be stacked more efficiently due to their straight perpendicular sides. The circular apertures were stacked horizontally and diagonally to utilize the space on the sieve surface. The oval sieve apertures, however, were stacked horizontally and vertically. This resulted in areas in the impact zone where no screening apertures were as shown in Figure 30. Although the sieves' open areas were designed to be similar, the impact area of the deflected particles was expected to be in the middle of the sieves and therefore the more densely packed sieve apertures were expected to produce results with higher efficiencies.

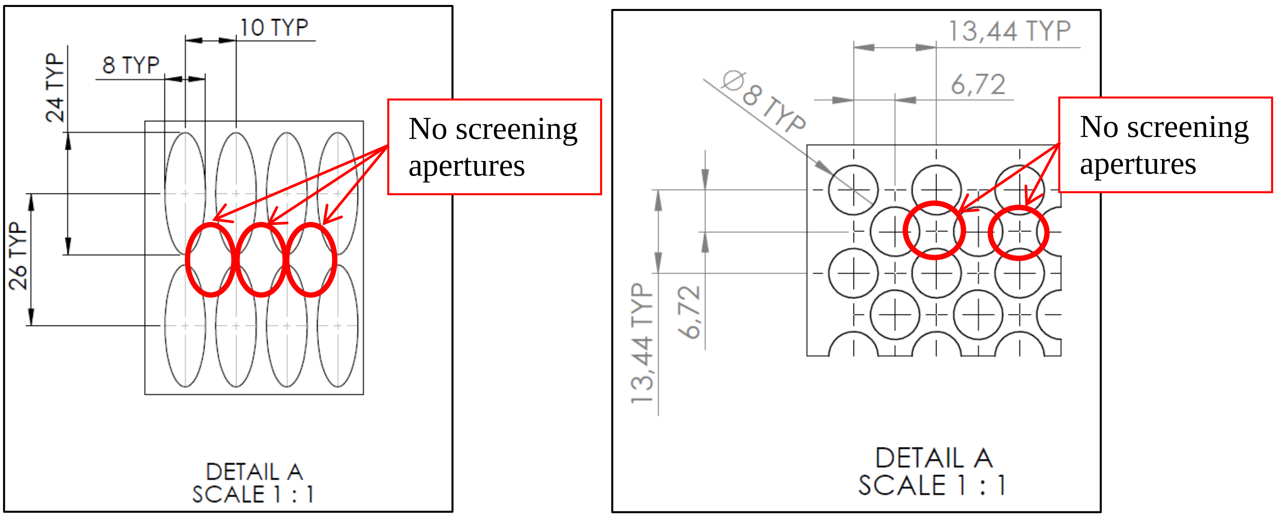

Figure 30: Detail A of the oval (Left) and circular (Right) sieves showing areas with no screening apertures.

2.3.4 Particles used in the experiment

The particles used in the experiment consist of white and yellow plastic pellets as well as the steel pellets. These pellets are spherical in nature with a diameter of 6 mm (see Figure 31). The densities of these spheres were calculated and are mentioned in the parameters of the LIGGGHTS simulations.

Iron ore particles will also be used in the experiment and the sizes will be greater than 4 mm but smaller than 8 mm. Figure 32 shows the 200 particles selected for the experiment while Figure 33 shows the particles on 1 x 1 mm scaled paper to gauge the sizes used. It should be noted that upon visual inspection the iron ore particles are of a slab nature with the aspect ratio of the particles ranging between 1.5 to 2. The particles will be selected to be smaller than the sieve aperture size so that there will be no large particles obstructing smaller particles from passing through the apertures. It should be noted also that this particle shape differs slightly from the cubic shape previously mentioned which could be expected to be produced by a VSI or HSI crusher. This is expected not to play an important role as the particles would be deflected towards the sieves at point-blank range. The DEM simulation of the physical experiment will use multi-bodies which would compare to the slab-shaped particles being experimented with.

Figure 31: Yellow pellets (left), white pellets (centre) and steel pellets (right)

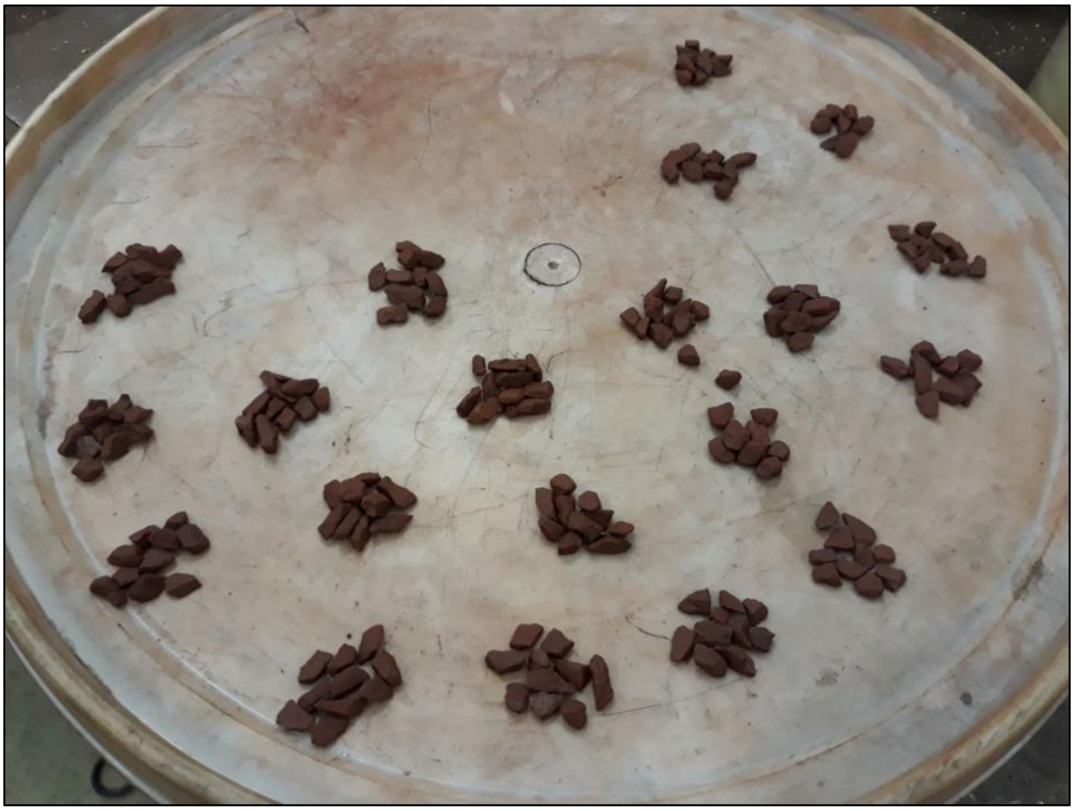

Figure 32: Particles used in the experiment.

Figure 33: Particle sizes and shapes seen on millimetre-scaled paper.

2.3.5 Probability of particles passing through the sieves

The physical experiment illustrates the principle of one-time sieving whereby each individual particle is only provided a single opportunity to pass through the various sieve shapes. As mentioned in the literature review the equations which govern the probability of a single particle passing through an aperture are given in Equations 2 to 5. These equations account for oblique impacts on the edges of the apertures with an angle θ correction, as shown earlier.

The particles' size of which 50% will pass through the sieve is 6 mm for all cases. This is due to all the particles being smaller than the sieve aperture. A value of 45° will be used for θ as this is the maximum angle that will still allow particles to deflect into the aperture openings. Using the square aperture size of 8 mm and the wire diameter (or distance between apertures) of 2 mm the probability of particles passing through all four types of sieves then yields:

Square:

$$\boldsymbol{p_{square}} = \left[\frac{(\mathbf{8} - \mathbf{6}\cos(\mathbf{45°}))}{(\mathbf{8}+\mathbf{2})}\right]^{\mathbf{2}}$$

$$\boldsymbol{p_{square}} = \mathbf{0.141}$$

$$\boldsymbol{p_{square}} = \mathbf{14.1}\%$$

Rectangle:

$$\boldsymbol{p_{rectangle}} = \left[\frac{(\mathbf{8} - \mathbf{6}\cos(\mathbf{45°}))\big((\mathbf{3})(\mathbf{8}) - \mathbf{6}\cos(\mathbf{45°})\big)}{(\mathbf{8}+\mathbf{2})\big((\mathbf{3})(\mathbf{8})+\mathbf{2}\big)}\right]$$

$$\boldsymbol{p_{rectangle}} = \mathbf{0.286}$$

$$\boldsymbol{p_{rectangle}} = \mathbf{28.6}\%$$

Circle:

$$p_{circle} = \frac{\pi}{4}\left[\frac{(\mathbf{8} - \mathbf{6}\cos(\mathbf{45°}))}{(\mathbf{8}+\mathbf{2})}\right]^2$$

$$\boldsymbol{p_{circle}} = \mathbf{0.111}$$

$$\boldsymbol{p_{circle}} = \mathbf{11.1}\%$$

Oval:

$$p_{oval} = \frac{\pi}{4}\left[\frac{(\mathbf{8} - \mathbf{6}\cos(\mathbf{45°}))\big((\mathbf{3})(\mathbf{8}) - \mathbf{6}\cos(\mathbf{45°})\big)}{(\mathbf{8}+\mathbf{2})\big((\mathbf{3})(\mathbf{8})+\mathbf{2}\big)}\right]$$

$$\boldsymbol{p_{oval}} = \mathbf{0.224}$$

$$\boldsymbol{p_{oval}} = \mathbf{22.4}\%$$

These values will be compared to the values obtained in the physical experiment and will be discussed in Section 4.3.

2.4 DEM Simulation of the Physical Experiment

This section explains how the parameters required for the LIGGGHTS DEM simulation are determined. It is also reasonable to include the results of the experiments here since they pertain to the DEM simulations.

2.4.1 LIGGGHTS simulation setup of physical experiment

A LIGGGHTS simulation of the physical experiment will be performed to compare the results obtained in the simulation versus the results obtained in the physical experiment. In order to replicate the real-life scenario it is important to calibrate the DEM LIGGGHTS parameters. As previously stated in Chapter 1 the parameters will be measured, calculated or determined experimentally, or they would be acquired from literature. The cohesion energy density is omitted from the simulation as only dry material is considered.

The following parameters will be measured, calculated or determined experimentally:

1. Coefficient of restitution – measured
2. Particle shape – visually inspected (refer to Figure 33)
3. Coefficient of static friction – determined experimentally
4. Particle size – measured
5. Particle density (plastic and steel spheres)
6. Time step – calculated using the critical Rayleigh time step, Equation 10.

The following parameters will be acquired from literature:

1. Particle density (iron ore particles)
2. Young’s Modulus (E)
3. Poisson’s ratio
4. Coefficient of rolling friction (for spherical particles)

2.4.1.1 *Coefficient of restitution*

The coefficient of restitution between the 8 mm VRN500 steel plate and all the pellets, as well as between the VRN500 steel plate and the iron ore particles, will be determined by using the following procedure (see Figure 34 for the test setup):.

- The particles are individually dropped from a height between 12 mm – 20 mm.
- They will bounce off the steel plate to a maximum height, which is recorded with a video camera against a millimetre scale background.
- This procedure is repeated 50 times for each particle type.
- Every time the particle is dropped the drop height and the maximum height to which the particle bounced is recorded by analyzing the video footage. Equation 8 is used to calculate the coefficient of restitution.

The results of the experiment showed that the coefficient of restitution of the iron ore particle on the 8 mm VRN500 steel plate was 0.56 while the coefficient of restitution of the yellow, white and steel pellets on the 8 mm VRN500 steel plate were 0.9, 0.74 and 0.67 respectively (see Table 6 below). The iron ore particle to particle coefficient of restitution is also shown in Table 6. The coefficient of restitution of the particles on the sieve plate was not considered because the one-time sieving technique is being tested here.

Table 6: Measured coefficient of restitution values

Parameter	**Iron Ore Particle to Particle COR**[1]	**Yellow Pellets to 8 mm VRN500 Steel Plate COR**	**White Pellets to 8 mm VRN500 Steel Plate COR**	**Steel Pellets to 8 mm VRN500 Steel Plate COR**	**Iron-ore to 8 mm VRN500 Steel Plate COR**
Minimum	0.46	0.83	0.66	0.58	0.38
Maximum	0.74	0.96	0.84	0.77	0.68
Average	0.61	0.9	0.74	0.67	0.56
Standard Deviation	0.08	0.03	0.05	0.05	0.05

Since the standard deviations are fairly small, the average coefficient of restitution values will be used in the DEM simulations.

[1] The numerical figures of the column titled "Particle to Particle Coefficient of Restitution" are sourced from Guya (2018) in the section titled 4.1.1 Coefficient of restitution test results.

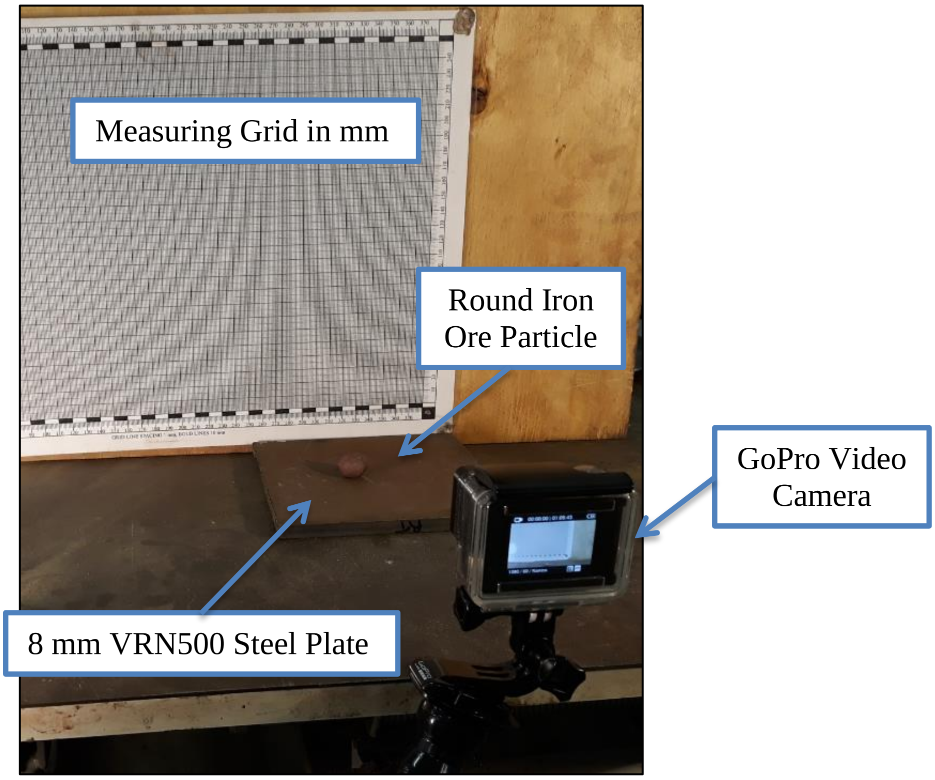

Figure 34: COR testing setup for 8 mm VRN500 steel plate and iron ore particle.

2.4.1.2 Coefficient of static friction

The coefficient of static friction is measured by using an inclined plane. The device consists of a steel pan which is hinged at a point with a protractor measuring the angle of the pan (see Figure 35). The spherical pellet types were rigidly glued to separate rigid bodies to ensure that they did not roll or move when an external force was applied to them. Each particle type was then positioned on the steel pan while it was lifted slowly (see Figure 36). Once the particle began to move the angled plane was locked into place so that the angle can be read off the protractor.

It was anticipated that the size of the iron ore particle being tested would not have an effect on the outcome of the coefficient therefore only the small iron ore particles were tested (particles 1 - 5 in Figure 37). Four combinations were tested, as follows:

1. Coefficient of static friction between VRN500 and yellow plastic pellets
2. Coefficient of static friction between VRN500 and white plastic pellets
3. Coefficient of static friction between VRN500 and steel pellets
4. Coefficient of static friction between VRN500 and small iron ore particles (-14 mm)

The test was performed by using the side of each iron ore particle which had the largest surface area facing down against the steel plate. The reason was so that the centre of gravity would be lower and during the inclination process the particles would resist rolling down the incline.

The angles of the inclined plane were measured for each of the four particle types and were used in Equation 9 to produce the corresponding coefficients of static friction. These results are presented in Table 7.

These coefficients are based on the comparison of the four experiments mentioned above. The steel to be used in space would be VRN500 and the particle size to be used in the experiment would be small iron ore particles (-14 mm).

Figure 35: Starting position of the inclined plane before the experiment has started.

Figure 36: Position of the particle while plane is being inclined (current angle of 21°).

Table 7: Coefficients of static friction between VRN500 steel plate and different particles

	Yellow Pellets to VRN500 Steel Plate	**White Pellets to VRN500 Steel Plate**	**Steel Pellets to VRN500 Steel Plate**	**Small Iron-ore Particles to VRN500 Steel Plate**
Minimum	0.38	0.40	0.42	0.51
Maximum	0.47	0.47	0.51	1.00
Average	0.43	0.42	0.46	0.71
Standard Deviation	0.04	0.03	0.05	0.12

As mentioned above the coefficient of static friction for small iron ore particles were tested. Figure 37 below illustrates the small iron ore particles (-14 mm) shown on millimetre scaled paper.

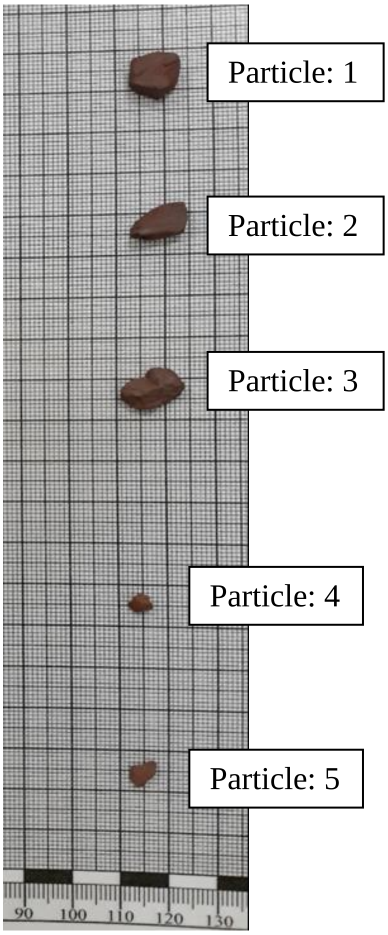

Figure 37: Scale of small iron ore particles on millimetre scale

2.4.1.3 Particle size

The simulations of the physical experiments of the controlled case (with the spherical pellets) will be simulated using single spheres with diameters of 6 mm. The particles will be selected to ensure that they are constant and would pass through the sieve apertures. This would allow the results to be compared to the theoretical calculated results as well.

All the iron ore particles used in the simulation of the physical experiment will be -6 mm on the longest 2 sides. The particles in the DEM simulation will be made up to be multi-spherical bodies to improve the accuracy of the simulation versus the physical experiment. They will be purposefully chosen to be undersize as this will give results of the passing success rate with no oversize particles blocking the shaped apertures. This will provide each particle an equal opportunity to pass through the sieve apertures.

Similar to the physical experiment the simulation of the physical experiment will only allow the particles to have one chance to pass through the sieve for the single impact experiment being simulated here.

2.4.1.4 Particle densities

The following Table 8 represents the values of particle densities calculated for each of the pellets and iron ore particles used in the physical experiment.

Table 8: Particle densities calculated for the plastic and steel pellets

Type of Particle	Diameter (m)	Mass (kg)	Density (kg/m³)
Yellow Plastic Pellet	6,00E-03	1,15E-04	1016,82
White Plastic Pellet	6,00E-03	2,50E-04	2210,49
Steel Airsoft Pellet	6,00E-03	3,60E-04	3183,10

The iron ore was given the particle density will be specified as 3280 kg/m³ (T Frangakis 2020, personal communication, 14 February).

2.4.1.5 Time Step

Equation 10 will be used to determine the Rayleigh time step for the simulation of the physical experiment. A particle shear modulus of 2 MPa will be used to ensure a reasonable simulation time, of approximately 10 minutes, while maintaining a good level of accuracy of the results.

For the iron ore, with d_P (smallest particle diameter in any of the clumped particles - 0.56 mm diameter) = 0.56 mm

ρ_P (Particle Density) = 3280 kg/m³

G_P (Particle Shear Modulus) = 2 MPa

γ_P (Particle Poisson's Ratio) = 0.283 (Li et al., 2017)

The equation then yields:

$$T_R = \frac{\pi \ (0.56\times10^{-3})\sqrt{\frac{3280}{2\times10^{6}}}}{2\,(0.1631 \times 0{,}283 + 0.8766)}$$

$$T_R = \ 3.9 \times 10^{-5}\ s$$

Table 9 below represents the time step calculations for each of the particles, using the appropriate particle diameters, Poisson's ratios and densities.

Table 9: Timesteps calculated for each particle type

	Timestep (s)
Yellow pellets	2.3×10^{-4}
White pellets	3.4×10^{-4}
Steel pellets	4.1×10^{-4}
Iron ore particles	3.9×10^{-5}

The timestep parameter will be chosen to be the worst case which is the iron ore particle case which has a value of 3.9×10^{-5} s. However, to be conservative this will be reduced further by a factor of 2 for better accuracy of the solution. Therefore the value used for all the simulations will be:

$$\mathbf{1.95 \times 10^{-5}\ s}$$

2.4.1.6 Coefficients of restitution and static friction matrix

The DEM simulations are expected to be sensitive to the coefficient of restitution as well as static friction. It is customary in DEM simulations to explore a range of values for these parameters in order to assess which combination thereof yields the most accurate results when compared with a physical experiment. Since this application is of sieving particles in zero gravity the vertical tube experiment described in Section 2.3.1 will be used to calibrate these parameters, even though they could be measured experimentally as previously described. In this case the coefficients of restitution and static friction were each varied between 0.1 and 0.9 during simulations of the plastic and steel spheres, and iron ore particles. The number of particles passing through the sieve in the vertical tube experiment will be compared with that of the DEM simulation with these parameters varied in order to determine the combination of restitution and static friction coefficients which give the most accurate results.

Appendix D shows the tabulated results of the physical experiment and all the combinations of the DEM simulations with the most accurate combinations of parameters highlighted. Table 10 below shows a summary of the results while Section 4.5 contains the discussion of the results.

Table 10: Best calculated combinations of the coefficients of restitution and static friction.

	Yellow pellets	White pellets	Steel pellets	Iron ore particles
Coefficient of Restitution	0.7	0.6	0.6	0.2
Coefficient of Static Friction	0.1	0.6	0.3	0.7
Maximum Deviation %	16.1	18.9	16.1	16.7

The results in Table 10 show that the coefficients of restitution are consistently high for the spherical pellets while the unsymmetrical iron ore particles are low. This may suggest that the shape of the particle affects the coefficient of restitution. The static friction coefficients do not display any particular pattern that could be commented on. The simulations were extremely sensitive to both parameters with a 0.1 change in either parameter sometimes meant a 10% change in efficiency.

2.4.1.7 Summary of LIGGGHTS Parameters

Table 11 below summarises the values which were physically tested through experimentation and used in the initial simulation of the physical experiment.

Table 11: Values of LIGGGHTS parameters used in the physical experiment

	Yellow Pellets	**White Pellets**	**Steel pellets**	**Iron-ore Particles**
LIGGGHTS Parameter	**Value (Units of measurement)**			
1. Coefficient of restitution*	0.9→0.7	0.74→0.6	0.67→0.6	0.56→0.2
2. Particle shape (discussed in 2.4.2)	Single sphere			Multi-bodies
3. Particle density (ρ) (kg/m³)	1017	2211	3183	3280
4. Young's modulus (E) (Pa)	$5\text{x}10^{6}$			
5. Cohesion energy density	No cohesion			
6. Coefficient of static friction*	0.43→0.1	0.42→0.6	0.46→0.3	0.71→0.7
7. Poisson's ratio (υ)	0.3**			0.283
8. Particle size (mm)	6			-6
9. Time step (s)	$1.95 \text{ x } 10^{-5}$			
10. Gravity (m/s²)	9.81			

*The coefficients of restitution and coefficients of static friction are shown first as their initial experimented value and then as their best-combination value. The best-combination value will be used in further simulations.

**Estimated based on the value of the iron ore's Poisson's ratio. As mentioned previously this value does not significantly affect the behavior of bulk material flow in DEM simulations.

2.4.2 Iron ore particles used in the LIGGGHTS simulation of the physical experiment

The particles used in the LIGGGHTS simulation of the physical experiment were made up of spherical multi-bodies. Three particles below in Figure 38 to Figure **43** illustrate how the particles have been modeled with different sizes of spheres to replicate the shape of the 3 actual particles. Each of the three particles were scaled by multiplying the particles by the following scales: 1.0, 1.25, 1.5 and 2.0. The factor-multiplied particles resulted in 12 different particles which were used in the DEM simulation of the physical experiment.

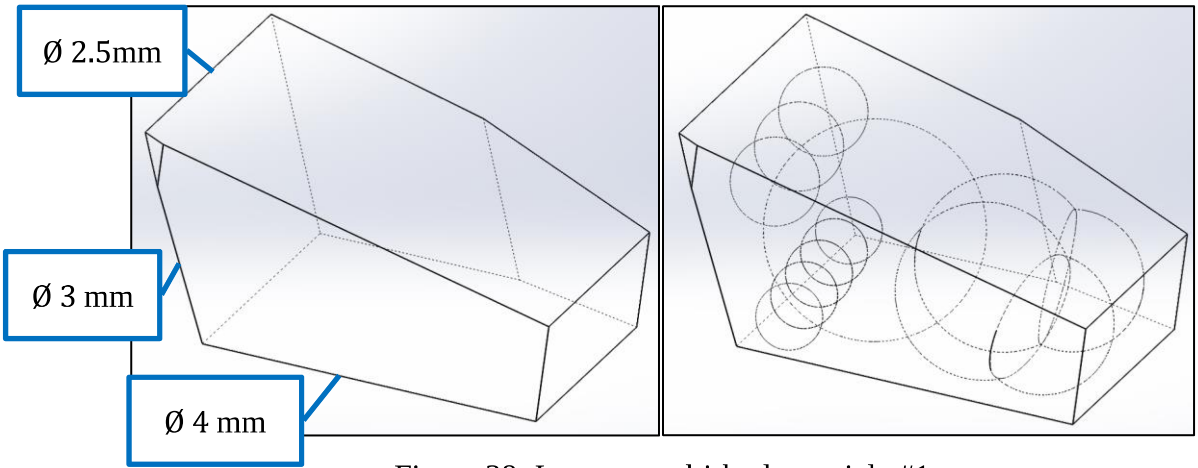

Figure 38: Iron ore multi-body particle #1

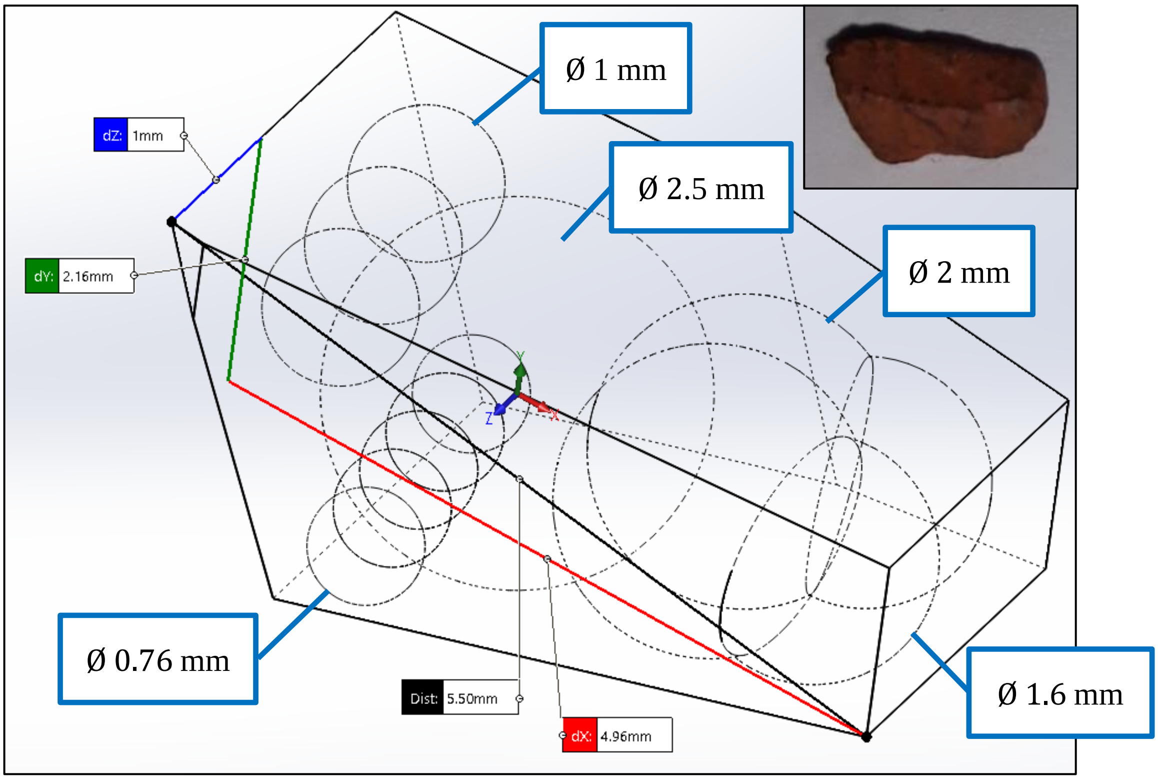

Figure 39: Iron ore multi-body particle #1 with reference dimensions

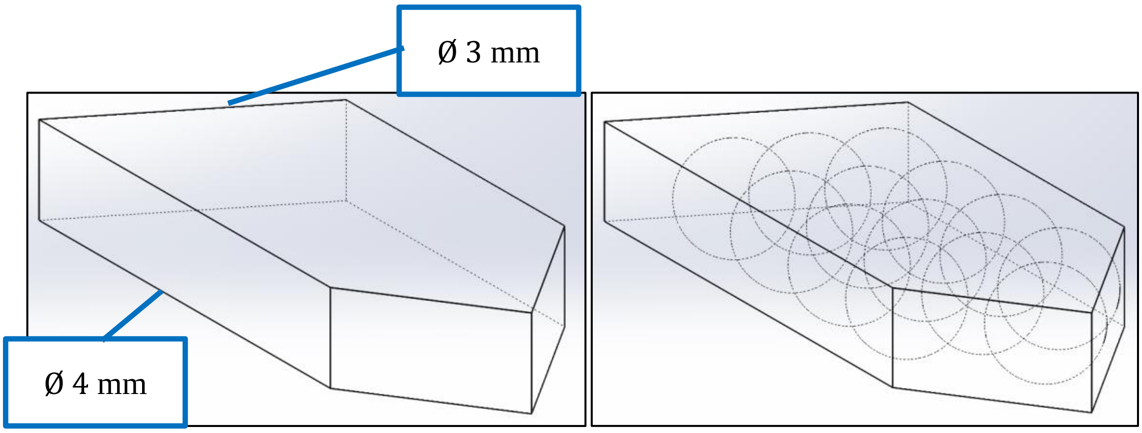

Figure 40: Iron ore multi-body particle #2

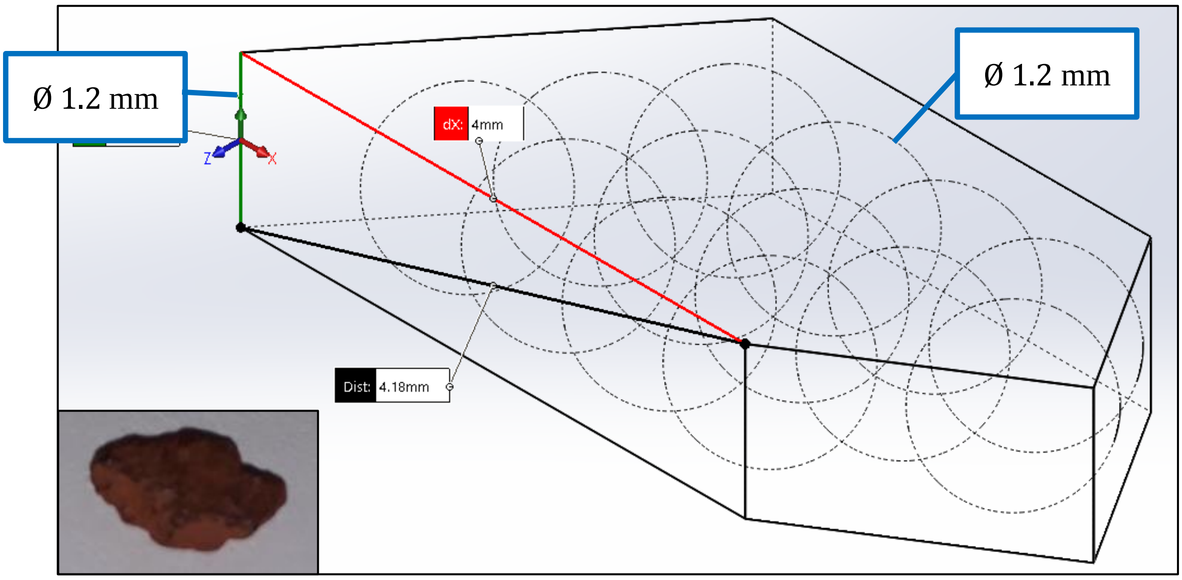

Figure 41: Iron ore multi-body particle #2 with reference dimensions

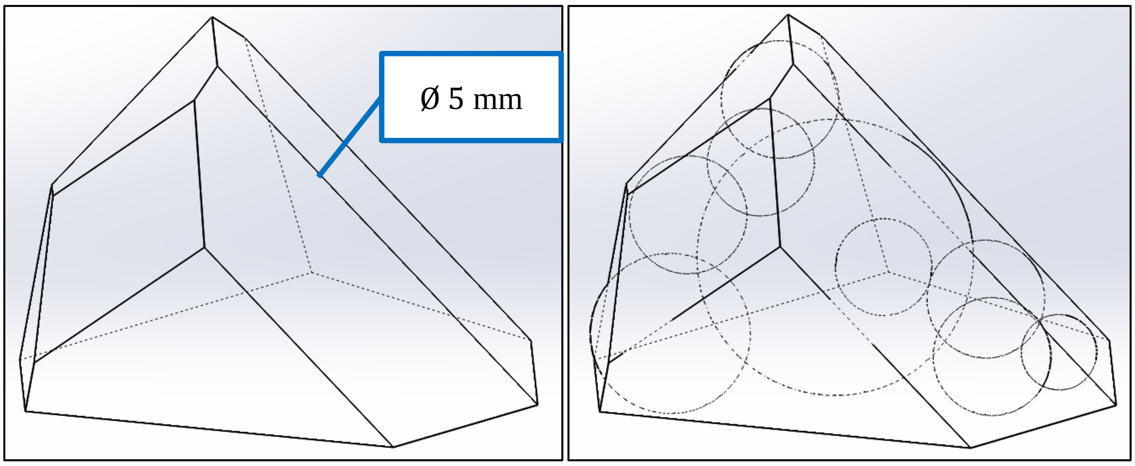

Figure 42: Iron ore multi-body particle #3

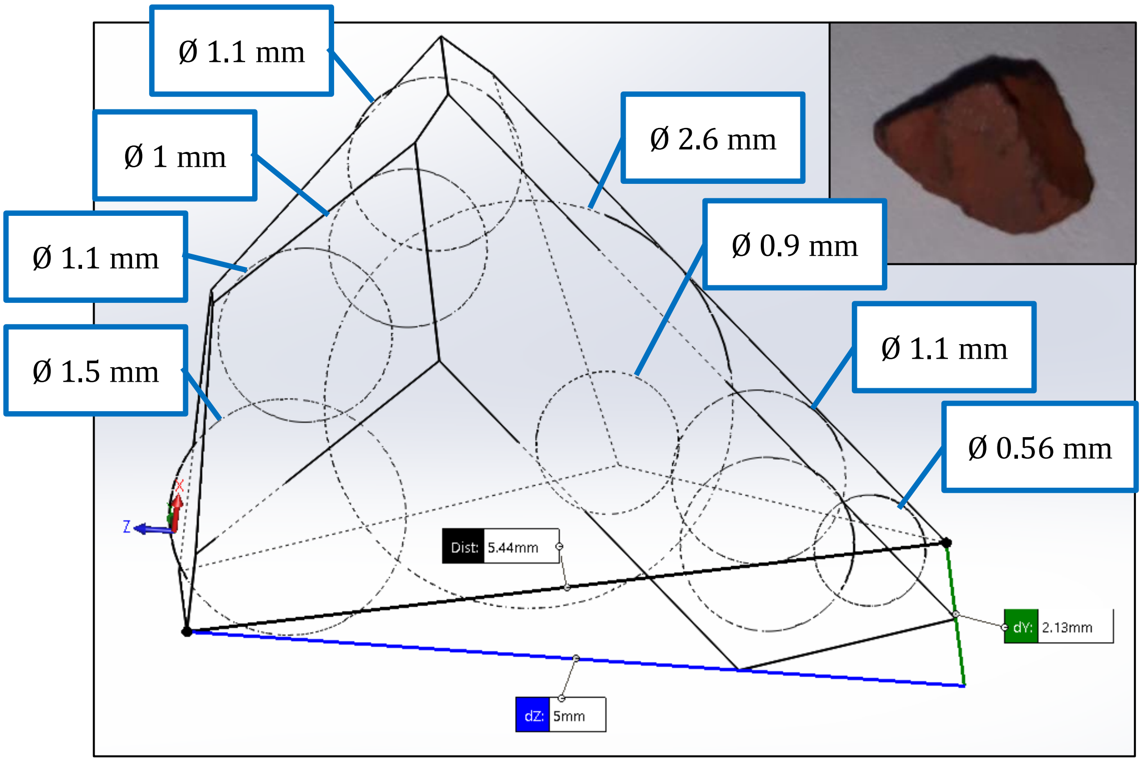

Figure 43: Iron ore multi-body particle #3 with reference dimensions

2.4.3 Other LIGGGHTS simulation details

The follow additional simulation details were used in conjunction with the parameters provided in Table 11 in order to run the simulation of the vertical tube test:

- Contact model used – Hertzian without cohesion
- Runtime – 0.39 s (real simulated time), 10 minutes (computation time)
- Number of simulations – 16 in total (4 particle types and 4 sieve geometries)
- Geometry – The geometry modeled for the simulation of the vertical tube experiment are referenced as follows:
  - Figure 27: Concept of physical experimental setup.
  - Appendix A – Design of Experiment Rig
  - Appendix B – Experiment Sieves

2.5 Final LIGGGHTS DEM Simulation – Zero-g Case

2.5.1 Space mine concept

Screw conveyors, crushing stations and screening chambers will all form part of the space mining process. Figure 44 shows a concept of a 3-dimensional layout of a space mining process that could potentially be used. Due to the lack of gravity in space the current Earth-bound screen designs would not work and therefore the technique of the tested one-time sieving is proposed as the preferred form of screening to be used in zero gravity environments. The concept of the one-time passing process is backed-up by the preliminary simulation results whereby more than 30% of the particles (on average) were screened in the first particle-sieve interaction than during any of the other seven strokes of the sieve box. This solution not only transports the oversize or unscreened particles to a crushing station for further down-sizing but it also transports the screened particles into a tunnel which enters the screw conveyor and is then pushed outwards due to centrifugal forces into a separate tunnel.

The blue arrows represent the oversize and unscreened particles and the orange arrows represent the screened particles. The use of a hydraulically actuated flapper gate at the top of the screen chamber divides the material into either a crushing station or the screw conveyor and which is further guided into a separate undersize particle tunnel. The desired mine process will indicate whether the undersize material would need to be re-circulated for further processing. Depending on the desired sizes of the particles, the oversize particles or the unscreened undersize particles would be fed back into the screening process or would be transported to the crushing station to be crushed further.

The screw conveyor is one of the only machines that could transport particles from one place to another in a zero gravity environment as it does not rely on gravity to transport particles. It works by producing linear particle movement from a screw-type rotary motion. It will also reduce the speed of the particles which were impacted by the sieving plates and feed them in a controlled manner into the side of the next sieving chamber.

The screening concept is to screen particles in the screening chamber by guiding sieve plates in these "tubes" which would hit an inserted stream of particles (see Figure 44). The particles are inserted from the side of the sieve chamber at a relatively low velocity so that the high velocity sieve (moving perpendicularly to the inserted particles) would hit larger particles and allow smaller particles to pass through. This action represents the one-time passing process which was tested in Sections 2.2.5 and 2.4.

The sieving mechanism would most likely work on a belt or chain drive system and would be positioned above each screening chamber (this is not shown). Every second plate on the drive system would be a sieving plate and every other plate would be a blank plate. The first sieving plate would perform the sieving function, which will be tested in the simulation of the space case, and would guide the oversize and unscreened particles to the right of the flapper gate into one of the crushing stations. Once they have been crushed they would be transported into the end portion of the screw conveyor and fed into the next screening chamber at a controlled rate. The second blank plate would guide the screened particles to the left of the flapper gate into the screw conveyor section where they will be given a centrifugal force which would push them into the undersize tunnel and escorted to a different location where they would be needed. Once both the sieve plate and the blank plate have performed their function they would be transported back, via the belt or chain drive system, to the beginning of the same screening chamber to perform the process again.

When the particles have made a full rotation through the space mining process they will have undergone 4 one-time screening opportunities.

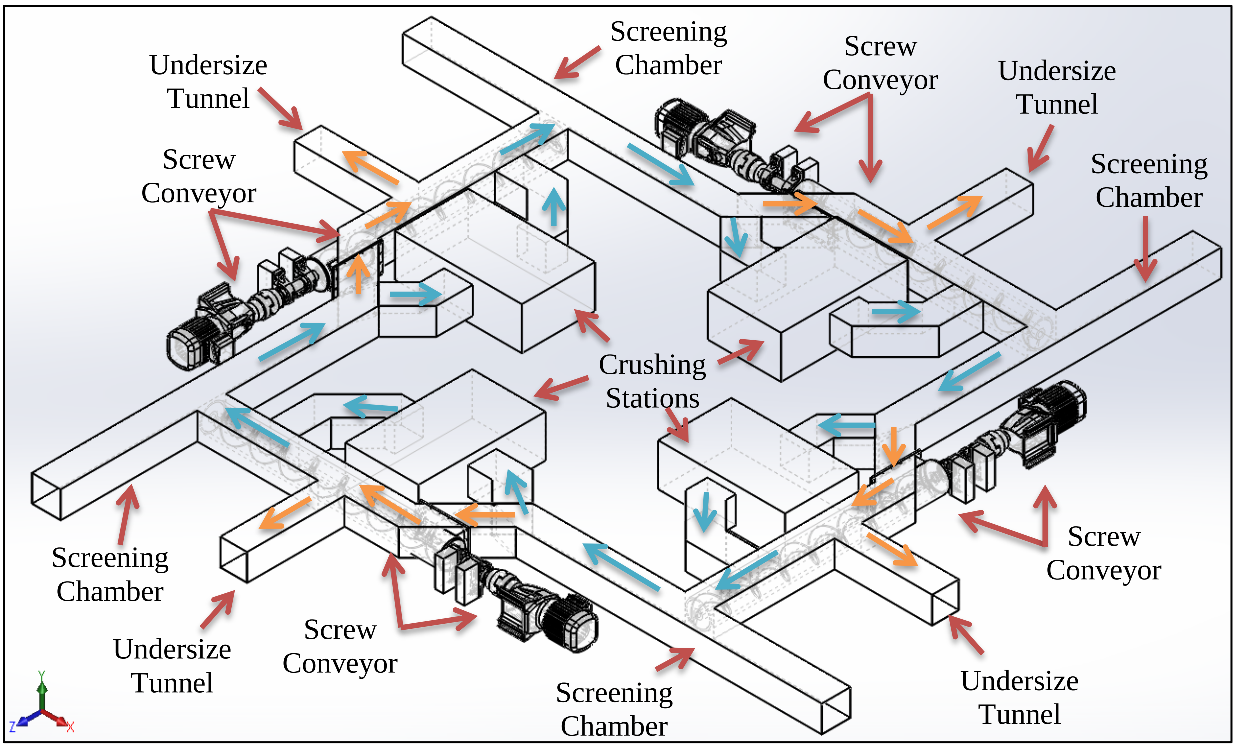

Figure 44: 3-Dimensional schematic of a potential space mining plant.

2.5.2 LIGGGHTS simulation setup – zero-g case

The final simulation would simulate how particles could be screened in the actual space scenario. As mentioned before a typical space mine would consist of asteroids being broken up, crushed and screened to obtain the particle sizes which could be used in 3D steel printers. Therefore the simulation only represents the screening process of the space mine concept.

The sieve chamber is designed as a 200 x 200 mm square tube with a side entry for the insertion of the stream of screenable particles (see Figure 45). The curved compartment at the end of the sieve chamber geometry is modeled in such a way as to trap the oversize particles so that they do not flow back into the screening area for counting purposes. As mentioned before the space application would not have this compartment but would allow the oversize particles to be guided to a crushing station for further downsizing.

All the sieves in their respective simulations are set to move at a velocity of 1.0 m/s in the x-direction as this ensured that at the time of sieve-on-particle impact the particles were spread out over the entire surface of the sieve. The concept of the sieve is completed when the "sweeping" solid flat plate component follows the sieve plate and pushes all the undersize particles (which are now separated from the oversize particles) into an undersize compartment or "stockpile" (this portion of the concept has been omitted from the simulation).

One limiting factor with this concept will be that the number of particles being screened will need to be kept as low as possible to optimize the efficiency but still promote throughput to conserve the amount of energy introduced into the system. The disadvantage of screening many particles at the same time in a zero gravity environment was observed in the results of the preliminary simulation where the sieve boxes performed more efficiently when only 200 particles were being screened compared to the case where 600 and 1800 particles were being screened. Therefore only 100 particles were inserted into each of the simulations.

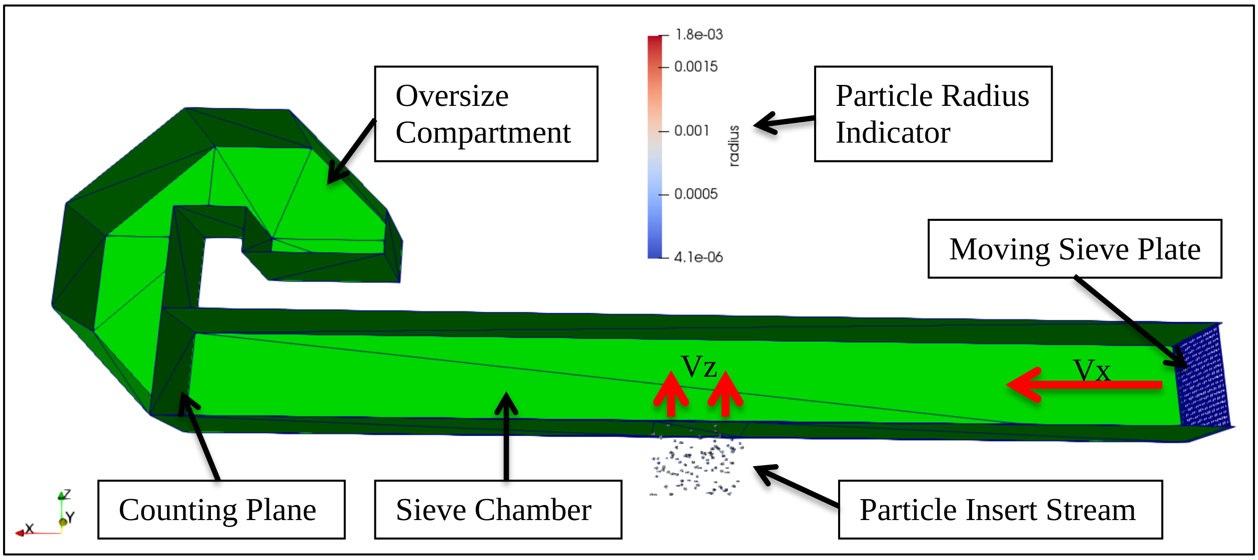

Figure 45: LIGGGHTS DEM simulation setup

The DEM parameters, which were previously calibrated, were used for the simulation of the zero-g space case (see Table 11). The particles are all inserted randomly across the insertion plane from the side of the sieve chamber at a velocity of 0.15 m/s in the z-direction while the moving sieve plate approached the particles at 1 m/s (in the x-direction).

2.5.3 Sieves used in the final zero-g space case simulation

As previously mentioned the flat sieve geometries performed the best with the least amount of issues and therefore they were used for the final zero-g space case simulation. Aside from the difference in screening performance with regards to efficiency, the extruded sieve geometries also showed cases of pegging which blocked apertures from screening particles further (as discussed in the preliminary results).

Due to the flat sieve configurations being used the results obtained in the final zero-g space case simulation could be compared to the physical experiment as well as the LIGGGHTS simulation of the physical experiment.

Table 12 below shows the open area as well as the percentage open area of the four sieve geometries. The manufacturing drawings of the four sieve geometries which were used in the simulations can be found in Appendix C – DEM Space Case Sieves

Table 12: Open area and percentages of the four shaped sieve geometries used in the final simulation.

	Open Area (m^2)	**Open Area (%)**
Square	0.02067	33.08
Rectangular	0.02016	32.26
Circular	0.02006	32.09
Oval	0.02006	32.09

2.5.4 Particles used in the LIGGGHTS simulation – zero-g space case

The particles used in the final zero-g space case simulation are of the same shape and size of the DEM simulation of the physical experiment as this is the size of particle which has been calibrated for the zero-g space case simulation. All the particles are analysed as a compilation of spheres which forms multibody particles with LIGGGHTS analysing them as such. This gives the particles more realistic movement characteristics when contacting each other as well as the boundary walls. A quantity of 100 of 12 differently shaped and scaled particles are inserted via a stream through the side of the sieve chamber.

Chapter 3 Results

3.1 Summary of Chapter 3

This chapter will address the results obtained for the physical experiments, simulations of the physical experiments and the final zero gravity simulations. The various sieves aperture shapes experimented and simulated will be compared to one another. The particle behaviour and the visual inspections of each experiment and simulation will also be discussed.

3.2 Vertical tube experiment results

A vertical tube drop test was performed to test the probability of a particle passing through different sieve apertures in a single impact. The experiment was first performed by dropping 50 single particles. These results have been summarized in Table 13. These values will be compared to the values which were theoretically calculated for each sieve shape in Section 2.3.5.

Table 13: Efficiency of particles passing through types of sieves

	Square	Rectangular	Circular	Oval
Yellow Pellets	16%	34%	12%	22%
White Pellets	14%	42%	12%	24%
Steel Pellets	14%	36%	12%	26%
Iron Ore Particles	13%	39%	10%	23%

The next physical experiment performed was conducted by dropping each set of particles all at once down the vertical pipe. This experiment was repeated three times for each particle type. The results for the four material types (yellow and white plastic spherical pellets, steel spherical pellets and iron ore) used in the experiment with the four sieve shapes are shown below in Table 14 to Table 17.

Table 14: Average efficiency for square sieve with pellets and iron ore particles.

Square Sieve												
Material Type	Yellow Pellets			White Pellets			Steel Pellets			Iron Ore Particles		
# of particles dropped	50	50	50	50	50	50	50	50	50	200	200	200
# of particles passed	11	7	6	11	8	7	12	9	8	21	25	27
% Success	22%	14%	12%	22%	16%	14%	24%	18%	16%	11%	13%	14%
Average % Success	16%			17%			19%			12%		

Table 15: Average efficiency for rectangular sieve with pellets and iron ore particles.

Rectangular Sieve												
Material Type	Yellow Pellets			White Pellets			Steel Pellets			Iron Ore Particles		
# of particles dropped	50	50	50	50	50	50	50	50	50	200	200	200
# of particles passed	16	15	15	23	19	14	16	17	13	43	54	80
% Success	32%	30%	30%	46%	38%	28%	32%	34%	26%	22%	27%	40%
Average % Success	31%			37%			31%			30%		

Table 16: Average efficiency for circular sieve with pellets and iron ore particles.

Circular Sieve												
Material Type	Yellow Pellets			White Pellets			Steel Pellets			Iron Ore Particles		
# of particles dropped	50	50	50	50	50	50	50	50	50	200	200	200
# of particles passed	2	7	8	5	2	6	8	9	6	13	24	18
% Success	4%	14%	16%	10%	4%	12%	16%	18%	12%	7%	12%	9%
Average % Success	11%			9%			15%			9%		

Table 17: Average efficiency for oval sieve with pellets and iron ore particles.

Oval Sieve												
Material Type	Yellow Pellets			White Pellets			Steel Pellets			Iron Ore Particles		
# of particles dropped	50	50	50	50	50	50	50	50	50	200	200	200
# of particles passed	9	12	15	10	13	12	12	7	9	50	51	50
% Success	18%	24%	30%	20%	26%	24%	24%	14%	18%	25%	26%	25%
Average % Success	24%			23%			19%			25%		

It can be seen that when each set of particles were dropped all at once the performance of the sieves were generally worse compared to when the particles were dropped individually. This is due to the congestion of particles obstructing other particles from passing through the apertures once they have deflected off the sieve plate. It should also be noted that some aperture shapes performed better in the congested case than in the uncongested case.

3.2.1 Deflection angle

The deflection angled was observed using a Hero 4 Silver GoPro camera. The best setting at which to see the deflection angle in slow-motion was using the WVGA mode while recording at 240 frames per second with the wide angle option. The camera was set up approximately 200 mm away from the initial impact point. The images were clear enough to see the particles impacting against the deflector plate and bounce off in the direction of the sieve and impact against the sieve or penetrate the sieve apertures. The camera frames were, however, not clear enough to see the interaction of the particle shape with the deflector plate. This seemed to be the determining factor for whether the particle rebounded off the deflector plate as was expected or not. A large percentage of particles, approximately 80%, rebounded off the plate as expected and some did not rebound at all.

3.2.2 Impact position

Figure 46 below indicates the trajectory angles of the typical yellow, white, and steel pellets and the iron ore particles (represented with yellow, white, black and orange lines) during the experiment. The angle of trajectory, from the horizontal, was seen to be increasing as the coefficient of restitution decreased through the particle types. It was noted that the trajectory was such that the particles hit the sieve plate in the middle. Some particles would not deflect off the deflector plate as expected and would slide along its surface until they collided with the bottom of the sieve plate. The behaviour of these particles suggests that the orientation in which the particle impacts the deflector plate is important to correctly determine the deflection angle. The deflection angle is important as it determines at what angle the particles will interact with the sieve plate (90° being the optimum particle-to-sieve interaction angle).

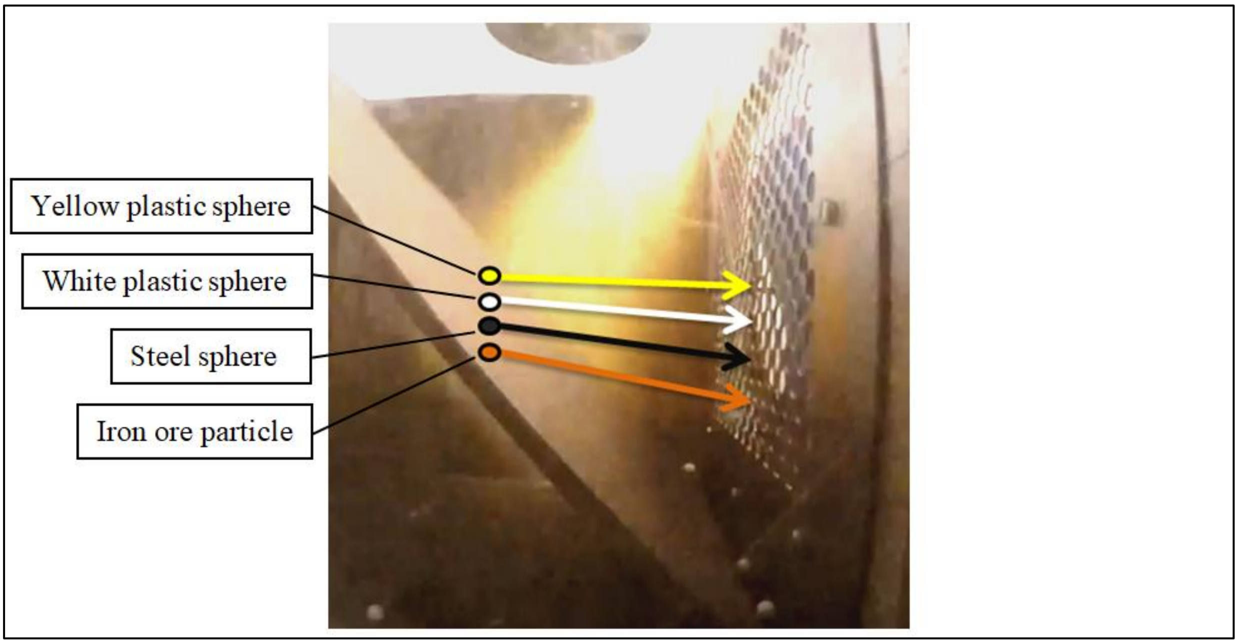

Figure 46: Deflection trajectory of each particle type.

3.3 *DEM simulation of the physical experiment results*

The simulation was run using the parameters which were discussed in Section 2.4.1.7. Each particle interacted with the sieve only once, after bouncing off the inclined plate. The reason for this is discussed later in Section 3.3.1. These simulations were used to calibrate the coefficient of restitution and the coefficient of static friction. As mentioned before these results were within an accuracy of 18.9 % of the physical experiment. A summary of the results of the physical experiment are tabulated in Table 18 below. The calculated probabilities have also been added for easy comparison and it is clear that the results obtained were as expected.

Table 18: Results of the DEM simulation of the physical experiments.

Percentage of particles passing through types of mesh				
	Square	Rectangular	Circular	Oval
Yellow Pellets	14%	26%	10%	26%
White Pellets	14%	30%	10%	20%
Steel Pellets	16%	26%	16%	22%
Iron Ore Particles	14%	28%	10%	24%
Calculated Probabilities	14,1%	28,6%	11,1%	22,4%

3.3.1 Impact point

The following figures (Figure 47 and Figure 48) show where the first particle of each particle type impacts the sieves. The vertical pipe was positioned such that it would allow the particles to deflect off the deflector plate and move towards the sieve at point blank range to ensure allow all the particles a chance to interact with the sieve apertures. After the iron ore particles collide with the deflector plate the particles are seen to have an angular velocity which cause the particles to spin while moving towards the sieve plates. This is further discussed in Section 3.3.2.

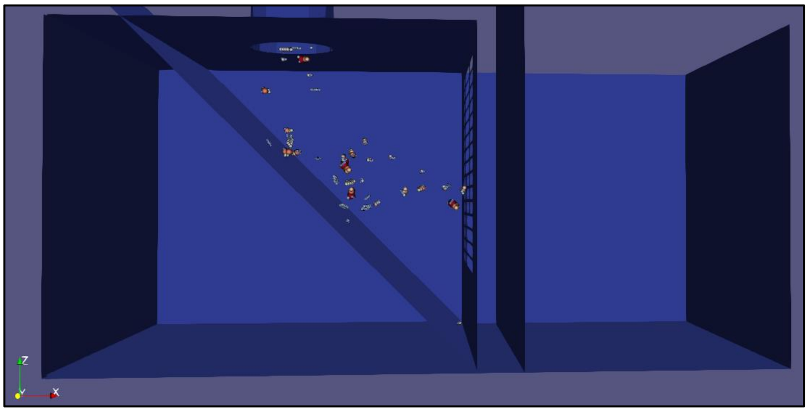

Figure 47: Impact point of iron ore particles

Figure 48 below shows the simulations of the physical experiments for the yellow, white and the steel particles at frame 13. The initial contact point between each of the particles and the sieves differs between the three. It should be noted that only difference between the parameters of these spherical particles are the densities, the coefficients of restitution and the coefficients of static friction.

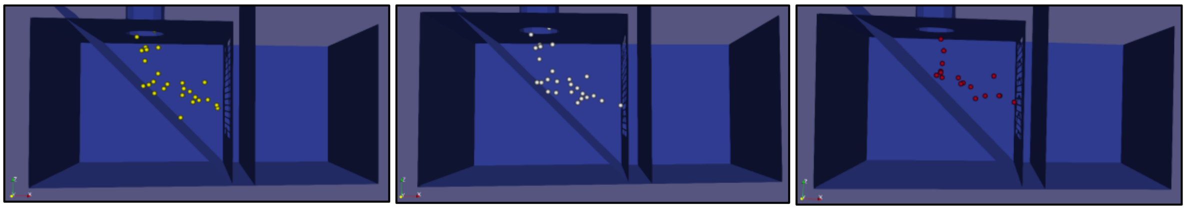

Figure 48: Impact point of yellow (left), white (middle) and steel pellets (right) simulated.

It can be seen in the figures above that the impact point varies between the four different particle types. Figure 47 also shows some particles sliding along the deflector plate. This was also noted on the video footage of the physical experiment with the iron ore particles.

The simulations, when compared to the video footage, showed similar particle-on-sieve impact positions which provided an additional verification process. The yellow pellets performed equally well in the simulation of the rectangular sieves as with the oval sieve. The same could be said about the steel pellets in the simulations for the square and circular sieves. The results of the physical experiment were within a 10% variance of the theoretical predictions, for the different types of sieves.

3.3.2 Particle movement – maximum bounding sphere

As mentioned before, once the particle (moving at approximately 6.26 m/s) impacts the deflection plate, the particles are given an angular velocity. This rotational velocity does not affect the spherical pellet's interaction with the sieves – especially in terms of the probability of the particles passing through the apertures. But when the iron ore particles are considered the rotation causes each particle to gain a theoretical maximum bounding sphere. This sphere is hypothetically drawn around the entire particle to ensure all the small spheres which make up the complete body are encapsulated. This means that the particle would rotate around its centre of mass with a larger spherical presence (as seen in Figure 49) due to its fast spinning nature relative to its lateral movement towards the sieve. As a result the probabilities of the fast spinning particles passing through the various sieve apertures are reduced.

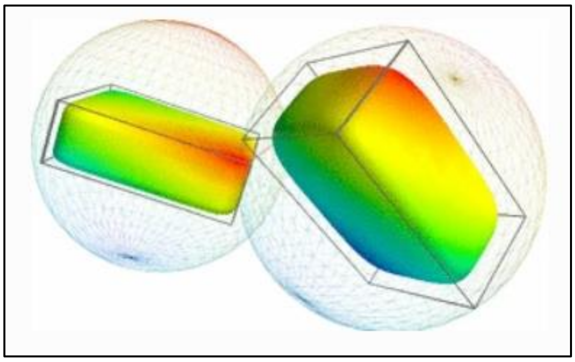

Figure 49: Max bounding spheres around simulated particles (Podlozhnyuk, Pirker and Kloss, 2016)

The following figure (Figure 50) shows the simulation for the square sieve configuration with iron ore particles. It shows the movement of iron ore particles through the sieve as well as through the counting plane. The figure depicts the spinning particles interacting with the sieve apertures.

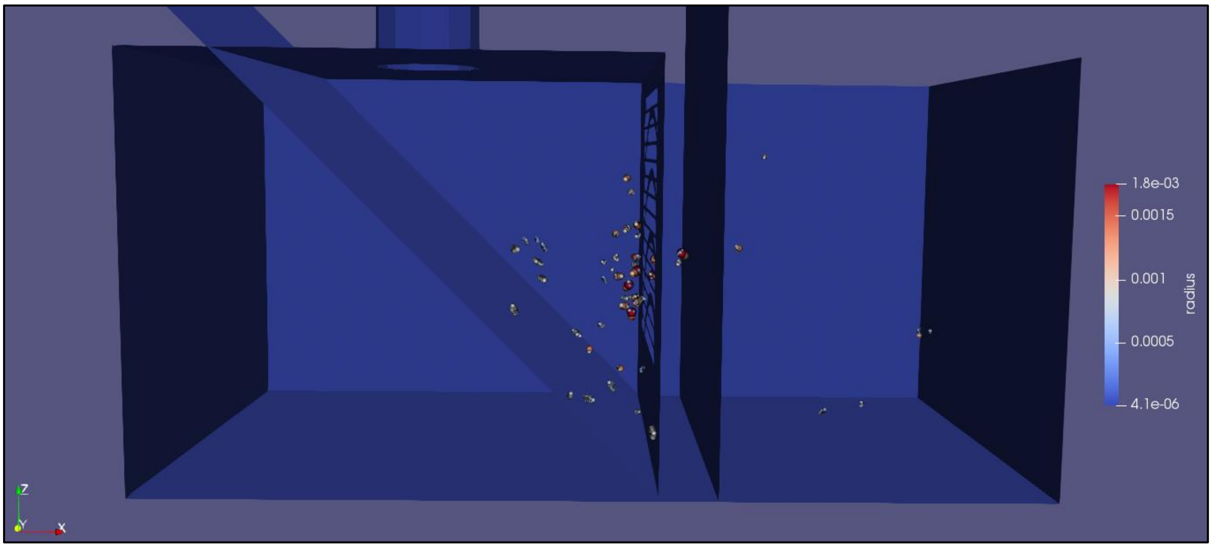

Figure 50: Iron ore particle movement through square sieve.

The following table (Table 19) shows the minimum and maximum bounding spheres of the 12 scaled multibody iron ore particles simulated which were calculated by LIGGGHTS. The minimum bounding sphere diameter would be measured at the smallest cross sectional area of the particle with its long axis positioned perpendicular to the sieve and the maximum bounding sphere diameter would be measured at the largest cross sectional area of the particle with its long axis positioned parallel to the sieve. The minimum and maximum probabilities may be calculated for each individually scaled particle (shown in Table 20) by using the minimum and maximum bounding sphere diameters respectively. The minimum to maximum probability range is also summarised in Table 20. This range essentially provides the probability of a particle to pass through a particular sieve in any orientation.

Table 19: Minimum and maximum bounding sphere diameters for each of the scaled iron ore particles

Minimum and Maximum Bounding Spheres Diameters (mm)					
		Scale			
		1	1,25	1,5	2
Particle #1	Minimum Sphere	3,20	4,00	4,80	6,40
	Maximum Sphere	4,87	6,09	7,31	9,74
Particle #2	Minimum Sphere	2,38	2,98	3,57	4,76
	Maximum Sphere	4,92	6,15	7,38	9,84
Particle #3	Minimum Sphere	3,72	4,65	5,58	7,44
	Maximum Sphere	5,26	6,58	7,89	10,52

Table 20: Probabilities of each scaled iron ore particle passing through each sieve

			Probabilities (%)				Range (%)
Square Sieve	Particle #1	Minimum Prob.	32,92	26,75	21,21	12,07	0.31 – 39.91
		Maximum Prob.	20,76	13,66	8,03	1,24	
	Particle #2	Minimum Prob.	39,91	34,77	29,98	21,48	
		Maximum Prob.	20,44	13,33	7,74	1,09	
	Particle #3	Minimum Prob.	28,83	22,20	16,44	7,50	
		Maximum Prob.	18,32	11,23	5,86	0,31	
Rectangular Sieve	Particle #1	Minimum Prob.	47,97	42,11	36,50	26,02	3.57 – 54.22
		Maximum Prob.	36,02	27,99	20,53	7,32	
	Particle #2	Minimum Prob.	54,22	49,66	45,23	36,78	
		Maximum Prob.	35,68	27,60	20,09	6,83	
	Particle #3	Minimum Prob.	44,13	37,54	31,27	19,74	
		Maximum Prob.	33,39	24,94	17,15	3,57	
Circular Sieve	Particle #1	Minimum Prob.	25,85	21,01	16,66	9,48	0.25 – 31.34
		Maximum Prob.	16,30	10,73	6,31	0,97	
	Particle #2	Minimum Prob.	31,34	27,31	23,55	16,87	
		Maximum Prob.	16,05	10,47	6,08	0,85	
	Particle #3	Minimum Prob.	22,64	17,44	12,91	5,89	
		Maximum Prob.	14,39	8,82	4,60	0,25	
Oval Sieve	Particle #1	Minimum Prob.	37,67	33,07	28,67	20,44	2.81 – 42.59
		Maximum Prob.	28,29	21,99	16,13	5,75	
	Particle #2	Minimum Prob.	42,59	39,00	35,52	28,89	
		Maximum Prob.	28,03	21,67	15,78	5,36	
	Particle #3	Minimum Prob.	34,66	29,48	24,56	15,51	
		Maximum Prob.	26,22	19,59	13,47	2,81	

3.4 *Final LIGGGHTS DEM simulation results – space case*

Each flat sieve type was used in the different simulations for all four particles; yellow & and white plastic pellets, steel pellets as well as the iron ore particles. 100 of each type of particle were inserted in their respective simulation therefore the efficiency of the sieve type was determined simply by counting the number of particles which were screened. The simulations below only cover the screening process that could occur in space. For simplification of the simulation, the concept of transporting the screened and unscreened particles to other mining processes for further processing is omitted.

The results obtained for the final DEM simulations of the space case are tabulated below in Table 21. Each sieve shape was simulated with each particle type so that all the results could be compared.

Table 21: Results obtained for the LIGGGHTS simulation for the space case.

Efficiency of DEM Simulation of Space Case				
	Square	Rectangular	Circular	Oval
Yellow Pellets	9%	22%	10%	17%
White Pellets	7%	20%	9%	16%
Steel Pellets	10%	22%	10%	18%
Iron ore Particles	21%	35%	16%	31%
Calculated Probabilities	14,1%	28,6%	11,1%	22,4%

3.4.1 Space case simulation

Figure 51 below shows the initial setup of the space case simulation where the moving sieve was changed and simulated with each type of particle until each of the four particle types were simulated with each sieve configurations. This resulted in 16 simulations being run.

Figure 52 and Figure 53 show the simulation for the square sieve configuration. The figures show the movement of particles into the screening chamber and thereafter they collide with the moving sieve while allowing the undersize particles to pass through the apertures. All the oversize particles as well as the particles which impact the sieve between apertures are forced towards the counting plane. Once the sieve plate touches the counting plane the counting plane counts all the particles which passed through it during the simulation and because it is known that 100 particles are inserted into the system, the difference between these two values is the amount of screened particles. The particles which are not sieved are transported to the left (where a crushing station may be) while the screened particles left in the chamber would be collected and used in a 3-D printer.

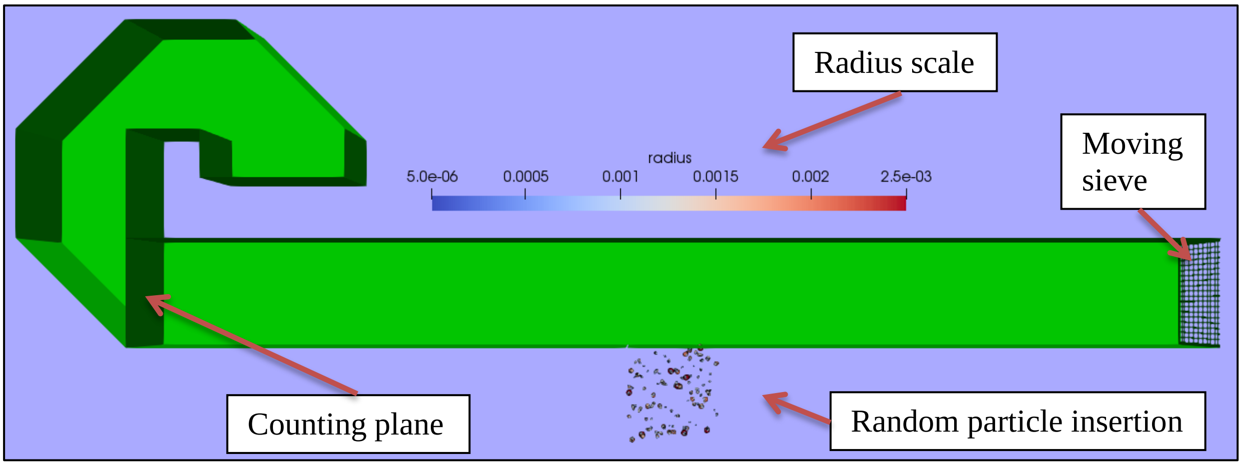

Figure 51: Initial setup of the space case simulation

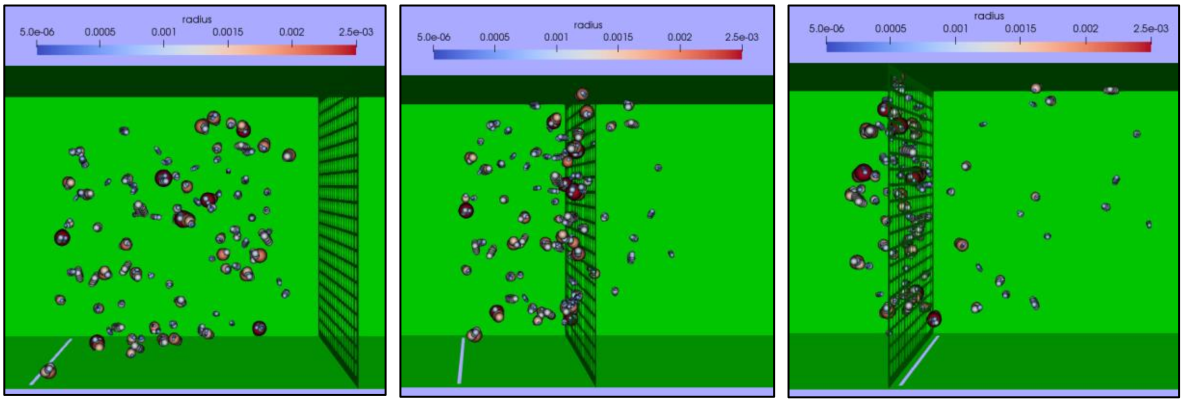

Figure 52: Movement of particles in the space case simulation for the square sieve.

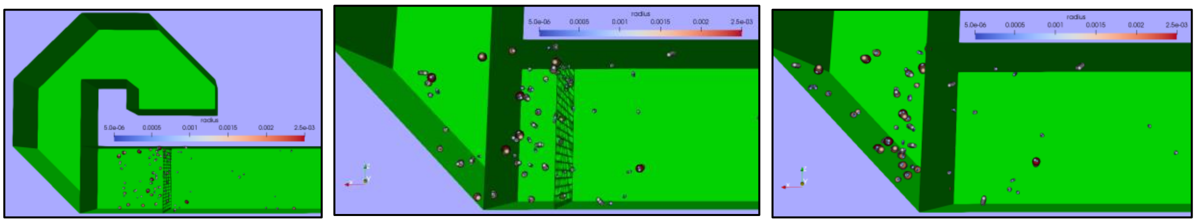

Figure 53: Space case simulation with oversize particles moving through counting plane

A high percentage of iron ore particles passed through the sieve while the spherical particles all displayed results which were below the theoretical efficiency values. Table 21 shows that the rectangular apertures consisted of the highest efficiencies while the next best was the oval apertures. The square and the circular apertures performed, on average, similarly.

Chapter 4 Discussion

4.1 Summary of Chapter 4

This chapter will discuss the results obtained for the preliminary simulations, physical experiments and final simulations. Each experiment and simulation will initially be analysed in isolation and thereafter a comparative exercise will be conducted in order to draw conclusions about all of the influencing factors as well as the relevant parameters.

4.2 Preliminary LIGGGHTS simulation

The preliminary simulations were set up to compare the efficiencies of four aperture shapes (square, rectangular, circular and oval) as well as the extruded aperture concept of the shapes. The simulations also varied the amount of particles which were inserted in the sieve box to analyse the effect of the number of particles have on the performance of the sieves. The extruded concept was based on the idea that the slanted sides may guide the particles through the apertures at the specified cut-size. A sieve box was created with the sieve plane dividing the box in two. Particles of four sizes (2, 3, 5 and 6 mm) were inserted in the top chamber while the entire sieve box would stroke eight times at a specified stroking angle. The sieve box impacted the particles and transferred kinetic energy into the particles. The particles which passed through the sieve plate would be counted and the efficiency of each sieve would be calculated while excluding the oversize particles which could not pass through the sieve. This process was repeated for stroking angles of the sieve box from 0° to 90° while the angle varied in increments of 15°.

As expected the sieve which produced the best results was the sieve with rectangular apertures. Efficiencies of approximately 90% were achieved with the 200 particle simulations and with the rectangular extruded sieve at strokes of 75° and 90°. The high efficiency can be attributed to the eight strokes of the sieve box compared to the 20% - 25% efficiency which was obtained during the first of the eight strokes in the simulation.

The flat sieves performed the better when compared to the extruded sieve configuration when there was more interference from other particles as was the case when the particle count was 600 and 1800.

It may be seen from the results in Figure 23 to Figure 26 that all the sieves performed worse as more particles were introduced to the screening box. This is due to the many interactions with the other particles instead of interactions with the sieve surface. The collisions with other particles also meant that in the vertical strokes some particles would deflect off other particles and transfer the vertical kinetic energy into horizontal kinetic energy which is not beneficial for screening purposes. As mentioned in the observations that the particles formed a bed of particle 3 – 5 particles high which only allowed the bottom layer to have an opportunity to be screened. Another contributing factor to the poor performance is the lack of stratification – the term previously used to describe the phenomenon of smaller particles moving to the bottom of a pile of particles when vibrated (where gravity plays an important role).

The highest proportion of particles which were screened was the smallest particle size where between 55% and 70% of the total particles screened were Ø2 mm particles while the remainders were the Ø3 mm particles.

As expected, the sieve types performed the best as the stroke angle was gradually changed to the vertical direction (90°). This allowed the particles to initially move towards the sieve without the effect of foreshortening.

It may be noted that on almost every occasion of simulations of the extruded sieve types that the efficiencies were low at stroking angles between 0° - 30°. The efficiencies then increased from strokes of 45° and above. The extruded sieve designs made it extremely difficult for particles to pass back through the sieve once they had passed into the bottom screening chamber. The extruded sieve type retained up to 90% of the particles which had passed through the sieve during the eight strokes, whereas the flat sieve types, on some occasions, lost up to 40% of the particles which had been screened due to them passing back through the sieve.

One unexplained result was observed for the 600 and 1800 particle simulations (as shown in Figure 23 to 26). The efficiency decreased from the stroke angles 30° to 60° after which it increased again. It is first seen subtly in the 600 particle simulations of the rectangular, circular and oval sieves but is then amplified by the 1800 particles simulations of all the sieve types. The reason for this is still unknown.

On average, the sieves which performed from the best to worst were as follows: rectangular, oval, circular and square sieves types.

The results in the preliminary simulations showed the following important aspects which affected the subsequent research in this report:

- The flat sieve performed better between the two sieve configurations (flat vs extruded) for stroking angles less than 60°, and with the 600 and 1800 number of particles. Therefore due to the complexity of manufacturing the extruded sieve configuration, the flat sieve would be used in the future experiments and simulations.
- The efficiency of the sieves increased as the stroking angle varied towards the 90° angle. Therefore the vertical tube experiment, the simulation thereof and the space case simulation would all have the particles interacting with the sieves at 90°, or angles close to 90°.
- Approximately 20% - 25% of screened particles were screened in the first stroke of the sieve box. With the extruded sieve configuration screening, on average, 5% more than the flat sieve during the first stroke. This promoted the idea of the one-time sieving technique.
- Attempting to screen too many particles at the same time is not beneficial for the efficiency. Efficiency came down to ensuring each particle comes into contact with the sieve as this increased the opportunities for particles to pass through apertures. It was shown that having additional particles in the simulations had obstructed other particles from having an opportunity to interact with the sieve. This meant that the vertical tube experiment, the simulation thereof as well as the space case simulation would have minimal particles in it to ensure every particle would have an opportunity to be screened in the single impact.

4.3 Probability of particles passing through sieves

The probabilities calculated in Section 2.3.5 from first principles provide a solid basis against which the experiment and the simulation results may be compared. The calculation is based on the spherical size of particle passing through the aperture and the area of the aperture itself, allowing for an oblique impact up to 45° with the edge of the apertures. The results of the calculations show that the rectangular aperture shape (28.6% probability) should perform the best followed by the oval apertures (22.4%), then the square apertures (14.1%) and lastly the circular apertures (11.1% probability). Unfortunately the calculations only apply a rough estimate for the probabilities of the complex multibodies such as the iron ore particles. The probability calculations for the multibody particles would depend on the cross sectional area and the orientation of the particles at the time of the particle-on-sieve interaction.

4.4 Vertical tube experiment

A vertical drop test rig was constructed where a particle was allowed to fall under the action of gravity. It then impacted a surface inclined at 45° and rebounded towards a sieve oriented at nominally 90° to the direction of motion of the particles. Two types of plastic (yellow and white) spheres, steel spheres, as well as iron ore particles were dropped. Four types of different sieves were changed out; square, rectangular, circular and oval, where the rectangular and oval apertures were oriented vertically. 50 particles of each type of particle were first dropped individually to ensure no particles were obstructed allowing each particle to have an opportunity to interact with the sieve. After this experiment the same 50 particles of each type were dropped simultaneously and the efficiency of each particle type and each sieve type were recorded.

It may be seen in Figure 46 that the particles were not projected exactly perpendicular to the sieves and some were deflected at much smaller angles such as 30° - 45° to the horizontal especially in the case of the iron ore particles. The preliminary simulations showed that the elongated apertures of the rectangular and oval sieve types performed better in general due to counteraction of foreshortening.

The rectangular sieve type produced the highest efficiency (42%) for all particles and is tabulated in Table 13 in the 50-single particle drop test. The test whereby all the particles were dropped at the same time (Table 14 to Table 17) also yielded the same result indicating that the particles rebounding off the sieve plate do not obstruct other particles moving towards the sieve. It should be noted that the rectangular sieve apertures may allow for oversize particles to pass through should the longest side of a multibody particle be orientated in the same direction as the longest side of the aperture. This may also be said about the oval sieve aperture, but then what was the fundamental difference between these two sieve types? The rectangular sieve open area, as previously mentioned in Figure 16, is greater than any of the other sieve types therefore it will, statistically, allow more particles to pass through each aperture with less sieve interference. The stacking density of the rectangular sieve is also greater in the area where the particles impacted therefore particles had a greater probability of passing through the rectangular sieve type as shown in Section 2.3.5. Though, it should be noted that the corners of the square and rectangular apertures do not play a role when the particles are spherical.

The next best performing sieve was the oval sieve type with a highest efficiency of 26%. The longitudinal opening of the apertures aided in allowing more particles to pass through the sieve.

The square sieve performed the third best out of the four with it achieving an average efficiency of 16%. This was unusual to see as the preliminary simulation suggested that it would perform the worst. The densely stacked apertures were as densely packed as the preliminary simulation and therefore cannot be the only contributing factor to the success of the sieve.

The circular sieve performed the worst while achieving an average passing efficiency of only 12%. As mentioned in the previous section and referring to Figure 30 it makes sense that the areas between the apertures would repel many of the approaching particles. It was thought that the fact that only spherical particles were used in the preliminary simulations may have contributed to the success of the circular sieve type but the physical experiments showed that even with the spherical particles the circular sieve performed badly.

The probabilities calculated theoretically directly relate to the efficiency of the particles passing through the different types of apertures in the vertical tube experiment. On average, the particles performed as expected as they compare closely to the calculated probabilities with the following results: rectangular (27.5%), oval (23.0%), square (14.5%) and circular (11.5%). The only variance that can be seen may be contributed to the number of particles used in the experiment. More accurate results could have been obtained had more particles been used in the experiment.

It should be noted that Table 13 suggested that regardless of the parameters the best performing particle type between the yellow, white and steel pellets as well as the iron ore particles could not be distinguished. The results showed that the particle interaction point on the sieves did not entirely determine the probability of the particles passing through the apertures as the efficiencies remained consistent.

4.5 Calibration of DEM parameters

The DEM simulation of the physical experiment was set up initially with the experimented parameters as previously discussed in Section 2.4.1. The simulations yielded results which were very different to the vertical tube experiment. It is customary in DEM simulation to calibrate the DEM parameters by modifying the most influential parameters to replicate the physical experiment. The most influential parameters in the case of the vertical tube experiment were the coefficients of restitution and static friction. These two parameters were varied from 0.1 to 0.9 in increments of 0.1.

The simulations proved to be very sensitive to the values of these two parameters and yielded results which varied approximately 10% - 15% in some cases. It was interesting to note that the iron particles resulted in having the lowest coefficient of restitution (0.2) and highest coefficient of static friction (0.7) and this is what the originally determined parameters displayed. The rest of the particles also showed the best coefficient of restitution parameter to be consistent with the originally determined parameters, despite a lower coefficient of restitution being expected for the thin sieve plate that was used in the experiments.

4.6 DEM Simulation of the vertical tube experiment

The DEM simulation was set up to replicate the vertical tube experiment with all the same dimensions of the actual experiment. In the simulation of the physical experiment 50 particles of each type of pellet were tested and 200 iron ore particles tested. These were inserted into the vertical tube and collided with the deflector plate and bounced in the direction of the sieve plates. The sieves were modelled and positioned as they were on the physical experiment. As mentioned previously the calibrated DEM parameters for the coefficients of restitution and static friction were used for each type of particle.

The results obtained in the simulations (after calibration) when compared to the physical experiment are within a maximum deviation of 7% as shown in Table 22, with the majority of the DEM simulation results being slightly lower than the experiment. This is due to the calibration of the coefficients of restitution and the coefficients of static friction of all the particles.

Due to the high efficiencies obtained during the experiment for the rectangular and the oval sieves the coefficients were selected to represent similar efficiencies for the simulations. The coefficients selected were the combinations of the two parameters which best suited each particle type in the physical experiment.

One point to consider is that only 3 particles were modelled as multibodies and scaled for the LIGGGHTS simulations for the iron ore case. Had more particles been modelled this could have produced different results for the iron ore particle case.

Table 22: Comparison of the physical experiment and the DEM simulation of the physical experiment results

Material Type	**Sieve Type**	**Square Sieve**	**Rectangular Sieve**	**Circular Sieve**	**Oval Sieve**
Yellow pellet efficiencies	Physical experiment (%)	16	31	11	24
	DEM simulation of physical experiment (%)	14	26	10	26
	Deviation (%)	2	5	1	2
White pellet efficiencies	Physical experiment (%)	17	37	9	23
	DEM simulation of physical experiment (%)	14	30	10	20
	Deviation (%)	3	7	1	3
Steel pellet efficiencies	Physical experiment (%)	19	31	15	19
	DEM simulation of physical experiment (%)	16	26	16	22
	Deviation (%)	3	5	1	3
Iron ore particle efficiencies	Physical experiment (%)	12	30	9	25
	DEM simulation of physical experiment (%)	14	28	10	24
	Deviation (%)	2	2	1	1

4.7 LIGGGHTS Simulation of the space case

The screening chamber described in Section 2.5.1 was simulated in the final space case simulation. The sieve plate was given a velocity and moved down the stationary tunnel (at 1 m/s) where it met the inserted stream of particles moving, perpendicularly to the tunnel, at a relatively small velocity (0.15 m/s). The undersize particles which were in a position to be screened passed through the sieve while other particles were hit and moved with the sieve to the end of the tunnel where they would theoretically be conveyed to a crushing chamber for further processing. The calibrated parameters were used in these simulations while 100 of each particle type were tested in separate simulations. The four sieves were changed and experimented with each of the four particle types therefore a total of 16 simulations were run for the space case scenario.

The screenshots of the simulations of the various sieves show that the sieves met the particles in the middle of the sieving area, as shown in Figure 52. The screened particles either passed through the sieve untouched or touched part of the sieve and passed through. Some of the screened particles which touched the sieve either deflected off the edges of apertures or continued to roll on the sieve face for a while until they rolled into an aperture and were screened. The sieves performed as expected and the timestep which was selected was sufficiently small so as to ensure particles did not pass through the sieve where they physically should not have.

Table 21 compares the LIGGGHTS simulation of the simulated space case for the various sieves and particle types. The simulation of the space case for the yellow, white and steel pellets resulted in lower efficiencies than the calculated probabilities when compared to the theoretical probability that was calculated for all the sieve types. All of the results differed by more than 24% except for the circular sieve which only differed by approximately 15%. This was the case despite the particles interacting with the sieve close to the optimal 90°. The results motivate that the process of screening almost entirely relies upon chance. If the particle was in the right place at the right time in the right position it was screened, otherwise it was not.

As mentioned before one of the reasons why the physical experiment and the simulation of the physical experiment did not perform as well as expected is due to the particles interacting with the sieve at an angle other than the optimum 90°. This was because the deflection angle of the particles off the deflector plate was not exactly 90°. In the simulation of the space case the particles are allowed to interact with the sieves at approximately 81.5° due to the moving sieve plate and the moving particles. This meant that the simulation of the space case could therefore produce the best results (as proven in the preliminary simulation - the 90° stroke produced the best results).

As it can be seen the simulation of the LIGGGHTS space case for iron ore particles outperformed all the physical experiments and the simulations thereof. One contributing factor is that due to the zero gravity environment the effect of gravity on the particle's movement does not have to be considered. That being said the efficiencies were extremely high, approximately 1.5 times higher than what was expected. The particles were inserted in random orientations so that they could interact with the sieve in different positions. It was later found that the reason for the increased efficiency is due to the perceived "smaller particle" which was being screened due to the smaller cross sectional area of the particle in the specific orientation as the particle was interacting with the sieve apertures (see Table 19 for probabilities of the minimum and maximum bounding sphere diameters). In the physical experiment and the simulation thereof the multibody particles impacted with a deflector plate which gave the particles a large angular velocity which meant that each of the rotating particles had a maximum bounding sphere as discussed in Section 3.3.2. The maximum bounding spheres would be used to determine the probabilities in those two cases (physical experiment and the simulation thereof) but would not directly apply to the space case simulation because an angular velocity was not given to the particles. Therefore the range of probabilities, shown in Table 20, would apply to the space case simulation as these cover all the possible orientations which the particle may have interacted with the various sieves. As expected, the ranges of probabilities of the sieves show that the orders of performance were as expected as the results obtained during the simulation were within these ranges. It can also be seen that the iron ore particles were sensitive to orientation, particularly when they had large aspect ratios.

It may be noted that for the space case simulations for the iron ore particles the sieves performed the best to the worst in the following order: rectangular sieve, oval sieve, square sieve and the circular sieve. This is the same order as the simulation of the physical experiment.

4.8 Summary of the research

The research first conducted preliminary simulations with flat and extruded sieves to assess the effects of zero gravity on particle behaviour. This gave valuable insights which were used in the subsequent research. The theoretical probabilities for Ø6 mm particles were then calculated for square, rectangular, circular and oval sieves. This was followed by experiments to measure the parameters required for the LIGGGHTS simulations. A vertical tube experiment was then conducted and replicated using DEM simulation which was used to calibrate and validate the LIGGGHTS parameters. This then led to the simulation of the space case or zero gravity case.

The preliminary simulations showed that particles approaching the sieve plate at 90° far outperform any other approaching angle and that the extruded sieve aperture obtained results which were 5% - 10% higher than the flat sieve configurations for the simulations run with 200 particles. For the simulations with 600 and 1800 particles the extruded aperture sieves performed worse. The one major disadvantage was that near-size particles would block some apertures at times. Screening fewer particles was shown to increase the particle-to-sieve interactions which increased the efficiency whereas screens on Earth, instead, use the principal of stratification to their advantage by vibrating smaller particles to the surface of the sieve. The preliminary simulation also showed that in zero gravity the concept of one-time sieving was very effective. All the research and experiments conducted showed that the sieves were most effective in the following order (from best to worst): rectangular, oval, square and circular – this was proven by theoretical probability calculations, physical experiments and through simulations. The rectangular and oval apertures contain a larger unobstructed area for screening to take place therefore they showed superior efficiencies. LIGGGHTS proved to be a useful DEM simulation tool after the input parameters were calibrated and validated. It showed that the minimum and maximum bounding spheres are important parameters that need to be considered especially when screening non-spherical multibody particles in zero gravity.

Chapter 5 Conclusions and Recommendations

5.1 Conclusions

This report demonstrates that it is possible to predict how particles would behave in a zero gravity environment and sets out the screening mechanisms which play important roles in this determination.

The starting point for this report was carrying out preliminary simulations which indicated that more particles were screened in the first particle and sieve interaction than at any other interaction. The simulations were run with four particles and four sieve types. The best efficiencies were obtained when the stroking angle was at 90° to the particles. The rectangular sieve performed the best, followed by the oval, square and circular sieve, in that order. The simulations demonstrated that more particle-sieve interaction resulted in higher efficiencies.

The next step in the research was carrying out a vertical tube experiment. This experiment resulted in the following efficiencies for the sieves: rectangular (42%), oval (26%), square (16%) and circular (12%). The results from this experiment were then used to calibrate the coefficients of restitution and static friction for the four types of particles used in this report. The change of these parameters, although small, caused significant differences in the results, with some results changing approximately 10% with only a 0.1 change of either parameter.

The space case simulation was run with the same four particles and four sieves, and the results were directly comparable to the calculated probabilities and the physical experiment, with the exception of the iron ore particles. These were approximately 1.5 times higher, which was as a result of non-rotating particles appearing smaller from the perspective of the sieve due to the maximum bounding sphere phenomenon. Notably, these results still fell within the range of probabilities for the multibody particles.

One of the central conclusions of this report is that the main characteristics which govern the behaviour of particles during the screening process in a zero gravity environment are the coefficient of restitution, coefficient of static friction and the shape of the particle.

5.2 *Recommendations for discrete element method (DEM) in a zero gravity environment*

- An investigation into the impact angle of the particles onto the deflector plate would be informative and beneficial in similar lines of research. It will be important to investigate whether the approaching orientation of the particle towards the deflector plate has an effect on the deflection angle after impact. It would be beneficial to insert the stream of particles into the simulation with random orientations and an angular velocity but the angular velocity operation is not yet functioning in LIGGGHTS. More development work needs to go into the code to allow multibody particles to be given angular velocities. This could be done by having the particles hit a deflector plate before entering the sieving tube but the particles would need to be given a high initial velocity as in the case of the vertical tube experiment where the velocity impacted the deflector plate at 6.26 m/s. The high impact velocity would mean that the particles would spin extremely fast while interacting with the sieve thereby taking full advantage of the maximum bounding sphere theorem.
- The multibody particles used in the simulations should be modelled as accurately as possible to the actual particles which will be predicted. Should the simulation consist of only one impact point, such as in a space case, then the orientation of the moving particles at the point of screening may have a significant effect on the outcome of the results.
- The superior configuration based on efficiency, of sieve type during the preliminary simulation was the extruded sieve where the approaching angles of the particles were more than 60°. The limitations of the design were that the particles would be blocked in the apertures but if this could be solved the design has far more pros than cons. Some of the pros are that the extruded shapes add significant structural rigidity to the sieve, the efficiencies increased by at least 10% when compared to the flat sieve at stroking angles of 75° and 90°. The design of the extruded apertures discouraged particles from passing back through the apertures thus improving the particle retention rate. The difficulty in manufacturing the sieve types could be circumvented if some thought is applied to it. Therefore it would be useful to investigate this type of sieve design further.
- Multiple impact sieving should also be investigated. The preliminary simulation illustrated that it was possible to obtain up to 91% efficiency in only eight strokes of a

sieve box moving at 16 Hz which means it only took 0.5 seconds to do this therefore this avenue should be investigated further.

- Although this research proposed the one-time sieving technique as the preferred form of sieving it will need to be expanded on to include more particles so that the tonnages put through the screening process may increase. It is important to note that the tonnages put through the screening process are just as important as the efficiency of the process.
- Experiments on the probabilities of irregular shaped particles passing through sieve apertures should be investigated with a more rigorous statistical approach.
- Different materials should be analysed and investigated. This research only covered the sieving of plastic and steel pellets as well as iron ore but there will be many other types of minerals which would be mined in space.
- Section 4.2 mentions that the efficiency reduces between 30° and 60° stroking angles in the simulations with 600 and 1800 particles. These unexplained results should be investigated as this research a general trend of improved efficiencies as the stroking angles increased to the optimum 90°.stroking angle.

Project Schedule

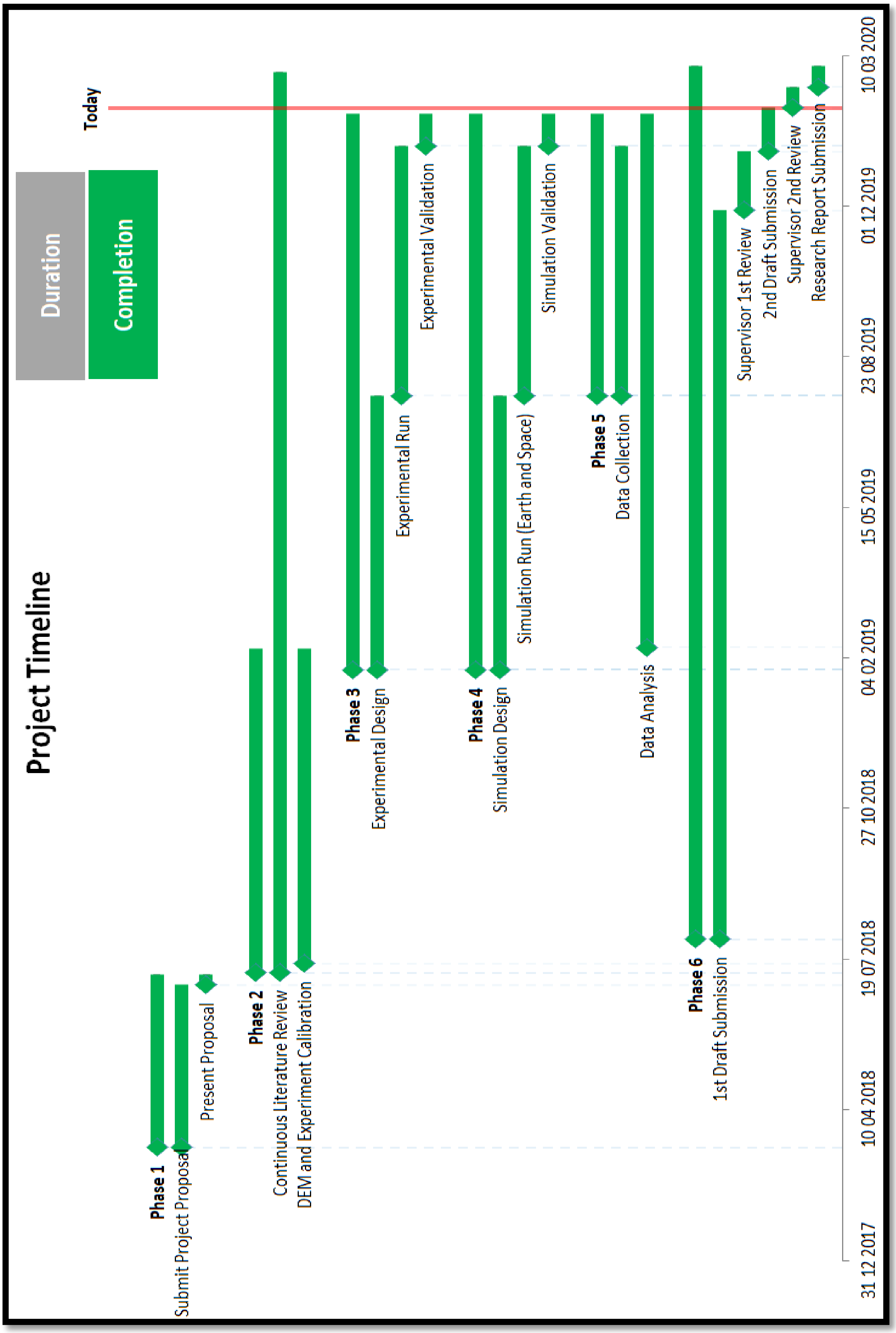

References

Arthur, I. (2016). *Asteroid Mining.* [video] Available at: https://youtu.be/3-3DjxhGaUg [Accessed 25 Mar. 2018].

Barrios, G., de Carvalho, R., Kwade, A. and Tavares, L. (2013). *Contact parameter estimation for DEM simulation of iron ore pellet handling.* Powder Technology, [online] 248, pp.84-93. Available at: http://www.elsevier.com/locate/powtec [Accessed 22 Jul. 2018].

Bennett, J. and Meepagala, R. (2005). *Coefficients of Restitution - The Physics Factbook.* [online] Hypertextbook.com. Available at: https://hypertextbook.com/facts/2006/restitution.shtml [Accessed 25 Jan. 2020].

Bhushan, B. and Kulkarni, A. (1996). *Effect of normal load on microscale friction measurements.* Thin Solid Films 278. Columbus, USA: Elsevier, pp.49-56.

Budynas, R., Nisbett, J. and Shigley, J. (2011). *Shigley's mechanical engineering design*. 9th ed. New York: McGraw-Hill.

Cavarretta, I., O'Sullivan, C., Ibraim, E., Lings, M., Hamlin, S. and Wood, D. (2012). *Characterization of artificial spherical particles for DEM validation studies*. Particuology, 10(2), pp.209-220.

Cfdem.com. 2016. *Gran Model Hertz Model — LIGGGHTS V3.X Documentation*. [online] Available at: <https://www.cfdem.com/media/DEM/docu/gran_model_hertz.html> [Accessed 19 October 2019].

Cherdo, L. (2019). *The best metal 3D printers in 2019 (March update) - From $5k and up.* [online] Aniwaa. Available at: https://www.aniwaa.com/best-of/3d-printers/best-metal-3d-printer/ [Accessed 3 Feb. 2020].

Cheung, G. and O'Sullivan, C. (2008). *Effective simulation of flexible lateral boundaries in two- and three-dimensional DEM simulations.* Particuology, 6(6), pp.483-500.

Cleary, P., Sinnott, M. and Morrison, R. (2009). *Separation performance of double deck banana screens -Part 1: Flow and separation for different accelerations.* Minerals Engineering, 22(14), pp.1218-1229.

Cleary, P., Sinnott, M. and Morrison, R. (2009). *Separation performance of double deck banana screens – Part 2: Quantitative predictions.* Minerals Engineering, 22(14), pp.1230-1244.

Coefficient of Friction Testing. (2019). [Blog] *JLW Instruments*. Available at: https://jlwforce.com/blogs/testing-applications/coefficient-of-friction-testing [Accessed 7 Jul. 2019].

Coetzee, C. (2017). *Review: Calibration of the discrete element method.* Powder Technology, 310, pp.104-142.

Cole, S. (2020). *Particle shear modulus - it can save you time.* [online] EDEM Simulation. Available at: https://www.edemsimulation.com/blog-and-news/blog/particle-shear-modulus-it-can-save-you-time/ [Accessed 25 Jan. 2020].

Combarros, M., Feise, H., Zetzener, H. and Kwade, A. (2014). *Segregation of particulate solids: Experiments and DEM simulations.* Particuology, 12, pp.25-32.

Coulter, S., Bras, B., Winslow, G. and Yester, S. (1998). *Designing for Material Separation: Lessons From Automotive Recycling.* Journal of Mechanical Design, 120(3), p.501.

Defender Rotary Screens. (2016). [ebook] *Valladolid-Spain: TORO Equipment, pp.1 - 3.* Available at: https://toroequipment.com/wp/wp-content/uploads/2015/09/Rotary-Screen-Pretreatment-Equipment.pdf [Accessed 22 Jul. 2018].

Delaney, G., Cleary, P., Hilden, M. and Morrison, R. (2012). *Testing the validity of the spherical DEM model in simulating real granular screening processes.* Chemical Engineering Science, 68(1), pp.215-226.

Diamcormining.com. (2018). *Final Recovery Methods | Diamcor Mining Inc..* [online] Available at: http://www.diamcormining.com/diamond_info/recovery_methods/ [Accessed 22 Jul. 2018].

Dong, K., Yu, A. and Brake, I. (2009). *DEM simulation of particle flow on a multi-deck banana screen.* Minerals Engineering, 22(11), pp.910-920.

Elskamp, F., Kruggel-Emden, H., Hennig, M. and Teipel, U. (2017). *A strategy to determine DEM parameters for spherical and non-spherical particles.* Granular Matter, 19(3).

Engineeringtoolbox.com. (2018). *Poisson's ratio.* [online] Available at: https://www.engineeringtoolbox.com/poissons-ratio-d_1224.html [Accessed 30 Jun. 2018].

Fernandez, J., Cleary, P., Sinnott, M. and Morrison, R. (2011). *Using SPH one-way coupled to DEM to model wet industrial banana screens.* Minerals Engineering, 24(8), pp.741-753.

Flint, A. L., L. E. Flint 2002. *2.2 Particle Density*. In: J. H. Dane, C. G. Topp, editors, *Methods of Soil Analysis: Part 4 Physical Methods*, SSSA Book Ser. 5.4. SSSA, Madison, WI. p. 229-240. doi:10.2136/sssabookser5.4.c10

FW:Thinking (2013). *The Future of Asteroid Mining.* [video] Available at: https://youtu.be/O9cLLNpo2f8 [Accessed 25 Mar. 2018].

Goswami, N. (2018). *China in Space Ambitions and Possible Conflict.* 1st ed. [ebook] Air University Press, pp.pp. 74-97. Available at: http://www.jstor.org/stable/26333878 [Accessed 3 Apr. 2018].

Grima, A. and Wypych, P. (2011). *Investigation into calibration of discrete element model parameters for scale-up and validation of particle–structure interactions under impact conditions.* Powder Technology, 212(1), pp.198-209.

Gump, D. (2014). *Space mining: David Gump at TEDxCibeles.* [video] Available at: https://youtu.be/OoNjSADM9H4 [Accessed 25 Mar. 2018].

Gupta, A. and Yan, D. (2006). *Mineral Processing Design and Operation.* Amsterdam: Elsevier Science, pp.293-353.

Guya, S. (2018). *Calibration of Discrete Element Modelling parameters for Bulk Materials Handling Applications,* Masters. University of the Witwatersrand.

Holzner, S. (2019). *How Surface Area Affects the Force of Friction - dummies.* [online] dummies. Available at: https://www.dummies.com/education/science/physics/how-surface-area-affects-the-force-of-friction/ [Accessed 14 Sep. 2019].

Horn, E. (2012), *The Calibration of Material Properties for Use in Discrete Element Methods*, Master's thesis, University of Stellenbosch: South Africa. Masters Dissertation.

Huang, X., Hanley, K., O'Sullivan, C. and Kwok, C. (2014). *Exploring the influence of interparticle friction on critical state behaviour using DEM.* International Journal for Numerical and Analytical Methods in Geomechanics, 38(12), pp.1276-1297.

Huang, X., Hanley, K., O'Sullivan, C. and Kwok, F. (2014). *Effect of sample size on the response of DEM samples with a realistic grading.* Particuology, 15, pp.107-115.

Jahani, M., Farzanegan, A. and Noaparast, M. (2015). *Investigation of screening performance of banana screens using LIGGGHTS DEM solver.* Powder Technology, 283, pp.32-47.

Jahani, Mohammad & Farzanegan, Akbar & Noaparast, Mohammad & Shafaei Tonkaboni, Sied Ziaedin. (2016). *DEM simulation of screening operation of banana screens by LIGGGHTS: Effect of design parameters.* Particuology.

Kloss, C., Goniva, C., Hager, A., Amberger, S. and Pirker, S., 2012. *Models, algorithms and validation for opensource DEM and CFD-DEM. Progress in Computational Fluid Dynamics, An International Journal*, [online] 12(2/3), pp.140-152. Available at: <http://www.cfdem.com/liggghtsr-open-source-discrete-element-method-particle-simulation-code> [Accessed 25 March 2018].

Lin, K., Zhang, Q. and Chen, X. (2010). *An evaluation of impacts of DEM resolution and parameter correlation on TOPMODEL modeling uncertainty.* Journal of Hydrology, 394(3-4), pp.370-383.

Li, J., Webb, C., Pandiella, S. and Campbell, G. (2003). *Discrete particle motion on sieves—a numerical study using the DEM simulation.* Powder Technology, 133(1-3), pp.190-202.

Li, T., Peng, Y., Zhu, Z., Zou, S. and Yin, Z. (2017). *Discrete Element Method Simulations of the Inter-Particle Contact Parameters for the Mono-Sized Iron Ore Particles.* [online] Available at: https://pdfs.semanticscholar.org/97d0/6dba6a70d4acfbaa3741ad477ff4ff8e1f27.pdf [Accessed 16 Sep. 2019].

Lupishko, D. and Belskaya, I. (1988). *On the Surface Composition of the M-Type Asteroids.* [ebook] Kharkov: Astronomical Observatory of Kharkov University, p.399. Available at: https://www.sciencedirect.com/science/article/pii/0019103589901863 [Accessed 2 Apr. 2018].

Metso. (2018). *Barmac® B Series™ Vertical Shaft Impact (VSI) crushers - Metso.* [online] Available at: https://www.metso.com/products/impact-crushers/vertical-shaft-impact-crusher-vsi-barmac-b/ [Accessed 14 May 2018].

Mineral Processing & Metallurgy. (2018). *Ore, Rock & Aggregate Screening (Complete Guide).* [online] Available at: https://www.911metallurgist.com/blog/screening [Accessed 10 Jun. 2018].

Musk, E. (2017). *Elon Musk Gives Updates on Mission to Mars.* [video] Available at: https://youtu.be/XcVpMJp9Th4 [Accessed 25 Mar. 2018].

NASA. (2020). *FY 2019 Budget.* [online] Available at: https://www.nasa.gov/content/fy-2019-budget [Accessed 19 Jan. 2020].

Olsen, L. and Carnes, B. (2001). *Screen Capacity Calculation.* Eugene: JCI, p.4.

O’Brien, M., Firth, B., Meyers, A., Nemeth, D. and Burger, A. (2002). *Improved Performance of Banana Screens in Drain and Rinse.* ACARP Project C8042. Australian Coal Association Research Program. (O’Brien et al., 2002).

O'Sullivan, C. and Cui, L. (2009). *Micromechanics of granular material response during load reversals: Combined DEM and experimental study.* Powder Technology, 193(3), pp.289-302.

O'Sullivan, C. and Bray, J., 2004. *Selecting a suitable time step for discrete element simulations that use the central difference time integration scheme. Engineering Computations*, [online] 21(2/3/4), pp.278-303. Available at: <https://www.researchgate.net/publication/241224401_Selecting_a_suitable_time_step_for_discrete_element_simulations_that_use_the_central_difference_time_integration_scheme> [Accessed 2 August 2020].

Padros, C. (2014). *Discrete Element Simulations with LIGGGHTS.* Master of Science. Swansea University.

Physicsnet.co.uk. (2018). *Young Modulus.* [online] Available at: http://physicsnet.co.uk/a-level-physics-as-a2/materials/young-modulus/ [Accessed 30 Jun. 2018].

Podlozhnyuk, A., Pirker, S. and Kloss, C., 2016. *Efficient implementation of superquadric particles in Discrete Element Method within an open-source framework. Computational Particle Mechanics*, [online] 4(1), pp.101-118. Available at: <https://link.springer.com/article/10.1007/s40571-016-0131-6> [Accessed 30 March 2020].

Popov, V., 2010. *Rigorous Treatment of Contact Problems – Hertzian Contact. Contact Mechanics and Friction*, [online] pp.55-70. Available at: <https://www.researchgate.net/publication/254653960_Rigorous_Treatment_of_Contact_Problems_-_Hertzian_Contact/link/0c96051fded463db02000000/download> [Accessed 19 March 2020].

Pstcc.edu. (2019). *The Coefficient of Kinetic Friction*. [online] Available at: http://www.pstcc.edu/departments/natural_behavioral_sciences/Web%20Physics/Experiment%2005web.htm [Accessed 7 Jul. 2019].

Ranjan, H. (2017). *A Methodology For DEM Parameter Calibration.* Masters. Purdue University.

Ren, B., Zhong, W., Chen, Y., Chen, X., Jin, B., Yuan, Z. and Lu, Y. (2012). *CFD-DEM simulation of spouting of corn-shaped particles.* Particuology, 10(5), pp.562-572.

Retsch.com. (2019). *Sieving methods of sieve analysis.* [online] Available at: https://www.retsch.com/applications/knowledge-base/sieve-analysis/ [Accessed 18 Nov. 2019].

Ross, S. (2001). *Near-Earth Asteroid Mining.* [ebook] Pasadena, California: California Institute of Technology. Available at: http://citeseerx.ist.psu.edu/viewdoc/download?doi=10.1.1.614.9343&rep=rep1&type=pdf [Accessed 25 Mar. 2018].

Sawant, G., Mohan, V. and Sawant, S. (2016). *Review Paper on Factors Affecting Efficiency of Vibration Screen.* 2nd ed. [ebook] Asian Journal of Convergence in Technology. Available at: http://www.asianssr.org [Accessed 19 Jul. 2018].

Science Plus (2016). *How Valuable is Asteroid Mining?.* [video] Available at: https://youtu.be/IkJqOKuGtIo [Accessed 25 Mar. 2018]. Screen Media. (2013). [ebook] Edenvale: FLSmidth, p.2. Available at: http://pumptech.co.za/products/FLSmidth_Screen_Media.pdf [Accessed 22 Jul. 2018].

Sebastian, B. and Tomasz, K. (2017). *New method and Device for Measuring Sliding Friction. In: International Scientific-Technical Conference "Innovations"*. [online] Lublin: Scientific Proceedings III, pp.141 - 142. Available at: http://innova-eng.eu/proceedings/2017/34.new%20method%20and%20device%20for%20measuring%20sliding%20friction.pdf [Accessed 7 Jul. 2019].

Silver.neep.wisc.edu. (2018). *What is Poisson's ratio?.* [online] Available at: http://silver.neep.wisc.edu/~lakes/PoissonIntro.html [Accessed 30 Jun. 2018].

Sonter, M. (1996). *The Technical and Economic Feasibility of Mining the Near-Earth Asteroids.* Masters of Science (Honours). University of Wollongong.

Space.com. (2018). *Is Space Big Enough for Two Asteroid-Mining Companies?.* [online] Available at: https://www.space.com/19380-asteroid-mining-spaceflight-competition.html [Accessed 25 Mar. 2018].

Sullivan, J. (2012). *Screening Theory and Practice.* [ebook] Triple/S Dynamics, p.1. Available at: https://www.sssdynamics.com/wp-content/themes/va/pdf/screeningtheory.pdf [Accessed 18 Nov. 2019].

Svoboda, J. and Fujita, T. (2003). Recent developments in magnetic methods of material separation. *Minerals Engineering,* 16(9), pp.785-792.

Sympatec. (2018). *QICPIC.* [online] Available at: https://www.sympatec.com/en/particle-measurement/sensors/dynamic-image-analysis/qicpic/ [Accessed 23 Jun. 2018.].

Tribology-abc.com. (2019). *How to measure friction?*. [online] Available at: http://www.tribology-abc.com/abc/friction.htm [Accessed 7 Jul. 2019].

Trio® Vertical Shaft Impact Crushers. (2016). [ebook] China: Weir Minerals, p.10. Available at: https://www.global.weir/products/product-catalogue/trio-mtv-series-modular-vertical-shaft-impactors/ [Accessed 14 May 2018].

Vibrating Screens. (1968). New York, N.Y: *Vibrating Screen Manufacturers Association.*

Wall, M. (2019). Starship and Super Heavy: SpaceX's Mars-Colonizing Transportation System. [online] Space.com. Available at: https://www.space.com/spacex-starship-super-heavy.html [Accessed 28 Nov. 2019].

Weerasekara, N., Powell, M., Cleary, P., Tavares, L., Evertsson, M., Morrison, R., Quist, J. and Carvalho, R. (2013). *The contribution of DEM to the science of comminution.* Powder Technology, 248, pp.3-24.

Williams, J. and Dwyer-Joyce, R., 2001. *Contact Between Solid Surfaces*. Boca Raton: CRC Press LLC.

Xinhai. (2018). *Vibrating Screen, Vibrating Screen Manufacturers, Vibrating Screen Working Principle , Vibrating Screening Machine – Xinhai.* [online] Available at: https://www.xinhaiepc.com/product/screens?utm_source=google&utm_medium=cpc&utm_network=g&utm_device=c&utm_criteria=Phrase&utm_adposition=1t3&utm_term=vibration%20screen&utm_content=a9_screening_vibrating_1&utm_campaign=cesh1_dewatering&epc1&gclid=CjwKCAjw1tDaBRAMEiwA0rYbSBrXpFSRILbUD77apj6znUswy6zcz8g2K3yIcvczq0GgFknFmeSy-RoC1tAQAvD_BwE [Accessed 22 Jul. 2018].

Yan, Z., Wilkinson, S.K., Stitt, E.H. *et al. Discrete element modelling (DEM) input parameters: understanding their impact on model predictions using statistical analysis. Comp. Part. Mech.* **2,** 283–299 (2015). https://doi.org/10.1007/s40571-015-0056-5

Zhou, C. and Ooi, J. (2009). *Numerical investigation of progressive development of granular pile with spherical and non-spherical particles.* Mechanics of Materials, 41(6), pp.707-714.

3D Printing for Beginners. (2018). *An introduction to DIY filament extrusion and extruders | 3D Printing for Beginners.* [online] Available at: http://3dprintingforbeginners.com/how-to-make-diy-filament-for-your-3d-printer/ [Accessed 22 Jul. 2018].

Appendix A – Design of Experiment Rig

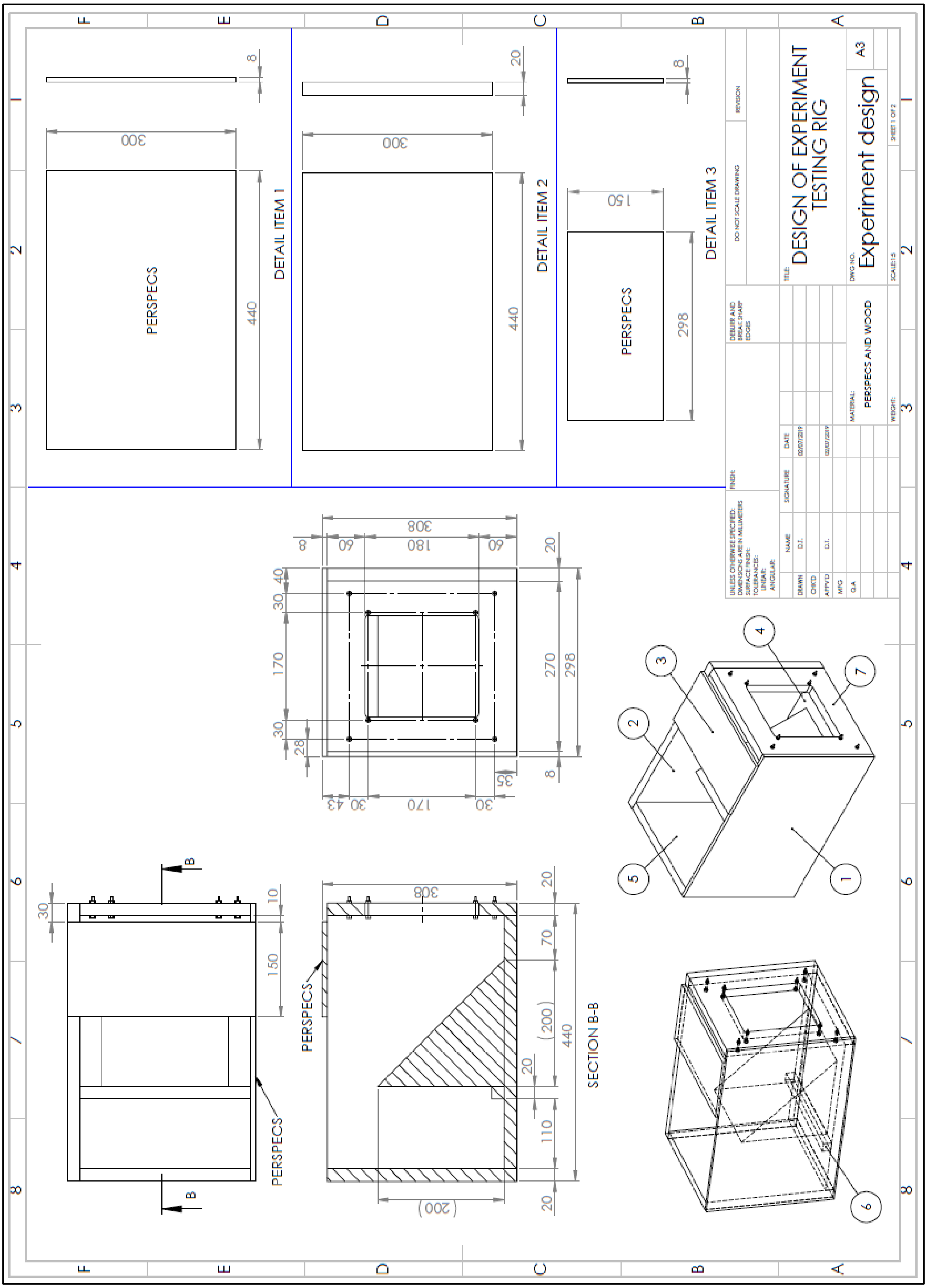

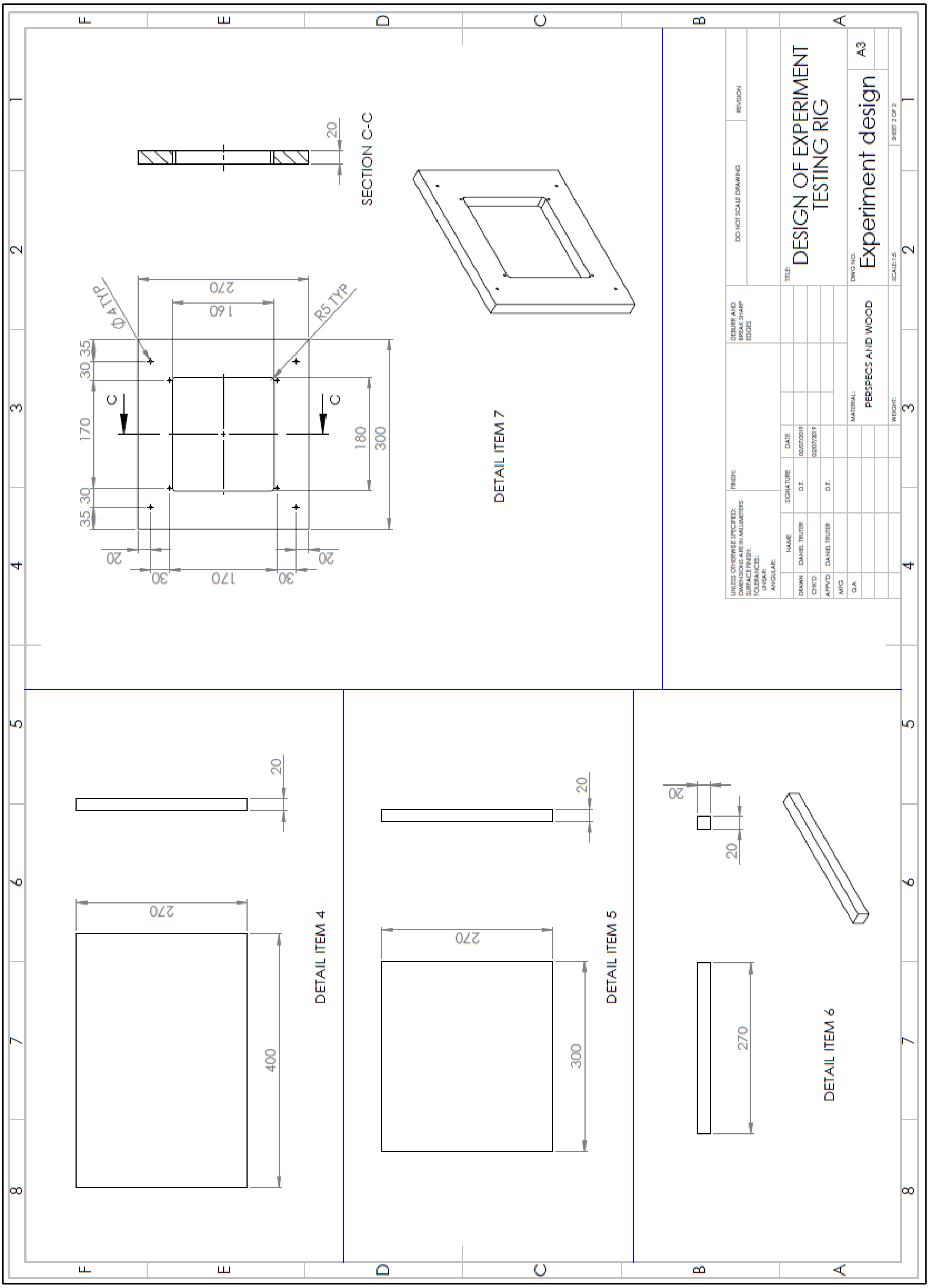
SECTION C-C
DETAIL ITEM 7
DETAIL ITEM 4
DETAIL ITEM 5
DETAIL ITEM 6
DESIGN OF EXPERIMENT TESTING RIG
Experiment design
PERSPECS AND WOOD
A3
DANIEL TRUTER
02/07/2019

Appendix B – Experiment Sieves

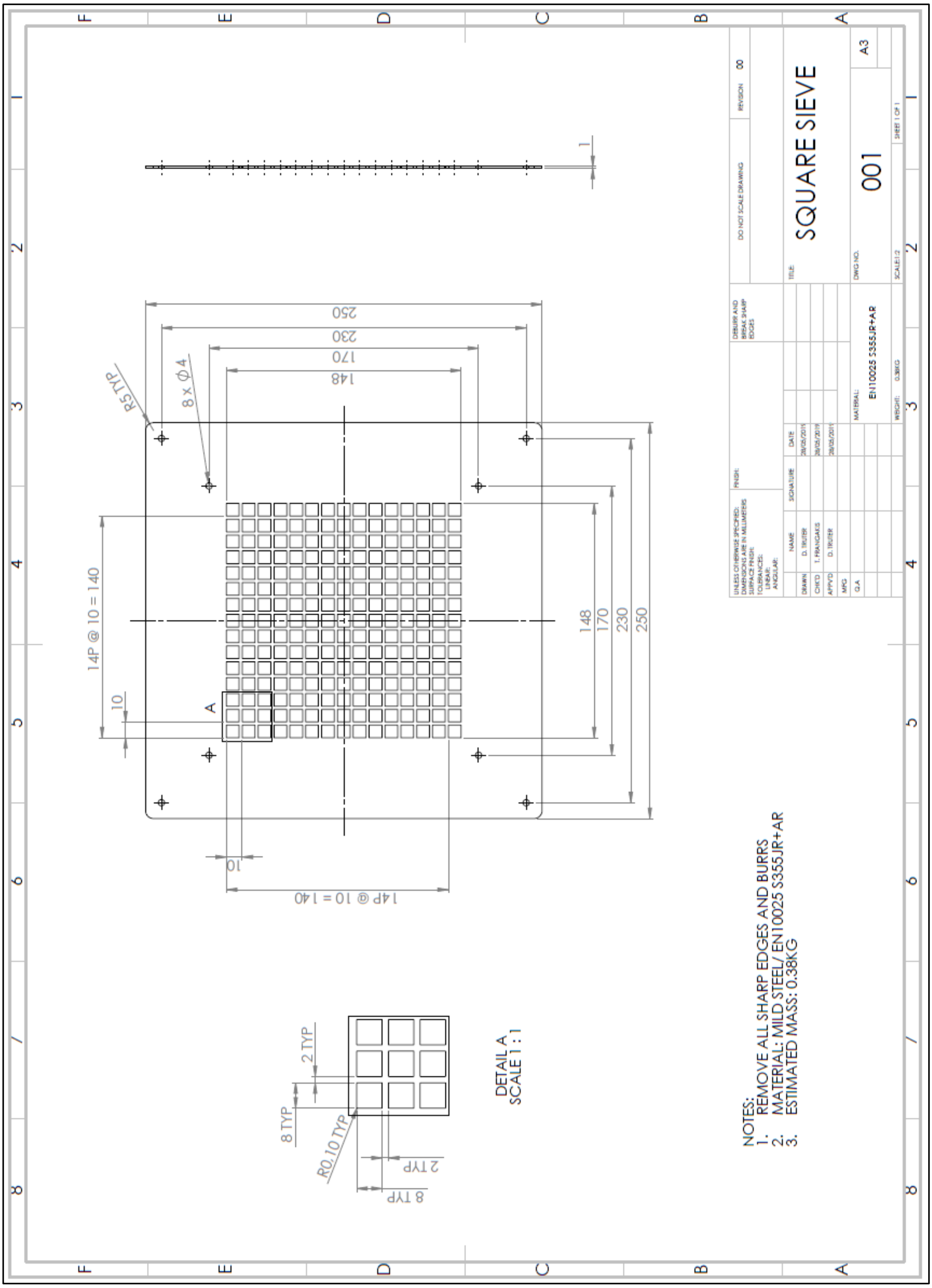

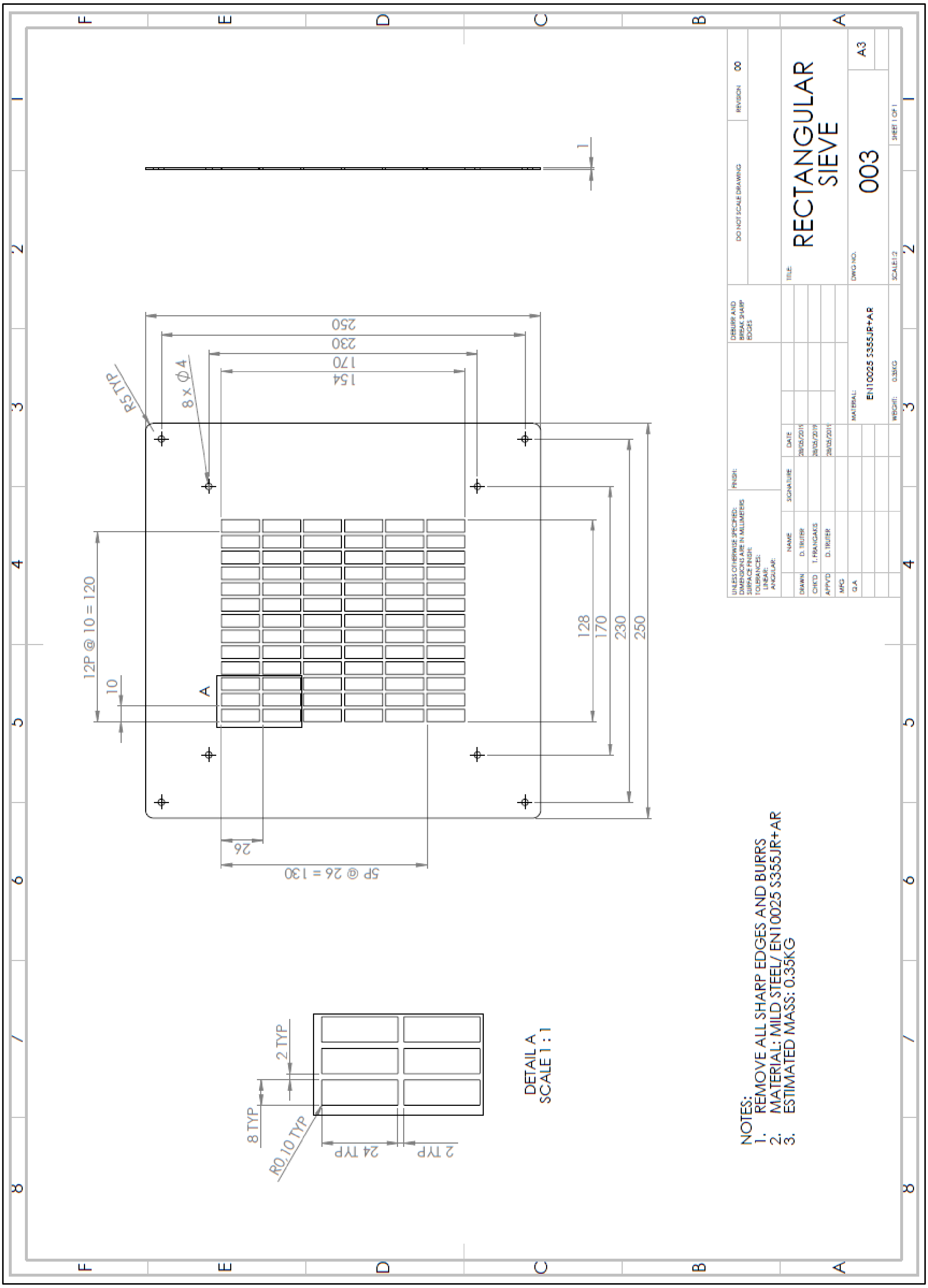
RECTANGULAR SIEVE
003
A3
DO NOT SCALE DRAWING
REVISION 00
DEBURR AND BREAK SHARP EDGES
MATERIAL: EN10025 S355JR+AR
DRAWN D. TRUTER
CHK'D T. FRANGAKIS
APPV'D D. TRUTER
250
230
170
154
R5 TYP
8 x Ø4
12P @ 10 = 120
10
A
128
170
230
250
26
5P @ 26 = 130
2 TYP
8 TYP
R0.10 TYP
24 TYP
2 TYP
DETAIL A
SCALE 1 : 1
NOTES:
1. REMOVE ALL SHARP EDGES AND BURRS
2. MATERIAL: MILD STEEL/ EN10025 S355JR+AR
3. ESTIMATED MASS: 0.35KG

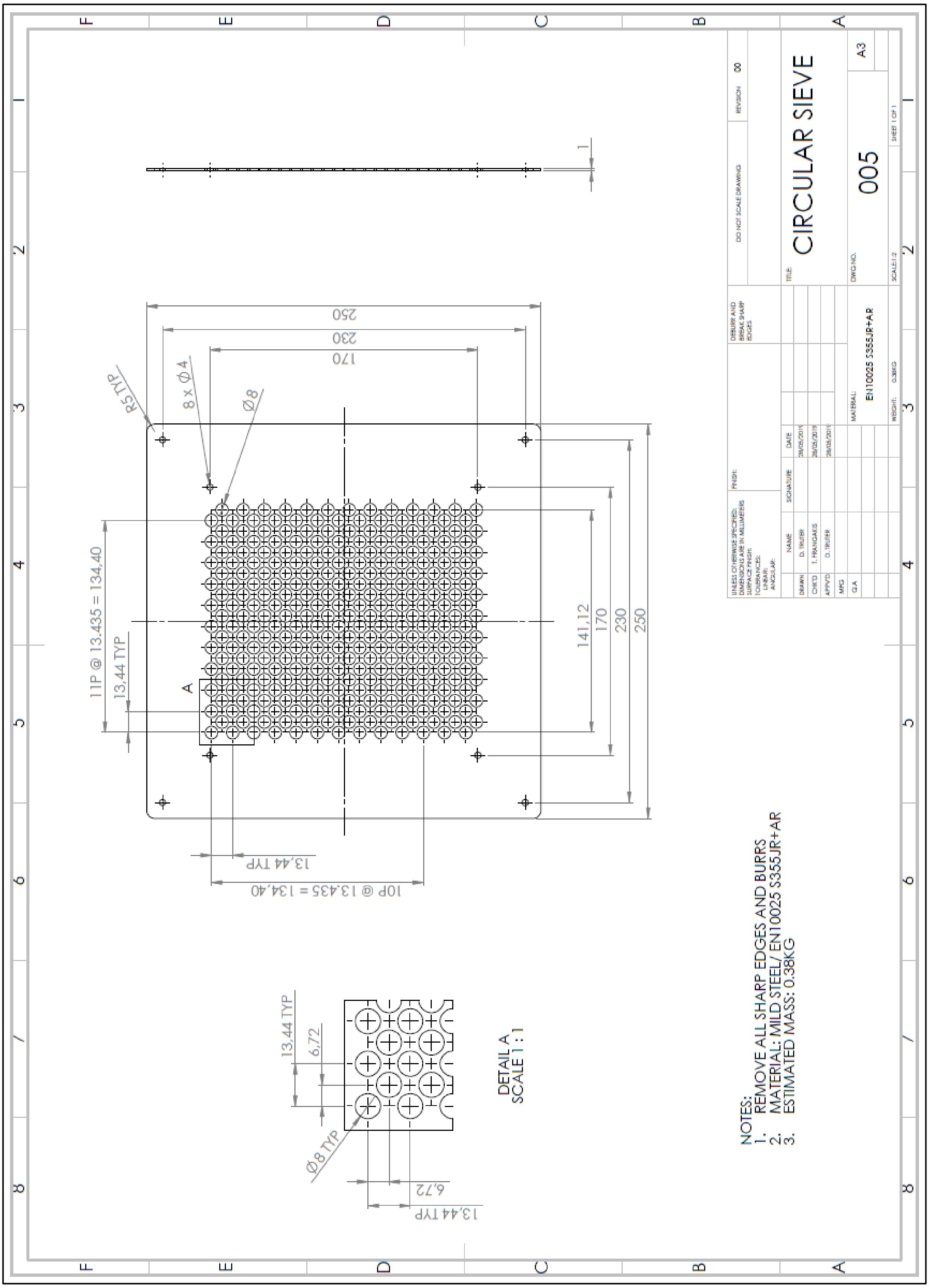

CIRCULAR SIEVE
005
A3
DO NOT SCALE DRAWING
REVISION 00
DEBURR AND BREAK SHARP EDGES
EN10025 S355JR+AR
250
230
170
141,12
R5 TYP
8 x Ø4
Ø8
11P @ 13.435 = 134,40
10P @ 13.435 = 134,40
13,44 TYP
6,72
Ø8 TYP
DETAIL A
SCALE 1 : 1
NOTES:
1. REMOVE ALL SHARP EDGES AND BURRS
2. MATERIAL: MILD STEEL/ EN10025 S355JR+AR
3. ESTIMATED MASS: 0.38KG

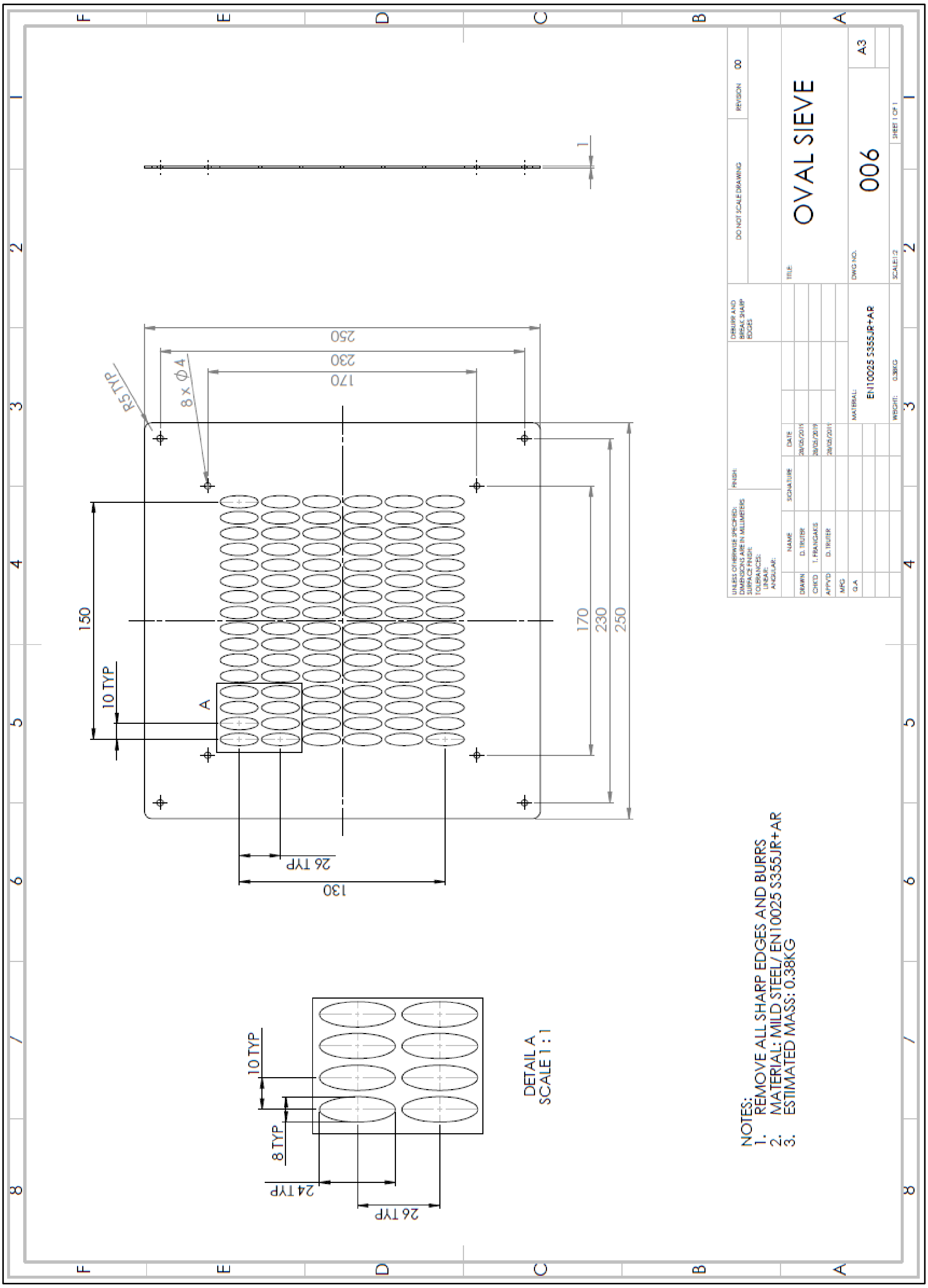

OVAL SIEVE
DO NOT SCALE DRAWING
REVISION 00
TITLE:
DWG NO.
006
A3
SCALE:1:2
SHEET 1 OF 1
WEIGHT: 0.38KG
MATERIAL:
EN10025 S355JR+AR
DEBURR AND BREAK SHARP EDGES
FINISH:
NAME
SIGNATURE
DATE
DRAWN
CHK'D
APPV'D
MFG
Q.A
250
230
170
8 x Ø4
R5 TYP
150
10 TYP
26 TYP
130
1
A
DETAIL A
SCALE 1 : 1
10 TYP
8 TYP
24 TYP
26 TYP
NOTES:
1. REMOVE ALL SHARP EDGES AND BURRS
2. MATERIAL: MILD STEEL/ EN10025 S355JR+AR
3. ESTIMATED MASS: 0.38KG

Appendix C – DEM Space Case Sieves

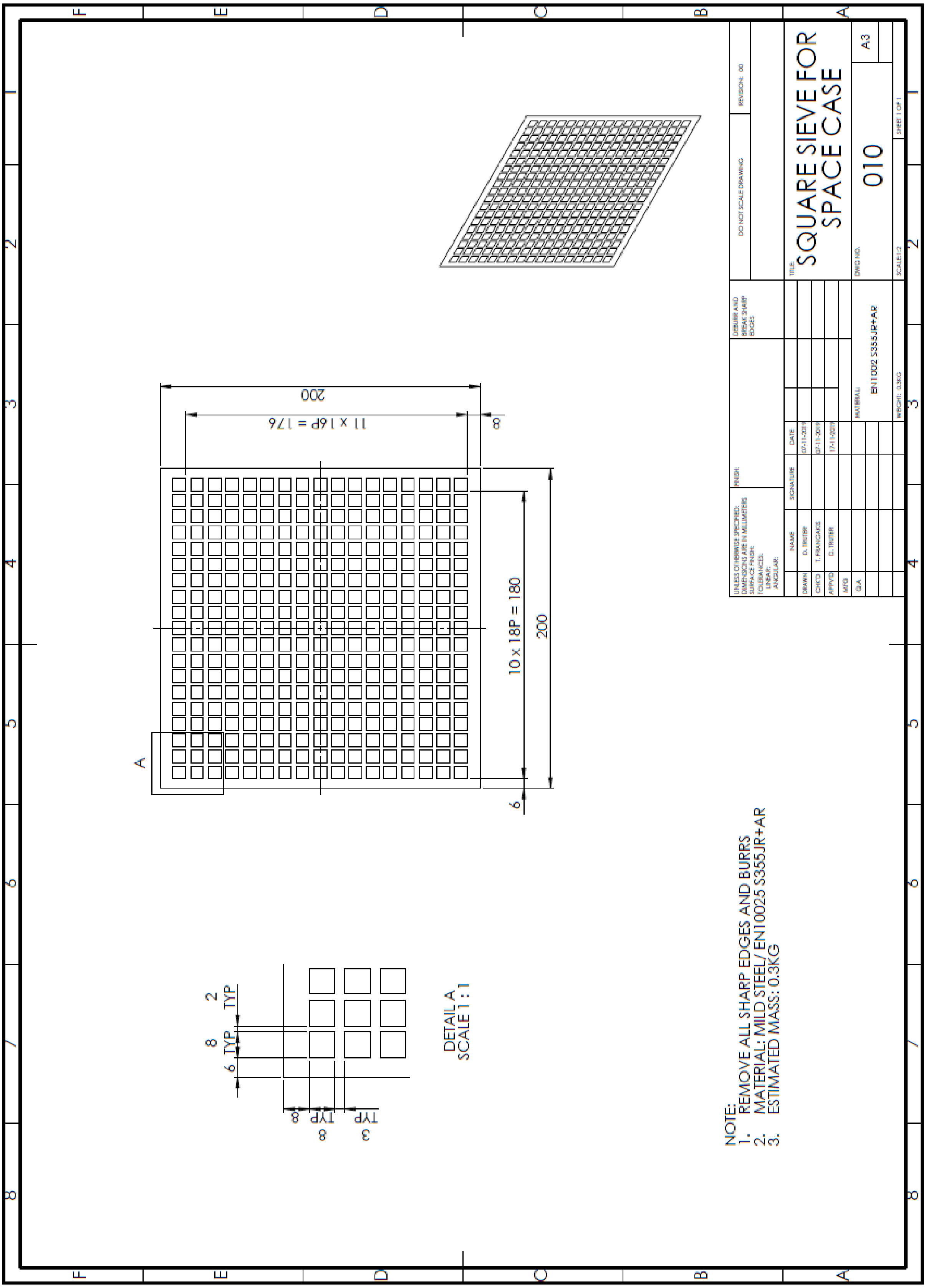

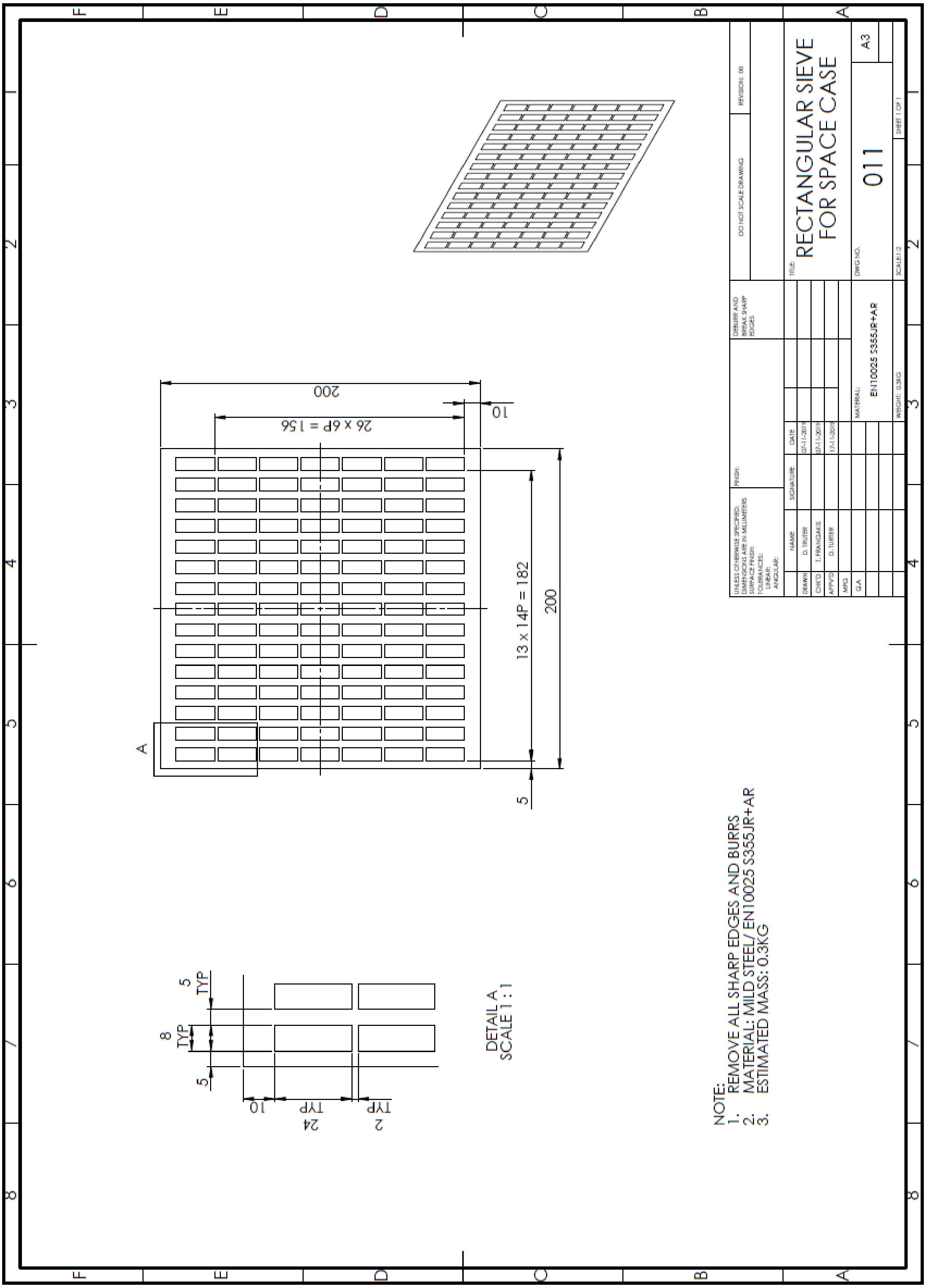

RECTANGULAR SIEVE FOR SPACE CASE
DWG NO. 011
A3
REVISION: 00
DO NOT SCALE DRAWING
DEBURR AND BREAK SHARP EDGES
UNLESS OTHERWISE SPECIFIED: DIMENSIONS ARE IN MILLIMETERS
DRAWN D. TRUTER
CHK'D T. FRANGAKIS
APPV'D D. TURTER
MATERIAL: EN10025 S355JR+AR
SCALE:1:2
SHEET 1 OF 1
200
26 x 6P = 156
10
13 x 14P = 182
200
5
A
DETAIL A
SCALE 1 : 1
5 TYP
8 TYP
5
10
24 TYP
2 TYP
NOTE:
1. REMOVE ALL SHARP EDGES AND BURRS
2. MATERIAL: MILD STEEL/ EN10025 S355JR+AR
3. ESTIMATED MASS: 0.3KG

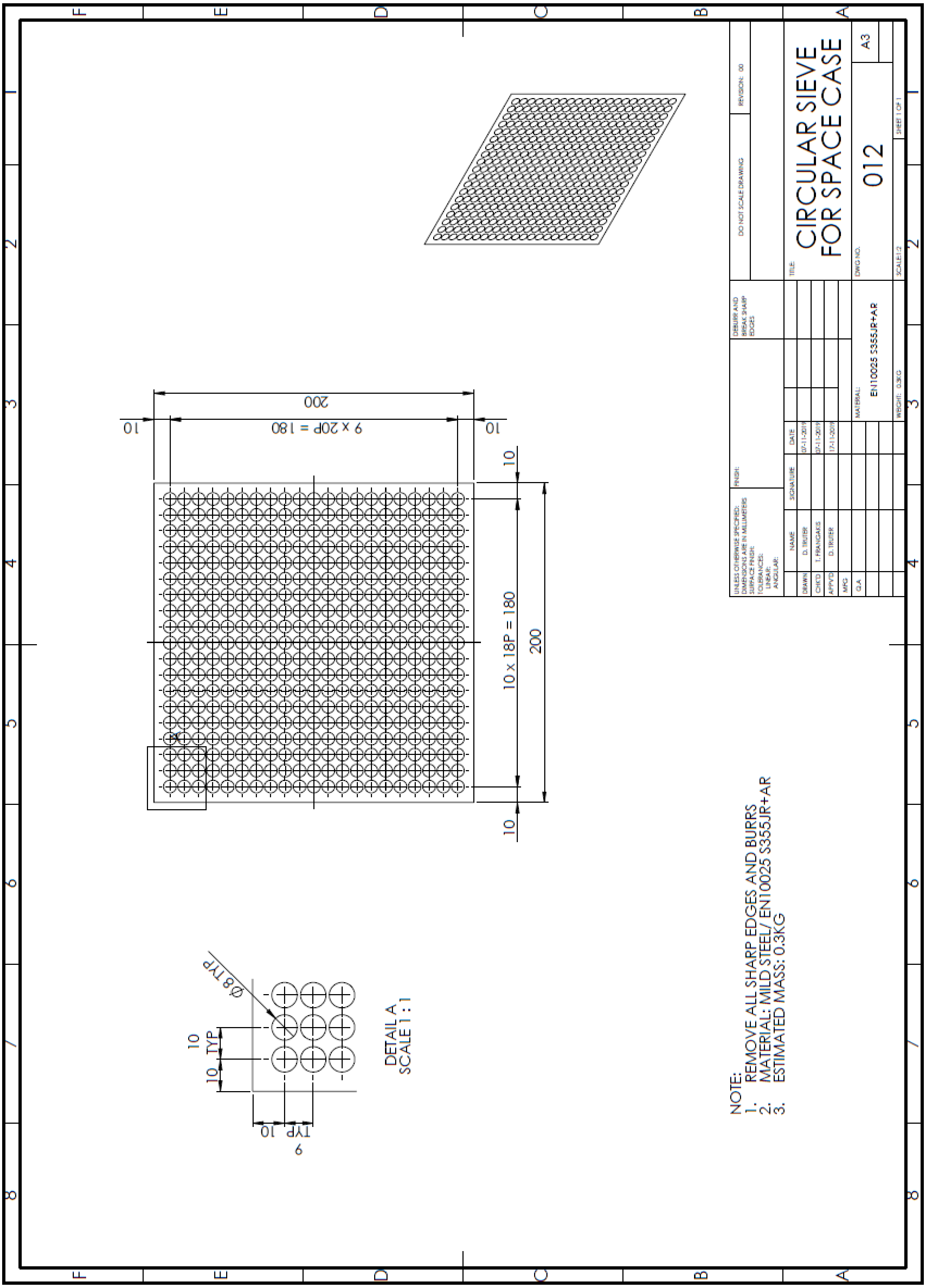
CIRCULAR SIEVE FOR SPACE CASE
012
A3
EN10025 S355JR+AR
200
9 x 20P = 180
10
10 x 18P = 180
Ø8 TYP
10 TYP
DETAIL A
SCALE 1 : 1
NOTE:
1. REMOVE ALL SHARP EDGES AND BURRS
2. MATERIAL: MILD STEEL/ EN10025 S355JR+AR
3. ESTIMATED MASS: 0.3KG

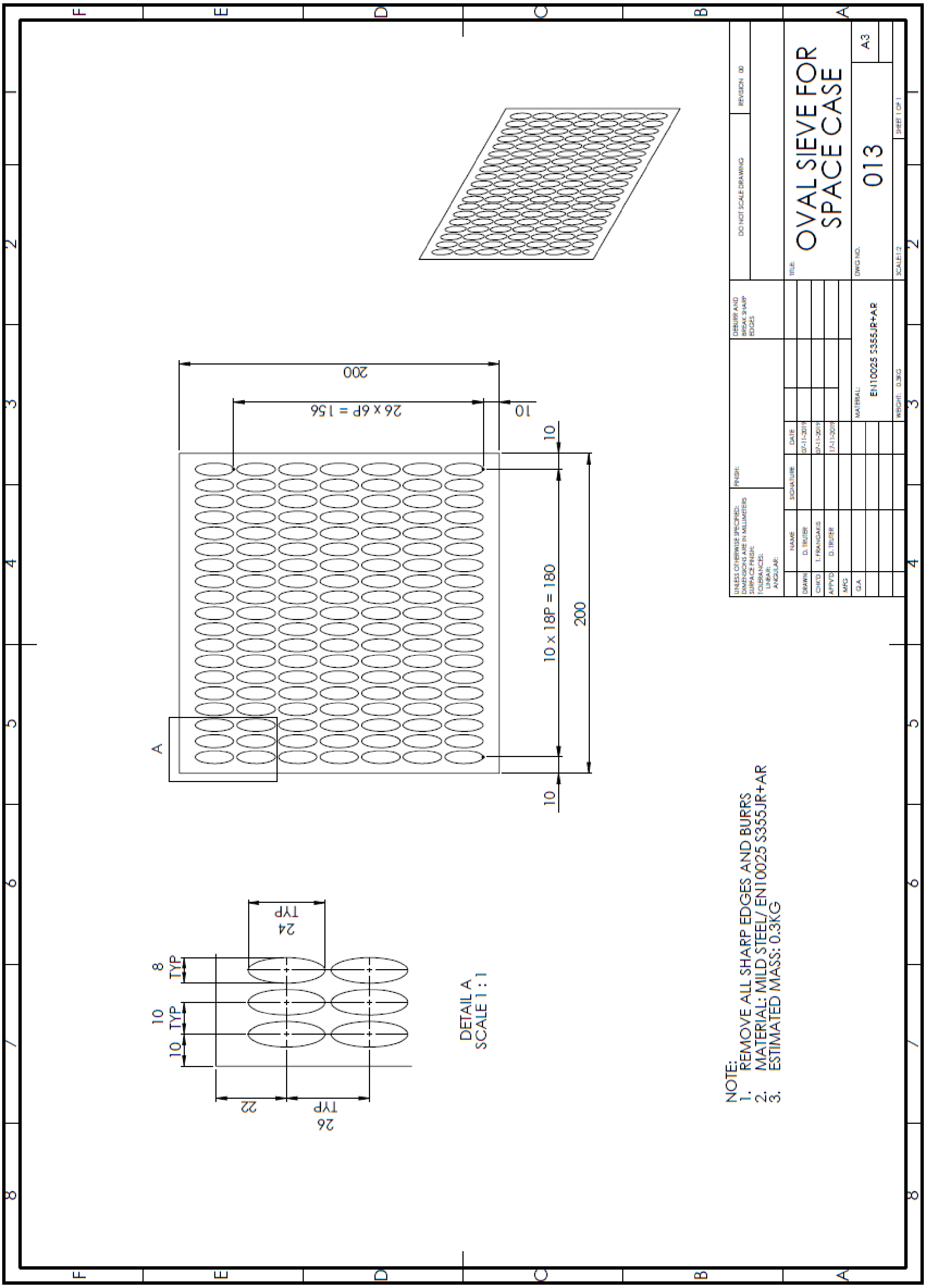

OVAL SIEVE FOR SPACE CASE
013
A3
DWG NO.
TITLE:
MATERIAL:
EN10025 S355JR+AR
WEIGHT: 0.3KG
SCALE:1:2
SHEET 1 OF 1
DO NOT SCALE DRAWING
REVISION 00
DEBURR AND BREAK SHARP EDGES
FINISH:
NAME
SIGNATURE
DATE
DRAWN
D. TRUTER
07-11-2019
CHK'D
T. FRANGAKIS
07-11-2019
APPV'D
D. TRUTER
17-11-2019
MFG
Q.A
200
26 x 6P = 156
10
10 x 18P = 180
A
DETAIL A
SCALE 1 : 1
24
TYP
8
22
26
NOTE:
1. REMOVE ALL SHARP EDGES AND BURRS
2. MATERIAL: MILD STEEL/ EN10025 S355JR+AR
3. ESTIMATED MASS: 0.3KG

Appendix D – DEM Parameter Calibration

Procedure for DEM parameter calibration:

1. The particle (yellow plastic pellet in this case) calibration started with running all the simulations with the oval sieve and the results recorded.
2. The cells were highlighted with the following colour coding:
   a. Blue – Near the physical experiment result or theoretical result (within approximately 10%)
   b. Orange – Within approximately 20% of the physical experiment result or theoretical result
   c. Red – Nowhere near the correct result
3. The yellow plastic pellets were tested on the next sieve (the circular sieve in this instance) on only the cells that were previously identified as blue or orange.
4. This procedure continued for the last two sieves while removing the coefficients which were nowhere near the correct results thereby leaving only the most correct answers.
5. A calculation was then performed regarding the closest correct combinations and this produced the coefficients which were selected.

Yellow Plastic Pellet: Coefficient of Restitution = 0.7 and Coefficient of Static Friction = 0.1

Yellow Pellet Coefficient Calibration with the Square Sieve (Experiment Efficiency = 16%, Theory = 14%)

CoR	CoSF	Particles Passed	% Efficiency	CoR	CoSF	Particles Passed	% Efficiency	CoR	CoSF	Particles Passed	% Efficiency	CoR	CoSF	Particles Passed	% Efficiency	CoR	CoSF	Particles Passed	% Efficiency	CoR	CoSF	Particles Passed	% Efficiency	CoR	CoSF	Particles Passed	% Efficiency	CoR	CoSF	Particles Passed	% Efficiency	CoR	CoSF	Particles Passed	% Efficiency
0,1	0,1	-	#VALUE!	0,2	0,1	-	#VALUE!	0,3	0,1	-	#VALUE!	0,4	0,1	7	0,14	0,5	0,1	-	#VALUE!	0,6	0,1	-	#VALUE!	0,7	0,1	7	0,14	0,8	0,1	-	#VALUE!	0,9	0,1	-	#VALUE!
0,1	0,2	-	#VALUE!	0,2	0,2	-	#VALUE!	0,3	0,2	-	#VALUE!	0,4	0,2	-	#VALUE!	0,5	0,2	-	#VALUE!	0,6	0,2	2	0,04	0,7	0,2		0	0,8	0,2		0	0,9	0,2	-	#VALUE!
0,1	0,3	-	#VALUE!	0,2	0,3	-	#VALUE!	0,3	0,3	-	#VALUE!	0,4	0,3	-	#VALUE!	0,5	0,3	-	#VALUE!	0,6	0,3		0	0,7	0,3	6	0,12	0,8	0,3		0	0,9	0,3	-	#VALUE!
0,1	0,4	-	#VALUE!	0,2	0,4	-	#VALUE!	0,3	0,4	-	#VALUE!	0,4	0,4	-	#VALUE!	0,5	0,4	-	#VALUE!	0,6	0,4	-	#VALUE!	0,7	0,4	-	#VALUE!	0,8	0,4	-	#VALUE!	0,9	0,4		0
0,1	0,5	-	#VALUE!	0,2	0,5	-	#VALUE!	0,3	0,5	-	#VALUE!	0,4	0,5	5	0,1	0,5	0,5	5	0,1	0,6	0,5	-	#VALUE!	0,7	0,5		0	0,8	0,5		0	0,9	0,5	-	#VALUE!
0,1	0,6	-	#VALUE!	0,2	0,6	-	#VALUE!	0,3	0,6	-	#VALUE!	0,4	0,6	5	0,1	0,5	0,6	-	#VALUE!	0,6	0,6		0	0,7	0,6	-	#VALUE!	0,8	0,6	4	0,08	0,9	0,6	-	#VALUE!
0,1	0,7	-	#VALUE!	0,2	0,7	-	#VALUE!	0,3	0,7	-	#VALUE!	0,4	0,7	-	#VALUE!	0,5	0,7	5	0,1	0,6	0,7		0	0,7	0,7	-	#VALUE!	0,8	0,7		0	0,9	0,7	-	#VALUE!
0,1	0,8	-	#VALUE!	0,2	0,8	-	#VALUE!	0,3	0,8	-	#VALUE!	0,4	0,8	-	#VALUE!	0,5	0,8	4	0,08	0,6	0,8		0	0,7	0,8	-	#VALUE!	0,8	0,8	-	#VALUE!	0,9	0,8	-	#VALUE!
0,1	0,9	-	#VALUE!	0,2	0,9	-	#VALUE!	0,3	0,9	-	#VALUE!	0,4	0,9	-	#VALUE!	0,5	0,9	4	0,08	0,6	0,9	-	#VALUE!	0,7	0,9		0	0,8	0,9	-	#VALUE!	0,9	0,9	-	#VALUE!

Yellow Pellet Coefficient Calibration with the Rectangular Sieve (Experiment Efficiency = 31%, Theory = 29%)

CoR	CoSF	Particles Passed	% Efficiency	CoR	CoSF	Particles Passed	% Efficiency	CoR	CoSF	Particles Passed	% Efficiency	CoR	CoSF	Particles Passed	% Efficiency	CoR	CoSF	Particles Passed	% Efficiency	CoR	CoSF	Particles Passed	% Efficiency	CoR	CoSF	Particles Passed	% Efficiency	CoR	CoSF	Particles Passed	% Efficiency	CoR	CoSF	Particles Passed	% Efficiency
0,1	0,1	-	#VALUE!	0,2	0,1	-	#VALUE!	0,3	0,1	-	#VALUE!	0,4	0,1	13	0,26	0,5	0,1	-	#VALUE!	0,6	0,1	-	#VALUE!	0,7	0,1	13	0,26	0,8	0,1	-	#VALUE!	0,9	0,1	-	#VALUE!
0,1	0,2	-	#VALUE!	0,2	0,2	-	#VALUE!	0,3	0,2	-	#VALUE!	0,4	0,2	-	#VALUE!	0,5	0,2	-	#VALUE!	0,6	0,2	13	0,26	0,7	0,2	10	0,2	0,8	0,2	10	0,2	0,9	0,2	-	#VALUE!
0,1	0,3	-	#VALUE!	0,2	0,3	-	#VALUE!	0,3	0,3	-	#VALUE!	0,4	0,3	-	#VALUE!	0,5	0,3	-	#VALUE!	0,6	0,3	11	0,22	0,7	0,3	13	0,26	0,8	0,3	9	0,18	0,9	0,3	-	#VALUE!
0,1	0,4	-	#VALUE!	0,2	0,4	-	#VALUE!	0,3	0,4	-	#VALUE!	0,4	0,4	-	#VALUE!	0,5	0,4	-	#VALUE!	0,6	0,4	-	#VALUE!	0,7	0,4	-	#VALUE!	0,8	0,4	-	#VALUE!	0,9	0,4	8	0,16
0,1	0,5	-	#VALUE!	0,2	0,5	-	#VALUE!	0,3	0,5	-	#VALUE!	0,4	0,5	13	0,26	0,5	0,5	7	0,14	0,6	0,5	-	#VALUE!	0,7	0,5	9	0,18	0,8	0,5	7	0,14	0,9	0,5	-	#VALUE!
0,1	0,6	-	#VALUE!	0,2	0,6	-	#VALUE!	0,3	0,6	-	#VALUE!	0,4	0,6	14	0,28	0,5	0,6	-	#VALUE!	0,6	0,6	10	0,2	0,7	0,6	-	#VALUE!	0,8	0,6	15	0,3	0,9	0,6	-	#VALUE!
0,1	0,7	-	#VALUE!	0,2	0,7	-	#VALUE!	0,3	0,7	-	#VALUE!	0,4	0,7	-	#VALUE!	0,5	0,7	8	0,16	0,6	0,7	7	0,14	0,7	0,7	-	#VALUE!	0,8	0,7	8	0,16	0,9	0,7	-	#VALUE!
0,1	0,8	-	#VALUE!	0,2	0,8	-	#VALUE!	0,3	0,8	-	#VALUE!	0,4	0,8	-	#VALUE!	0,5	0,8	9	0,18	0,6	0,8	10	0,2	0,7	0,8	-	#VALUE!	0,8	0,8	-	#VALUE!	0,9	0,8	-	#VALUE!
0,1	0,9	-	#VALUE!	0,2	0,9	-	#VALUE!	0,3	0,9	-	#VALUE!	0,4	0,9	-	#VALUE!	0,5	0,9	8	0,16	0,6	0,9	-	#VALUE!	0,7	0,9	9	0,18	0,8	0,9	-	#VALUE!	0,9	0,9	-	#VALUE!

Yellow Pellet Coefficient Calibration with the Circular Sieve (Experiment Efficiency = 11%, Theory = 11%)

CoR	CoSF	Particles Passed	% Efficiency	CoR	CoSF	Particles Passed	% Efficiency	CoR	CoSF	Particles Passed	% Efficiency	CoR	CoSF	Particles Passed	% Efficiency	CoR	CoSF	Particles Passed	% Efficiency	CoR	CoSF	Particles Passed	% Efficiency	CoR	CoSF	Particles Passed	% Efficiency	CoR	CoSF	Particles Passed	% Efficiency	CoR	CoSF	Particles Passed	% Efficiency
0,1	0,1	-	#VALUE!	0,2	0,1	-	#VALUE!	0,3	0,1	-	#VALUE!	0,4	0,1	7	0,14	0,5	0,1	-	#VALUE!	0,6	0,1	-	#VALUE!	0,7	0,1	5	0,1	0,8	0,1	-	#VALUE!	0,9	0,1	-	#VALUE!
0,1	0,2	-	#VALUE!	0,2	0,2	-	#VALUE!	0,3	0,2	-	#VALUE!	0,4	0,2	-	#VALUE!	0,5	0,2	-	#VALUE!	0,6	0,2	5	0,1	0,7	0,2	4	0,08	0,8	0,2	4	0,08	0,9	0,2	-	#VALUE!
0,1	0,3	-	#VALUE!	0,2	0,3	-	#VALUE!	0,3	0,3	-	#VALUE!	0,4	0,3	-	#VALUE!	0,5	0,3	-	#VALUE!	0,6	0,3	4	0,08	0,7	0,3	5	0,1	0,8	0,3	5	0,1	0,9	0,3	3	0,06
0,1	0,4	-	#VALUE!	0,2	0,4	-	#VALUE!	0,3	0,4	-	#VALUE!	0,4	0,4	-	#VALUE!	0,5	0,4	-	#VALUE!	0,6	0,4	1	0,02	0,7	0,4	2	0,04	0,8	0,4	1	0,02	0,9	0,4	5	0,1
0,1	0,5	-	#VALUE!	0,2	0,5	-	#VALUE!	0,3	0,5	-	#VALUE!	0,4	0,5	4	0,08	0,5	0,5	4	0,08	0,6	0,5	3	0,06	0,7	0,5	4	0,08	0,8	0,5	5	0,1	0,9	0,5	-	#VALUE!
0,1	0,6	-	#VALUE!	0,2	0,6	-	#VALUE!	0,3	0,6	-	#VALUE!	0,4	0,6	5	0,1	0,5	0,6	-	#VALUE!	0,6	0,6	4	0,08	0,7	0,6	2	0,04	0,8	0,6	7	0,14	0,9	0,6	2	0,04
0,1	0,7	-	#VALUE!	0,2	0,7	-	#VALUE!	0,3	0,7	-	#VALUE!	0,4	0,7	3	0,06	0,5	0,7	5	0,1	0,6	0,7	4	0,08	0,7	0,7	-	#VALUE!	0,8	0,7	4	0,08	0,9	0,7	3	0,06
0,1	0,8	-	#VALUE!	0,2	0,8	-	#VALUE!	0,3	0,8	-	#VALUE!	0,4	0,8	2	0,04	0,5	0,8	4	0,08	0,6	0,8	5	0,1	0,7	0,8	-	#VALUE!	0,8	0,8	-	#VALUE!	0,9	0,8	-	#VALUE!
0,1	0,9	-	#VALUE!	0,2	0,9	-	#VALUE!	0,3	0,9	-	#VALUE!	0,4	0,9	-	#VALUE!	0,5	0,9	7	0,14	0,6	0,9	-	#VALUE!	0,7	0,9	4	0,08	0,8	0,9	-	#VALUE!	0,9	0,9	3	0,06

Yellow Pellet Coefficient Calibration with the Oval Sieve (Experiment Efficiency = 24%, Theory = 22%)

CoR	CoSF	Particles Passed	% Efficiency	CoR	CoSF	Particles Passed	% Efficiency	CoR	CoSF	Particles Passed	% Efficiency	CoR	CoSF	Particles Passed	% Efficiency	CoR	CoSF	Particles Passed	% Efficiency	CoR	CoSF	Particles Passed	% Efficiency	CoR	CoSF	Particles Passed	% Efficiency	CoR	CoSF	Particles Passed	% Efficiency	CoR	CoSF	Particles Passed	% Efficiency
0,1	0,1	0	0	0,2	0,1	20	0,4	0,3	0,1	17	0,34	0,4	0,1	10	0,2	0,5	0,1	18	0,36	0,6	0,1	15	0,3	0,7	0,1	12	0,24	0,8	0,1	9	0,18	0,9	0,1	21	0,42
0,1	0,2	0	0	0,2	0,2	10	0,2	0,3	0,2	16	0,32	0,4	0,2	16	0,32	0,5	0,2	19	0,38	0,6	0,2	10	0,2	0,7	0,2	10	0,2	0,8	0,2	13	0,26	0,9	0,2	8	0,16
0,1	0,3	1	0,02	0,2	0,3	11	0,22	0,3	0,3	13	0,26	0,4	0,3	15	0,3	0,5	0,3	16	0,32	0,6	0,3	11	0,22	0,7	0,3	12	0,24	0,8	0,3	14	0,28	0,9	0,3	14	0,28
0,1	0,4	2	0,04	0,2	0,4	8	0,16	0,3	0,4	13	0,26	0,4	0,4	16	0,32	0,5	0,4	16	0,32	0,6	0,4	10	0,2	0,7	0,4	10	0,2	0,8	0,4	11	0,22	0,9	0,4	13	0,26
0,1	0,5	3	0,06	0,2	0,5	10	0,2	0,3	0,5	12	0,24	0,4	0,5	11	0,22	0,5	0,5	13	0,26	0,6	0,5	11	0,22	0,7	0,5	14	0,28	0,8	0,5	10	0,2	0,9	0,5	8	0,16
0,1	0,6	1	0,02	0,2	0,6	7	0,14	0,3	0,6	10	0,2	0,4	0,6	12	0,24	0,5	0,6	16	0,32	0,6	0,6	14	0,28	0,7	0,6	10	0,2	0,8	0,6	13	0,26	0,9	0,6	12	0,24
0,1	0,7	2	0,04	0,2	0,7	8	0,16	0,3	0,7	10	0,2	0,4	0,7	13	0,26	0,5	0,7	14	0,28	0,6	0,7	12	0,24	0,7	0,7	8	0,16	0,8	0,7	12	0,24	0,9	0,7	14	0,28
0,1	0,8	3	0,06	0,2	0,8	9	0,18	0,3	0,8	13	0,26	0,4	0,8	11	0,22	0,5	0,8	14	0,28	0,6	0,8	12	0,24	0,7	0,8	6	0,12	0,8	0,8	8	0,16	0,9	0,8	8	0,16
0,1	0,9	1	0,02	0,2	0,9	8	0,16	0,3	0,9	11	0,22	0,4	0,9	6	0,12	0,5	0,9	14	0,28	0,6	0,9	9	0,18	0,7	0,9	10	0,2	0,8	0,9	17	0,34	0,9	0,9	10	0,2

White Pellet: Coefficient of Restitution = 0.6 and Coefficient of Static Friction = 0.6

White Pellet Coefficient Calibration with the Square Sieve (Experiment Efficiency = 17%, Theory = 14%)

CoR	CoSF	Particles Passed	% Efficiency	CoR	CoSF	Particles Passed	% Efficiency	CoR	CoSF	Particles Passed	% Efficiency	CoR	CoSF	Particles Passed	% Efficiency	CoR	CoSF	Particles Passed	% Efficiency	CoR	CoSF	Particles Passed	% Efficiency	CoR	CoSF	Particles Passed	% Efficiency	CoR	CoSF	Particles Passed	% Efficiency	CoR	CoSF	Particles Passed	% Efficiency
0,1	0,1	0	0	0,2	0,1	-	#VALUE!	0,3	0,1	-	#VALUE!	0,4	0,1	-	#VALUE!	0,5	0,1	5	0,1	0,6	0,1	-	#VALUE!	0,7	0,1	-	#VALUE!	0,8	0,1	-	#VALUE!	0,9	0,1	-	#VALUE!
0,1	0,2	-	#VALUE!	0,2	0,2	-	#VALUE!	0,3	0,2	-	#VALUE!	0,4	0,2	-	#VALUE!	0,5	0,2	6	0,12	0,6	0,2	-	#VALUE!	0,7	0,2	2	0,04	0,8	0,2	-	#VALUE!	0,9	0,2	5	0,1
0,1	0,3	-	#VALUE!	0,2	0,3	-	#VALUE!	0,3	0,3	-	#VALUE!	0,4	0,3	-	#VALUE!	0,5	0,3	-	#VALUE!	0,6	0,3	-	#VALUE!	0,7	0,3	-	#VALUE!	0,8	0,3	-	#VALUE!	0,9	0,3	-	#VALUE!
0,1	0,4	-	#VALUE!	0,2	0,4	-	#VALUE!	0,3	0,4	6	0,12	0,4	0,4	-	#VALUE!	0,5	0,4	-	#VALUE!	0,6	0,4	-	#VALUE!	0,7	0,4	-	#VALUE!	0,8	0,4	-	#VALUE!	0,9	0,4	-	#VALUE!
0,1	0,5	0	0	0,2	0,5	-	#VALUE!	0,3	0,5	-	#VALUE!	0,4	0,5	-	#VALUE!	0,5	0,5	-	#VALUE!	0,6	0,5	-	#VALUE!	0,7	0,5	-	#VALUE!	0,8	0,5	4	0,08	0,9	0,5	-	#VALUE!
0,1	0,6	-	#VALUE!	0,2	0,6	-	#VALUE!	0,3	0,6	-	#VALUE!	0,4	0,6	-	#VALUE!	0,5	0,6	-	#VALUE!	0,6	0,6	7	0,14	0,7	0,6	-	#VALUE!	0,8	0,6	-	#VALUE!	0,9	0,6	-	#VALUE!
0,1	0,7	-	#VALUE!	0,2	0,7	-	#VALUE!	0,3	0,7	5	0,1	0,4	0,7	6	0,12	0,5	0,7	-	#VALUE!	0,6	0,7	-	#VALUE!	0,7	0,7	-	#VALUE!	0,8	0,7	-	#VALUE!	0,9	0,7	-	#VALUE!
0,1	0,8	-	#VALUE!	0,2	0,8	-	#VALUE!	0,3	0,8	-	#VALUE!	0,4	0,8	-	#VALUE!	0,5	0,8	-	#VALUE!	0,6	0,8	-	#VALUE!	0,7	0,8	-	#VALUE!	0,8	0,8	-	#VALUE!	0,9	0,8	-	#VALUE!
0,1	0,9	-	#VALUE!	0,2	0,9	-	#VALUE!	0,3	0,9	-	#VALUE!	0,4	0,9	-	#VALUE!	0,5	0,9	-	#VALUE!	0,6	0,9	-	#VALUE!	0,7	0,9	-	#VALUE!	0,8	0,9	-	#VALUE!	0,9	0,9	-	#VALUE!

White Pellet Coefficient Calibration with the Rectangular Sieve (Experiment Efficiency = 37%, Theory = 29%)

CoR	CoSF	Particles Passed	% Efficiency	CoR	CoSF	Particles Passed	% Efficiency	CoR	CoSF	Particles Passed	% Efficiency	CoR	CoSF	Particles Passed	% Efficiency	CoR	CoSF	Particles Passed	% Efficiency	CoR	CoSF	Particles Passed	% Efficiency	CoR	CoSF	Particles Passed	% Efficiency	CoR	CoSF	Particles Passed	% Efficiency	CoR	CoSF	Particles Passed	% Efficiency
0,1	0,1	-	#VALUE!	0,2	0,1	-	#VALUE!	0,3	0,1	-	#VALUE!	0,4	0,1	-	#VALUE!	0,5	0,1	14	0,28	0,6	0,1	-	#VALUE!	0,7	0,1	-	#VALUE!	0,8	0,1	-	#VALUE!	0,9	0,1	-	#VALUE!
0,1	0,2	-	#VALUE!	0,2	0,2	-	#VALUE!	0,3	0,2	-	#VALUE!	0,4	0,2	-	#VALUE!	0,5	0,2	14	0,28	0,6	0,2	-	#VALUE!	0,7	0,2	12	0,24	0,8	0,2	-	#VALUE!	0,9	0,2	15	0,3
0,1	0,3	-	#VALUE!	0,2	0,3	2	0,04	0,3	0,3	-	#VALUE!	0,4	0,3	-	#VALUE!	0,5	0,3	-	#VALUE!	0,6	0,3	-	#VALUE!	0,7	0,3	-	#VALUE!	0,8	0,3	11	0,22	0,9	0,3	-	#VALUE!
0,1	0,4	-	#VALUE!	0,2	0,4	3	0,06	0,3	0,4	15	0,3	0,4	0,4	-	#VALUE!	0,5	0,4	-	#VALUE!	0,6	0,4	-	#VALUE!	0,7	0,4	6	0,12	0,8	0,4	-	#VALUE!	0,9	0,4	-	#VALUE!
0,1	0,5	-	#VALUE!	0,2	0,5	1	0,02	0,3	0,5	-	#VALUE!	0,4	0,5	-	#VALUE!	0,5	0,5	-	#VALUE!	0,6	0,5	-	#VALUE!	0,7	0,5	9	0,18	0,8	0,5	13	0,26	0,9	0,5	-	#VALUE!
0,1	0,6	-	#VALUE!	0,2	0,6	-	#VALUE!	0,3	0,6	-	#VALUE!	0,4	0,6	-	#VALUE!	0,5	0,6	-	#VALUE!	0,6	0,6	15	0,3	0,7	0,6	-	#VALUE!	0,8	0,6	10	0,2	0,9	0,6	-	#VALUE!
0,1	0,7	-	#VALUE!	0,2	0,7	3	0,06	0,3	0,7	12	0,24	0,4	0,7	14	0,28	0,5	0,7	-	#VALUE!	0,6	0,7	-	#VALUE!	0,7	0,7	10	0,2	0,8	0,7	4	0,08	0,9	0,7	10	0,2
0,1	0,8	-	#VALUE!	0,2	0,8	3	0,06	0,3	0,8	-	#VALUE!	0,4	0,8	-	#VALUE!	0,5	0,8	-	#VALUE!	0,6	0,8	8	0,16	0,7	0,8	-	#VALUE!	0,8	0,8	10	0,2	0,9	0,8	8	0,16
0,1	0,9	-	#VALUE!	0,2	0,9	-	#VALUE!	0,3	0,9	-	#VALUE!	0,4	0,9	-	#VALUE!	0,5	0,9	9	0,18	0,6	0,9	9	0,18	0,7	0,9	-	#VALUE!	0,8	0,9	-	#VALUE!	0,9	0,9	-	#VALUE!

White Pellet Coefficient Calibration with the Circular Sieve (Experiment Efficiency = 9%, Theory = 11%)

CoR	CoSF	Particles Passed	% Efficiency	CoR	CoSF	Particles Passed	% Efficiency	CoR	CoSF	Particles Passed	% Efficiency	CoR	CoSF	Particles Passed	% Efficiency	CoR	CoSF	Particles Passed	% Efficiency	CoR	CoSF	Particles Passed	% Efficiency	CoR	CoSF	Particles Passed	% Efficiency	CoR	CoSF	Particles Passed	% Efficiency	CoR	CoSF	Particles Passed	% Efficiency
0,1	0,1	-	#VALUE!	0,2	0,1	-	#VALUE!	0,3	0,1	-	#VALUE!	0,4	0,1	-	#VALUE!	0,5	0,1	6	0,12	0,6	0,1	-	#VALUE!	0,7	0,1	-	#VALUE!	0,8	0,1	9	0,18	0,9	0,1	-	#VALUE!
0,1	0,2	-	#VALUE!	0,2	0,2	7	0,14	0,3	0,2	-	#VALUE!	0,4	0,2	-	#VALUE!	0,5	0,2	5	0,1	0,6	0,2	7	0,14	0,7	0,2	6	0,12	0,8	0,2	8	0,16	0,9	0,2	5	0,1
0,1	0,3	-	#VALUE!	0,2	0,3	6	0,12	0,3	0,3	7	0,14	0,4	0,3	-	#VALUE!	0,5	0,3	-	#VALUE!	0,6	0,3	7	0,14	0,7	0,3	-	#VALUE!	0,8	0,3	6	0,12	0,9	0,3	7	0,14
0,1	0,4	-	#VALUE!	0,2	0,4	5	0,1	0,3	0,4	6	0,12	0,4	0,4	-	#VALUE!	0,5	0,4	-	#VALUE!	0,6	0,4	-	#VALUE!	0,7	0,4	4	0,08	0,8	0,4	7	0,14	0,9	0,4	-	#VALUE!
0,1	0,5	-	#VALUE!	0,2	0,5	6	0,12	0,3	0,5	-	#VALUE!	0,4	0,5	-	#VALUE!	0,5	0,5	-	#VALUE!	0,6	0,5	2	0,04	0,7	0,5	6	0,12	0,8	0,5	4	0,08	0,9	0,5	7	0,14
0,1	0,6	-	#VALUE!	0,2	0,6	-	#VALUE!	0,3	0,6	-	#VALUE!	0,4	0,6	1	0,02	0,5	0,6	-	#VALUE!	0,6	0,6	5	0,1	0,7	0,6	-	#VALUE!	0,8	0,6	5	0,1	0,9	0,6	-	#VALUE!
0,1	0,7	-	#VALUE!	0,2	0,7	4	0,08	0,3	0,7	6	0,12	0,4	0,7	5	0,1	0,5	0,7	-	#VALUE!	0,6	0,7	2	0,04	0,7	0,7	4	0,08	0,8	0,7	4	0,08	0,9	0,7	5	0,1
0,1	0,8	-	#VALUE!	0,2	0,8	4	0,08	0,3	0,8	-	#VALUE!	0,4	0,8	3	0,06	0,5	0,8	-	#VALUE!	0,6	0,8	5	0,1	0,7	0,8	7	0,14	0,8	0,8	6	0,12	0,9	0,8	4	0,08
0,1	0,9	-	#VALUE!	0,2	0,9	-	#VALUE!	0,3	0,9	-	#VALUE!	0,4	0,9	3	0,06	0,5	0,9	6	0,12	0,6	0,9	5	0,1	0,7	0,9	7	0,14	0,8	0,9	-	#VALUE!	0,9	0,9	-	#VALUE!

White Pellet Coefficient Calibration with the Oval Sieve (Experiment Efficiency = 23%, Theory = 22%)

CoR	CoSF	Particles Passed	% Efficiency	CoR	CoSF	Particles Passed	% Efficiency	CoR	CoSF	Particles Passed	% Efficiency	CoR	CoSF	Particles Passed	% Efficiency	CoR	CoSF	Particles Passed	% Efficiency	CoR	CoSF	Particles Passed	% Efficiency	CoR	CoSF	Particles Passed	% Efficiency	CoR	CoSF	Particles Passed	% Efficiency	CoR	CoSF	Particles Passed	% Efficiency
0,1	0,1	0	0	0,2	0,1	26	0,52	0,3	0,1	16	0,32	0,4	0,1	16	0,32	0,5	0,1	14	0,28	0,6	0,1	16	0,32	0,7	0,1	17	0,34	0,8	0,1	10	0,2	0,9	0,1	23	0,46
0,1	0,2	1	0,02	0,2	0,2	14	0,28	0,3	0,2	15	0,3	0,4	0,2	21	0,42	0,5	0,2	14	0,28	0,6	0,2	14	0,28	0,7	0,2	9	0,18	0,8	0,2	14	0,28	0,9	0,2	13	0,26
0,1	0,3	1	0,02	0,2	0,3	9	0,18	0,3	0,3	14	0,28	0,4	0,3	16	0,32	0,5	0,3	15	0,3	0,6	0,3	12	0,24	0,7	0,3	16	0,32	0,8	0,3	12	0,24	0,9	0,3	13	0,26
0,1	0,4	0	0	0,2	0,4	12	0,24	0,3	0,4	14	0,28	0,4	0,4	16	0,32	0,5	0,4	21	0,42	0,6	0,4	6	0,12	0,7	0,4	11	0,22	0,8	0,4	12	0,24	0,9	0,4	15	0,3
0,1	0,5	1	0,02	0,2	0,5	10	0,2	0,3	0,5	19	0,38	0,4	0,5	15	0,3	0,5	0,5	18	0,36	0,6	0,5	9	0,18	0,7	0,5	13	0,26	0,8	0,5	10	0,2	0,9	0,5	14	0,28
0,1	0,6	1	0,02	0,2	0,6	15	0,3	0,3	0,6	15	0,3	0,4	0,6	14	0,28	0,5	0,6	15	0,3	0,6	0,6	10	0,2	0,7	0,6	16	0,32	0,8	0,6	10	0,2	0,9	0,6	17	0,34
0,1	0,7	3	0,06	0,2	0,7	11	0,22	0,3	0,7	14	0,28	0,4	0,7	13	0,26	0,5	0,7	18	0,36	0,6	0,7	13	0,26	0,7	0,7	10	0,2	0,8	0,7	12	0,24	0,9	0,7	14	0,28
0,1	0,8	3	0,06	0,2	0,8	13	0,26	0,3	0,8	15	0,3	0,4	0,8	14	0,28	0,5	0,8	15	0,3	0,6	0,8	10	0,2	0,7	0,8	10	0,2	0,8	0,8	10	0,2	0,9	0,8	12	0,24
0,1	0,9	3	0,06	0,2	0,9	15	0,3	0,3	0,9	15	0,3	0,4	0,9	10	0,2	0,5	0,9	12	0,24	0,6	0,9	10	0,2	0,7	0,9	9	0,18	0,8	0,9	17	0,34	0,9	0,9	15	0,3

Steel Pellets: Coefficient of Restitution = 0.6 and Coefficient of Static Friction = 0.3

Steel Pellet Coefficient Calibration with the Square Sieve (Experiment Efficiency = 19%, Theory = 14%)

CoR	CoSF	Particles Passed	% Efficiency	CoR	CoSF	Particles Passed	% Efficiency	CoR	CoSF	Particles Passed	% Efficiency	CoR	CoSF	Particles Passed	% Efficiency	CoR	CoSF	Particles Passed	% Efficiency	CoR	CoSF	Particles Passed	% Efficiency	CoR	CoSF	Particles Passed	% Efficiency	CoR	CoSF	Particles Passed	% Efficiency	CoR	CoSF	Particles Passed	% Efficiency
0,1	0,1	0	0	0,2	0,1	0	0	0,3	0,1	12	0,24	0,4	0,1	4	0,08	0,5	0,1	7	0,14	0,6	0,1	9	0,18	0,7	0,1	11	0,22	0,8	0,1	12	0,24	0,9	0,1	13	0,26
0,1	0,2	0	0	0,2	0,2	0	0	0,3	0,2	5	0,1	0,4	0,2	5	0,1	0,5	0,2	9	0,18	0,6	0,2	5	0,1	0,7	0,2	10	0,2	0,8	0,2	8	0,16	0,9	0,2	8	0,16
0,1	0,3	0	0	0,2	0,3	0	0	0,3	0,3	4	0,08	0,4	0,3	5	0,1	0,5	0,3	6	0,12	0,6	0,3	8	0,16	0,7	0,3	9	0,18	0,8	0,3	11	0,22	0,9	0,3	6	0,12
0,1	0,4	0	0	0,2	0,4	0	0	0,3	0,4	4	0,08	0,4	0,4	4	0,08	0,5	0,4	7	0,14	0,6	0,4	4	0,08	0,7	0,4	7	0,14	0,8	0,4	7	0,14	0,9	0,4	9	0,18
0,1	0,5	0	0	0,2	0,5	0	0	0,3	0,5	4	0,08	0,4	0,5	6	0,12	0,5	0,5	9	0,18	0,6	0,5	6	0,12	0,7	0,5	10	0,2	0,8	0,5	8	0,16	0,9	0,5	7	0,14
0,1	0,6	0	0	0,2	0,6	0	0	0,3	0,6	3	0,06	0,4	0,6	4	0,08	0,5	0,6	6	0,12	0,6	0,6	7	0,14	0,7	0,6	5	0,1	0,8	0,6	6	0,12	0,9	0,6	4	0,08
0,1	0,7	0	0	0,2	0,7	0	0	0,3	0,7	4	0,08	0,4	0,7	3	0,06	0,5	0,7	8	0,16	0,6	0,7	6	0,12	0,7	0,7	6	0,12	0,8	0,7	9	0,18	0,9	0,7	9	0,18
0,1	0,8	0	0	0,2	0,8	0	0	0,3	0,8	4	0,08	0,4	0,8	4	0,08	0,5	0,8	10	0,2	0,6	0,8	3	0,06	0,7	0,8	5	0,1	0,8	0,8	4	0,08	0,9	0,8	6	0,12
0,1	0,9	0	0	0,2	0,9	0	0	0,3	0,9	5	0,1	0,4	0,9	4	0,08	0,5	0,9	7	0,14	0,6	0,9	6	0,12	0,7	0,9	6	0,12	0,8	0,9	6	0,12	0,9	0,9	7	0,14

Steel Pellet with the Rectangle Sieve (Exp. Eff. = 31%, Theory = 29%)

CoR	CoSF	Particles Passed	% Efficiency	CoR	CoSF	Particles Passed	% Efficiency	CoR	CoSF	Particles Passed	% Efficiency	CoR	CoSF	Particles Passed	% Efficiency	CoR	CoSF	Particles Passed	% Efficiency	CoR	CoSF	Particles Passed	% Efficiency	CoR	CoSF	Particles Passed	% Efficiency	CoR	CoSF	Particles Passed	% Efficiency	CoR	CoSF	Particles Passed	% Efficiency
0,1	0,1	-	#VALUE!	0,2	0,1	-	#VALUE!	0,3	0,1	-	#VALUE!	0,4	0,1	-	#VALUE!	0,5	0,1	17	0,34	0,6	0,1	17	0,34	0,7	0,1	14	0,28	0,8	0,1	16	0,32	0,9	0,1	21	0,42
0,1	0,2	-	#VALUE!	0,2	0,2	-	#VALUE!	0,3	0,2	-	#VALUE!	0,4	0,2	-	#VALUE!	0,5	0,2	18	0,36	0,6	0,2	17	0,34	0,7	0,2	18	0,36	0,8	0,2	16	0,32	0,9	0,2	19	0,38
0,1	0,3	-	#VALUE!	0,2	0,3	-	#VALUE!	0,3	0,3	-	#VALUE!	0,4	0,3	-	#VALUE!	0,5	0,3	17	0,34	0,6	0,3	13	0,26	0,7	0,3	10	0,2	0,8	0,3	20	0,4	0,9	0,3	21	0,42
0,1	0,4	-	#VALUE!	0,2	0,4	-	#VALUE!	0,3	0,4	-	#VALUE!	0,4	0,4	-	#VALUE!	0,5	0,4	12	0,24	0,6	0,4	14	0,28	0,7	0,4	10	0,2	0,8	0,4	22	0,44	0,9	0,4	20	0,4
0,1	0,5	-	#VALUE!	0,2	0,5	-	#VALUE!	0,3	0,5	-	#VALUE!	0,4	0,5	-	#VALUE!	0,5	0,5	9	0,18	0,6	0,5	12	0,24	0,7	0,5	12	0,24	0,8	0,5	15	0,3	0,9	0,5	15	0,3
0,1	0,6	-	#VALUE!	0,2	0,6	-	#VALUE!	0,3	0,6	-	#VALUE!	0,4	0,6	-	#VALUE!	0,5	0,6	11	0,22	0,6	0,6	10	0,2	0,7	0,6	7	0,14	0,8	0,6	13	0,26	0,9	0,6	12	0,24
0,1	0,7	-	#VALUE!	0,2	0,7	-	#VALUE!	0,3	0,7	-	#VALUE!	0,4	0,7	-	#VALUE!	0,5	0,7	12	0,24	0,6	0,7	18	0,36	0,7	0,7	7	0,14	0,8	0,7	13	0,26	0,9	0,7	18	0,36
0,1	0,8	-	#VALUE!	0,2	0,8	-	#VALUE!	0,3	0,8	-	#VALUE!	0,4	0,8	-	#VALUE!	0,5	0,8	15	0,3	0,6	0,8	16	0,32	0,7	0,8	12	0,24	0,8	0,8	12	0,24	0,9	0,8	19	0,38
0,1	0,9	-	#VALUE!	0,2	0,9	-	#VALUE!	0,3	0,9	-	#VALUE!	0,4	0,9	-	#VALUE!	0,5	0,9	17	0,34	0,6	0,9	11	0,22	0,7	0,9	13	0,26	0,8	0,9	10	0,2	0,9	0,9	15	0,3

Steel Pellet with the Circle Sieve (Exp. Eff. = 15%, Theory = 11%)

CoR	CoSF	Particles Passed	% Efficiency	CoR	CoSF	Particles Passed	% Efficiency	CoR	CoSF	Particles Passed	% Efficiency	CoR	CoSF	Particles Passed	% Efficiency	CoR	CoSF	Particles Passed	% Efficiency	CoR	CoSF	Particles Passed	% Efficiency	CoR	CoSF	Particles Passed	% Efficiency	CoR	CoSF	Particles Passed	% Efficiency	CoR	CoSF	Particles Passed	% Efficiency
0,1	0,1	-	#VALUE!	0,2	0,1	-	#VALUE!	0,3	0,1	-	#VALUE!	0,4	0,1	-	#VALUE!	0,5	0,1	10	0,2	0,6	0,1	4	0,08	0,7	0,1	8	0,16	0,8	0,1	10	0,2	0,9	0,1	14	0,28
0,1	0,2	-	#VALUE!	0,2	0,2	-	#VALUE!	0,3	0,2	-	#VALUE!	0,4	0,2	-	#VALUE!	0,5	0,2	3	0,06	0,6	0,2	8	0,16	0,7	0,2	7	0,14	0,8	0,2	8	0,16	0,9	0,2	12	0,24
0,1	0,3	-	#VALUE!	0,2	0,3	-	#VALUE!	0,3	0,3	-	#VALUE!	0,4	0,3	-	#VALUE!	0,5	0,3	12	0,24	0,6	0,3	8	0,16	0,7	0,3	8	0,16	0,8	0,3	11	0,22	0,9	0,3	13	0,26
0,1	0,4	-	#VALUE!	0,2	0,4	-	#VALUE!	0,3	0,4	-	#VALUE!	0,4	0,4	-	#VALUE!	0,5	0,4	12	0,24	0,6	0,4	14	0,28	0,7	0,4	7	0,14	0,8	0,4	8	0,16	0,9	0,4	8	0,16
0,1	0,5	-	#VALUE!	0,2	0,5	-	#VALUE!	0,3	0,5	-	#VALUE!	0,4	0,5	-	#VALUE!	0,5	0,5	7	0,14	0,6	0,5	9	0,18	0,7	0,5	6	0,12	0,8	0,5	5	0,1	0,9	0,5	8	0,16
0,1	0,6	-	#VALUE!	0,2	0,6	-	#VALUE!	0,3	0,6	-	#VALUE!	0,4	0,6	-	#VALUE!	0,5	0,6	3	0,06	0,6	0,6	2	0,04	0,7	0,6	4	0,08	0,8	0,6	9	0,18	0,9	0,6	12	0,24
0,1	0,7	-	#VALUE!	0,2	0,7	-	#VALUE!	0,3	0,7	-	#VALUE!	0,4	0,7	-	#VALUE!	0,5	0,7	6	0,12	0,6	0,7	6	0,12	0,7	0,7	3	0,06	0,8	0,7	6	0,12	0,9	0,7	10	0,2
0,1	0,8	-	#VALUE!	0,2	0,8	-	#VALUE!	0,3	0,8	-	#VALUE!	0,4	0,8	-	#VALUE!	0,5	0,8	6	0,12	0,6	0,8	6	0,12	0,7	0,8	6	0,12	0,8	0,8	13	0,26	0,9	0,8	3	0,06
0,1	0,9	-	#VALUE!	0,2	0,9	-	#VALUE!	0,3	0,9	-	#VALUE!	0,4	0,9	-	#VALUE!	0,5	0,9	5	0,1	0,6	0,9	6	0,12	0,7	0,9	12	0,24	0,8	0,9	9	0,18	0,9	0,9	3	0,06

Steel Pellet with the Oval Sieve (Exp. Eff. = 19%, Theory = 22%)

CoR	CoSF	Particles Passed	% Efficiency	CoR	CoSF	Particles Passed	% Efficiency	CoR	CoSF	Particles Passed	% Efficiency	CoR	CoSF	Particles Passed	% Efficiency	CoR	CoSF	Particles Passed	% Efficiency	CoR	CoSF	Particles Passed	% Efficiency	CoR	CoSF	Particles Passed	% Efficiency	CoR	CoSF	Particles Passed	% Efficiency	CoR	CoSF	Particles Passed	% Efficiency
0,1	0,1	0	0	0,2	0,1	35	0,7	0,3	0,1	15	0,3	0,4	0,1	22	0,44	0,5	0,1	12	0,24	0,6	0,1	23	0,46	0,7	0,1	18	0,36	0,8	0,1	16	0,32	0,9	0,1	30	0,6
0,1	0,2	0	0	0,2	0,2	15	0,3	0,3	0,2	19	0,38	0,4	0,2	18	0,36	0,5	0,2	21	0,42	0,6	0,2	14	0,28	0,7	0,2	23	0,46	0,8	0,2	23	0,46	0,9	0,2	23	0,46
0,1	0,3	0	0	0,2	0,3	17	0,34	0,3	0,3	17	0,34	0,4	0,3	13	0,26	0,5	0,3	15	0,3	0,6	0,3	11	0,22	0,7	0,3	19	0,38	0,8	0,3	22	0,44	0,9	0,3	18	0,36
0,1	0,4	0	0	0,2	0,4	16	0,32	0,3	0,4	19	0,38	0,4	0,4	16	0,32	0,5	0,4	16	0,32	0,6	0,4	11	0,22	0,7	0,4	17	0,34	0,8	0,4	17	0,34	0,9	0,4	22	0,44
0,1	0,5	0	0	0,2	0,5	15	0,3	0,3	0,5	16	0,32	0,4	0,5	13	0,26	0,5	0,5	21	0,42	0,6	0,5	12	0,24	0,7	0,5	18	0,36	0,8	0,5	18	0,36	0,9	0,5	21	0,42
0,1	0,6	0	0	0,2	0,6	15	0,3	0,3	0,6	15	0,3	0,4	0,6	15	0,3	0,5	0,6	21	0,42	0,6	0,6	9	0,18	0,7	0,6	20	0,4	0,8	0,6	14	0,28	0,9	0,6	14	0,28
0,1	0,7	0	0	0,2	0,7	16	0,32	0,3	0,7	16	0,32	0,4	0,7	17	0,34	0,5	0,7	21	0,42	0,6	0,7	11	0,22	0,7	0,7	20	0,4	0,8	0,7	13	0,26	0,9	0,7	20	0,4
0,1	0,8	0	0	0,2	0,8	17	0,34	0,3	0,8	12	0,24	0,4	0,8	16	0,32	0,5	0,8	19	0,38	0,6	0,8	10	0,2	0,7	0,8	17	0,34	0,8	0,8	16	0,32	0,9	0,8	21	0,42
0,1	0,9	0	0	0,2	0,9	15	0,3	0,3	0,9	13	0,26	0,4	0,9	12	0,24	0,5	0,9	18	0,36	0,6	0,9	13	0,26	0,7	0,9	12	0,24	0,8	0,9	17	0,34	0,9	0,9	22	0,44

Iron Ore particle: Coefficient of Restitution = 0.2 and Coefficient of Static Friction = 0.7

Iron Ore Coefficient Calibration with the Square Sieve (Experiment Efficiency = 12%, Theory = 14%)

CoR	CoSF	Particles Passed	% Efficiency	CoR	CoSF	Particles Passed	% Efficiency	CoR	CoSF	Particles Passed	% Efficiency	CoR	CoSF	Particles Passed	% Efficiency	CoR	CoSF	Particles Passed	% Efficiency	CoR	CoSF	Particles Passed	% Efficiency	CoR	CoSF	Particles Passed	% Efficiency	CoR	CoSF	Particles Passed	% Efficiency	CoR	CoSF	Particles Passed	% Efficiency
0,1	0,1	0	0	0,2	0,1	-	#VALUE!	0,3	0,1	0	0	0,4	0,1	-	#VALUE!	0,5	0,1	-	#VALUE!	0,6	0,1	-	#VALUE!	0,7	0,1	-	#VALUE!	0,8	0,1	-	#VALUE!	0,9	0,1		0
0,1	0,2	2	0,04	0,2	0,2	-	#VALUE!	0,3	0,2	-	#VALUE!	0,4	0,2	-	#VALUE!	0,5	0,2	-	#VALUE!	0,6	0,2	-	#VALUE!	0,7	0,2	-	#VALUE!	0,8	0,2	-	#VALUE!	0,9	0,2	-	#VALUE!
0,1	0,3	6	0,12	0,2	0,3	10	0,2	0,3	0,3	8	0,16	0,4	0,3	14	0,28	0,5	0,3	-	#VALUE!	0,6	0,3	-	#VALUE!	0,7	0,3	-	#VALUE!	0,8	0,3		0	0,9	0,3		0
0,1	0,4	6	0,12	0,2	0,4	8	0,16	0,3	0,4	9	0,18	0,4	0,4	-	#VALUE!	0,5	0,4	22	0,44	0,6	0,4	-	#VALUE!	0,7	0,4	-	#VALUE!	0,8	0,4	-	#VALUE!	0,9	0,4		0
0,1	0,5	7	0,14	0,2	0,5	5	0,1	0,3	0,5	12	0,24	0,4	0,5	11	0,22	0,5	0,5	14	0,28	0,6	0,5	18	0,36	0,7	0,5	-	#VALUE!	0,8	0,5	-	#VALUE!	0,9	0,5		0
0,1	0,6	10	0,2	0,2	0,6	3	0,06	0,3	0,6	9	0,18	0,4	0,6	11	0,22	0,5	0,6	9	0,18	0,6	0,6	8	0,16	0,7	0,6	-	#VALUE!	0,8	0,6	-	#VALUE!	0,9	0,6		0
0,1	0,7	4	0,08	0,2	0,7	7	0,14	0,3	0,7	-	#VALUE!	0,4	0,7	6	0,12	0,5	0,7	4	0,08	0,6	0,7	19	0,38	0,7	0,7	-	#VALUE!	0,8	0,7		0	0,9	0,7		0
0,1	0,8	6	0,12	0,2	0,8	8	0,16	0,3	0,8	15	0,3	0,4	0,8	9	0,18	0,5	0,8	10	0,2	0,6	0,8	-	#VALUE!	0,7	0,8		0	0,8	0,8		0	0,9	0,8	-	#VALUE!
0,1	0,9	9	0,18	0,2	0,9	6	0,12	0,3	0,9	7	0,14	0,4	0,9	11	0,22	0,5	0,9	9	0,18	0,6	0,9	-	#VALUE!	0,7	0,9		0	0,8	0,9		0	0,9	0,9	-	#VALUE!

Iron Ore Coefficient Calibration with the Rectangular Sieve (Experiment Efficiency = 30%, Theory = 29%)

CoR	CoSF	Particles Passed	% Efficiency	CoR	CoSF	Particles Passed	% Efficiency	CoR	CoSF	Particles Passed	% Efficiency	CoR	CoSF	Particles Passed	% Efficiency	CoR	CoSF	Particles Passed	% Efficiency	CoR	CoSF	Particles Passed	% Efficiency	CoR	CoSF	Particles Passed	% Efficiency	CoR	CoSF	Particles Passed	% Efficiency	CoR	CoSF	Particles Passed	% Efficiency
0,1	0,1	-	#VALUE!	0,2	0,1	-	#VALUE!	0,3	0,1	-	#VALUE!	0,4	0,1	-	#VALUE!	0,5	0,1	-	#VALUE!	0,6	0,1	-	#VALUE!	0,7	0,1	-	#VALUE!	0,8	0,1	-	#VALUE!	0,9	0,1		0
0,1	0,2		0	0,2	0,2	-	#VALUE!	0,3	0,2	-	#VALUE!	0,4	0,2	-	#VALUE!	0,5	0,2	-	#VALUE!	0,6	0,2	-	#VALUE!	0,7	0,2	-	#VALUE!	0,8	0,2	-	#VALUE!	0,9	0,2	-	#VALUE!
0,1	0,3	-	#VALUE!	0,2	0,3		0	0,3	0,3	17	0,34	0,4	0,3		0	0,5	0,3	-	#VALUE!	0,6	0,3	-	#VALUE!	0,7	0,3	-	#VALUE!	0,8	0,3		0	0,9	0,3		0
0,1	0,4	-	#VALUE!	0,2	0,4	10	0,2	0,3	0,4	15	0,3	0,4	0,4	-	#VALUE!	0,5	0,4		0	0,6	0,4	-	#VALUE!	0,7	0,4	-	#VALUE!	0,8	0,4	-	#VALUE!	0,9	0,4		0
0,1	0,5	-	#VALUE!	0,2	0,5	6	0,12	0,3	0,5		0	0,4	0,5		0	0,5	0,5		0	0,6	0,5		0	0,7	0,5	-	#VALUE!	0,8	0,5	-	#VALUE!	0,9	0,5		0
0,1	0,6	-	#VALUE!	0,2	0,6	-	#VALUE!	0,3	0,6	13	0,26	0,4	0,6		0	0,5	0,6	19	0,38	0,6	0,6	18	0,36	0,7	0,6	-	#VALUE!	0,8	0,6	-	#VALUE!	0,9	0,6		0
0,1	0,7	-	#VALUE!	0,2	0,7	14	0,28	0,3	0,7	-	#VALUE!	0,4	0,7	13	0,26	0,5	0,7	14	0,28	0,6	0,7		0	0,7	0,7	-	#VALUE!	0,8	0,7		0	0,9	0,7		0
0,1	0,8	10	0,2	0,2	0,8	12	0,24	0,3	0,8		0	0,4	0,8	10	0,2	0,5	0,8		0	0,6	0,8	-	#VALUE!	0,7	0,8		0	0,8	0,8		0	0,9	0,8	-	#VALUE!
0,1	0,9	8	0,16	0,2	0,9	12	0,24	0,3	0,9	8	0,16	0,4	0,9		0	0,5	0,9	14	0,28	0,6	0,9	-	#VALUE!	0,7	0,9		0	0,8	0,9		0	0,9	0,9	-	#VALUE!

Iron Ore Coefficient Calibration with the Circular Sieve (Experiment Efficiency = 9%, Theory = 11%)

CoR	CoSF	Particles Passed	% Efficiency	CoR	CoSF	Particles Passed	% Efficiency	CoR	CoSF	Particles Passed	% Efficiency	CoR	CoSF	Particles Passed	% Efficiency	CoR	CoSF	Particles Passed	% Efficiency	CoR	CoSF	Particles Passed	% Efficiency	CoR	CoSF	Particles Passed	% Efficiency	CoR	CoSF	Particles Passed	% Efficiency	CoR	CoSF	Particles Passed	% Efficiency
0,1	0,1	-	#VALUE!	0,2	0,1	-	#VALUE!	0,3	0,1	-	#VALUE!	0,4	0,1	-	#VALUE!	0,5	0,1	-	#VALUE!	0,6	0,1	-	#VALUE!	0,7	0,1	-	#VALUE!	0,8	0,1	-	#VALUE!	0,9	0,1		0
0,1	0,2		0	0,2	0,2	-	#VALUE!	0,3	0,2	-	#VALUE!	0,4	0,2	-	#VALUE!	0,5	0,2	-	#VALUE!	0,6	0,2	-	#VALUE!	0,7	0,2	-	#VALUE!	0,8	0,2	-	#VALUE!	0,9	0,2	-	#VALUE!
0,1	0,3	-	#VALUE!	0,2	0,3		0	0,3	0,3	6	0,12	0,4	0,3		0	0,5	0,3	-	#VALUE!	0,6	0,3	-	#VALUE!	0,7	0,3	-	#VALUE!	0,8	0,3		0	0,9	0,3		0
0,1	0,4	-	#VALUE!	0,2	0,4		0	0,3	0,4	5	0,1	0,4	0,4	-	#VALUE!	0,5	0,4		0	0,6	0,4	-	#VALUE!	0,7	0,4	-	#VALUE!	0,8	0,4	-	#VALUE!	0,9	0,4		0
0,1	0,5	-	#VALUE!	0,2	0,5		0	0,3	0,5		0	0,4	0,5		0	0,5	0,5		0	0,6	0,5		0	0,7	0,5	-	#VALUE!	0,8	0,5	-	#VALUE!	0,9	0,5		0
0,1	0,6	-	#VALUE!	0,2	0,6	-	#VALUE!	0,3	0,6	9	0,18	0,4	0,6		0	0,5	0,6		0	0,6	0,6	6	0,12	0,7	0,6	-	#VALUE!	0,8	0,6	-	#VALUE!	0,9	0,6		0
0,1	0,7	-	#VALUE!	0,2	0,7	5	0,1	0,3	0,7	-	#VALUE!	0,4	0,7	7	0,14	0,5	0,7	13	0,26	0,6	0,7		0	0,7	0,7	-	#VALUE!	0,8	0,7		0	0,9	0,7		0
0,1	0,8		0	0,2	0,8	6	0,12	0,3	0,8		0	0,4	0,8		0	0,5	0,8		0	0,6	0,8	-	#VALUE!	0,7	0,8		0	0,8	0,8		0	0,9	0,8	-	#VALUE!
0,1	0,9		0	0,2	0,9	11	0,22	0,3	0,9		0	0,4	0,9		0	0,5	0,9	11	0,22	0,6	0,9	-	#VALUE!	0,7	0,9		0	0,8	0,9		0	0,9	0,9	-	#VALUE!

Iron Ore Coefficient Calibration with the Oval Sieve (Experiment Efficiency = 25%, Theory = 22%)

CoR	CoSF	Particles Passed	% Efficiency	CoR	CoSF	Particles Passed	% Efficiency	CoR	CoSF	Particles Passed	% Efficiency	CoR	CoSF	Particles Passed	% Efficiency	CoR	CoSF	Particles Passed	% Efficiency	CoR	CoSF	Particles Passed	% Efficiency	CoR	CoSF	Particles Passed	% Efficiency	CoR	CoSF	Particles Passed	% Efficiency	CoR	CoSF	Particles Passed	% Efficiency
0,1	0,1	0	0	0,2	0,1	1	0,02	0,3	0,1	12	0,24	0,4	0,1	23	0,46	0,5	0,1	22	0,44	0,6	0,1	21	0,42	0,7	0,1	17	0,34	0,8	0,1	20	0,4	0,9	0,1	15	0,3
0,1	0,2	13	0,26	0,2	0,2	6	0,12	0,3	0,2	22	0,44	0,4	0,2	21	0,42	0,5	0,2	19	0,38	0,6	0,2	16	0,32	0,7	0,2	20	0,4	0,8	0,2	21	0,42	0,9	0,2	17	0,34
0,1	0,3	7	0,14	0,2	0,3	13	0,26	0,3	0,3	15	0,3	0,4	0,3	15	0,3	0,5	0,3	22	0,44	0,6	0,3	21	0,42	0,7	0,3	16	0,32	0,8	0,3	15	0,3	0,9	0,3	14	0,28
0,1	0,4	4	0,08	0,2	0,4	13	0,26	0,3	0,4	13	0,26	0,4	0,4	18	0,36	0,5	0,4	14	0,28	0,6	0,4	16	0,32	0,7	0,4	20	0,4	0,8	0,4	18	0,36	0,9	0,4	15	0,3
0,1	0,5	7	0,14	0,2	0,5	10	0,2	0,3	0,5	9	0,18	0,4	0,5	14	0,28	0,5	0,5	15	0,3	0,6	0,5	14	0,28	0,7	0,5	24	0,48	0,8	0,5	16	0,32	0,9	0,5	12	0,24
0,1	0,6	10	0,2	0,2	0,6	14	0,28	0,3	0,6	11	0,22	0,4	0,6	10	0,2	0,5	0,6	15	0,3	0,6	0,6	15	0,3	0,7	0,6	17	0,34	0,8	0,6	20	0,4	0,9	0,6	11	0,22
0,1	0,7	8	0,16	0,2	0,7	12	0,24	0,3	0,7	17	0,34	0,4	0,7	11	0,22	0,5	0,7	9	0,18	0,6	0,7	12	0,24	0,7	0,7	17	0,34	0,8	0,7	15	0,3	0,9	0,7	12	0,24
0,1	0,8	9	0,18	0,2	0,8	15	0,3	0,3	0,8	10	0,2	0,4	0,8	9	0,18	0,5	0,8	12	0,24	0,6	0,8	19	0,38	0,7	0,8	13	0,26	0,8	0,8	15	0,3	0,9	0,8	19	0,38
0,1	0,9	14	0,28	0,2	0,9	11	0,22	0,3	0,9	15	0,3	0,4	0,9	9	0,18	0,5	0,9	14	0,28	0,6	0,9	16	0,32	0,7	0,9	11	0,22	0,8	0,9	13	0,26	0,9	0,9	16	0,32

Appendix E – Preliminary Simulation Result Tables

Results of each of the sieve configurations and each of the aperture shapes were simulated with 200, 600 and 1800 particles and were vibrated at the different angles of stroke. The following four tables represent the results of all the particles which passed through the sieve and counting plane.

Square sieve configurations:

Percentage (%) of particles passing through the counting plane						
	200 Particles		600 Particles		1800 Particles	
Angle of Stroke	Square Sieve	Square Ext Sieve	Square Sieve	Square Ext Sieve	Square Sieve	Square Ext Sieve
0°	7,0	4,0	8,7	4,0	5,3	4,0
15°	19,0	7,0	14,7	7,7	8,4	4,9
30°	26,0	20,0	25,7	21,0	18,9	14,4
45°	49,0	39,0	36,0	32,3	19,0	14,1
60°	66,0	71,0	49,0	44,7	28,2	22,1
75°	70,0	76,0	59,0	64,7	48,8	37,2
90°	71,0	81,0	73,7	69,3	56,9	45,8

Rectangular sieve configurations:

Percentage (%) of particles passing through the counting plane						
	200 Particles		600 Particles		1800 Particles	
Angle of Stroke	Rect Sieve	Rect Ext Sieve	Rect Sieve	Rect Ext Sieve	Rect Sieve	Rect Ext Sieve
0°	23,0	13,0	23,3	21,3	13,2	11,0
15°	35,0	30,0	27,3	23,3	17,6	16,1
30°	45,0	44,0	41,3	44,3	30,0	25,0
45°	70,0	69,0	47,3	52,0	25,8	27,7
60°	77,0	86,0	57,7	68,0	34,2	33,6
75°	82,0	91,0	70,0	80,0	56,6	45,2
90°	81,0	90,0	76,7	84,0	58,0	50,8

Circular sieve configurations:

Percentage (%) of particles passing through the counting plane						
	200 Particles		600 Particles		1800 Particles	
Angle of Stroke	Circular Sieve	Circular Ext Sieve	Circular Sieve	Circular Ext Sieve	Circular Sieve	Circular Ext Sieve
0°	7,0	2,0	7,3	3,0	4,9	2,5
15°	14,0	3,0	13,0	3,3	9,2	4,5
30°	31,0	16,0	27,7	16,0	20,3	12,2
45°	42,0	37,0	31,3	19,3	17,6	9,6
60°	64,0	60,0	46,7	37,3	31,3	22,0
75°	75,0	74,0	64,3	62,0	53,4	40,4
90°	71,0	84,0	74,3	71,0	56,6	45,0

Oval sieve configurations:

Percentage (%) of particles passing through the counting plane						
	200 Particles		600 Particles		1800 Particles	
Angle of Stroke	Oval Sieve	Oval Ext Sieve	Oval Sieve	Oval Ext Sieve	Oval Sieve	Oval Ext Sieve
0°	15,0	5,0	20,0	12,7	13,1	5,6
15°	32,0	15,0	25,0	12,3	16,7	8,6
30°	39,0	26,0	38,7	27,0	27,8	19,1
45°	63,0	52,0	45,3	36,0	26,3	20,0
60°	71,0	84,0	62,3	54,3	31,8	28,1
75°	78,0	83,0	71,3	69,0	48,3	42,3
90°	79,0	85,0	74,3	72,0	57,8	46,9

Results of each of the sieve configurations and each of the aperture shapes were simulated with 200, 600 and 1800 particles and were vibrated at the different angles of stroke. The following four tables represent the results of all the particles which passed through the sieve and counting plane excluding the particles which passed back though the sieve. This shows the amount of particles which were sieved and that were retained in the sieve chamber.

Square sieve configurations:

Percentage (%) of particles passing counting plane excluding particles which passed back through the Sieve						
	200 Particles		600 Particles		1800 Particles	
Angle of Stroke	Square Sieve	Square Ext Sieve	Square Sieve	Square Ext Sieve	Square Sieve	Square Ext Sieve
0°	7,0	4,0	11,0	4,3	5,6	4,7
15°	19,0	8,0	15,0	7,3	8,4	4,7
30°	21,0	20,0	22,0	20,0	17,6	13,1
45°	38,0	38,0	25,7	29,0	12,9	11,0
60°	50,0	52,0	36,0	34,3	14,7	16,7
75°	44,0	62,0	44,0	53,0	31,2	28,0
90°	49,0	72,0	49,7	57,7	42,8	38,3

Rectangular sieve configurations:

Percentage (%) of particles passing counting plane excluding particles which passed back through the Sieve						
	200 Particles		600 Particles		1800 Particles	
Angle of Stroke	Rect Sieve	Rect Ext Sieve	Rect Sieve	Rect Ext Sieve	Rect Sieve	Rect Ext Sieve
0°	24,0	16,0	24,3	22,7	12,8	11,5
15°	33,0	29,0	27,7	23,7	16,1	14,8
30°	34,0	38,0	31,7	36,3	25,6	21,6
45°	59,0	47,0	31,0	38,7	17,8	19,9
60°	51,0	66,0	38,0	48,3	17,6	21,8
75°	50,0	68,0	47,0	59,0	34,7	33,9
90°	52,0	70,0	50,3	68,0	40,1	41,9

Circular sieve configurations:

Percentage (%) of particles passing counting plane excluding particles which passed back through the Sieve								
	200 Particles			600 Particles			1800 Particles	
Angle of Stroke	Circular Sieve	Circular Ext Sieve		Circular Sieve	Circular Ext Sieve		Circular Sieve	Circular Ext Sieve
0°	8,0	2,0		8,0	4,0		5,1	2,8
15°	13,0	3,0		12,0	5,0		9,3	4,5
30°	29,0	18,0		26,0	14,3		19,3	11,9
45°	34,0	33,0		21,0	17,0		10,7	8,0
60°	46,0	49,0		32,0	30,3		19,3	10,1
75°	55,0	58,0		46,3	46,3		37,4	30,1
90°	59,0	68,0		52,7	59,7		42,8	36,9

Oval sieve configurations:

Percentage (%) of particles passing counting plane excluding particles which passed back through the Sieve								
	200 Particles			600 Particles			1800 Particles	
Angle of Stroke	Oval Sieve	Oval Ext Sieve		Oval Sieve	Oval Ext Sieve		Oval Sieve	Oval Ext Sieve
0°	14,0	8,0		20,7	15,0		13,6	5,9
15°	30,0	14,0		22,0	12,3		15,9	8,0
30°	31,0	23,0		33,0	25,0		23,8	17,6
45°	49,0	43,0		28,0	31,7		18,7	15,6
60°	49,0	63,0		39,0	39,0		17,4	18,4
75°	58,0	60,0		49,7	51,0		32,4	32,1
90°	56,0	76,0		53,7	61,3		41,9	35,9

Appendix F – Preliminary Simulation Best and Worst Results

The preliminary simulation consisted of a series of tests. Different strokes ranging between 0° and 90° in increments of 15° were analysed. These strokes were tested on 4 different sieve shapes with 2 different sieve geometries for each shape. Furthermore, 200, 600 and 1800 particles were inserted into the simulation box configurations in different simulations. Therefore the total number of simulations run was: 7x4x2x3 = 168.

The results below show only the best and the worst performing sieve configurations (flat and extruded) for a specific shape which allowed the most first time passes at each stroke. For each 200, 600 and 1800 particles inserted these the images of the results will be shown below.

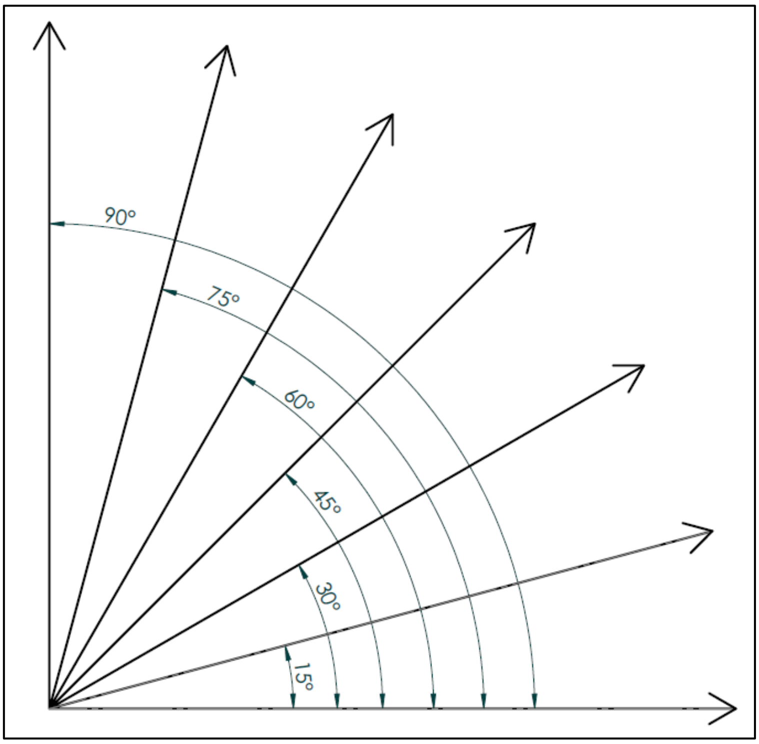

Square Sieve

1. For the Square Sieve with 200 Particles
    a. The worst performing simulation was the 0° stroke with a 7% passing rate.

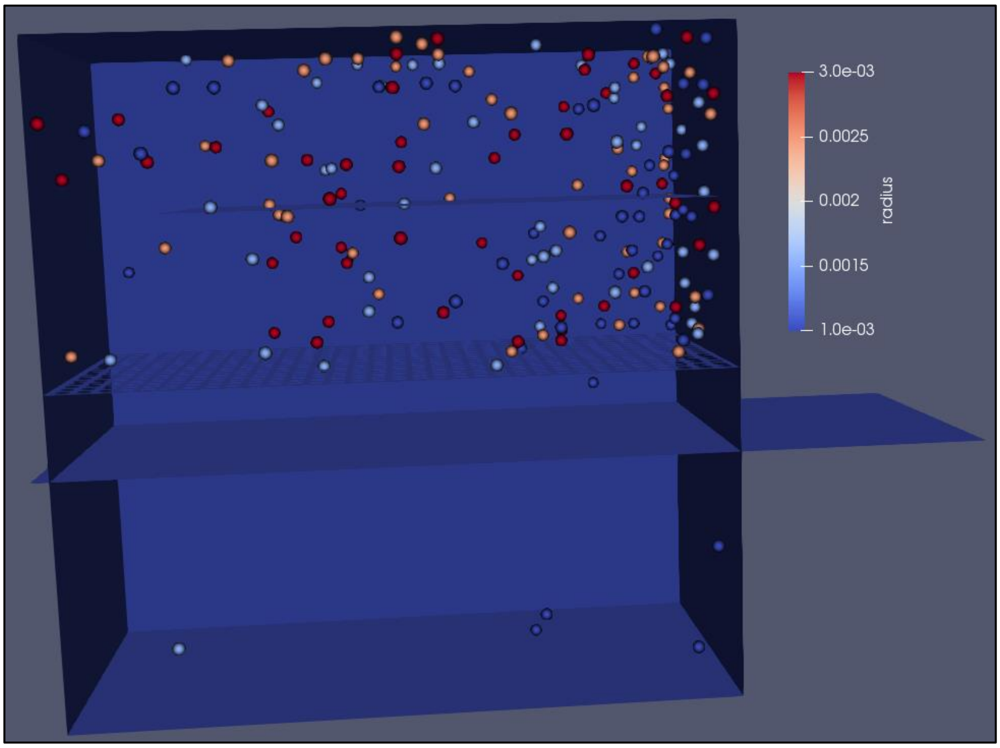

    b. The best performing simulation was the 90° stroke with a 71% passing rate.

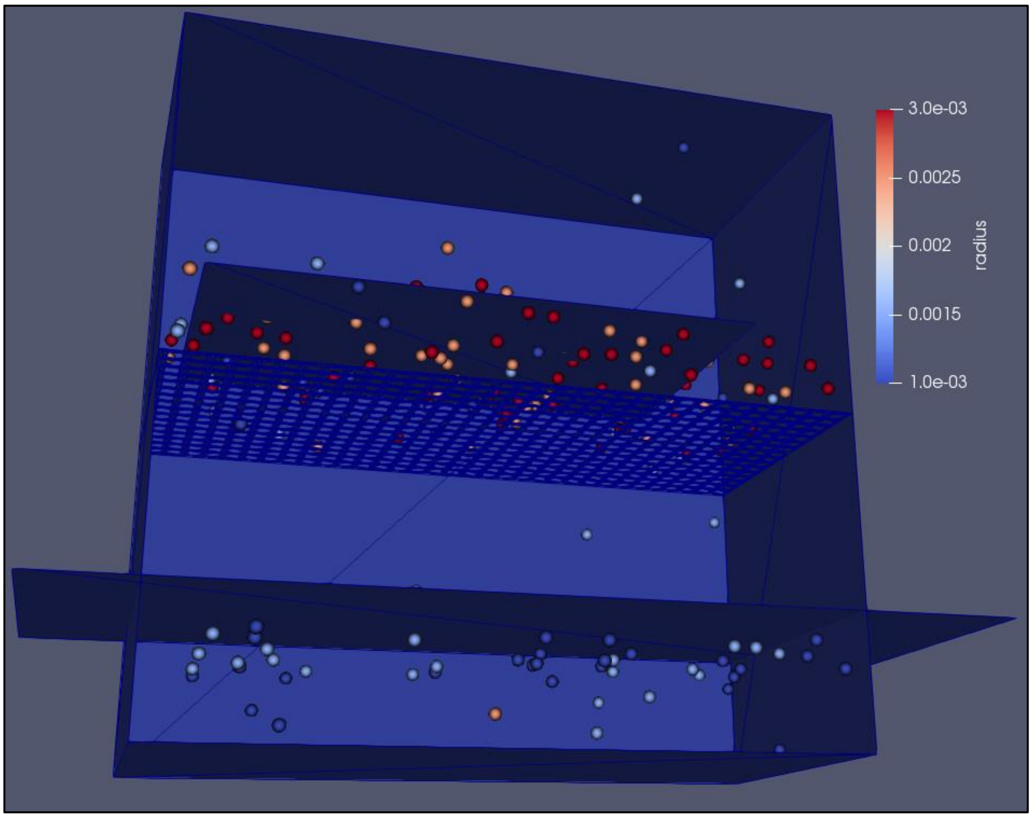

2. For the Square Sieve with 600 Particles
    a. The worst performing simulation was the 0° stroke with an 8.7% passing rate.

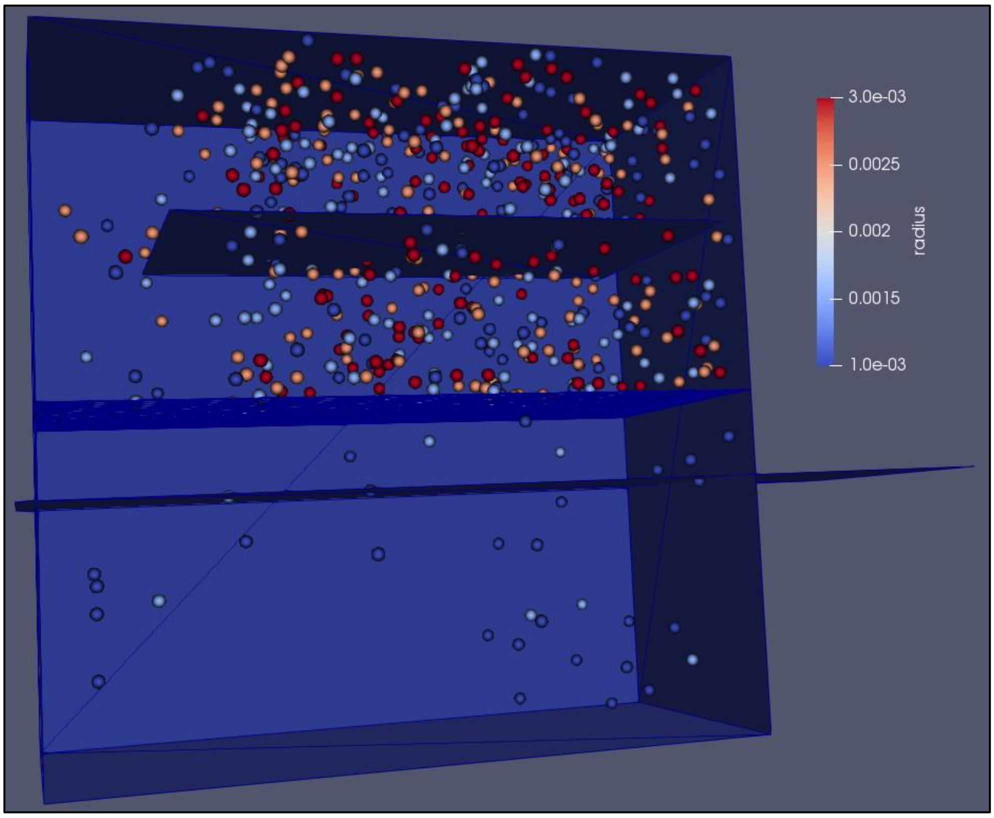

    b. The best performing simulation was the 90° stroke with a 73.7% passing rate.

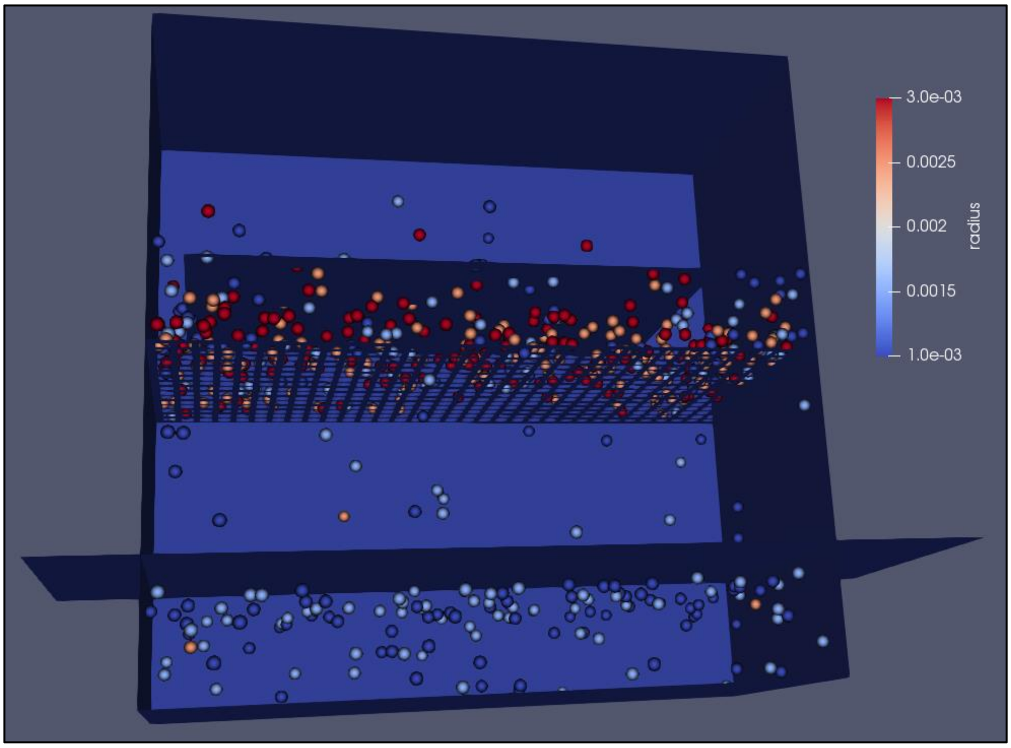

3. For the Square Sieve with 1800 Particles

   a. The worst performing simulation was the 0° stroke with a 5.3% passing rate.

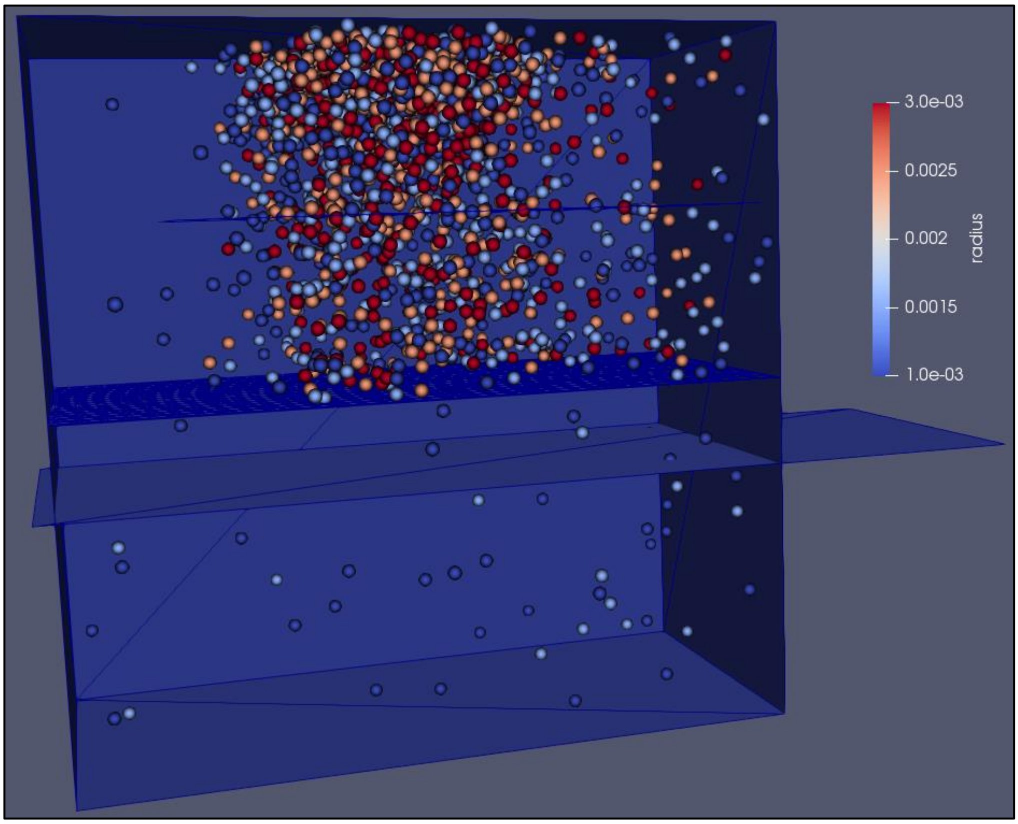

   b. The best performing simulation was the 90° stroke with a 56.9% passing rate.

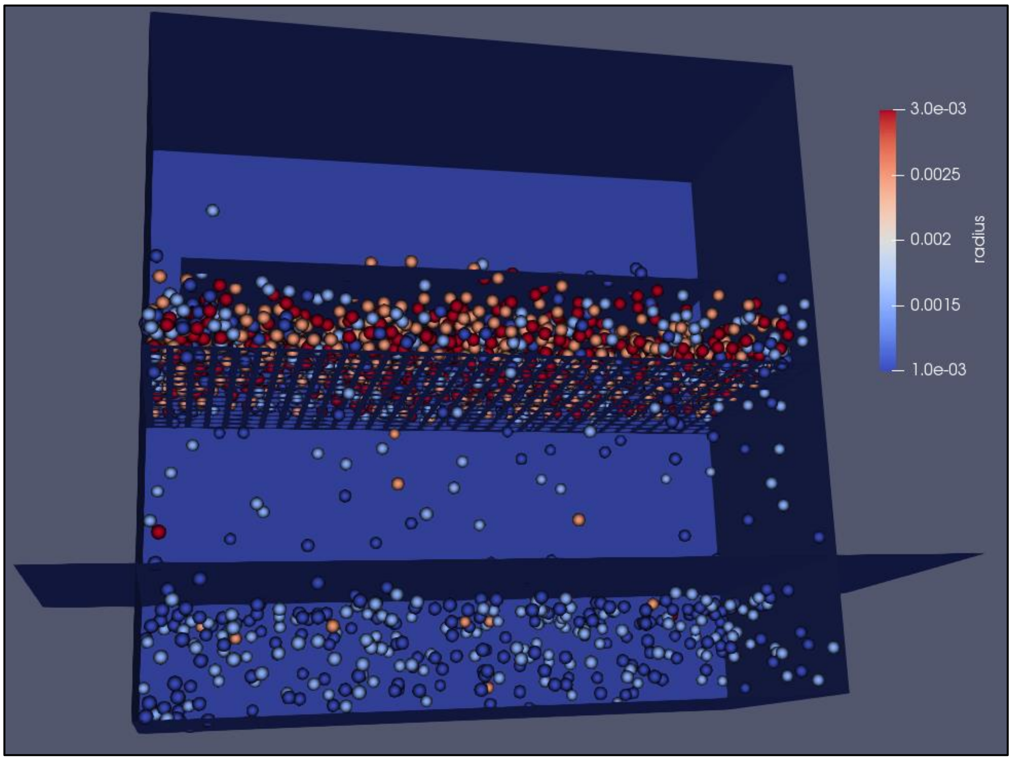

Square Extruded Sieve

1. For the Square Extruded Sieve with 200 Particles
    a. The worst performing simulation was the 0° stroke with a 4% passing rate.

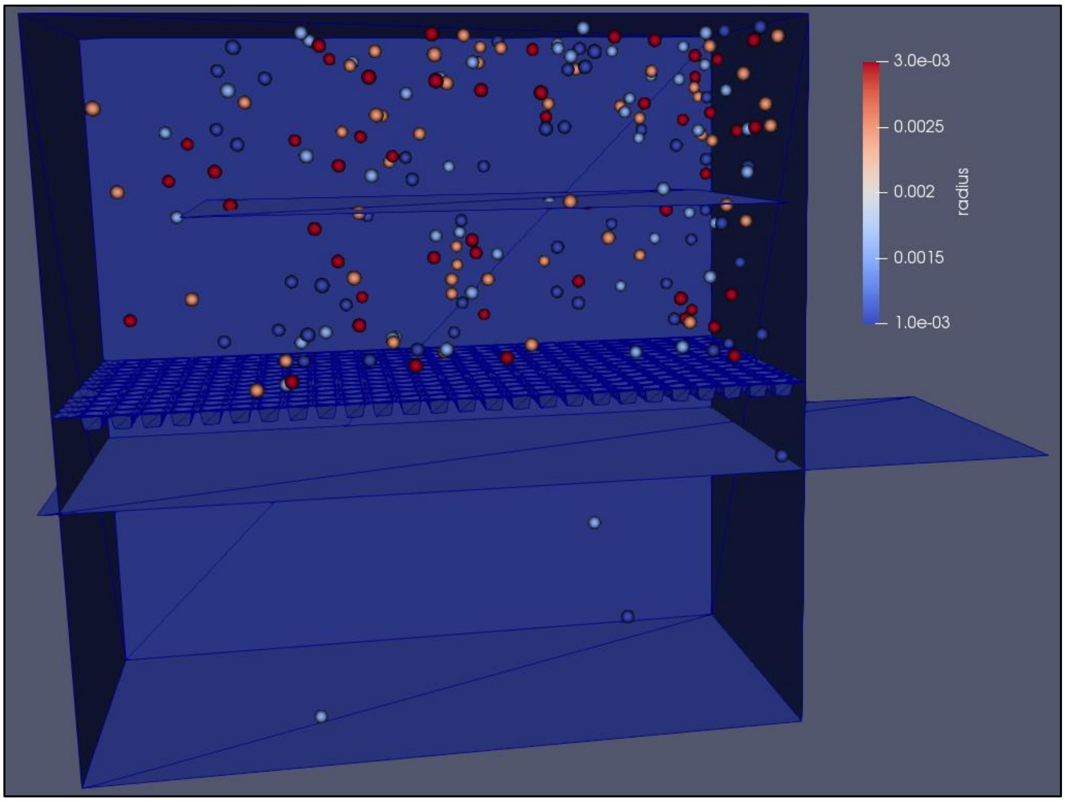

    b. The best performing simulation was the 90° stroke with a 81% passing rate.

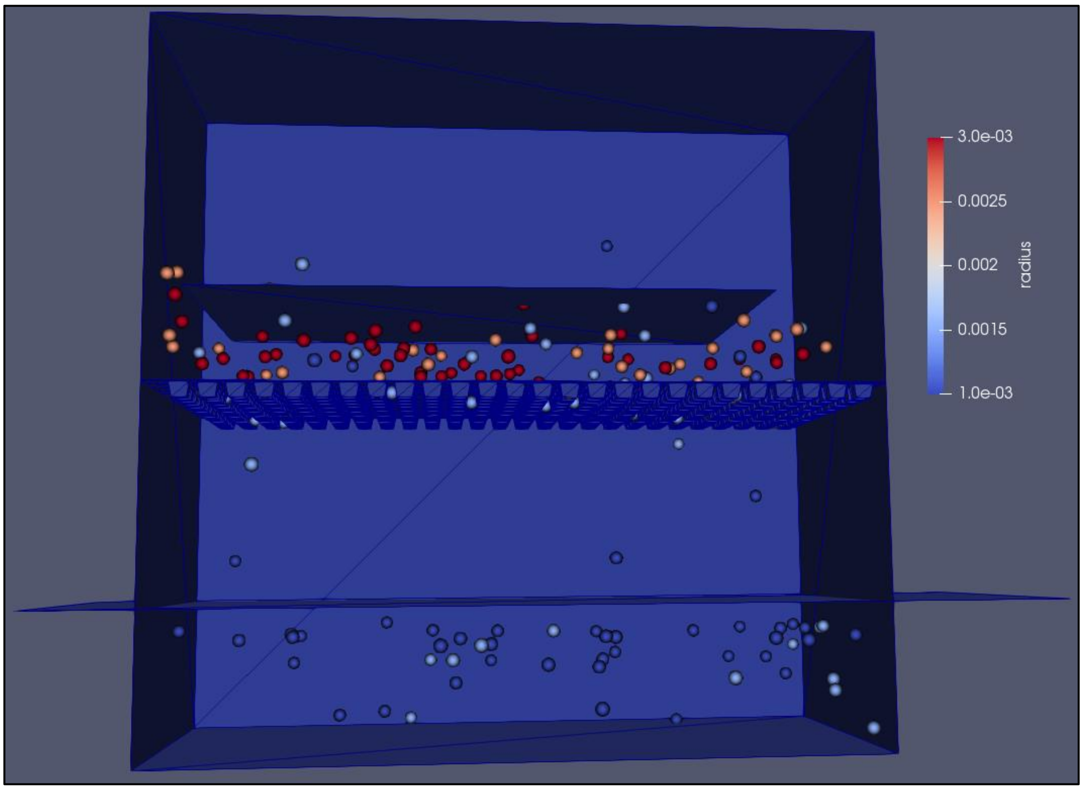

2. For the Square Extruded Sieve with 600 Particles

   a. The worst performing simulation was the 0° stroke with a 4% passing rate.

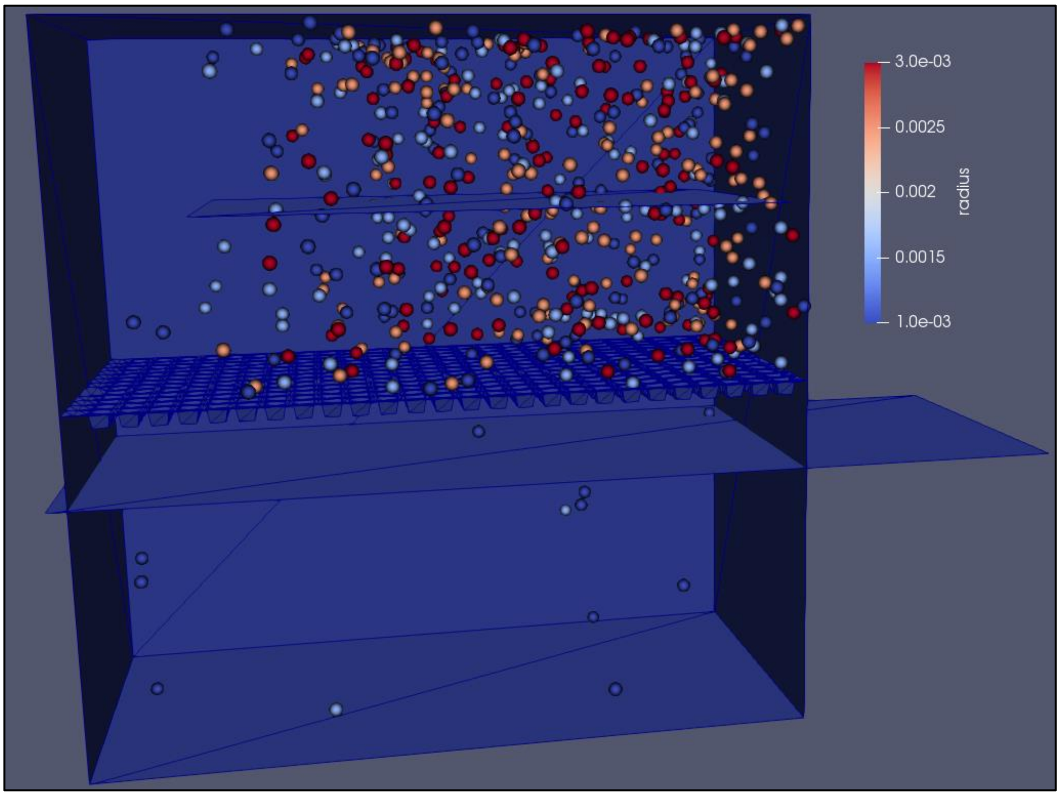

   b. The best performing simulation was the 90° stroke with a 69.3% passing rate.

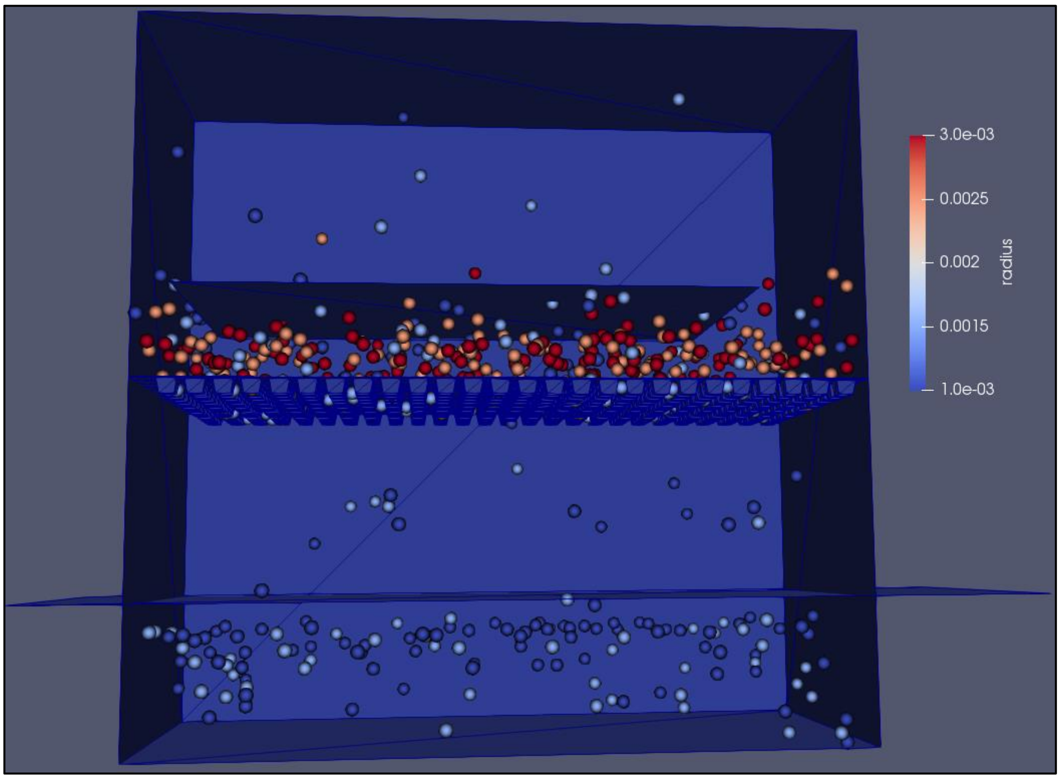

3. For the Square Extruded Sieve with 1800 Particles

   a. The worst performing simulation was the 0° stroke with a 4% passing rate.

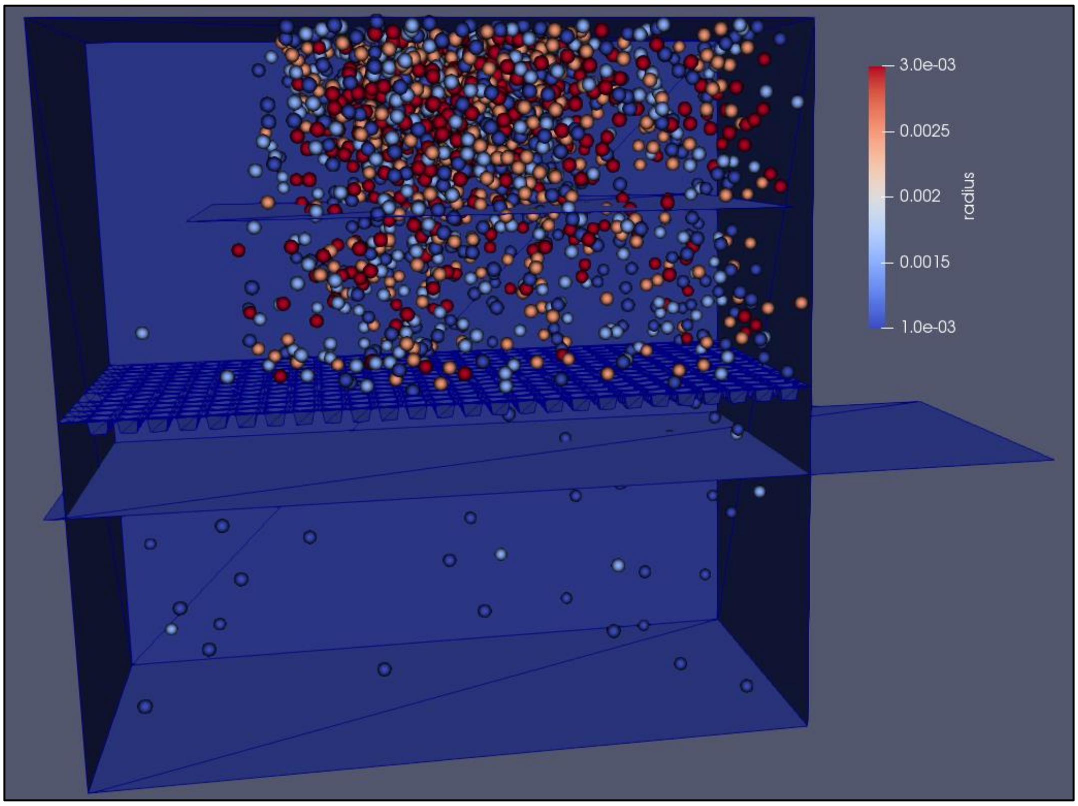

   b. The best performing simulation was the 90° stroke with a 45.8% passing rate.

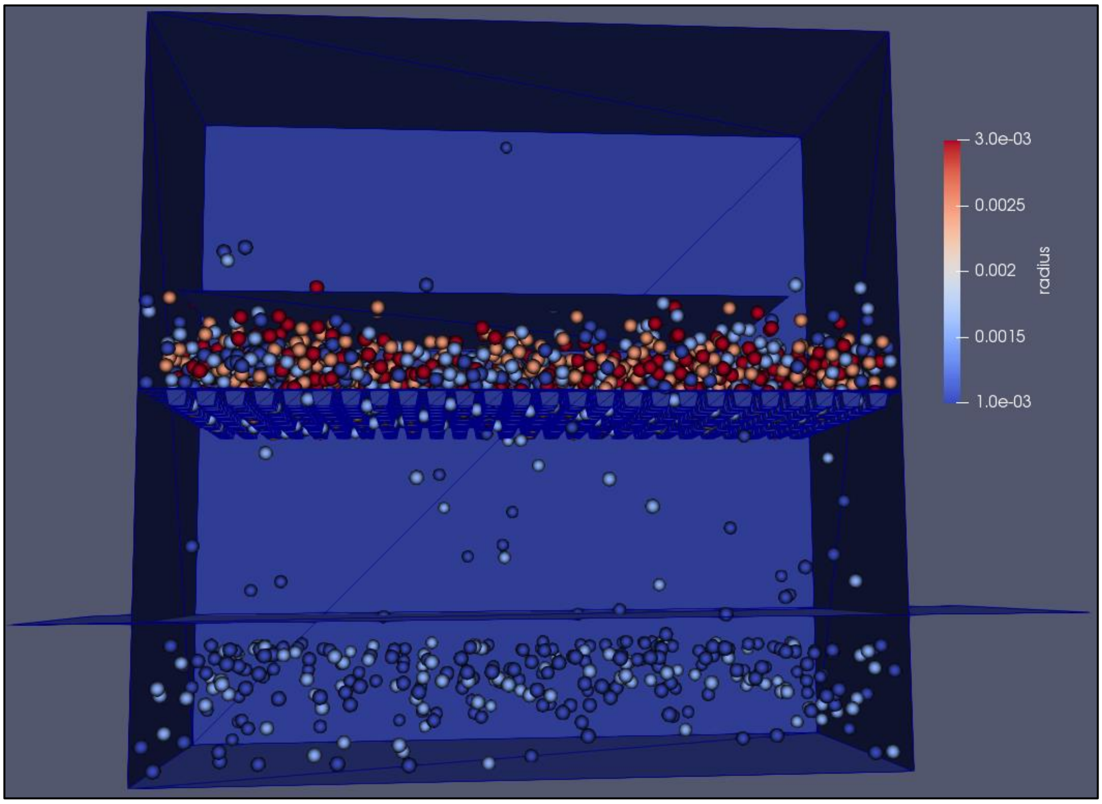

Rectangular Sieve

1. For the Rectangular Sieve with 200 Particles
   a. The worst performing simulation was the 0° stroke with a 23% passing rate.

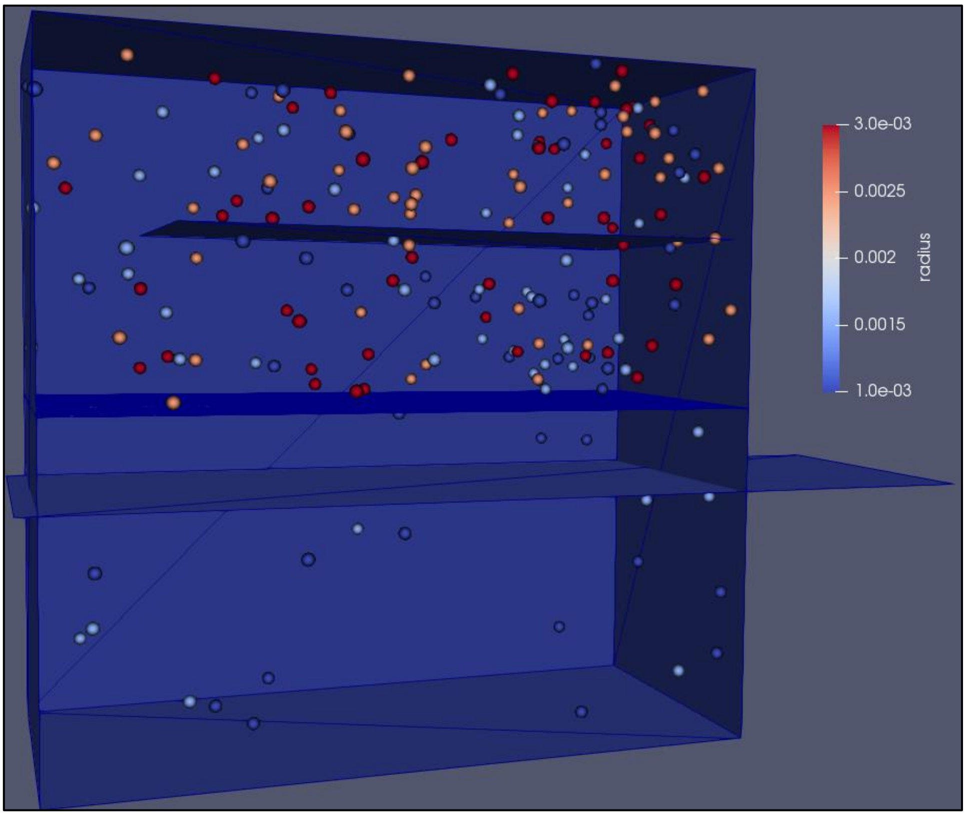

   b. The best performing simulation was the 75° stroke with a 82% passing rate.

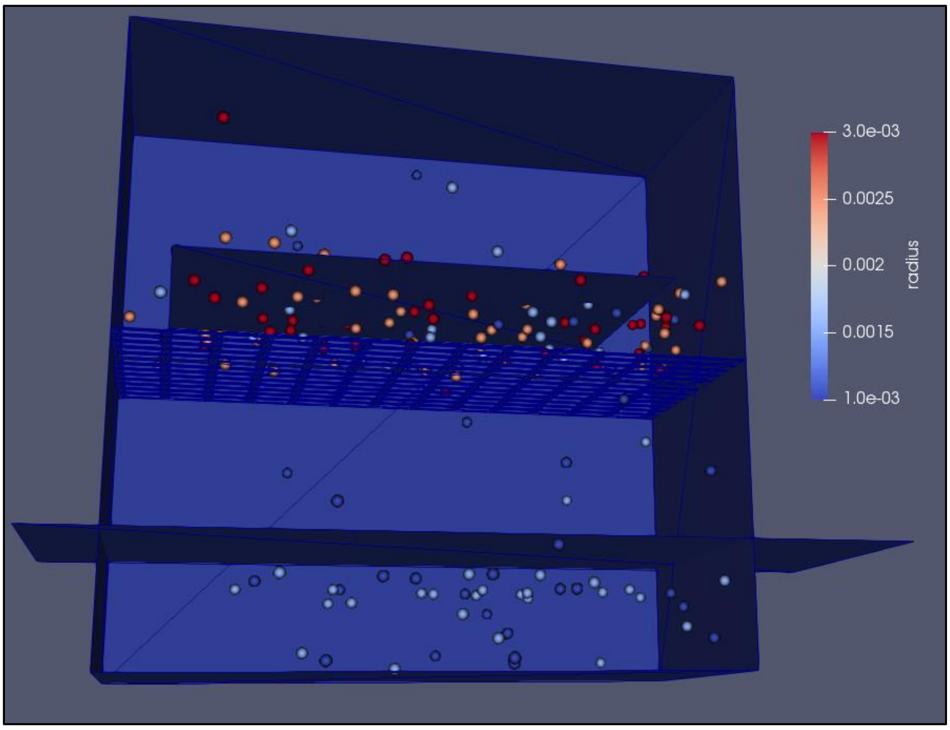

2. For the Rectangular Sieve with 600 Particles

   a. The worst performing simulation was the 0° stroke with a 23.3% passing rate.

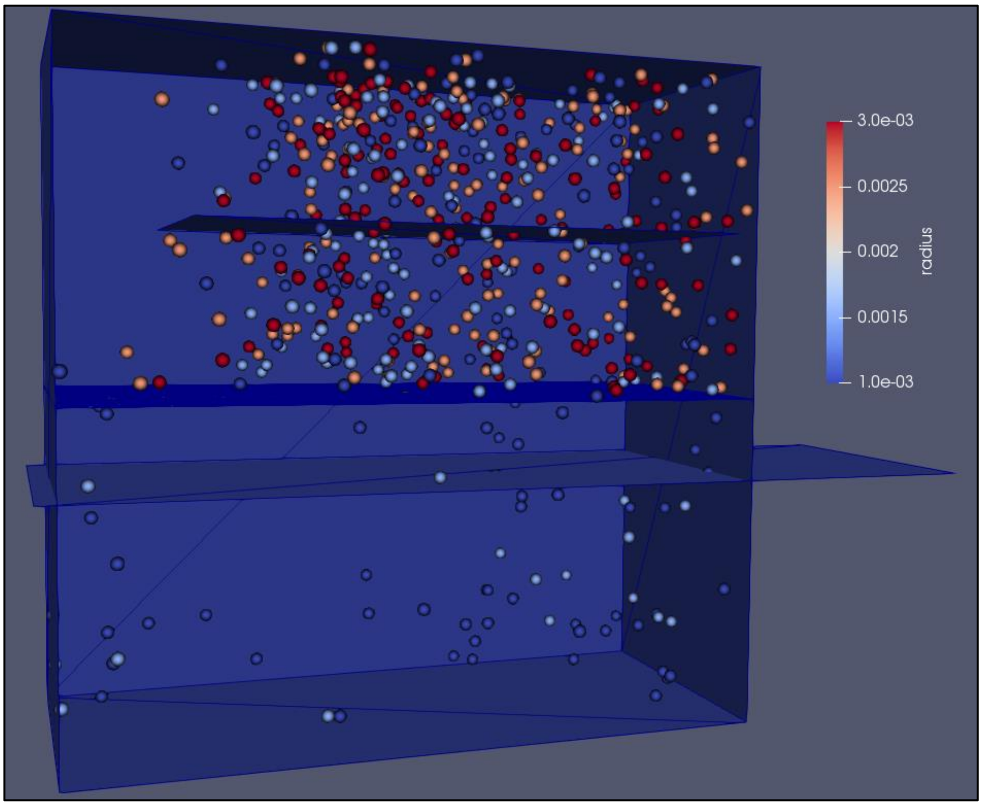

   b. The best performing simulation was the 90° stroke with a 76.7% passing rate.

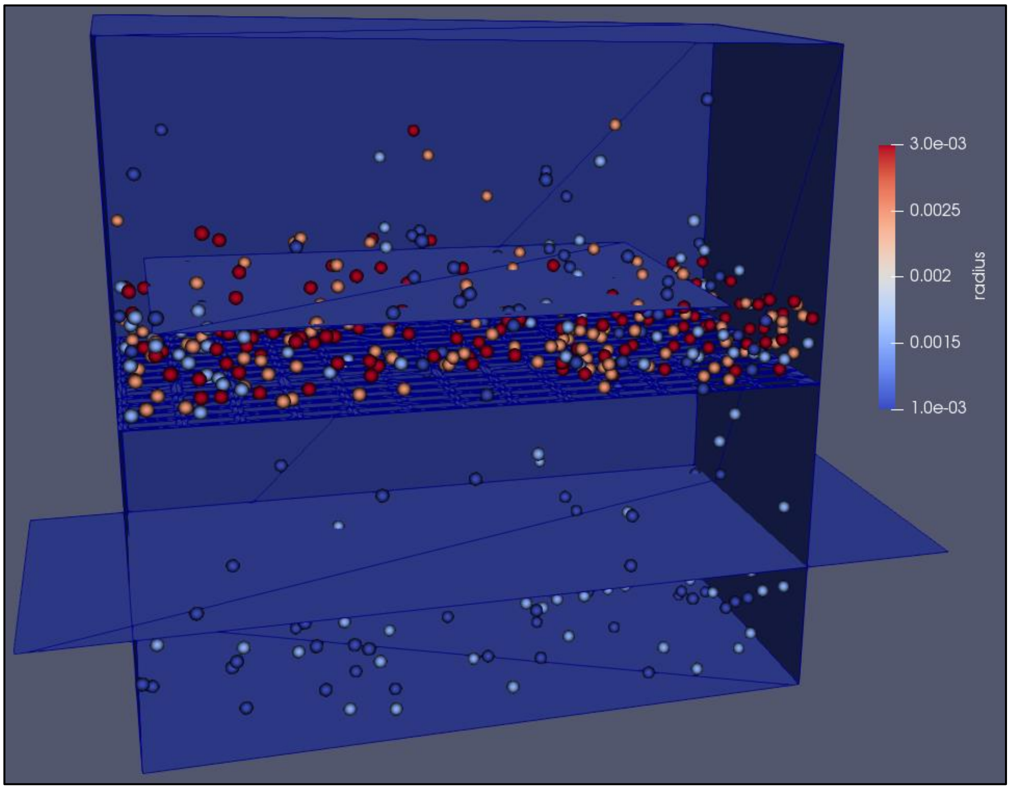

3. For the Rectangular Sieve with 1800 Particles

   a. The worst performing simulation was the 0° stroke with a 13.2% passing rate.

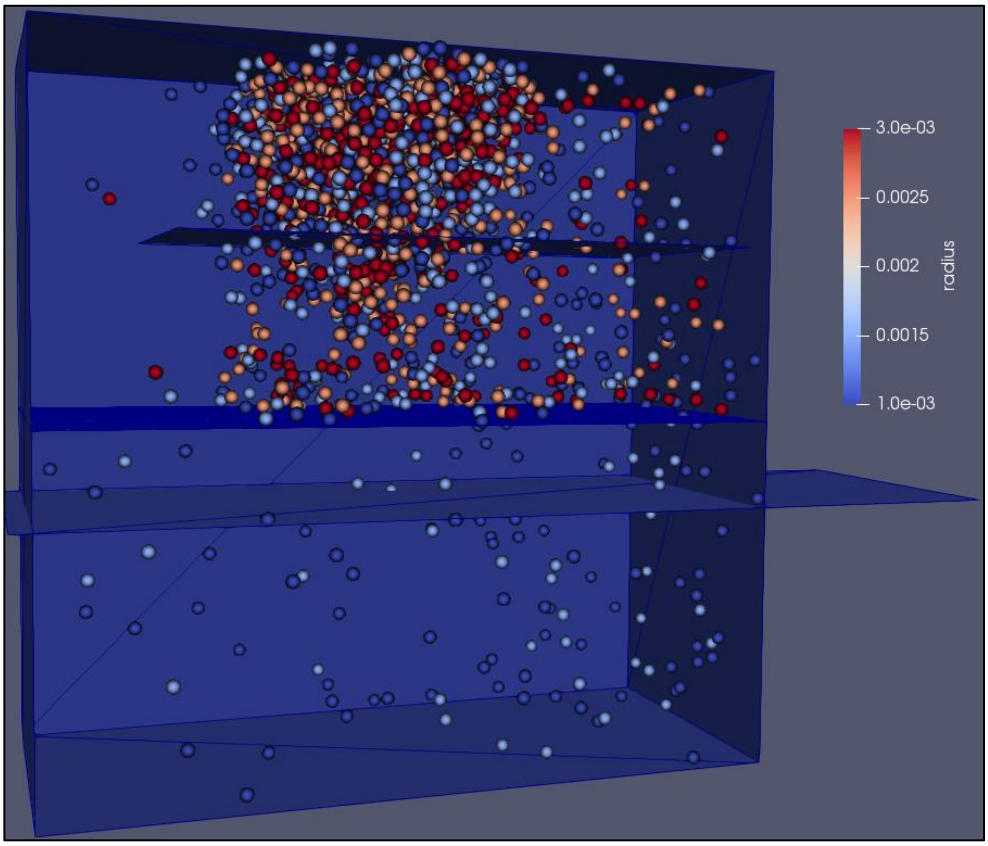

   b. The best performing simulation was the 90° stroke with a 58% passing rate.

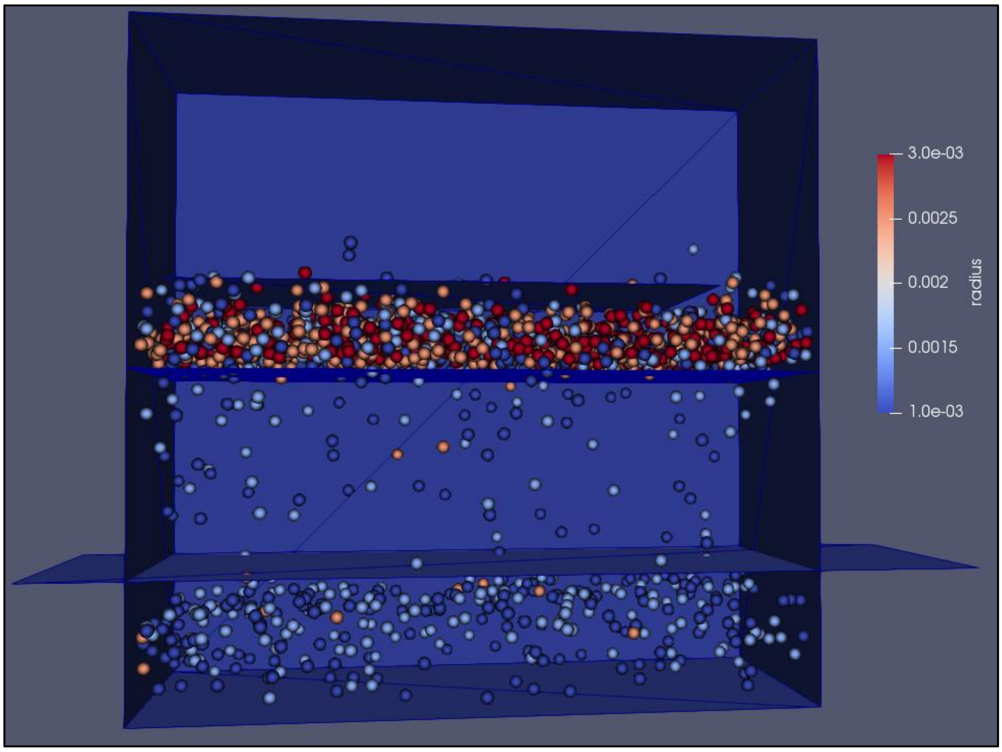

Rectangular Extruded Sieve

1. For the Rectangular Extruded Sieve with 200 Particles
    a. The worst performing simulation was the 0° stroke with a 13% passing rate.

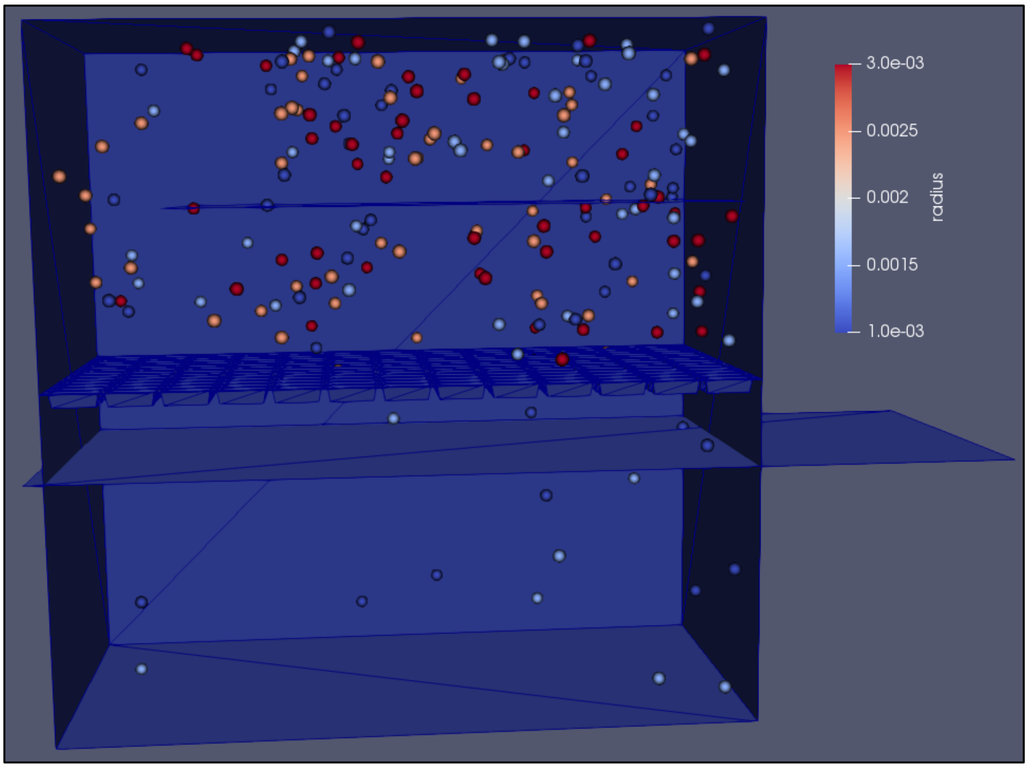

    b. The best performing simulation was the 75° stroke with a 91% passing rate.

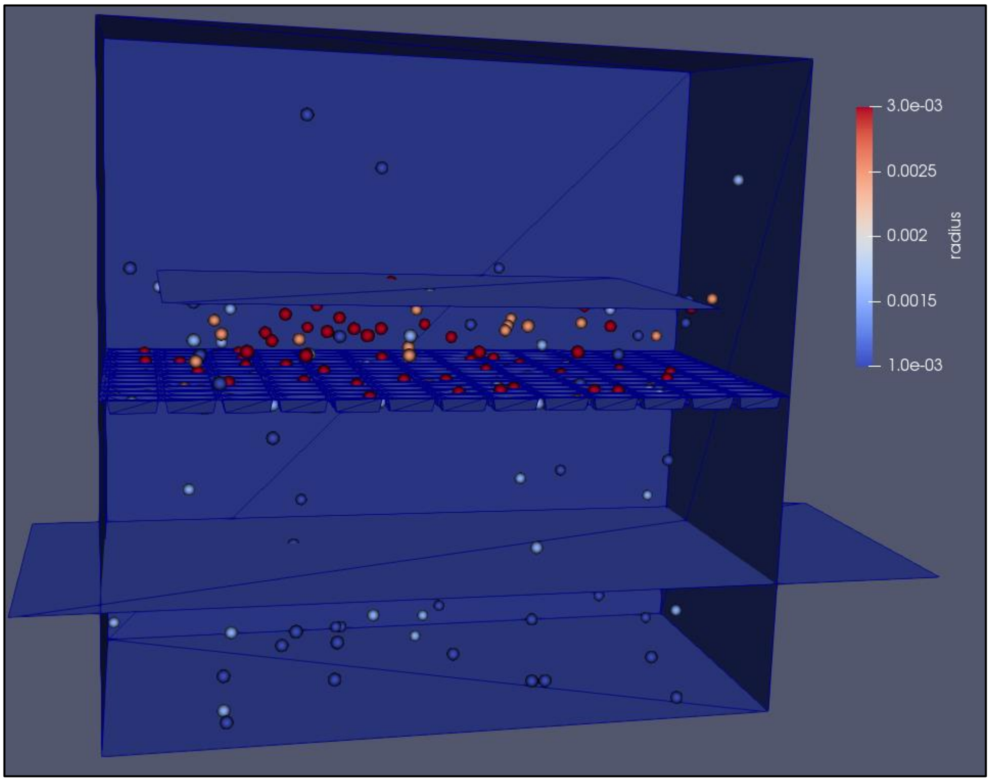

2. For the Rectangular Extruded Sieve with 600 Particles

    a. The worst performing simulation was the 0° stroke with a 21.3% passing rate.

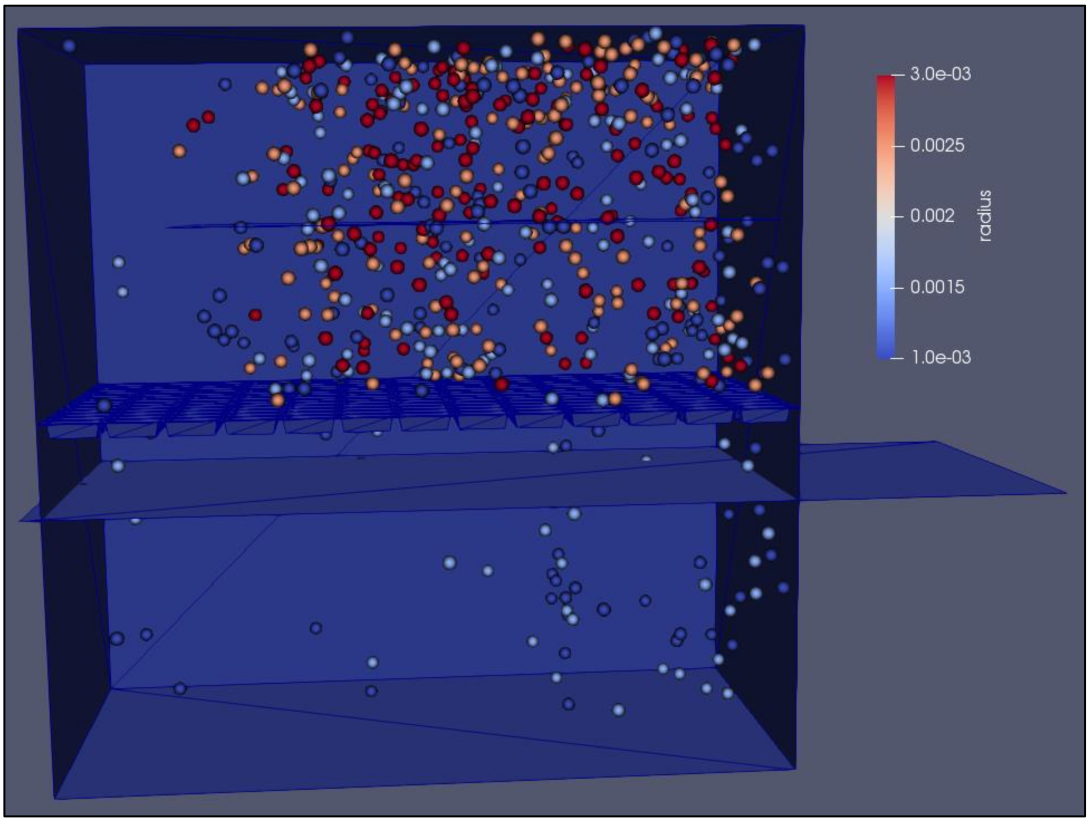

    b. The best performing simulation was the 90° stroke with a 84% passing rate.

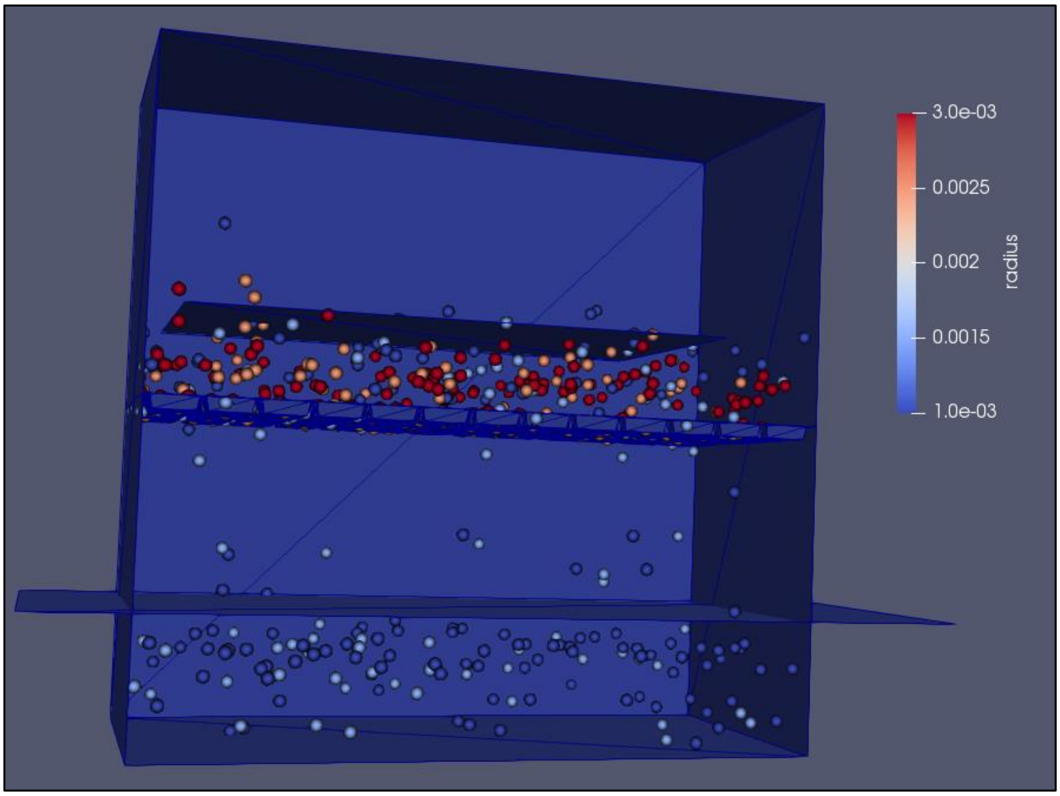

3. For the Rectangular Extruded Sieve with 1800 Particles

    a. The worst performing simulation was the 0° stroke with a 11% passing rate.

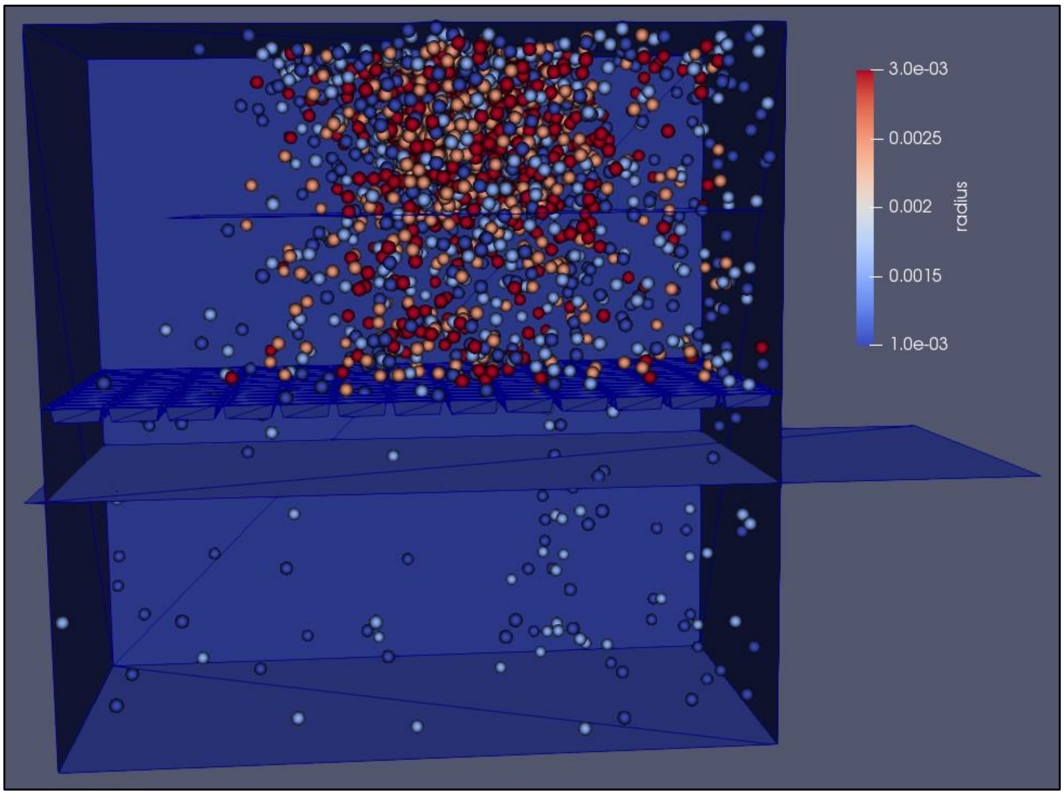

    b. The best performing simulation was the 90° stroke with a 50.8% passing rate.

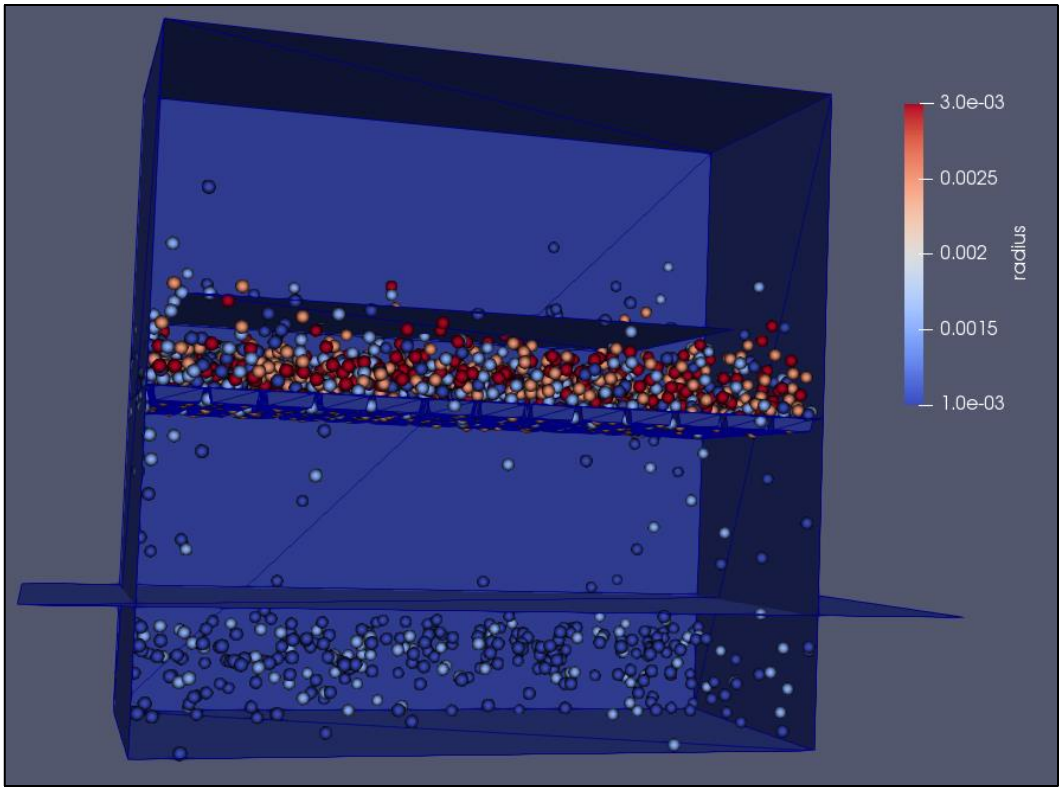

Circular Sieve

1. For the Circular Sieve with 200 Particles
   a. The worst performing simulation was the 0° stroke with a 7% passing rate.

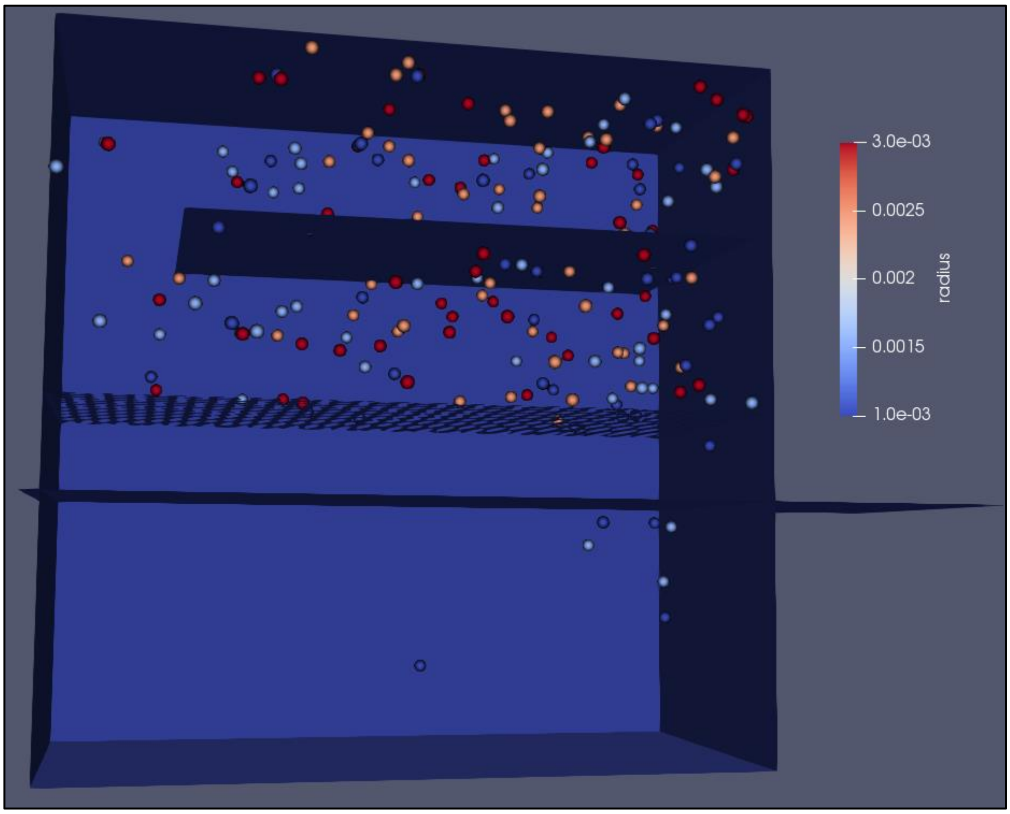

   b. The best performing simulation was the 75° stroke with a 75% passing rate.

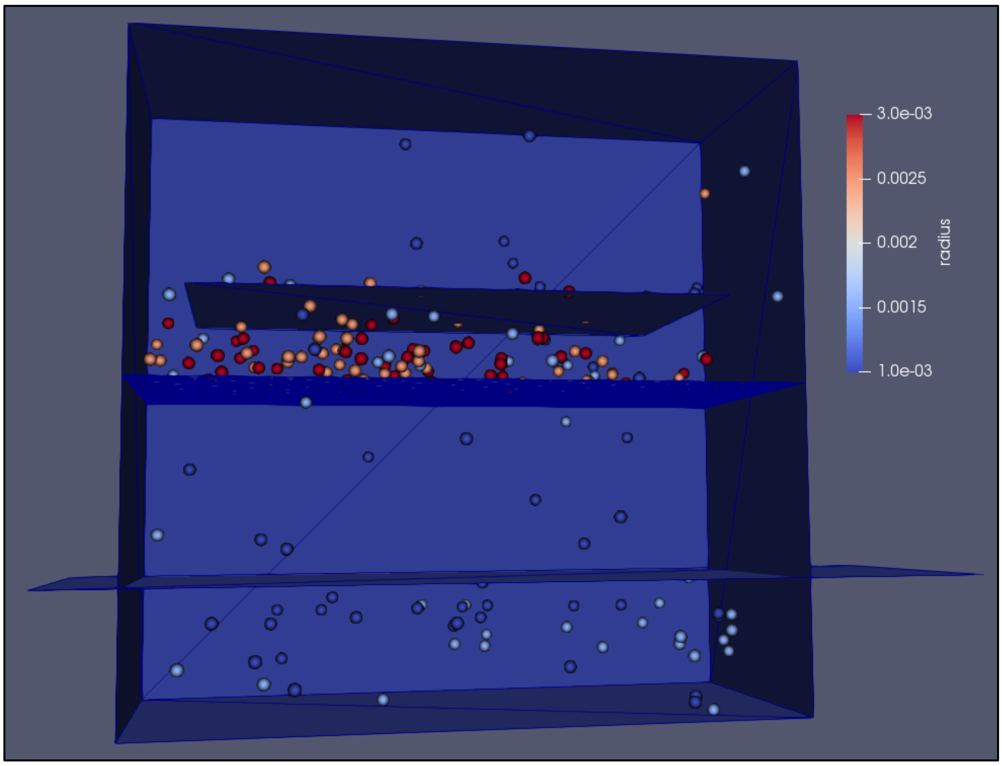

2. For the Circular Sieve with 600 Particles

   a. The worst performing simulation was the 0° stroke with a 7.3% passing rate.

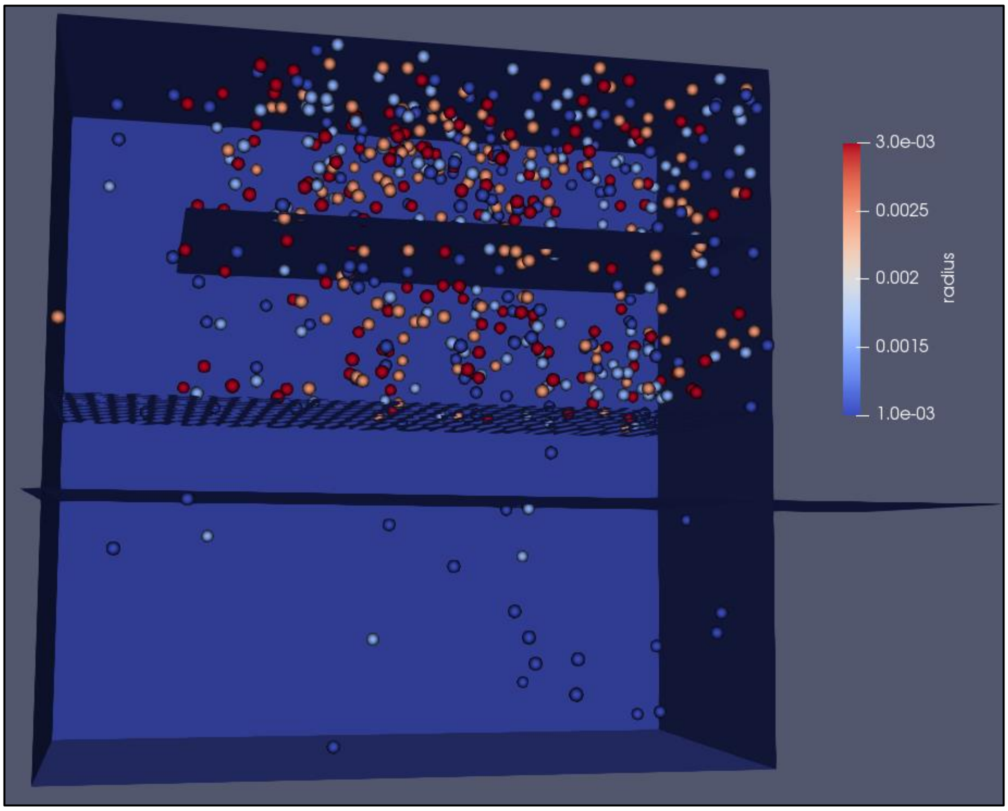

   b. The best performing simulation was the 90° stroke with a 74.3% passing rate.

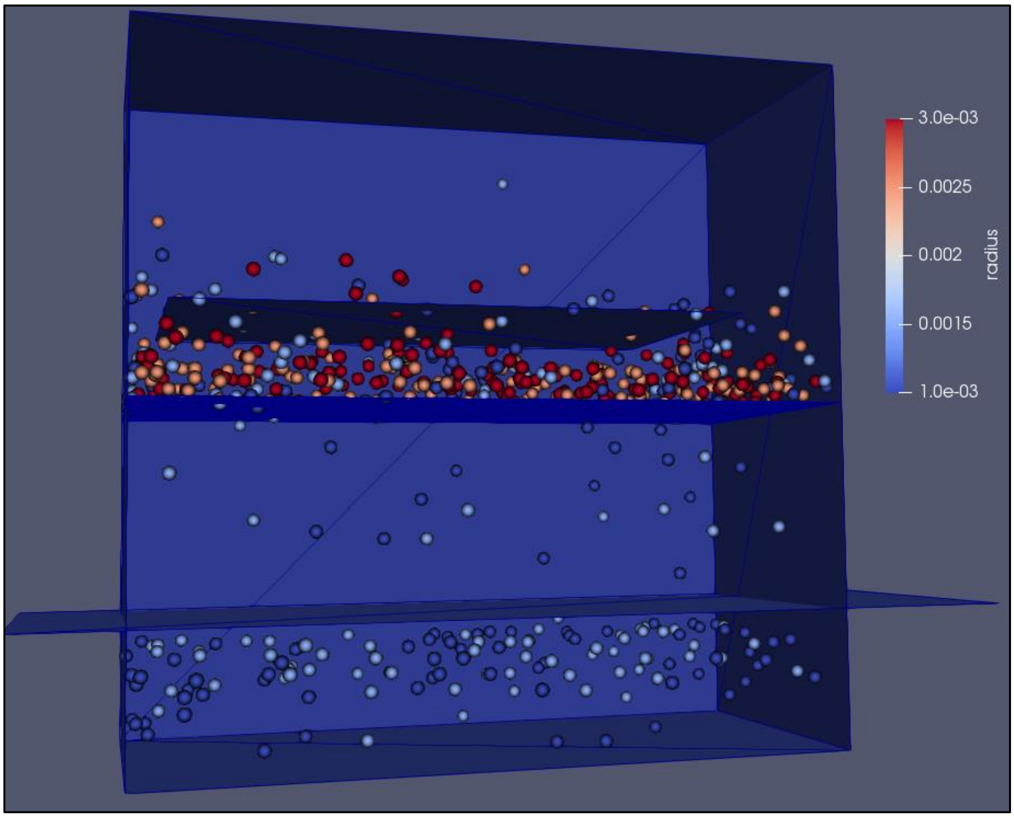

3. For the Circular Sieve with 1800 Particles

   a. The worst performing simulation was the 0° stroke with a 4.9% passing rate.

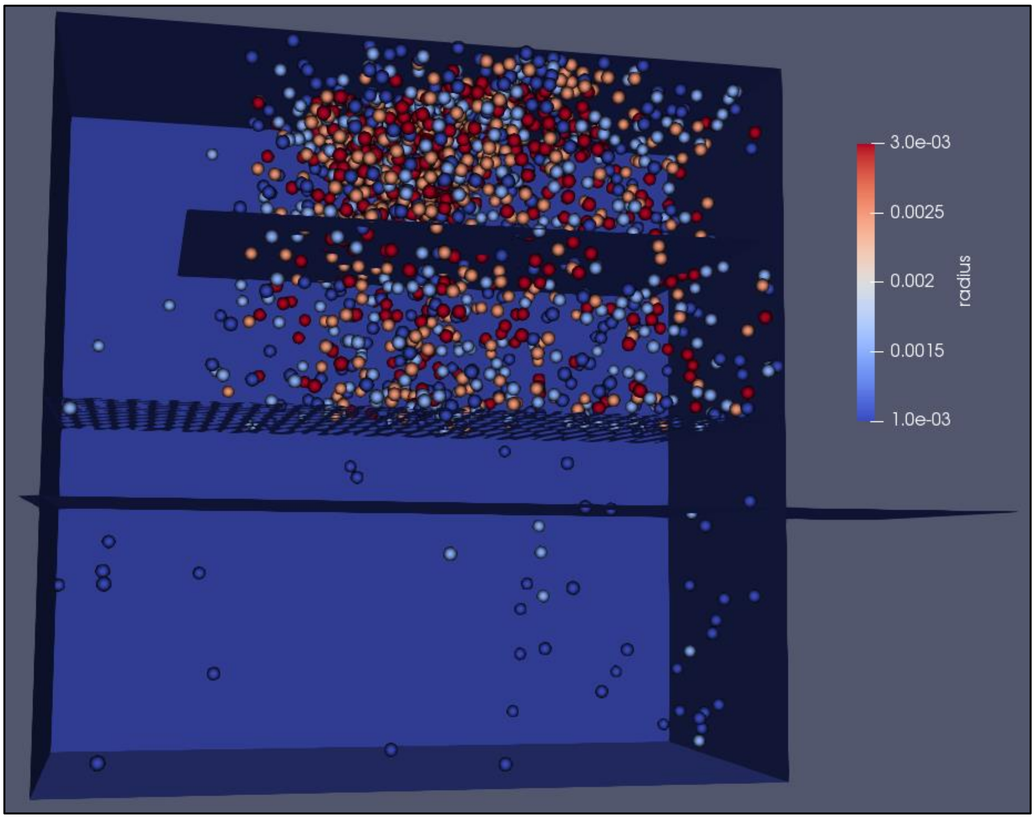

   b. The best performing simulation was the 90° stroke with 56.6% passing rate.

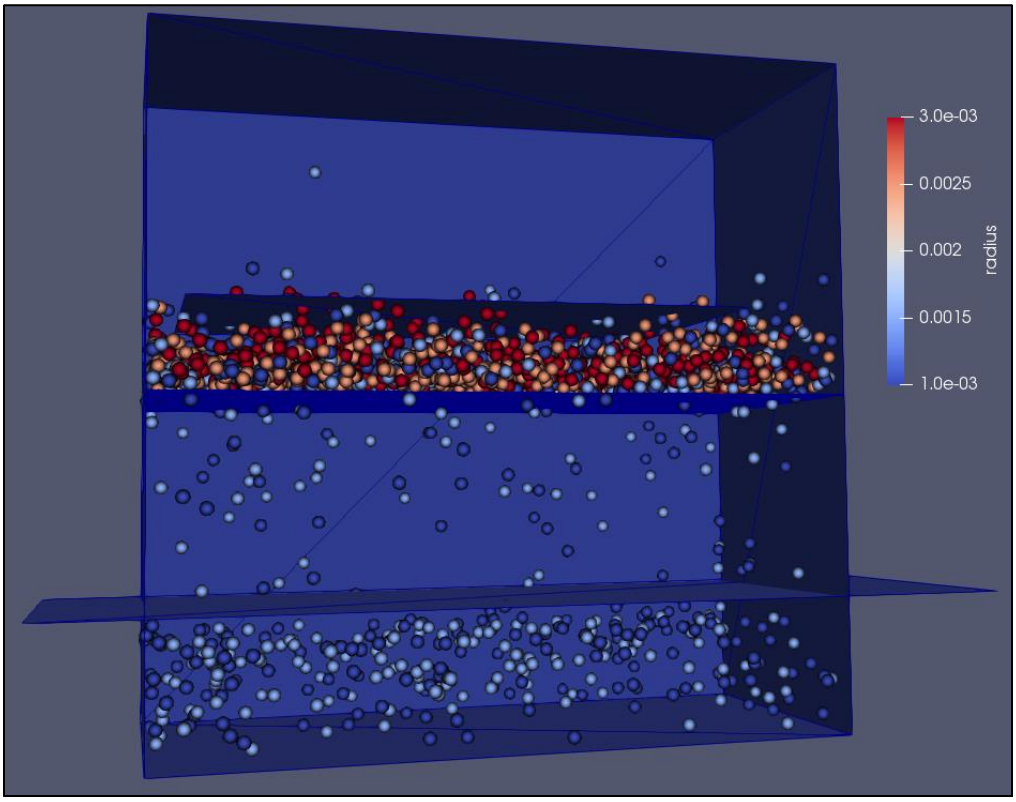

Circular Extruded Sieve

1. For the Circular Extruded Sieve with 200 Particles
   a. The worst performing simulation was the 0° stroke with a 2% passing rate.

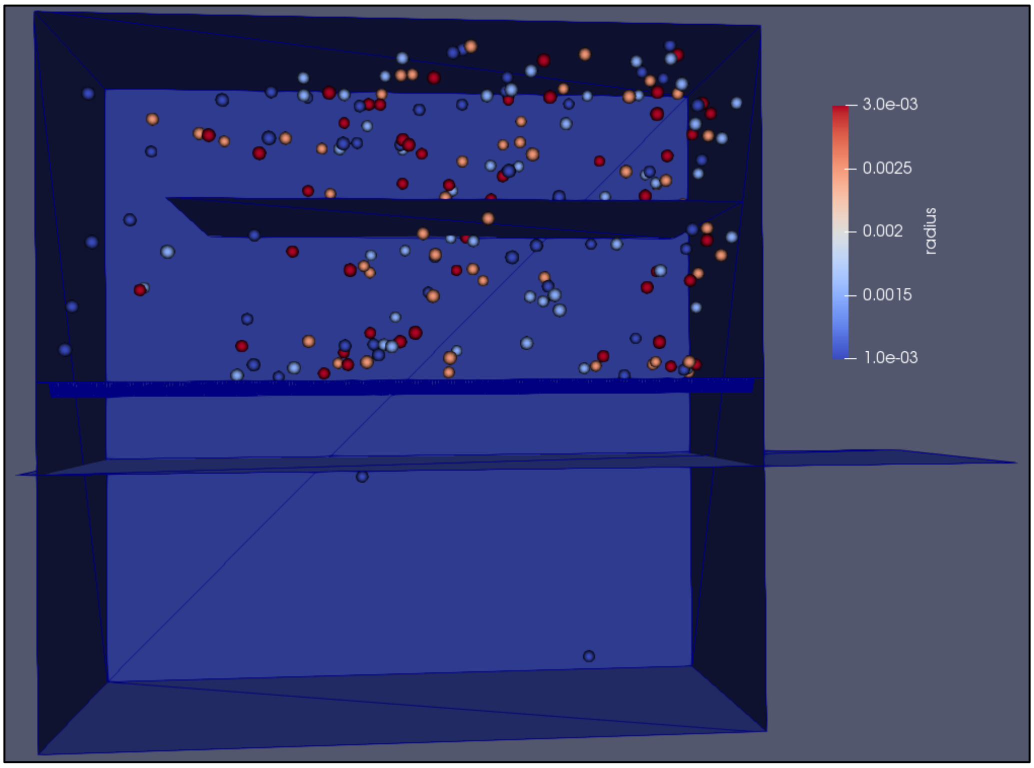

   b. The best performing simulation was the 90° stroke with an 84% passing rate.

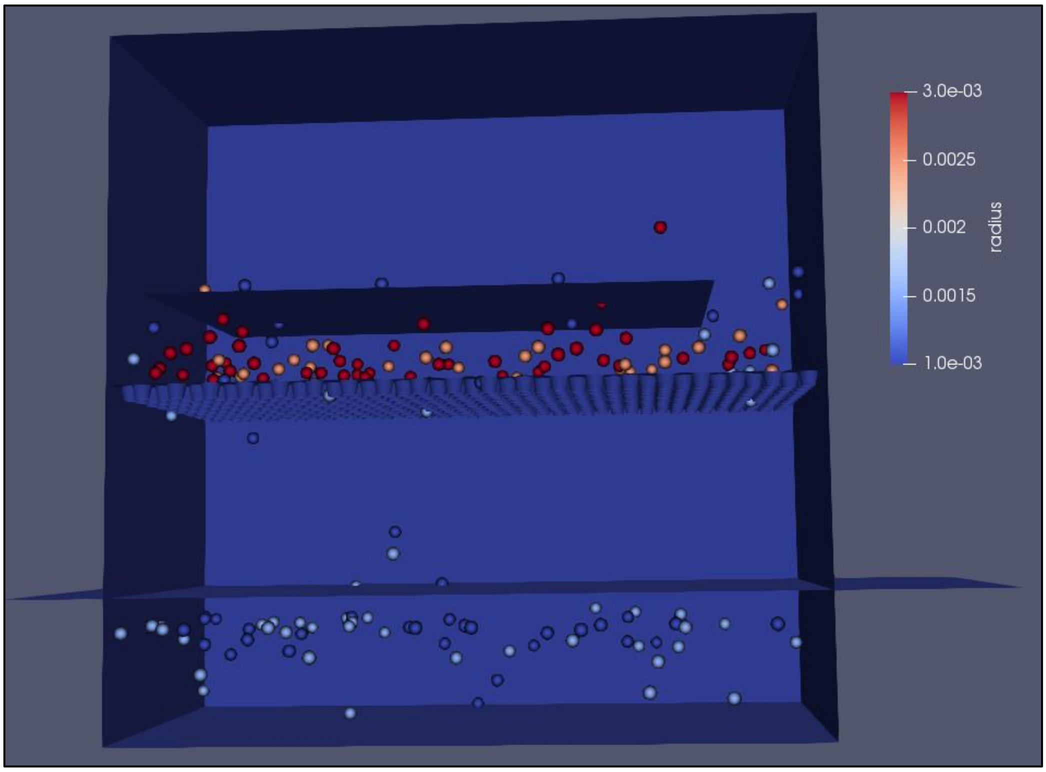

2. For the Circular Extruded Sieve with 600 Particles

   a. The worst performing simulation was the 0° stroke with a 3% passing rate.

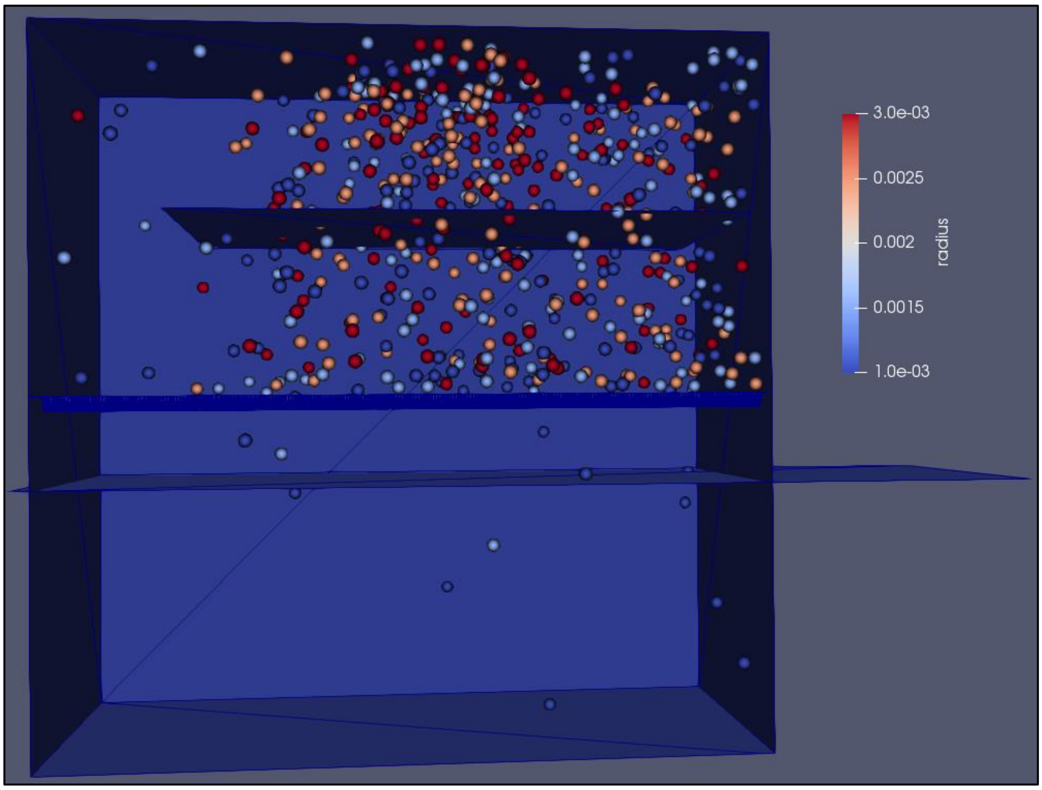

   b. The best performing simulation was the 90° stroke with a 71% passing rate.

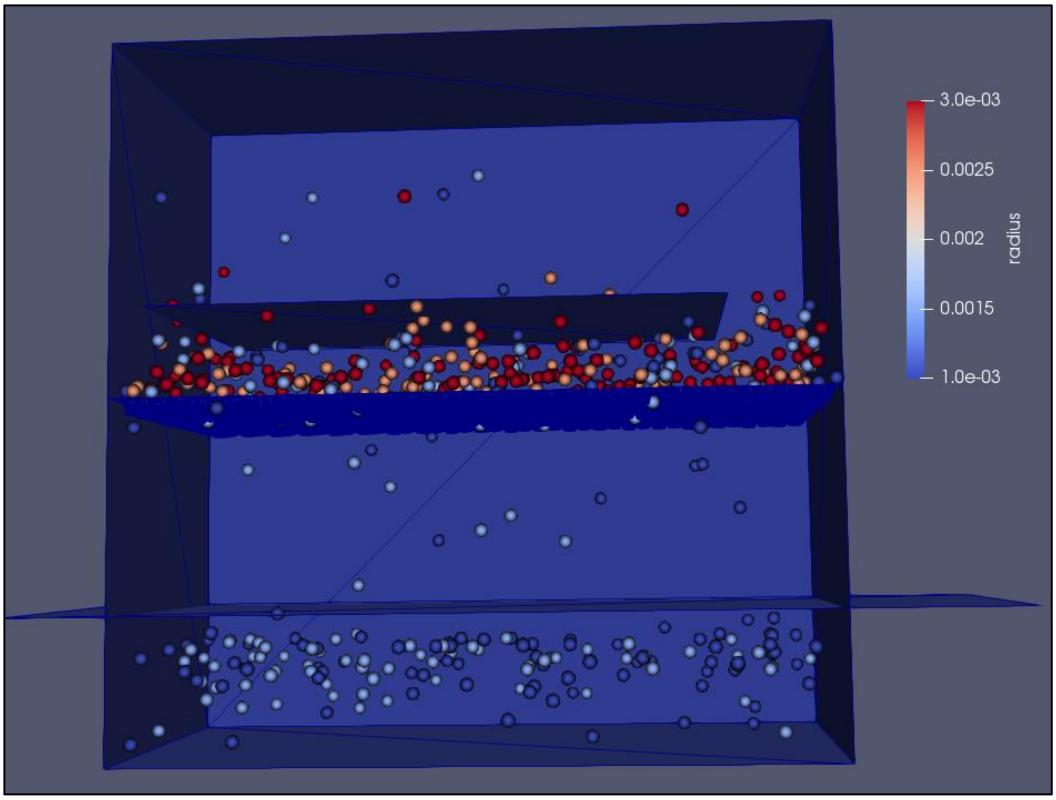

3. For the Circular Extruded Sieve with 1800 Particles

   a. The worst performing simulation was the 0° stroke with a 2.5% passing rate.

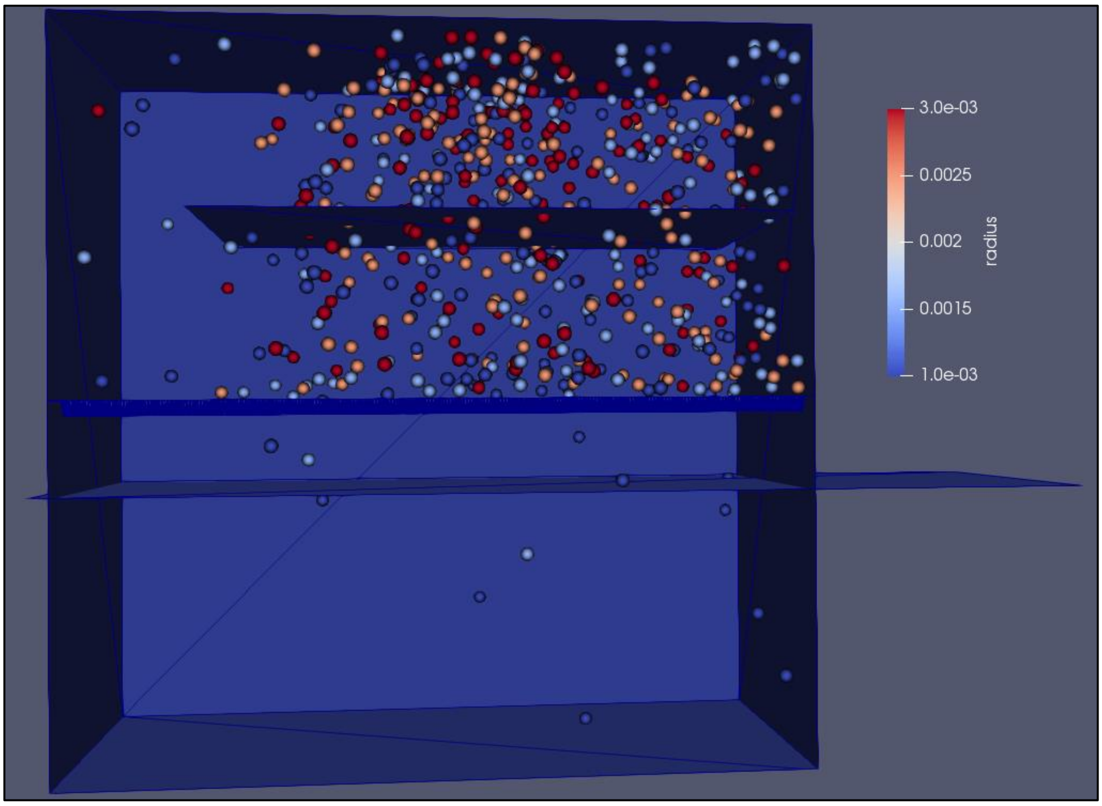

   b. The best performing simulation was the 90° stroke with a 45% passing rate.

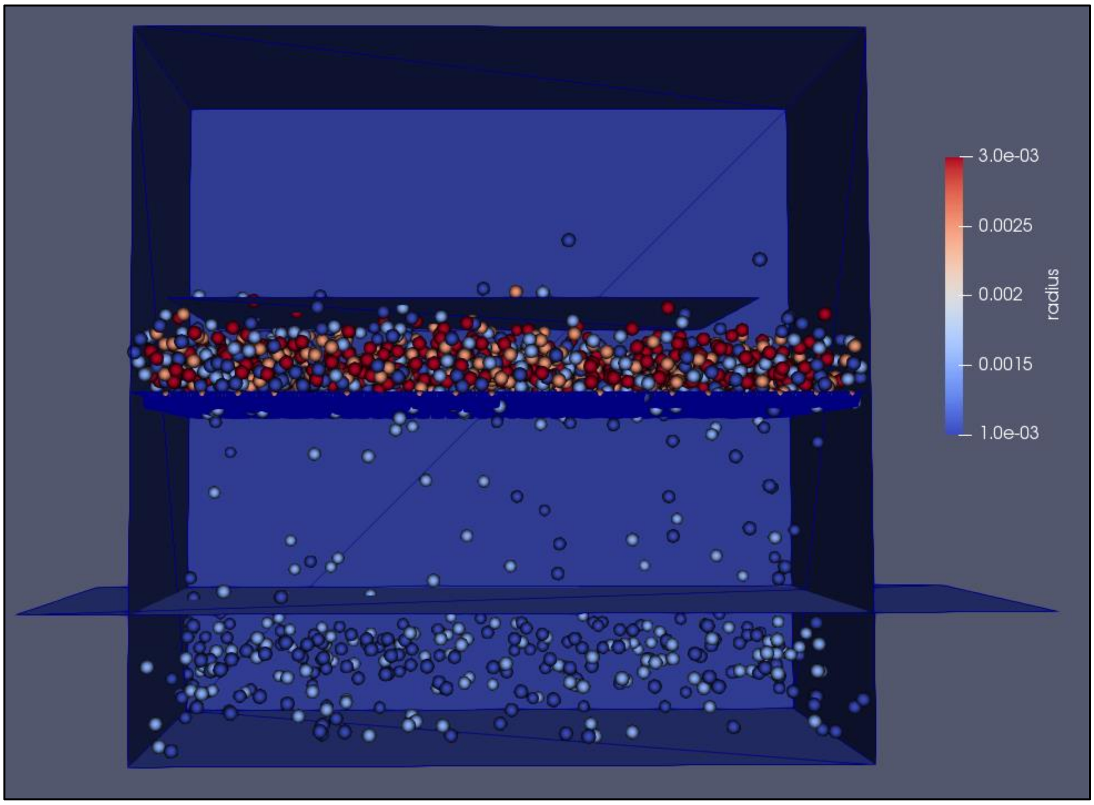

Oval Sieve

1. For the Oval Sieve with 200 Particles

   a. The worst performing simulation was the 0° stroke with a 15% passing rate.

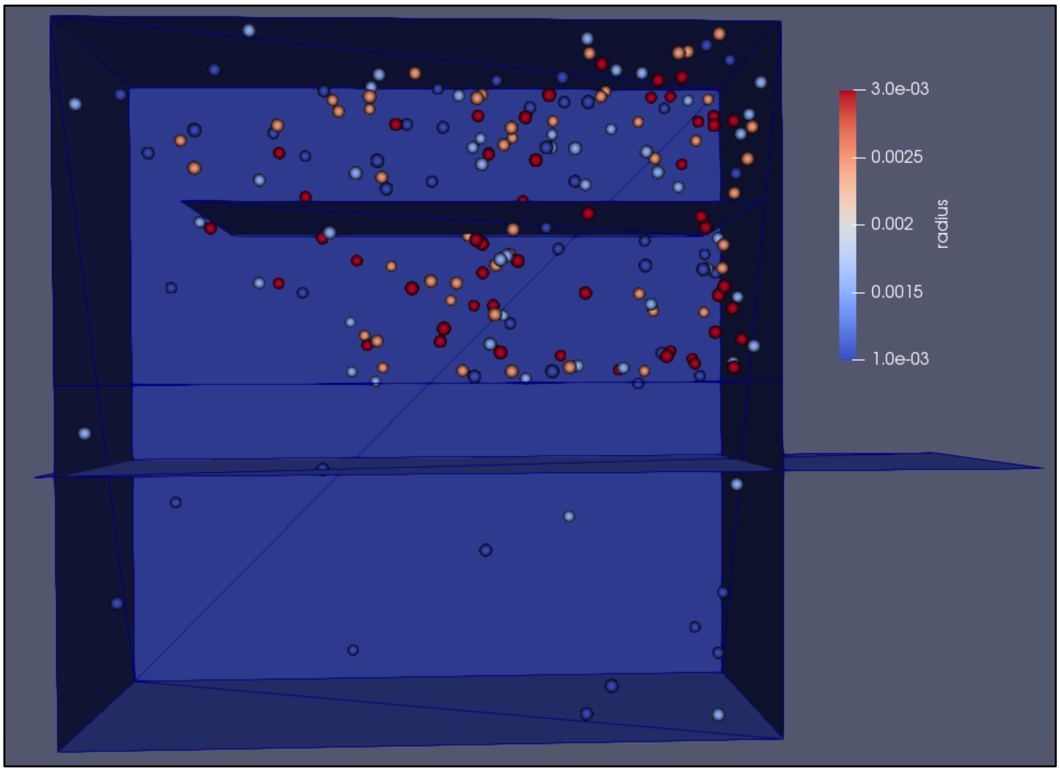

   b. The best performing simulation was the 90° stroke with a 79% passing rate.

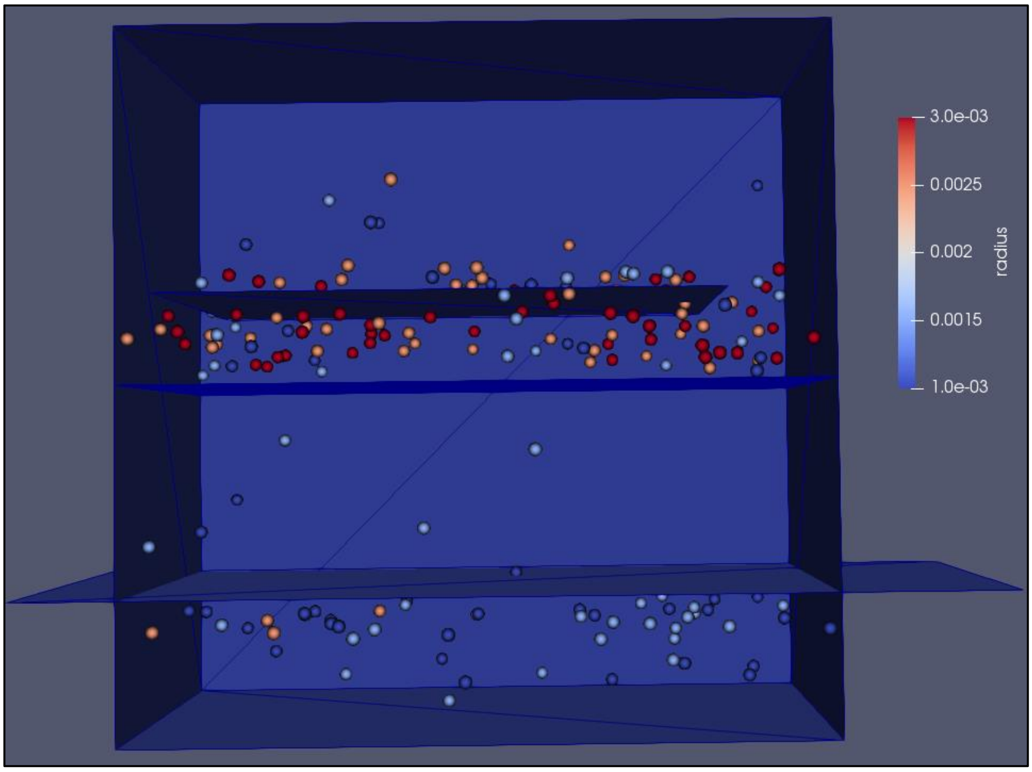

2. For the Oval Sieve with 600 Particles

   a. The worst performing simulation was the 0° stroke with a 20% passing rate.

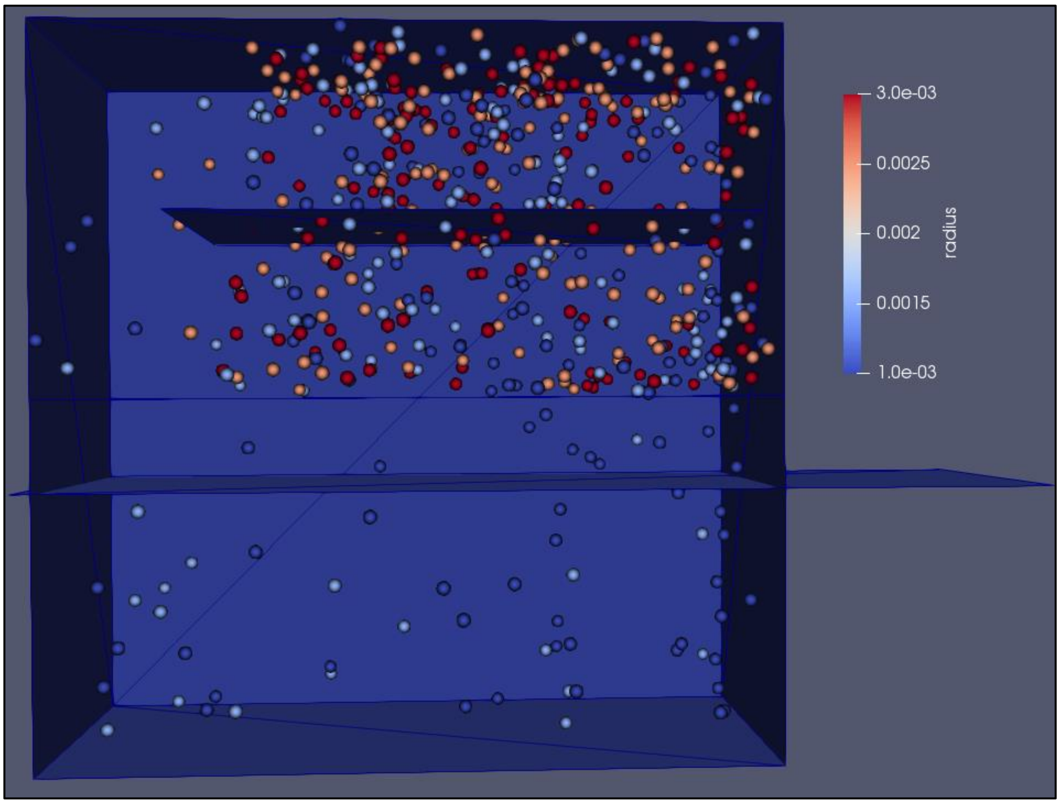

   b. The best performing simulation was the 90° stroke with a 74.3% passing rate.

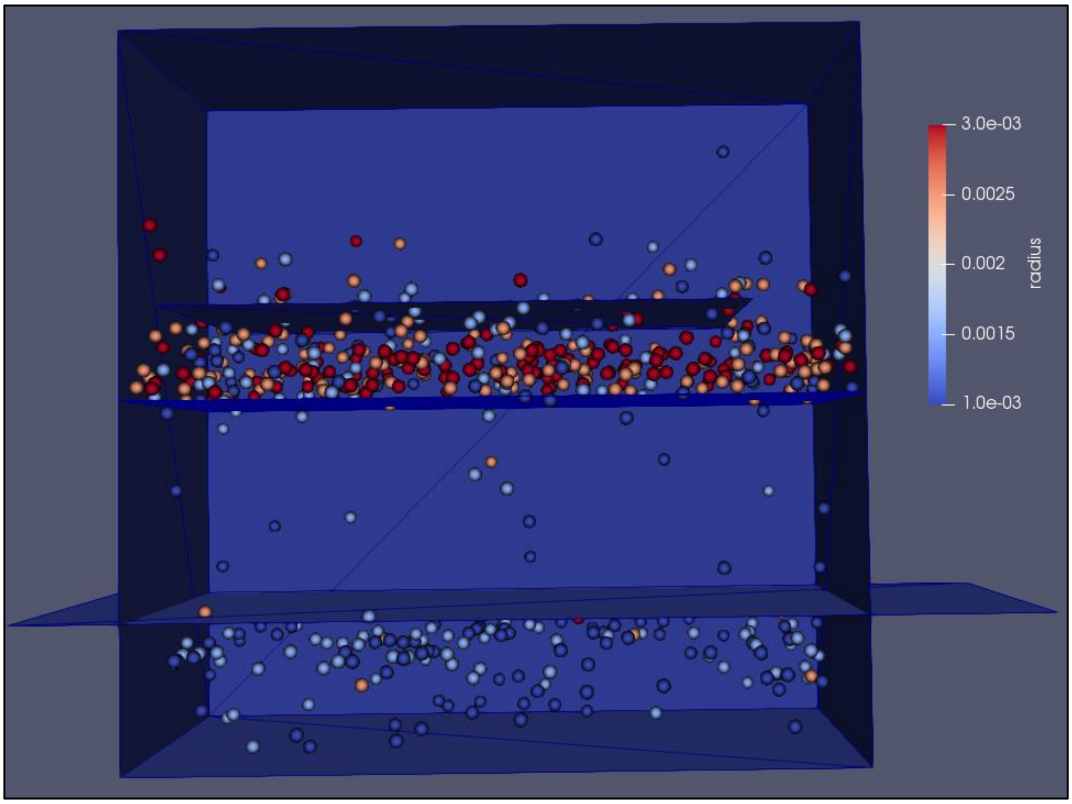

3. For the Oval Sieve with 1800 Particles

   a. The worst performing simulation was the 0° stroke with a 13.1% passing rate.

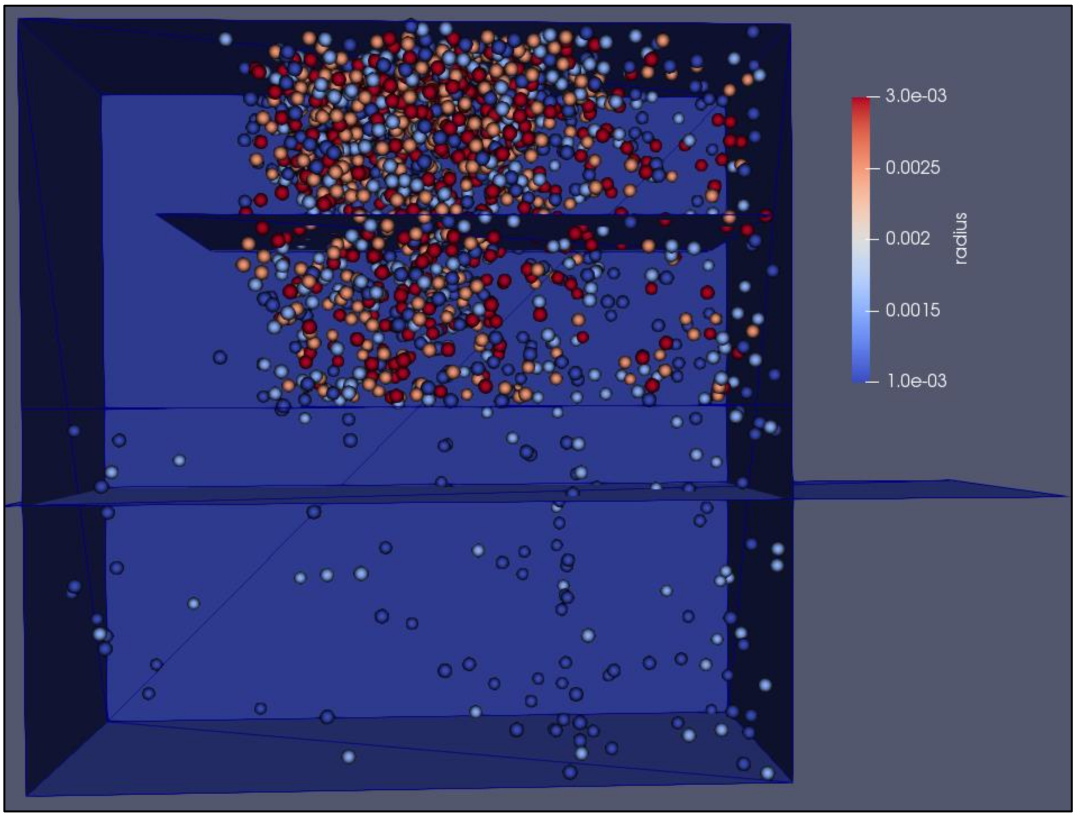

   b. The best performing simulation was the 90° stroke with a 57.8% passing rate.

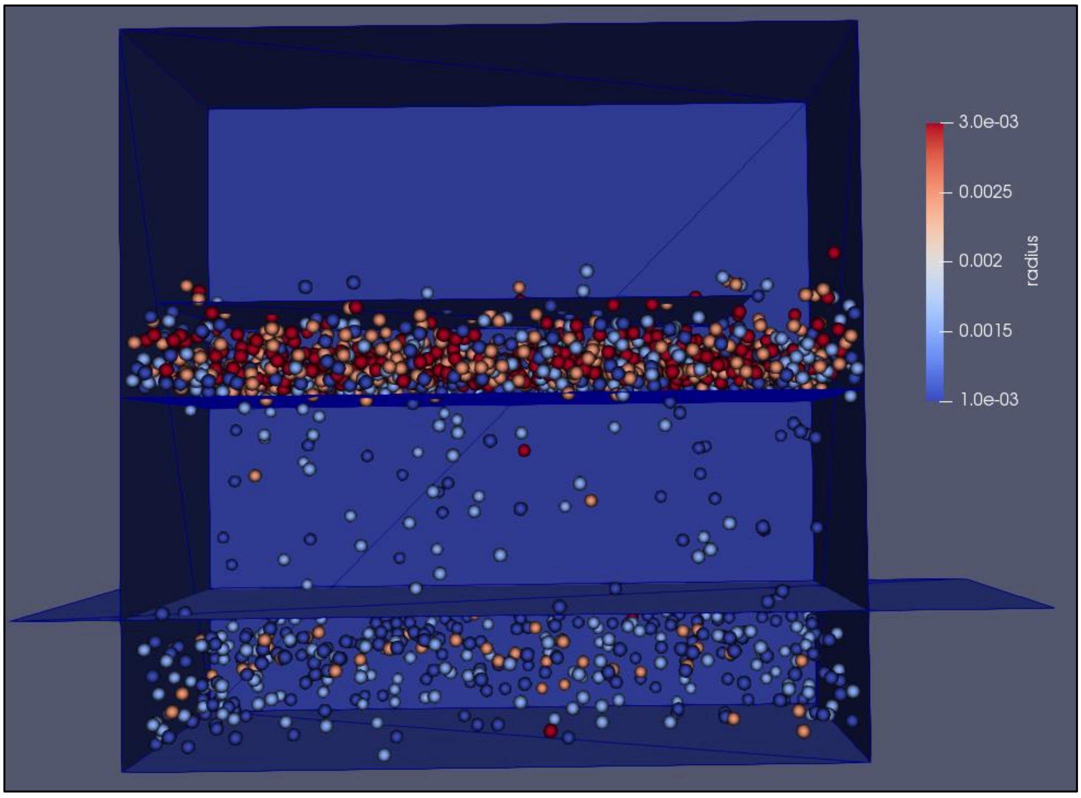

Oval Extruded Sieve

1. For the Oval Extruded Sieve with 200 Particles
   a. The worst performing simulation was the 0° stroke with a 5% passing rate.

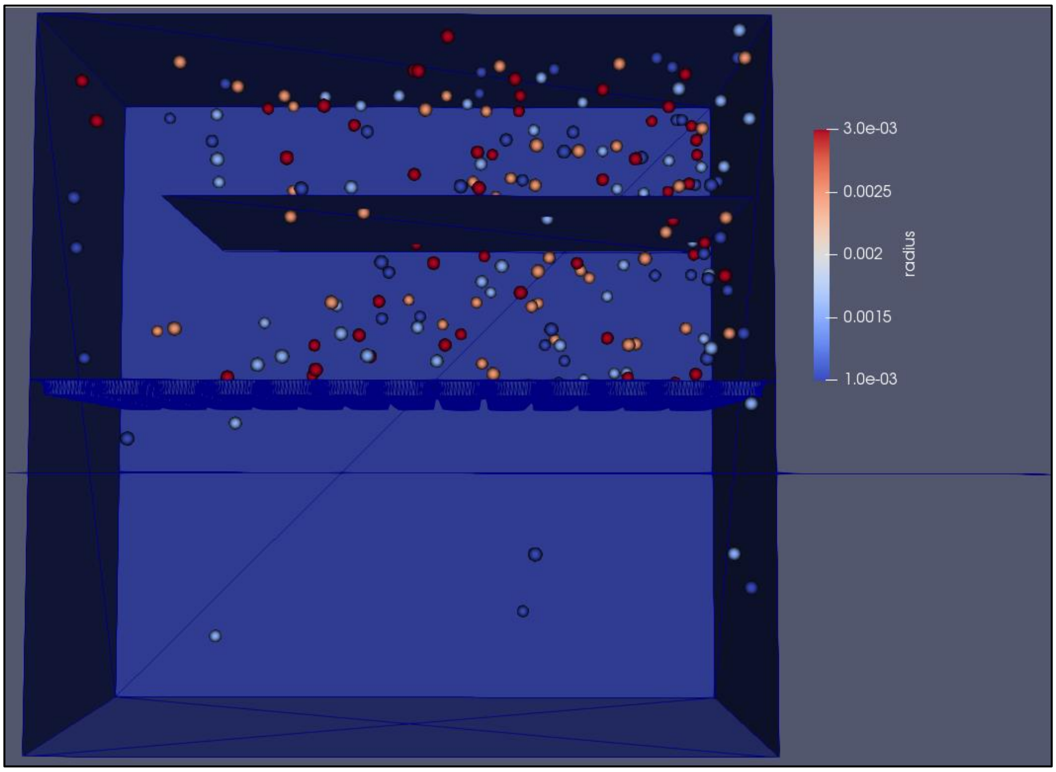

   b. The best performing simulation was the 90° stroke with an 85% passing rate.

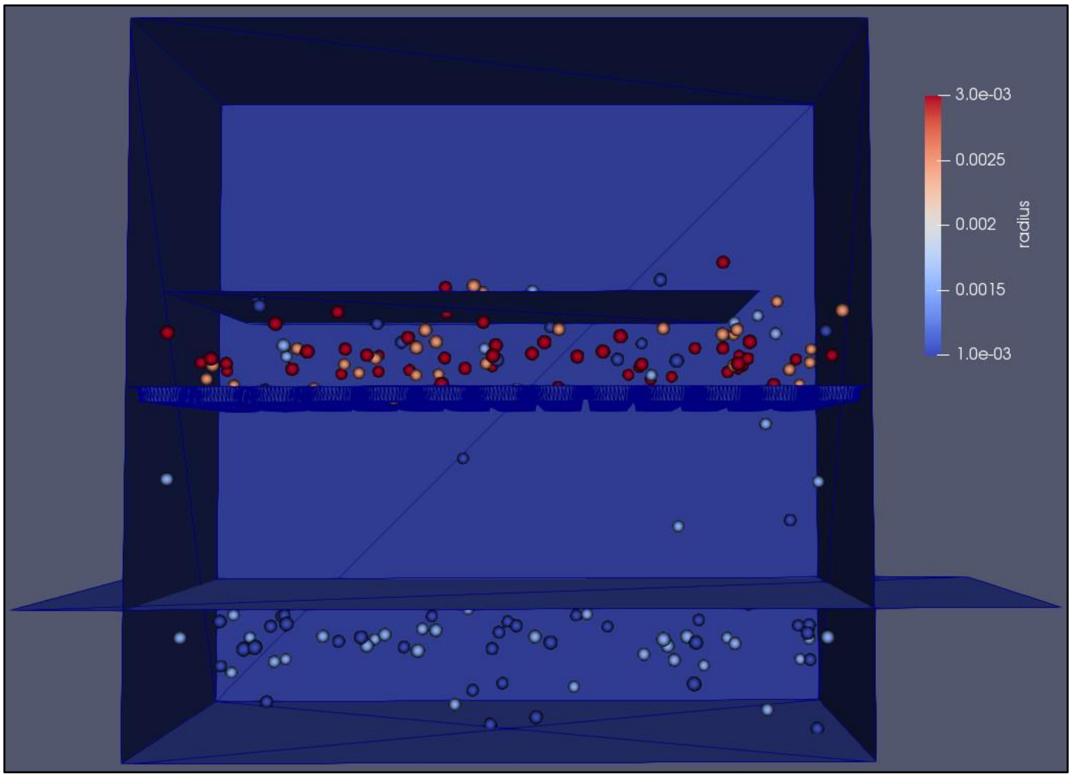

2. For the Oval Extruded Sieve with 600 Particles
    a. The worst performing simulation was the 15° stroke with a 12.3% passing rate.

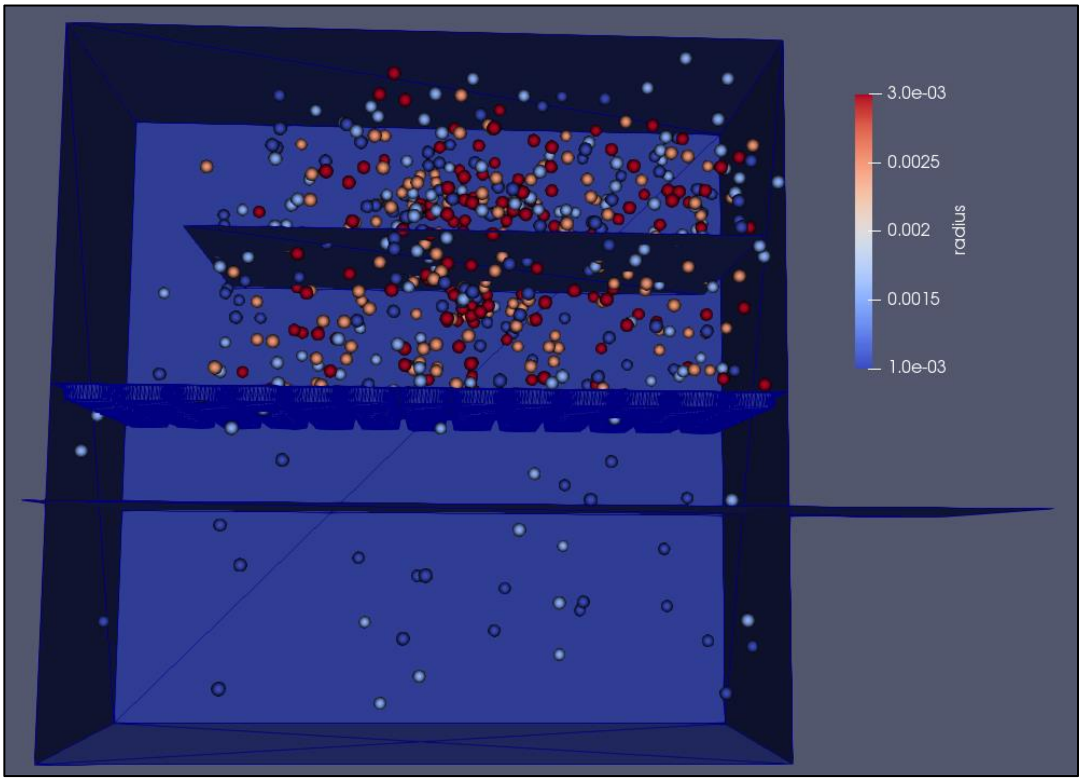

    b. The best performing simulation was the 90° stroke with a 72% passing rate.

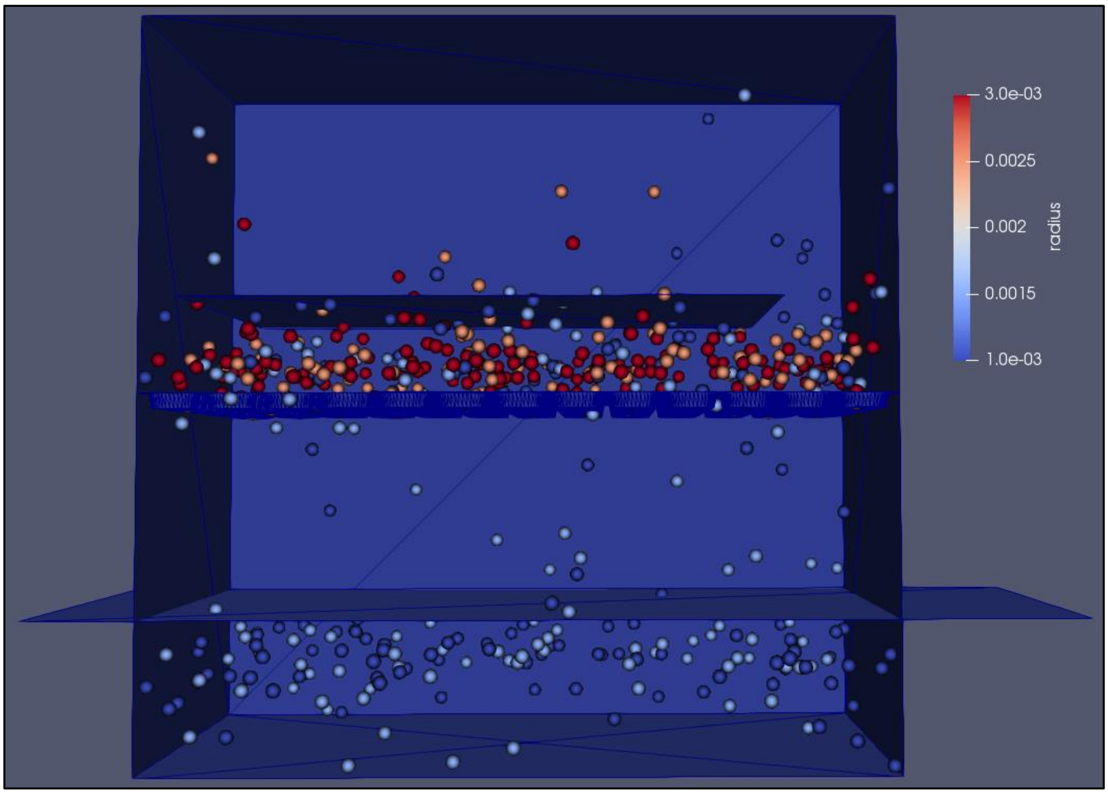

3. For the Oval Extruded Sieve with 1800 Particles

    a. The worst performing simulation was the 0° stroke with a 5.6% passing rate.

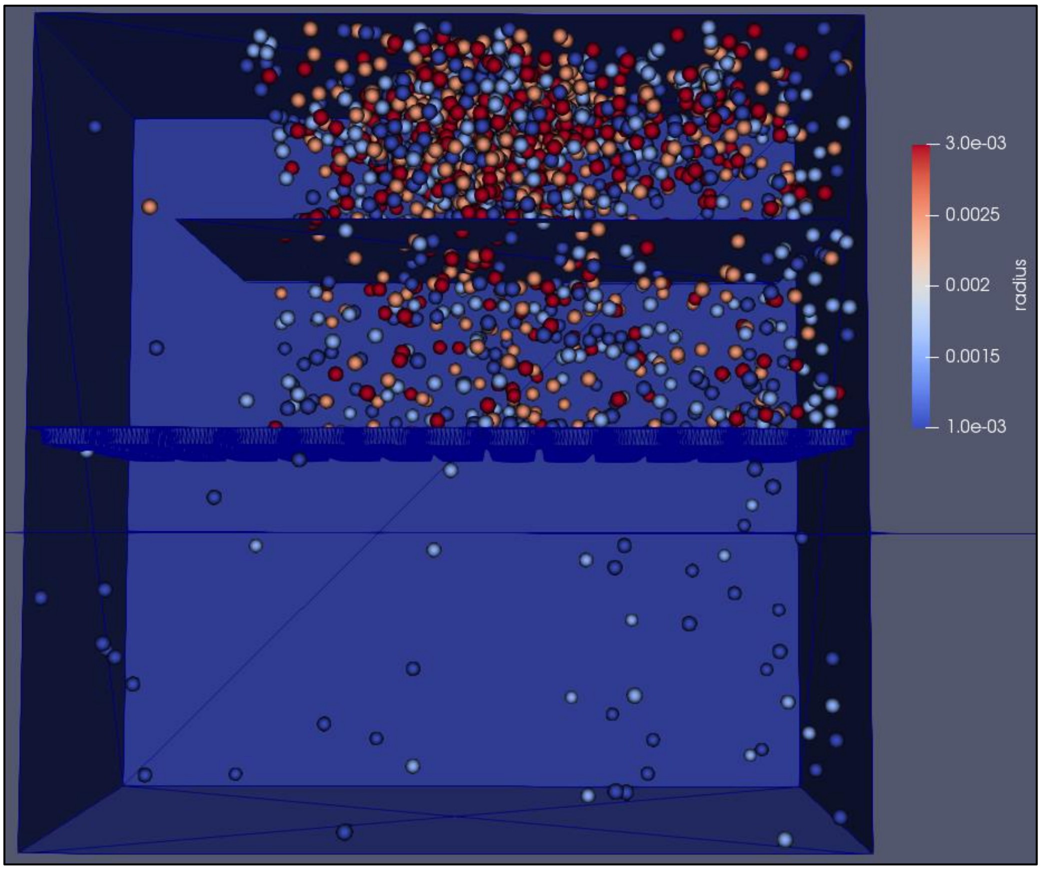

    b. The best performing simulation was the 90° stroke with a 46.9% passing rate.